Characterization of Stromal Cell-Derived Factor-1 (SDF-1) and Glycoprotein nmb (GPNMB) in Cardiac Pathophysiology

Dissertation

zur Erlangung des akademischen Grades

doctor rerum naturalium (Dr. rer. nat.)

im Fach Biologie

eingereicht an der

Mathematisch-Naturwissenschaftlichen Fakultät I

der Humboldt-Universität zu Berlin

von

Silke Mühlstedt, M.Sc.

Präsident der Humboldt-Universität zu Berlin

Prof. Dr. Jan-Hendrik Olbertz

Dekan der Mathematisch-Naturwissenschaftlichen Fakultät I

Prof. Dr. Stefan Hecht

Gutachter: 1. Prof. Dr. Harald Saumweber

2. Prof. Dr. Michael Bader

3. PD Dr. Cemil Özcelik

Tag der mündlichen Prüfung: 15.01.2013

Abstract

Ischemic heart diseases are the major cause of death worldwide due to the limited mitotic capacity and subsequent lack of regeneration in the heart. The chemokine SDF-1 is one of the most promising novel therapeutic targets due to its ability to influence inflammatory and repair processes in the damaged heart by attracting leukocytes as well as stem/progenitor cells. However, the exact role of different cardiac cell types in this process remains elusive and underlying mechanisms have been controversially discussed due to recent reports that demonstrated detrimental effects of SDF-1 in cardiac repair. In order to clarify the role of the chemokine and its receptor CXCR4 in myocardial regeneration, we generated transgenic rats overexpressing SDF-1 exclusively in cardiomyocytes and subjected these animals to myocardial infarct experiments. Whereas the overexpression of the chemokine did not alter the function and morphology of the hearts at baseline, transgenic rats demonstrated a deterioration of cardiac function and remodeling upon induction of infarction. This finding was accompanied by higher levels of fibrosis, neutrophil blood counts and macrophage infiltration into the cardiac tissue. On the other hand, we found no alterations of stem/progenitor cell recruitment or neovascularization in SDF-1-overexpressing animals. In conclusion, our findings confirm that the SDF-1/CXCR4 axis can have adverse effects on cardiac repair by affecting the inflammatory state of the healing heart. We therefore suggest a careful evaluation of the pleiotropic functions of the chemokine and its receptor in a cell type- and context-specific manner.

Furthermore, a microarray-based screening was conducted in rat hearts 24 hours after myocardial infarction with the aim to discover yet unknown molecules that might have an impact on cardiac pathophysiology. This screening yielded the glycoprotein GPNMB, which is known to be involved in inflammatory and fibrotic processes after tissue injury. However, its role in the heart remains elusive and we thus studied the protein further using DBA/2J mice that lack functional levels of GPNMB due to a spontaneous point mutation. Whereas the cardiac function and morphology in these mice were found to be normal at baseline, experimental induction of myocardial infarction revealed a preservation of cardiac function in the mutant mice in association with less dilatation of the heart as well as higher red blood cell and hemoglobin levels in the blood. Moreover, the absence of GPNMB resulted in an altered function and distribution of monocyte/macrophage subsets that are known to be critically involved in cardiac healing. These results indicate a role of GPNMB in repair processes of the heart after experimental ischemic injury and prompted us to analyze its relevance in human cardiac diseases. We found increased levels of the glycoprotein in plasma of patients after acute myocardial infarction in comparison to healthy individuals. In contrast, GPNMB was not elevated in plasma from patients suffering from chronic coronary artery disease. In

conclusion, our findings suggest that GPNMB might constitute a novel therapeutic target and biomarker of acute myocardial infarction.

Keywords: myocardial infarction, inflammation, SDF-1, cardiac remodeling, macrophages, GPNMB

Zusammenfassung

Ischämische Herzerkrankungen stellen die weltweit häufigste Todesursache dar, was auf die eingeschränkte mitotische Kapazität des Herzens und die sich daraus ergebende mangelnde Regeneration zurückzuführen ist. Das Chemokin SDF-1 zählt zu den vielversprechendsten neuen Therapietargets, da es durch die Anlockung von Leukozyten und Stamm- und Vorläuferzellen sowohl entzündliche als auch regenerative Prozesse im beschädigten Herzen beeinflussen kann. Die Funktion, welche die verschiedenen kardialen Zelltypen dabei einnehmen, ist jedoch unbekannt. Auch die zugrunde liegenden Mechanismen werden kontrovers diskutiert, da jüngste Veröffentlichungen nachteilige Effekte von SDF-1 auf die Heilung des Herzens beschrieben haben. Um den Einfluss des Chemokins und seines Rezeptors CXCR4 auf die myokardiale Regeneration aufzuklären, wurden in der vorliegenden Arbeit transgene Ratten, die SDF-1 ausschließlich in Kardiomyozyten überexprimieren, generiert und im experimentellen Herzinfarktmodell untersucht. Während die Überexpression des Chemokins keinen Einfluss auf die basale Funktion und Struktur des Herzens hatte, zeigte sich eine Verschlechterung der kardialen Funktion und des Remodelings in den transgenen Tieren nach Myokardinfarktinduktion. Des Weiteren ließ sich eine verstärkte Fibrosebildung, ein Anstieg der Zahl neutrophiler Granulozyten im Blut sowie eine erhöhte Einwanderung von Makrophagen in die Herzen transgener Ratten feststellen. Dagegen hatte die kardiale Überexpression von SDF-1 keine Auswirkung auf die Anlockung von Stamm- und Vorläuferzellen oder die Blutgefäßneubildung nach Herzinfarkt. Diese Daten bestätigen, dass kardiales SDF-1 eine nachteilige Wirkung auf die Heilung des Herzens ausüben kann, indem es die entzündlichen Prozesse im geschädigten Gewebe beeinflusst. Die vielfältigen Effekte des Chemokins und seines Rezeptors sollten daher immer im Hinblick auf die unterschiedlichen Krankheitsbilder und beteiligten Zelltypen bewertet werden.

Ferner wurde im Rahmen der vorliegenden Arbeit ein Microarray-basiertes Screening in kardialem Rattengewebe 24 Stunden nach Herzinfarkt durchgeführt. Ziel dieser Studie war es, neuartige Moleküle zu identifizieren, deren Rolle in der Pathophysiologie des Herzens bislang unbekannt ist. Das Screening brachte das Glykoprotein GPNMB hervor, welches bekanntermaßen an entzündlichen und fibrotischen Prozessen nach Gewebeschädigung beteiligt ist. Die Funktion von GPNMB im Herzen ist jedoch nicht erforscht, weshalb wir das Protein nachfolgend mit Hilfe des DBA/2J Mausstamms untersuchten. DBA/2J Mäuse tragen eine Spontanmutation des GPNMB Gens, wodurch in den Tieren kein funktionelles Protein vorhanden ist. Die Phänotypisierung der Mäuse zeigte, dass das Fehlen von GPNMB weder zu strukturellen Auffälligkeiten noch zu Veränderungen der basalen Funktion des Herzens führt. Im experimentellen Herzinfarktmodell zeigten die DBA/2J Mäuse jedoch eine verbesserte kardiale Funktion begleitet von einer verringerten Herzdilatation sowie erhöhten Erythrozyten- und Hämoglobinkonzentrationen im peripheren Blut. Weiterführende

Experimente ergaben zudem Veränderungen in der Funktion und Verteilung von Monozyten- und Makrophagensubpopulationen, welche nachweislich an kardialen Heilungsprozessen beteiligt sind. Diese Ergebnisse lassen darauf schließen, dass GPNMB eine wichtige Rolle in regenerativen Vorgängen des Herzens nach Myokardinfarkt spielt und veranlassten uns, die Relevanz des Glykoproteins für humane Herzerkrankungen zu untersuchen. Proteinbestimmungen von GPNMB im Plasma ergaben erhöhte Konzentrationen des Glykoproteins in Proben von Patienten nach akutem Myokardinfarkt im Vergleich zu Plasmaproben von gesunden Individuen. Dagegen war GPNMB im Plasma von Patienten, die an chronischer koronarer Herzkrankheit leiden, nicht verändert. Zusammenfassend weisen die Ergebnisse der vorliegenden Arbeit darauf hin, dass GPNMB nicht nur ein vielversprechendes Therapietarget, sondern auch einen potenziellen Biomarker für akuten Myokardinfarkt darstellt.

Schlagwörter: Herzinfarkt, Entzündung, SDF-1, kardiales Remodeling, Makrophagen, GPNMB

Table of Contents

ABSTRACT ..... **I**

ZUSAMMENFASSUNG ..... **III**

TABLE OF CONTENTS ..... **V**

1 INTRODUCTION **1**

1.1 ISCHEMIC HEART DISEASE **1**

1.1.1 Acute Myocardial Infarction 1

1.1.2 Myocardial Remodeling of the Ischemic Heart 2

1.1.2.1 Cell Death 2

1.1.2.2 Inflammation and the Role of Infiltrating Macrophages 3

1.1.2.3 Neurohormonal Activation 4

1.1.2.4 ECM Remodeling and Fibrosis 5

1.1.2.5 Cardiac Hypertrophy 6

1.1.3 Cardiac Biomarkers 6

1.1.4 Therapeutic Options 8

1.1.4.1 Invasive therapy 9

1.1.4.2 Medical therapy 9

1.1.4.3 Stem Cell-Based Approaches 10

1.2 THE CHEMOKINE SDF-1/CXCL12 AND MYOCARDIAL INFARCTION **13**

1.2.1 Chemokines and Their Involvement in Ischemic Cardiac Injury 13

1.2.2 The Chemokine SDF-1/CXCL12 and its Receptor CXCR4 14

1.2.3 Therapeutic Targeting of the SDF-1/CXCR4 Axis in Myocardial Infarction 16

1.2.4 Platelet-derived SDF-1 and its Role in Cardiac Repair 19

1.2.5 Negative Impact of SDF-1/CXCR4-Based Therapy in Myocardial Infarction 20

1.3 GPNMB/OSTEOACTIVIN **22**

1.3.1 Biology of the Glycoprotein GPNMB/Osteoactivin 22

1.3.2 Functional Role of GPNMB/Osteoactivin in Disease Processes 24

2 AIM OF THE STUDY **27**

3 MATERIAL AND METHODS **28**

3.1 MATERIAL **28**

3.1.1 Chemicals and Reagents 28

3.1.2 Enzymes, Markers and Kits 29

3.1.3 Antibodies 30

3.1.4 Oligonucleotides 31

3.1.5 Mouse and Rat Strains 34

3.1.6 Lab Equipment and Expendable Material 35

3.2 METHODS **36**

3.2.1 DNA Analysis 36

3.2.1.1 DNA Isolation for Genotyping 36

3.2.1.2 DNA Isolation for Southern Blot ... 36
3.2.1.3 Determination of Nucleic Acid Concentration ... 37
3.2.1.4 DNA Extraction from Agarose Gels ... 37
3.2.1.5 Sequencing ... 37
3.2.1.6 Polymerase Chain Reaction (PCR) ... 37
3.2.1.7 Long Template PCR ... 38
3.2.1.8 Southern Blot ... 39
3.2.2 RNA Analysis ... 41
3.2.2.1 RNA Extraction from Tissue ... 41
3.2.2.2 RNA Extraction from Cells ... 41
3.2.2.3 Reverse Transcription ... 41
3.2.2.4 Quantitative Real Time PCR (qRT-PCR) ... 42
3.2.2.5 5´ RLM-RACE ... 42
3.2.2.6 Microarray ... 43
3.2.3 Protein Biochemistry ... 44
3.2.3.1 Protein Isolation from Cells and Organs ... 44
3.2.3.2 Measurement of Protein Concentration ... 44
3.2.3.3 SDS Polyacrylamide Gel Electrophoresis (SDS-PAGE) ... 44
3.2.3.4 Western Blot ... 45
3.2.3.5 Enzyme-linked Immunosorbent Assay (ELISA) ... 45
3.2.4 Isolation and Culture of Adult Rat Cardiomyocytes ... 46
3.2.5 Isolation and Culture of Murine Macrophages ... 46
3.2.6 Animal Work ... 47
3.2.6.1 Animal Husbandry ... 47
3.2.6.2 Generation of SDF-1 Transgenic Rats ... 47
3.2.6.3 Generation of SDF-1 Conditional Knockout Mice ... 47
3.2.6.4 Echocardiography ... 48
3.2.6.5 Cardiac MRI ... 48
3.2.6.6 Isoprenaline Infusion via Minipumps ... 49
3.2.6.7 Induction of Myocardial Infarction ... 50
3.2.6.8 Collection of Organs and Blood Composition Analysis ... 50
3.2.6.9 Preparation of Thrombocytes from Mice ... 50
3.2.7 Flow Cytometry ... 51
3.2.7.1 Preparation of Cells for Flow Cytometry ... 51
3.2.7.2 Antibody Staining and Measurement ... 51
3.2.8 Histology ... 51
3.2.8.1 Preparation of Paraffin Sections ... 51
3.2.8.2 Preparation of Cryosections ... 52
3.2.8.3 Sirius Red Staining of Cryosections ... 52
3.2.8.4 Immunofluorescence Staining ... 52
3.2.9 Patient Population ... 53
3.2.10 Statistics ... 53

4 RESULTS 54

4.1 Generation and Basic Characterization of SDF-1α Transgenic Rats 54

4.1.1 Generation of SDF-1α Transgenic Rats 54

4.1.2 Transgene Insertion and Expression Analysis 54

4.1.3 SDF-1 mRNA Levels and Protein Content in Rat Tissues 56

4.1.4 Basic Phenotyping of SDF-1α Transgenic Rats 57

4.2 Myocardial Regeneration in SDF-1α Transgenic Rats 58

4.2.1 Impaired Cardiac Function in SDF-1α Transgenic Rats after MI 58

4.2.2 Gene Expression Analysis in SDF-1α Transgenic Rats after MI 63

4.2.3 Histological Analysis in SDF-1α Transgenic Rats after MI 65

4.2.4 Altered Cell Recruitment in SDF-1α Transgenic Rats after MI 68

4.2.5 Higher SDF-1 Plasma Levels in Transgenic Rats after MI 72

4.3 Generation and Basic Characterization of Platelet-Specific SDF-1 Knockout Mice 72

4.3.1 Generation of Platelet-Specific SDF-1 cKO Mice 72

4.3.2 Basic Phenotyping of Platelet-Specific SDF-1 cKO Mice 75

4.4 A Screening for Novel Factors in the Pathophysiology of Myocardial Infarction 76

4.4.1 Design and Evaluation of the Microarray Study 76

4.4.2 Identification of the Most Promising Candidate 78

4.5 Basic Characterization of the Selected Candidate GPNMB 80

4.5.1 GPNMB Expression Studies 80

4.5.2 DBA/2J Mice as Model to Study GPNMB *in vivo* 82

4.5.3 Basic Characterization of DBA/2J Mouse Strains 83

4.5.4 Altered Macrophage Phenotype in DBA/2J Mice 83

4.6 GPNMB as Novel Therapeutic Target and Biomarker of Ischemic Cardiac Diseases 86

4.6.1 Cardiac Function and Morphology in DBA/2J Mouse Strains after Isoprenaline Treatment 86

4.6.2 Blood Composition in DBA/2J Mouse Strains after Isoprenaline Treatment 88

4.6.3 Expression and Histological Analysis in DBA/2J Mouse Strains after Isoprenaline Treatment 89

4.6.4 Cardiac Function and Morphology in DBA/2J Strains after MI 92

4.6.5 Blood Composition and Cell Recruitment in DBA/2J Strains after MI 94

4.6.6 Expression and Histological Analysis in DBA/2J Strains after MI 98

4.6.7 GPNMB Levels in Plasma of Cardiac Disease Patients 101

5 DISCUSSION 103

5.1 Effect of Overexpression of SDF-1α in a Transgenic Rat Model 103

5.2 Generation of Platelet-Specific Conditional SDF-1 Knockout Mice 111

5.3 The Potential of GPNMB as Novel Therapeutic Target and Biomarker of Ischemic Heart Diseases 112

6 REFERENCES 120

7 APPENDIX 129

7.1 Abbreviations and Letter Symbols 129

7.1.1 Abbreviations 129

7.1.2 Letter Symbols 131
7.2 DANKSAGUNG 132
7.3 SELBSTSTÄNDIGKEITSERKLÄRUNG 133

1 Introduction

Cardiovascular diseases cause 30-40% of all deaths worldwide and are thus the most common cause of mortality.[1] Moreover, these conditions contribute significantly to healthcare costs with expenses of about 192 billion Euros per year in the EU.[2] Among cardiovascular diseases, ischemic heart diseases represent the largest group and are described in detail within the following paragraph.

1.1 Ischemic Heart Disease

Ischemic heart disease (also referred to as coronary artery disease) is a condition characterized by reduced supply of blood to the heart (ischemia). Its pathophysiological origin is atherosclerosis, which is the ongoing deposition of lipids (fatty acids and cholesterol) and white blood cells (such as macrophages) on the wall of coronary arteries. The resulting plaque formation leads to narrowing of the lumen of the blood vessels and subsequently reduces the supply of oxygen and nutrients to the heart muscle. This causes an imbalance between blood flow and the metabolic need of the myocardium. It might therefore deteriorate the function of the heart in an advanced state of the disease (≥75% luminal narrowing) and cause conditions such as stable angina pectoris, acute coronary syndromes (ACS) including myocardial infarction and heart failure. Major independent risk factors are hypertension, hypercholesterolemia, smoking and diabetes mellitus (hyperglycemia). These factors damage the endothelium of blood vessels and thus promote endothelial dysfunction, which plays a crucial role in the initiation of atherosclerosis.[3,4]

1.1.1 Acute Myocardial Infarction

Myocardial infarction (MI) or acute myocardial infarction (AMI), which is commonly known as heart attack, is defined as irreversible damage and loss of heart muscle due to dying myocardial cells and later myocardial scarring without heart muscle regrowth. It usually results from the sudden rupture of an atherosclerotic plaque with exposure of the subendothelial matrix, which leads to adhesion and subsequent activation of platelets. As a result, platelets aggregate and form a thrombus that partially or totally occludes the coronary vessel, followed by acute reduction of blood supply to the downstream portion of the myocardium. The susceptibility of a plaque to rupture mainly depends on inflammatory processes, which can increase the activity of macrophages at the site of the plaque. This leads to an enlarged lipid core and a thinner plaque cap, both characteristics of highly unstable plaques.[5] Clinical complications of AMI depend on the size and location of the infarction. In the acute phase, MI might cause arrhythmias, cardiogenic shock or formation of ventricular aneurysms and myocardial rupture. Moreover, MI may increase the predisposition to pericarditis and other long-term complications such as congestive heart failure.[6,7]

1.1.2 Myocardial Remodeling of the Ischemic Heart

The term “cardiac remodeling” comprises all pathological and structural changes in the heart after AMI such as infarct expansion, development of hypertrophy and reactive fibrosis as well as left ventricle (LV) dilatation. Therefore, post-infarction remodeling is the major determinant of impaired ventricular function, which may ultimately lead to the development of congestive heart failure with poor patient outcome (Fig. 1).

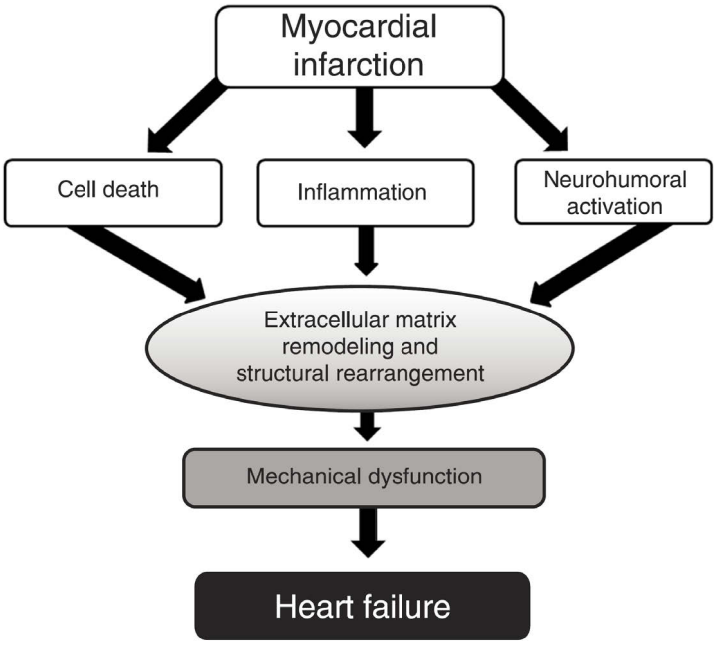

Fig. 1: Schematic illustration of the components of post-infarction remodeling.[8]

1.1.2.1 Cell Death

The hypoxic environment in the infarcted heart leads to irreversible injury of the myocardium due to cardiomyocyte death by necrosis and predominantly by apoptosis. The programmed apoptotic cell death, which accounts for loss of 2-12% of cells in the peri-infarct region of human hearts, has actually been described as an essential factor in the etiology of heart failure. The process in cardiomyocytes resembles most apoptotic signaling pathways found in extra-cardiac cell types and is based on the activation and function of cysteinyl-aspartate-directed proteases (caspases). Apoptosis is initiated by altered expression of members of the Bcl-2 family of proteins that are key regulatory components of the apoptotic process. Pro-apoptotic proteins (e.g. Bax, Bak) increase, whereas anti-apoptotic factors (e.g. Bcl-2, Bcl-xL) decrease as early as 3 hours after AMI. This shift of expression of pro-death and pro-survival proteins disrupts the integrity of mitochondrial membranes and results in the activation of caspases and formation of an “apoptosome” complex that facilitates DNA fragmentation and cell death.[8-10]

1.1.2.2 Inflammation and the Role of Infiltrating Macrophages

In the ischemic heart tissue, dying cardiomyocytes release pro-inflammatory and chemoattractive molecules, which lead to the recruitment of inflammatory cells (neutrophils, lymphocytes and monocytes) to the site of injury. The subsequent inflammatory response is essential for post-infarction healing, but prolonged inflammation may also exert deleterious effects on cardiac structure and function. Thus, the process must be tightly controlled. A key component in the regulation of the early inflammatory process is nuclear factor-kappa B (NF-κB), a transcription factor that is activated in injured hearts by local factors including reactive oxygen species (ROS). NF-κB triggers the expression of pro-inflammatory cytokines, as well as adhesion molecules and chemokines such as monocyte chemoattractant protein-1 (MCP-1 or CCL2), which in turn results in leukocyte infiltration into the injured myocardium. However, other components of the innate immune system such as toll-like receptors (TLRs) as well as the complement system might also be involved in the recruitment and activation of inflammatory cells early after myocardial infarction. The first cells that extravasate into the infarct zone within the first hours after onset of ischemia are neutrophils. Neutrophils are important mediators of the inflammatory process since they secrete molecules that attract other inflammatory cells, e.g. monocytes/macrophages. These mononuclear phagocytes dominate the cellular infiltrate for the first two weeks after AMI and are crucial for appropriate healing after AMI since they contribute to inflammation, angiogenesis and collagen deposition. Moreover, they degrade cell debris and phagocytose neutrophils as well as dead cardiomyocytes. In order to orchestrate the diverse functions of these cells, the injured heart modulates its chemokine expression profile over time, which leads to a biphasic recruitment of blood monocyte subsets. Early (during the first 3 days) after infarction, Ly-6C^{high} (Gr-1^{high}) monocytes (that give rise to M1 macrophages) are recruited via expression of the chemokine receptor CCR2. Cells of this subtype fulfill phagocytic, proteolytic and inflammatory functions and digest injured tissue. Ly-6C^{low} (Gr-1^{low}) monocytes (that preferentially become M2 macrophages) express the CX3CR1 receptor and dominate later (between 4 and 7 days) after MI. These recruited or resident “patrolling” cells exhibit reparative functions by promoting angiogenesis, myofibroblast accumulation and deposition of collagen (Fig. 2).[11-15]

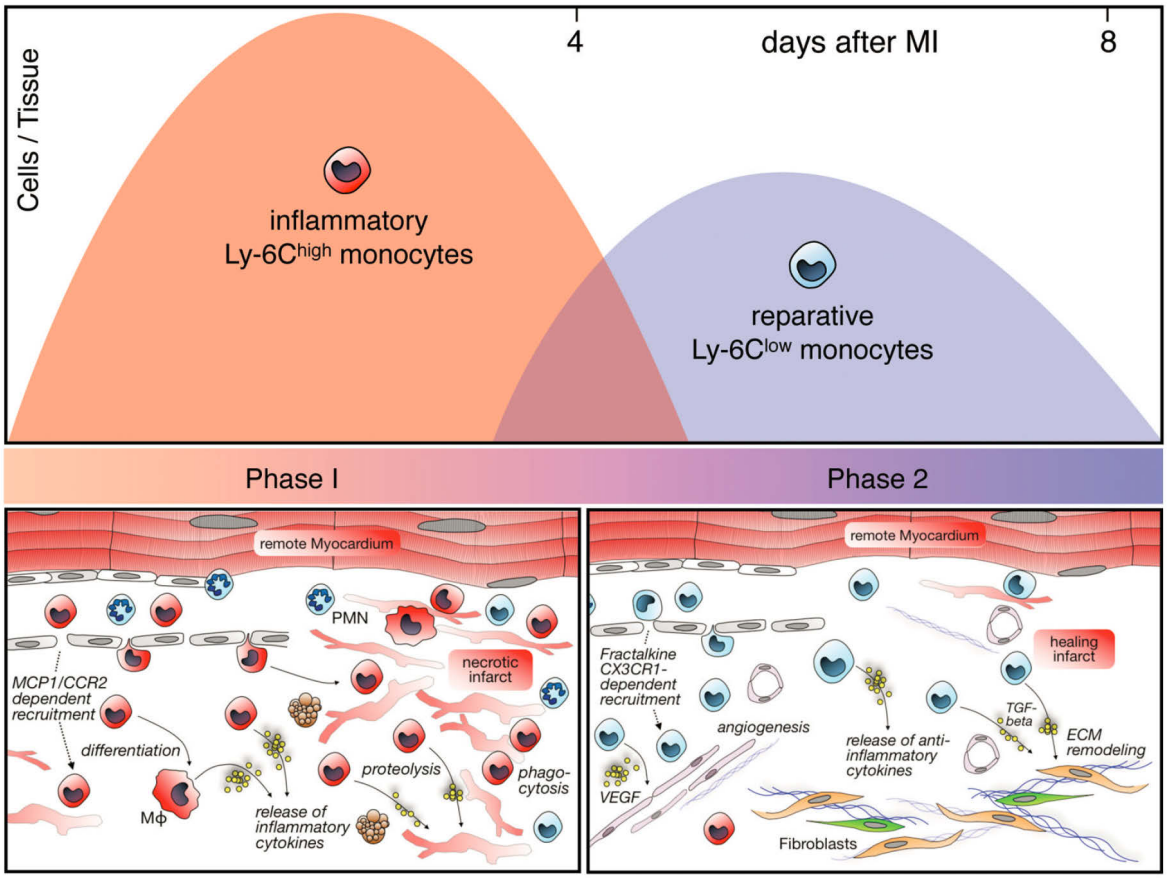

Fig. 2: Biphasic recruitment of monocytes to the post-MI mouse heart. Two different monocyte subsets (defined by their Ly-6C expression levels) are recruited to the infarcted heart at different time points and exert various functions (depicted in the lower panel). PMN: neutrophil; Mφ: macrophage; ECM: extracellular matrix.[15]

Different monocyte subsets that support various functions have also been described in humans.[11,16,17] Circulating $CD14^+$ $CD16^-$ cells resemble mouse $Ly6C^{high}$ monocytes, increase early in AMI patients and their peak levels (on day 2.6 after AMI) have been negatively correlated with extent of myocardial recovery.[18] On the other hand, $CD14^{low}$ $CD16^+$ monocytes, which peak later after myocardial infarction (on day 4.8), share a phenotype similar to mouse $Ly6C^{low}$ monocytes with potent antigen-presenting capacity but low phagocytic activity. A third, intermediate $CD14^+$ $CD16^+$ subset with unique dynamic and functional characteristics has been recently identified.[19]

1.1.2.3 Neurohormonal Activation

In order to maintain adequate levels of cardiac output and systemic blood flow, an adaptive neurohormonal response is activated post-MI. This response includes the activation of the sympathetic beta-adrenergic system as well as the cardiac renin-angiotensin-aldosterone system (RAAS). The early activation of the beta-adrenergic system leads to increased catecholamine synthesis and norepinephrine turnover. Stimulation of beta-adrenergic receptors type 1 (B_1-AR) in the heart exerts detrimental, pro-hypertrophic effects on the myocardium (whereas B_2-AR are cardio-protective). The RAAS regulates blood pressure and electrolytic homeostasis at basal levels. It is induced upon AMI because macrophages and

myofibroblasts produce angiotensinogen, whereas endothelial cells and macrophages synthetize angiotensin converting enzyme (ACE). This results in high concentrations of angiotensin II in the inflamed tissue. Moreover, the expression of AT1 receptors is increased post-MI, which in turn leads to higher levels of aldosterone. Both angiotensin II and aldosterone are key components of the remodeling process. Angiotensin II directly influences the myocardium via activation of AT1 receptors, resulting in the development of myocyte hypertrophy, cardiac fibrosis and apoptosis. Furthermore, the peptide mediates the release of chemokines that support the inflammatory process by recruiting neutrophils. Aldosterone is particularly important for the development of fibrosis by stimulating collagen synthesis in the myocardium. The protein also induces endothelial dysfunction and hypertrophy and hence aldosterone levels correlate with the severity of the disease. If the neurohormonal activation persists, the contractile function of the myocardial tissue will be impaired due to changes of the calcium metabolism within the cardiomyocytes. Therefore, components of the beta-adrenergic system and the cardiac RAAS play an important role in cardiac remodeling and development of heart failure and are thus promising therapeutic targets.[8,13,20]

1.1.2.4 ECM Remodeling and Fibrosis

The extra-cellular matrix (ECM) is a dynamic complex that surrounds the myocytes and is critical for the structural integrity of the heart. It is predominantly composed of collagen type I and III as well as fibroblasts and it also includes the proteolytic enzymes matrix metalloproteinases (MMPs) and their counterparts tissue inhibitors of MMPs (TIMPs). An altered balance between degradation and preservation of ECM is a critical step in the development of cardiac remodeling. During the early inflammatory phase after AMI, interstitial collagen fibers and other cardiac extracellular matrix components are degraded at the site of initial injury due to increased MMPs/TIMPs ratios. This leads to infarct expansion, a process which includes wall thinning, chamber dilatation and increased wall stress. Thus, a short-term inhibition of MMPs can be beneficial for the healing process. The degraded ECM network is replaced by a fibrin-based provisional matrix. Matrix fragments and the plasma-derived provisional matrix play an important role in leukocyte recruitment linking tissue injury with the inflammatory response. In parallel, pathways are activated that inhibit pro-inflammatory signals and induce the transition from the inflammatory to the proliferative phase. This phase includes the clearance of the provisional matrix and secretion of fibronectin as “second order” matrix as essential steps. Deposition of fibronectin and upregulation of pro-fibrotic cytokines (e.g. TGF-β1 and CTGF) in response to oxidative stress promote the conversion of fibroblasts and/or circulating progenitor cells to myofibroblasts. These cells rapidly accumulate and are responsible for the synthesis of ECM proteins and collagen, which is detectable as early as three days after AMI within all regions of the left ventricle (infarcted and non-infarcted). The increased collagen deposition in the infarct region during the final maturation phase is

necessary for the formation of a scar that prevents further expansion. However, the collagen production in the remote myocardium by interstitial fibroblasts results in changes of the LV architecture and geometry. Therefore, ECM remodeling and fibrosis contribute significantly to the remodeling of the injured heart and the impairment of cardiac function.[8,21-25]

1.1.2.5 Cardiac Hypertrophy

Cardiac hypertrophy is a complex adaptive process that initially allows the organism to maintain and improve cardiac output and to decrease ventricular wall tension upon loss of myocardial tissue after MI. However, sustained cardiac hypertrophy becomes detrimental and can lead to arrhythmias as well as heart failure and is therefore a significant predictor of cardiovascular mortality. It is characterized by increased myocyte cell size that is accompanied by assembly of additional sarcomeres in order to maximize force generation in the absence of cell division. Cardiomyocyte hypertrophy is typically paralleled by the reactivation of a cardiac fetal gene expression program (e.g. re-expression of β-MHC) and increased synthesis of atrial and B-type natriuretic peptides (ANP and BNP). Another common feature of the condition is an altered expression of critical calcium cycling/handling proteins (e.g. SERCA), which can be manifested in alterations of the action potential shape and excitation-contraction coupling process. The predominant stimuli for the hypertrophic process are mechanical factors, but hormones and cytokines such as angiotensin II, thyroid hormone, insulin and epidermal growth factor (EGF) can be also involved in the initiation of hypertrophy. The subsequent activation of intracellular signaling pathways involves the activation of protein kinase C (PKC), mitogen activated protein kinase (MAPK) superfamily, phosphoinositide-3-kinase (PI3K-Akt) and calcineurin-NFAT. The resulting changes in transcriptional regulation of gene expression play a crucial role in hypertrophy development and transition to a failing state.[8,26-28]

1.1.3 Cardiac Biomarkers

The basis of diagnosing ACS and myocardial infarction is a combination of evaluating the clinical history of a patient, results from ECG and stress testing as well as cardiac biomarker levels in the blood. A cardiac marker is a protein that functions as indicator of myocardial damage since it is released into the circulation if the ischemia in the heart is severe enough to damage myocardial cell membranes. Several cardiac biomarkers are available to evaluate the heart function and myocardial injury in the context of ischemic symptoms. For many years, creatine kinase (CK) was the gold standard marker for myocardial injury. CK is a simple and cost-efficient test, but the protein is also expressed in non-cardiac tissue such as skeletal muscle. Thus, elevated CK levels can result from other conditions, e.g. skeletal muscle diseases. The CK-MB (CK-muscle brain) fraction, which is more specific for cardiac muscle than striated muscle, can be measured to overcome this problem. It peaks early

(within 10-24 hours of myocardial necrosis) and it has a short duration since it returns to normal levels within 2-3 days (Figure 3). Therefore, CK-MB is useful for diagnosing reinfarction and MI extension. However, CK-MB is less sensitive than troponins.[5,29,30] Troponins are the most sensitive and specific markers at present to diagnose myocardial damage. Both troponins (troponin I and T) are components of the cardiac muscle and are released into the bloodstream upon myocardial injury. They begin to increase within 3-4 hours, peak around 12 hours after MI and remain elevated up to 5-10 days for troponin I and up to two weeks for troponin T. Due to this timing, troponins have a low sensitivity in the early phase after MI (< 6 hours after symptom onset) and repeated measurements are needed for correct diagnosis. Furthermore, they are less appropriate to diagnose recurrent infarction than CK-MB. However, even minor elevation of troponin signifies adverse prognosis and helps to determine high-risk patients and to select the most suitable therapy. Thus, high sensitive-Troponin T (hs-TnT) is now the biomarker of preference defined by the European Society of Cardiology and the American College of Cardiology Foundation/American Heart Association (ACCF/AHA) guidelines.[31,32]

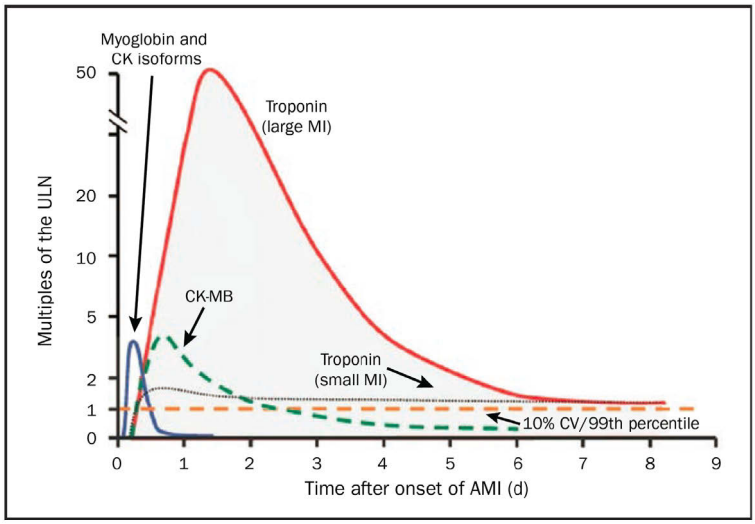

Fig. 3: Comparison of cardiac biomarkers in the first days (d) after onset of acute myocardial infarction (AMI). The dashed lines illustrate the upper limit of normal (ULN), defined as the 99th percentile from a normal reference population without myocardial damage.[5]

Another marker recommended by these guidelines is myoglobin. This protein binds oxygen and is a sensitive marker of myocardial injury. However, it is not specific for cardiac muscle since it is also expressed in skeletal muscle. For this reason, myoglobin is less used than the other markers, but it has the advantage of rising earlier than CK-MB or troponin with a peak after 2 hours. Thus, the elevation of myoglobin levels can be helpful for early detection of myocardial damage and for excluding MI. Myoglobin can be also used to determine the reperfusion after thrombolysis.[5] Glycogen phosphorylase isoenzyme BB (GPBB) is an enzyme expressed in cardiac and brain tissue but is considered to be heart muscle-specific due to the blood-brain barrier. During ischemic cardiac damage, GPBB is converted in its

soluble form and released into the circulation where it can be detected already 1-3 hours after initial damage. It is therefore described as a novel and specific marker especially for the early diagnosis of acute coronary syndrome.[33] Additional molecules have been described such as soluble lectin-like oxidized lipoprotein receptor (sLOX)-1[34] or MMP-9[35] that reflect plaque rupture and vulnerability rather than myocardial damage and might be useful as markers for diagnosis in earliest stages of acute coronary syndrome.

There are also cardiac markers available for chronic ischemic heart diseases. BNP is released from ventricular myocardium in conditions of systolic and diastolic LV dysfunction, acute coronary syndrome, stable coronary artery disease, valvular heart disease, right ventricular failure or ventricular hypertrophy. Higher BNP levels are associated with higher mortality rates and bigger infarctions. BNP is an approved marker for congestive heart failure.[30,36,37] C-reactive protein (CRP) is an acute phase protein and elevated during inflammation. It is also part of the plaque formation and might therefore reflect extent of plaque formation and predict the risk for plaque rupture and acute coronary events. In addition, CRP correlates with mortality rates and can be helpful to distinguish patients with high and low risk (even if troponin levels are normal).[30,38,39]

In summary, several markers exist for acute as well as chronic ischemic injury of the heart. However, none of them is completely sensitive and specific for myocardial infarction. Moreover, the rise of these proteins in the circulation can take 2-24 hours followed by the laboratory measurement that also takes time. Therefore, cardiac biomarkers alone are not useful in the acute phase diagnosis and should be accompanied by ECG measurements and history evaluation. Furthermore, novel cardiac markers are needed for the prognosis of the condition and efficiency of the therapy. Nevertheless, multi-marker approaches can be useful. For example, it has been reported that the mortality risk can be evaluated based on the parallel measurement of troponin I, CRP and BNP since it increases with the number of elevated markers.[40] In line with this, the ACCF/AHA guidelines suggest the measurement of troponin, CK-MB and myoglobin for patients with suspected ACS without ST-segment elevation.

1.1.4 Therapeutic Options

Over the last decades, considerable progress was achieved for the treatment of ischemic heart diseases and acute coronary syndromes. As a result, morbidity and mortality rates after AMI have been improved. However, the incidence of heart failure continues to increase significantly because existing therapeutic options focus only on cause-dependent interventions. They cannot reduce necrosis of the myocardium or induce cardiac repair due to the terminally differentiated state of the heart. The major treatment goal is the alleviation of ischemia and the prevention of recurring adverse events. In principle, there are two strategies

(early invasive versus conservative) for the treatment of acute coronary syndromes. The early invasive strategy includes cardiac catheterization within 4-24 hours after admission and revascularization via coronary artery bypass graft (CABG) or percutaneous coronary intervention (PCI). Accurate diagnosis and identification of high-risk patients who profit most from aggressive medical therapy and early invasive strategies is of great importance. In contrast, the conservative strategy focuses on initial medical therapy followed by catheterization and revascularization only if ischemia persists. Recent pooled data revealed similar outcomes of both strategies for low-risk patients.[41]

1.1.4.1 Invasive therapy

Coronary angiography is important to define the coronary anatomy and diagnose patients with significant stenosis and severe lesions who need surgical intervention. For reperfusion, CABG has been the gold standard approach. However, the development of PCI and improvement of stenting techniques (bare-metal or drug-eluting stents) allowed the consideration of this approach as alternative treatment option.[42] CABG and PCI improve ventricular function and remodeling as well as collateral blood flow and thereby decrease infarct expansion, ventricular aneurysm formation and mortality. However, there are also important limitations to the early invasive strategy. There are risks of major bleeding and stroke and stent implantation has been associated with neo-intimal proliferation, stent thrombosis and restenosis that result in recurrent MI. Also, the optimal timing of intervention remains unclear and the benefit of invasive approaches in low-risk patients has been questioned.[41]

1.1.4.2 Medical therapy

The conservative medical strategy is applied in all patients suffering from chronic ischemic diseases (e.g. stable angina) and acute coronary syndromes alone or in combination with invasive reperfusion. The main objective of the medical therapy includes anti-ischemic, anti-thrombotic and lipid-lowering effects.[5]

The ACCF/AHA guidelines (2011 update) recommend the use of nitroglycerin, beta blockers, calcium antagonists and inhibitors of the RAAS for anti-ischemic therapy.[31,32] Organic nitrates such as nitroglycerin function as vasodilator thereby improving the blood flow to ischemic areas through the generation of nitric oxide (NO) in the vasculature. Nitroglycerin is administered as sublingual tablet or injected intravenously if symptoms persist. Beta blockers are antagonists of β_1-adrenergic receptors in the heart muscle. They improve the cardiac function by reducing myocardial contractility and heart rate, which in turn decreases the cardiac workload and oxygen demand of the heart tissue. Similar effects have been described for calcium channel blockers. They inhibit the contraction of the myocardium and smooth muscle cells and thus reduce the myocardial oxygen demand and cause vasodilatation of the

coronary arteries. Finally, inhibitors of the RAAS such as ACE inhibitors or angiotensin II receptor blockers can be applied in order to improve cardiac function and remodeling via attenuation of ventricular dilatation and hypertrophy.

Platelets play a key role in the process of thrombus formation. With regard to this, antiplatelet drugs are a major part of anti-thrombotic therapy. However, these agents may increase the risk of severe bleeding. Therefore, the therapy should be carefully monitored especially if it is combined with invasive revascularization. Aspirin, which irreversibly inhibits the enzyme cyclooxygenase 1 (COX1), blocks the formation of thromboxane A_2 in platelets, thereby inhibiting platelet aggregation. It is furthermore used for long-term prevention of adverse events. Clopidogrel is another antiplatelet agent. It functions as irreversible antagonist of $P2Y_{12}$ adenosine diphosphate (ADP) receptors on platelet membranes. As a result of this blockage, the activation and aggregation of platelets is decreased and the blood viscosity is reduced. Moreover, GP IIb/IIIa inhibitors can be applied that inhibit fibrin-mediated cross-linking of platelets. The other major goal of anti-thrombotic therapy is the inhibition of coagulation as soon as possible. For anticoagulant therapy, indirect thrombin inhibitors, e.g. unfractionated or low-molecular-weight heparin, can be used. Furthermore, direct inhibitors of thrombin or factor Xa have been reported to decrease ischemic complications associated with acute coronary syndrome.

Lipid-lowering therapy with statins is beneficial in patients with ACS independent of baseline low density lipoprotein (LDL) cholesterol levels by reducing the mortality and incidence of subsequent MI, coronary revascularization and stroke. More recently, therapeutic angiogenesis has been described as promising strategy. The purpose of this novel approach is to stimulate the development of new blood vessels via administration of growth factors such as VEGF, FGF-1 or FGF-2.[43] Early clinical trials revealed great potential of the application of these factors for patients with advanced ischemic heart diseases. Nevertheless, more studies are required to elucidate underlying mechanisms and limitations.

1.1.4.3 Stem Cell-Based Approaches

Despite aggressive medical therapy, the prognosis remains poor in patients with large myocardial infarctions and severely impaired left ventricular function. Therefore, new strategies are needed to improve the healing of the cardiac wound in order to maintain structure and function of the heart. Recently, it has been reported that the inflammatory state of the heart after AMI induces not only the recruitment of terminally differentiated cells (e.g. lymphocytes, neutrophils and monocytes), but also influences the spontaneous mobilization of bone marrow (BM)-derived stem cells that express early cardiac and endothelial markers.[44] This led to the hypothesis that LV recovery can be enhanced by stimulating the self-repair mechanism.[45] Given that granulocyte colony-stimulating factor (G-CSF) is capable of mobilizing BM-derived stem/progenitor cells in the peripheral blood and has already been

widely used in clinical hematology, the idea of using this agent in patients after AMI arose. Several preclinical studies and small-scale trials of percutaneous G-CSF injection confirmed the safety and feasibility of the approach.[46-48] Moreover, these studies described a significant increase of $CD34^+$ cell numbers and in some cases a trend towards improved LV function and remodelling.[47,49] However, subsequent randomized and placebo-controlled trials such as REVIVAL-2[50], STEMMI[51] and G-CSF STEMI[52] showed no effects of G-CSF on LV function despite of significant bone marrow-derived stem cell mobilization. Due to these controversial results, exogenous stem cell delivery emerged as an alternative approach. In preclinical and clinical studies, several cell types and a variety of methods of delivery have been considered for stem cell therapy.[45,53-57] Autologous skeletal myoblasts (also called satellite cells) were used first due to several advantages such as myogenic differentiation potential, ischemic resistance and lack of immunosuppression. Initial small-scale trials described the feasibility of autologous skeletal myoblast transplantation accompanied by small benefits on cardiac function in patients with chronic heart diseases.[58] However, the safety of the approach was questioned due to the appearance of ventricular arrhythmias in several reports.[58-61] In contrast, other studies found no increased risk for arrhythmias.[62,63] This led to the initiation of large-scale randomized trials, which confirmed improvements in NYHA class and LV volumes.[63,64] Nevertheless, Menasché *et al*. did not observe improvements of LV function and again described a 2-fold higher risk for arrhythmia development in the cell-treated group. As another general barrier, trans-differentiation and electromechanical coupling between myoblasts and cardiomyocytes seems unlikely.[65,66]

Another cell type used in clinical trials are mesenchymal stem cells (MSCs), defined as non-hematopoietic stem cells with multi-lineage potential.[67] These cells have been described to give rise to fat, skeletal muscle, bone and cartilage as well as connective tissue and are also capable of differentiating into myocardium. Several randomized, placebo-controlled trials in patients with AMI proved the safety and feasibility of autologous[68] and allogeneic[69] MSC transplantation. Moreover, treatment was shown to improve LV function and attenuate remodeling. Thus, transplantation of MSCs appears to be a promising strategy with most prominent effects described in patients with AMI. A disadvantage of MSCs is that their fraction in BM mononuclear cells is marginal (0.01%).[70] An interesting approach to overcome this problem was reported by Kastritis *et al.* who administered a BM population consisting of culture-expanded MSCs together with endothelial progenitor cells (EPCs) in patients with acute or chronic MI[71]. The aim was to promote myogenesis (by MSCs) as well as angiogenesis (by EPCs). They could show that the approach is beneficial for LV function with significant improvements in patients with AMI. Stem and progenitor cells expressing hematopoietic and/or endothelial markers such as EPCs or hematopoietic stem cells (HSCs) have also been used in other clinical trials.[72-75] These studies showed that the administration

of suspensions enriched for $CD34^+$, $CD133^+$ or double-positive cells is safe and feasible. The transplantation of cells was shown to improve LV function and increase perfusion in both chronic[73] and acute[72] ischemia. These beneficial effects might be due to the angiogenic character of the cells that promotes neovascularization. Paracrine effects such as reduction of cardiomyocyte apoptosis might play a role as well. A major problem is the heterogeneity of the cell suspension and trans-differentiation into cardiomyocytes seems unlikely.

To date, most experience has been gained with transplanting BM-derived autologous mononuclear cell suspensions consisting of a mixture of HSCs, MSCs and EPCs in patients after AMI. Early small-scale studies demonstrated that the approach is safe and feasible and may improve cardiac contractility and remodelling.[76-78] Larger randomized and placebo-controlled trials showed mixed results regarding effects of mononuclear cell transplantation on cardiac function. The REPAIR-AMI trial (the largest to date) showed sustained LV recovery compared to controls.[79,80] In addition, Miettinen *et al.* demonstrated strongest improvements of global LV ejection fraction (LVEF) in patients with most severely impaired cardiac function at the time of admission.[81] Wollert and colleagues reported significant improvements in both regional and global LV function early after cell transplantation in the BOOST study.[82] However, the 18 months follow-up showed no long-term benefit compared to control patients.[83] Other investigations reported limited or no improvements of LVEF upon cell transplantation despite some advances in remodeling and perfusion.[84-86] Due to these conflicting results and on the basis of preclinical studies showing beneficial effects of BM cell injection together with G-CSF administration, several phase I clinical studies were conducted using this combination approach. The MAGIC trial reported significantly improved LV function compared to G-CSF treatment alone, but an unexpectedly high rate of in-stent restenosis was observed.[87] However, follow-up studies by Steinwender *et al*.[88], the MAGIC Cell-3-DES trial[89] and a recent report from Pasquet and colleagues[90] demonstrated significant improvements of LV function without increased incidences of restenosis. Hence, the combination of exogenous stem cell delivery and G-CSF administration to mobilize endogenous stem cells seems to be a promising approach. However, beneficial effects might be due to paracrine effects of the injected cells since evidence for true cardiac regeneration is lacking. Resident cardiac stem cells as well as inducible pluripotent stem (iPS) cells might be suitable candidates for future trials due to their high proliferative potential and great capacity for cardiac cell differentiation. Large-scale trials are necessary to further assess the role of stem cells in cardiac repair. Also, optimal protocols are needed regarding the time point of cell injection, cell numbers and cell type for therapy as well as methods of delivery.

1.2 The Chemokine SDF-1/CXCL12 and Myocardial Infarction

1.2.1 Chemokines and Their Involvement in Ischemic Cardiac Injury

Chemokines or chemotactic cytokines are a family of small (~ 8-14 kDa), structurally related proteins that are able to induce directed chemotaxis of leukocytes through interactions with their respective G protein-coupled seven-transmembrane receptors. They can be expressed constitutively and may be responsible for basal leukocyte trafficking and tissue maintenance (homeostatic chemokines) or they can be strongly upregulated during an immune response and may be an active part of the inflammatory reaction (inducible chemokines). Chemokines are classified into four subfamilies on the basis of the number of amino acids between the two N-terminal cysteine residues. They are designated CXC (α), CC (β), XC (γ or lymphotactin) and CX3C (δ or fractalkine) chemokines. The chemokine receptors belong to the family of G protein-coupled receptors and their nomenclature uses CXC, CC, XC or CX3C followed by R (for receptor) and then a number. CXC or α chemokines have one amino acid separating the first two cysteines and are further classified according to the presence of the motif glutamic acid-leucine-arginine (ELR) in the N-terminal region. CC chemokines have two adjacent cysteine residues and are the largest and most diverse subfamily. Lymphotactin is the only chemokine containing only one cysteine residue and the fourth group, fractalkine, has three amino acids separating the first two cysteines.[91,92]

Chemokines are known to be involved in all phases after myocardial infarction and a number of studies reported that the induction of these proteins is a prominent part of the inflammatory response after cardiac injury.[14,92-94] Increased circulating levels of CXC and CC chemokines have been found in patients suffering from AMI as well as congestive heart failure.[95-97] The upregulation of chemokine expression is mainly mediated by pro-inflammatory cytokines (e.g. TNFα and interleukin 1β (IL-1β)) as well as by ROS, complement activation and TLR signaling. ELR^+ CXC chemokines, e.g. CXCL8/IL-8 and other CXCR2-binding proteins, are critical regulators of neutrophil chemotaxis and activation. Neutrophils release chemotactic factors and recruit inflammatory monocytes from the spleen in a CCR2-dependent manner. Thus, inhibition of CXCL8/IL-8 in an experimental model of MI reduced the development of necrosis and preserved the cardiac function.[98] The role of other members of the ELR^+ CXC subfamily in cardiac wound healing is less extensively studied. However, it is known that CXCL1/GROα and MIP-2 are also induced after myocardial damage and that these ELR^+ chemokines might exert chemotactic and angiogenic actions mainly via the CXCR2 receptor. ELR^- CXC chemokines, e.g. CXCL9, CXCL10 and CXCL11, play a role in inflammation by recruiting T helper cells that express CXCR3. Moreover, members of this subfamily might have angiostatic (CXCL4/Pf4, CXCL9 and CXCL10) as well as antifibrotic (CXCL10) effects early after MI in order to prevent premature angiogenesis and fibrous tissue deposition in the

infarct region before formation of an appropriate matrix. The ELR$^-$ chemokine CXCL12 (also known as stromal cell-derived factor 1 or SDF-1) possesses the unique ability of recruiting CXCR4-expressing stem/progenitor cells in the ischemic tissue, which promotes angiogenesis (by attraction of EPCs and smooth muscle cell progenitors) and might also favor regenerative processes (by MSC recruitment).[45] CCL2/MCP-1 is the best studied CC chemokine and is described as a potent chemoattractant for mononuclear cells early (within 5 hours) after MI. Studies using CCL2 knockout mice revealed its crucial role in cardiac remodeling due to recruitment and activation of macrophages as well as induction of cytokine synthesis and myofibroblast differentiation in healing infarcts.[99] Other CC chemokines such as MCP-3, MIP-1α and -1β are also induced after ischemic cardiac injury, but their functions are less understood. Nevertheless, there are hints that CCL7/MCP-3 is capable of recruiting MSCs and circulating angiogenic cells to injured cardiac tissue and that its local overexpression improves cardiac remodeling.[100,101] Fractalkine (CX3CL1) is expressed on natural killer (NK) cells, monocytes and T lymphocytes. A study using a renal ischemia/reperfusion model revealed that the CX3CR1 receptor is a potent leukocyte chemoattractant and regulates the accumulation of reparative macrophages as well as fibrous tissue deposition.[102] These findings suggest that fractalkine and its receptor might also be involved in regeneration after ischemic injury of the heart.

In summary, chemokines are critical regulators of the post-infarction inflammatory response by induction of leukocyte infiltration and activity. In addition, they might influence repair processes by recruiting stem/progenitor cells to the site of injury. However, chemokines might have additional effects on myocardial healing beyond their chemotactic properties via influencing angiogenesis and fibrosis.

1.2.2 The Chemokine SDF-1/CXCL12 and its Receptor CXCR4

The ELR$^-$ chemokine SDF-1/CXCL12 has initially been characterized as a BM stromal-cell derived factor that is capable of stimulating pre-B cells.[103] Originally, two isoforms (SDF-1α and SDF-1β) have been identified in human and mouse that arise from a single gene through alternative splicing. Both variants are ubiquitously expressed in various cell types and tissues in a constitutive manner.[104] The predominant isoform SDF-1α comprises 3 exons and encodes an 89 amino acid protein, while SDF-1β consists of 4 exons and encodes a protein of 93 amino acids (of which the first 89 amino acids are identical to those of SDF-1α). Unlike all other chemokines of the CXC subfamily, the genes of which are clustered, the SDF-1 gene has been mapped to a unique chromosomal localization.[105] Moreover, SDF-1α and SDF-1β sequences are more than 92% identical and are highly conserved not only between human and mouse but also among lower vertebrates. These features suggest unique biological functions of SDF-1 different from those of other CXC subfamily members. Gleichmann *et al*.

identified a third splice variant, SDF-1γ, which is expressed in rat brain, heart and lung with highest levels found in heart tissue.[106] However, its expression remains unchanged upon myocardial infarction whereas SDF-1α mRNA is selectively induced in MI.[107] A recent study reported the identification of three additional human SDF-1 splice variants, SDF-1δ, SDF-1ε and SDF-1φ, in multiple tissues via RT-PCR.[108] More investigations are needed in order to understand the potential physiological relevance of these different SDF-1 isoforms and their functional differences.

Unlike other chemokines, SDF-1 had been shown to exclusively bind to the G protein-coupled seven-transmembrane receptor CXCR4 that is broadly expressed in immune cells as well as stem/progenitor cells in the bone marrow. The interaction between SDF-1 and CXCR4 exerts multiple G protein-dependent signaling pathways in target cells, resulting in diverse biological outcomes related to cell migration, adhesion and transcriptional activation.[45,109] The CXCR4-mediated activation of G_i proteins results in inhibition of adenylyl cyclases as well as activation of the Src family of tyrosine kinases and Rho GTPase, while $G_{\beta\gamma}$ activates phospholipase C-β (PLC-β) and PI3K. Moreover, binding of SDF-1 to CXCR4 can induce G protein-independent signaling pathways such as the JAK/STAT pathway. The CXCR4-mediated signaling may be regulated by receptor desensitization (involving arrestin) as well as phosphorylation and subsequent protein kinase C (PKC)-dependent internalization of the receptor.[109,110] Recent studies reported that SDF-1 also binds with high affinity to the seven-transmembrane receptor CXCR7/RDC1.[111] This protein is highly conserved in mammals and as CXCR4 expressed in a wide range of tissues. In addition to SDF-1, CXCR7 binds to the chemokine CXCL11/I-TAC, although with a lower affinity.[112] The characterization of $CXCR7^{-/-}$ mice revealed disrupted cardiac development resulting in rapid postnatal death of the animals despite normal hematopoiesis and neural development.[113] Even though it was shown that SDF-1 does not induce G protein-linked signaling through CXCR7, the atypical receptor may form heterodimers with CXCR4 and thereby affect cellular signaling networks.[114] However, the phenotypic differences observed in mice lacking CXCR4 or CXCR7 also raise the possibility of separate biological roles of both SDF-1 receptors.

The functions of SDF-1 and CXCR4 are diverse ranging from organogenesis during development to inflammation and tissue repair in adult organisms. The importance of the chemokine and its receptor was illustrated by the generation of CXCR4- and SDF-1-deficient mice, which exhibit an almost identical phenotype of perinatal lethality, defects of B-cell lymphopoiesis and myelopoiesis in fetal liver and bone marrow. Moreover, the mutants showed cardiac ventricular septal defects. These and other studies reveal that the SDF-1/CXCR4 axis is essential for hematopoiesis, organogenesis (e.g. cardiogenesis) and vascularization during embryonic development.[115-117] In adult life, SDF-1 plays an essential role in regulating the trafficking of immune cells (pre-B and T lymphocytes, monocytes) as

well as of stem/progenitor cells by inducing motility, chemotactic responses, adhesion and secretion of MMPs and angiopoietic factors in cells expressing CXCR4.[118] Accordingly, the SDF-1 receptor is expressed on the surface of several tissue-committed stem/progenitor cells such as skeletal muscle satellite cells[119], neural[120] or liver[121] stem cells. However, the SDF-1/CXCR4 axis is not only important for the mobilization and recruitment of these cells to the periphery, but plays also a crucial role in maintaining the stem cell niche in the bone marrow under steady state conditions. The analysis of conditional SDF-1 knockout mice revealed that the chemokine affects hematopoiesis and stem/progenitor cell homeostasis in the adult stage bone marrow.[122] The deletion of SDF-1 in adult mice led to the expansion of hematopoietic progenitors in BM and peripheral blood paralleled by reduction of long-term quiescent stem cells. The finding of disrupted hematopoiesis on the bone-lining surface strongly indicates the importance of SDF-1 for the organization of an osteoblastic stem/progenitor cell niche in adults. Furthermore, the SDF-1/CXCR4 axis is involved in the progression of certain types of cancers by promoting tumor growth, angiogenesis and metastatic spread to organs.[123] SDF-1 also plays an important role in human immunodeficiency virus (HIV) infection since CXCR4 acts as a co-receptor for entry of HIV in $CD4^+$ T cells.[124] Finally, it has been observed in various organs that the expression and secretion of SDF-1 is increased after tissue damage leading to direct trafficking of CXCR4-positive cells to the site of injury. Thus, the chemokine plays an important role not only in inflammation (by attracting lymphocytes) but also during tissue regeneration/repair (by attracting tissue-committed $CXCR4^+$ stem/progenitor cells from their niches).[125] In summary, SDF-1 and its receptor CXCR4 are instrumental in many pathophysiological conditions.

1.2.3 Therapeutic Targeting of the SDF-1/CXCR4 Axis in Myocardial Infarction

A first hint that SDF-1α, the major SDF-1 isoform in heart tissue, is involved in cardiac regeneration was the finding that it is strongly upregulated after experimental myocardial infarction.[107,126-128] Furthermore, higher SDF-1 levels have been found in serum samples and cardiac biopsies of patients after AMI.[129,130] Thereby, levels of circulating SDF-1α seem to correlate with numbers of progenitor cells in the periphery.[131] The induction of the chemokine is dependent on the hypoxia-inducible factor (HIF)-1α, a transcription factor that is activated at low oxygen concentrations.[132] HIF-1α also induces the expression of CXCR4 on progenitor cells, which might be helpful to attract these cells towards SDF-1 gradients.[133] Based on the chemoattractant properties of SDF-1, these observations led to the hypothesis that the chemokine and its receptor are involved in cardiac repair processes by influencing the inflammatory process via recruitment of leukocytes and the healing of the wound by chemoattraction of stem/progenitor cells.

In order to clarify the functional relevance and therapeutic potential of the SDF-1/CXCR4 axis, different approaches have been used over the past 10 years to manipulate the chemokine and/or its receptor in experimental models of ischemic cardiac diseases. Figure 4 summarizes the different models and outcomes of these preclinical studies. In most reports, SDF-1 was targeted directly by inducing its overexpression via local infusion or transplantation of engineered cells. For example, pretreatment of cultured myocytes with SDF-1α was shown to increase their resistance to hypoxic damage and administration of the chemokine *in vivo* 30 minutes before coronary occlusion decreased the infarct size.[128] The adenovirus-mediated SDF-1α (AdV-SDF-1) gene transfer did also induce cardiac preservation after AMI accompanied by increased neoangiogenesis and decreased apoptosis and fibrosis induction.[134,135] Moreover, a study by Saxena *et al.* revealed significantly better post-infarction cardiac function, prolonged myocardial survival and increased neoangiogenesis in mice upon intramyocardial injection of recombinant SDF-1α protein.[136] In line with this, plasmid-based (non-viral) transient SDF-1 gene transfer improved cardiac function and increased neoangiogenesis in a rodent model of heart failure.[137] Another approach is to induce overexpression of SDF-1 via engineered cells. The transplantation of SDF-1-expressing skeletal myoblasts eight weeks after AMI in rats improved cardiac function.[138] Supporting these results, Elmadbouh *et al.* reported improved cardiac function and neoangiogenesis upon transplantation of SDF-1α-overexpressing skeletal myoblasts at the time of AMI induction in rats.[139] Moreover, the intramyocardial injection of MSCs overexpressing SDF-1α in a heterotopic transplanted working heart model increased the survival of the myocardium as well as neoangiogenesis and decreased apoptotic cell death.[140] The transplantation of SDF-1-overexpressing fibroblasts 8 weeks after infarction was also shown to improve the cardiac function and to induce homing of c-Kit$^+$ stem cells.[126]

A general limitation in the use of SDF-1 is its short half-life and lack of lesion-directed accumulation due to the rapid diffusion of the chemokine and the degradation upon tissue injury by proteolytic enzymes, e.g. MMP-2/9 or CD26/dipeptidylpeptidase IV (DPPIV).[141] The low enrichment in the injured heart tissue and the proteolytic degradation of SDF-1 might limit its therapeutic effect after AMI. Therefore, inhibiting the degradation of the chemokine has evolved as a promising approach. Segers and colleagues designed a bioengineered protease-resistant variant of SDF-1 called S-SDF-1 (S4V). Intramyocardial delivery of this fusion protein after AMI improved the function of the heart and increased the recruitment of stem cells and the capillary density.[142] Moreover, a study by Zaruba *et al*. combined genetic and pharmacologic inhibition of DPPIV with G-CSF treatment. This led to the stabilization of myocardial SDF-1 protein, which in turn resulted in increased homing of CXCR4-positive progenitor cells (induced by G-CSF) towards infarcted areas.[143] This was accompanied by preserved cardiac function through increased angiogenesis and cardiomyocyte survival as

well as reduced cardiac remodeling. The same research group demonstrated that parathyroid hormone functions as DPPIV inhibitor and thus increases stem cell homing to the injured heart associated with attenuated ischemic cardiomyopathy.[144] A recent study by Ziegler *et al*. reported the generation of a recombinant, bifunctional molecule that consists of a SDF-1 domain and a glycoprotein VI (GPVI) domain.[145] The aim of using this SDF-1-GPVI fusion protein in a mouse model of MI was to anchor SDF-1 to tissue lesions with destroyed vascular integrity by the platelet receptor GPVI and thereby enhance the SDF-1-mediated recruitment of stem/progenitor cells to the site of myocardial damage. Indeed, administration of SDF-1-GPVI resulted in reduced infarct sizes, enhanced capillary density and preserved cardiac function after MI accompanied by enhanced recruitment of BM-derived cells. These findings indicate that the stabilization of local SDF-1 protein in ischemic tissue represents a promising new strategy to promote cardiac repair.

A number of studies focused on modulating the expression of CXCR4 on various stem/progenitor cells rather than targeting SDF-1. Intravenous infusion of MSCs overexpressing CXCR4 in rats after AMI resulted in enhanced engraftment of the stem cells accompanied by increased neoangiogenesis and alleviated left ventricular remodeling.[146] In line with this, a study by Cheng *et al.* revealed improved cardiac performance and less deleterious fibrosis upon infusion of CXCR4-expressing MSCs 24 h after coronary occlusion in rats.[147] Moreover, it has been shown that the cultivation of BM-derived cells *in vitro* leads to induced CXCR4 expression.[148] The transplantation of these cultivated cells restored blood flow and enhanced ischemic tissue neovascularization in a murine hind limb ischemia model. These results suggest that the modification of the CXCR4 receptor might be a promising approach to improve the post-MI myocardial repair besides or in addition to the manipulation of SDF-1.

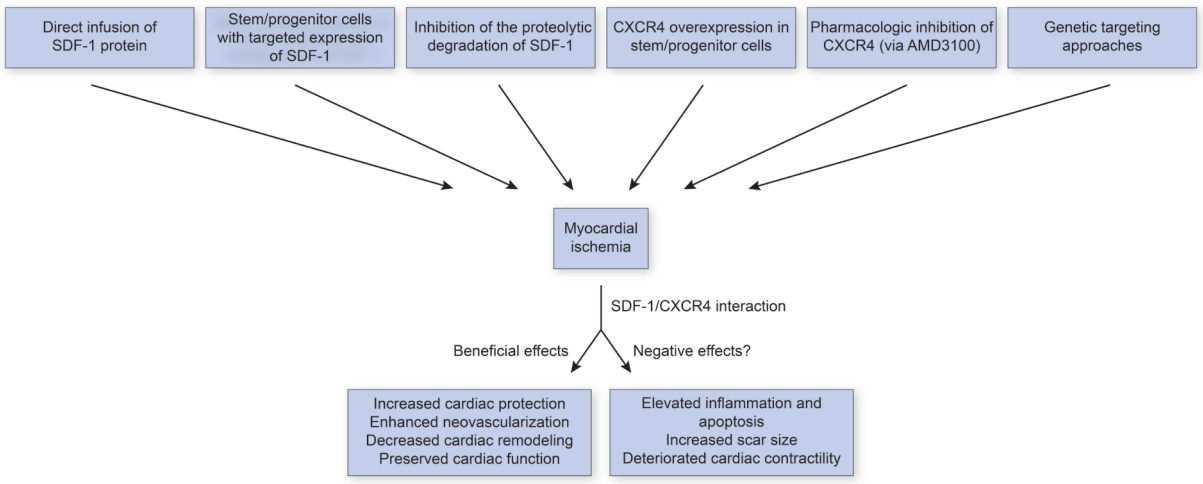

Fig. 4: Schematic representation of the various approaches used to manipulate the SDF-1/CXCR4 axis and possible effects of the chemokine and its receptor in experimental models of ischemic cardiac damage. Modified from Ghadge *et al*.[45]

In summary, the majority of studies revealed protective effects of the SDF-1/CXCR4 axis on cardiac repair processes that can be explained by three potential mechanisms.[149] First, neoangiogenesis may be supported via recruitment of CXCR4-expressing EPCs or via direct activation of proangiogenic pathways. Second, the SDF-1/CXCR4 axis may activate pro-survival factors (e.g. protein kinase B (PKB/Akt) and ERK) and thus reduce cardiomyocyte apoptosis. Third, SDF-1 may be involved in induction of regenerative processes through recruitment of $CXCR4^+$ stem/progenitor cells. On the basis of the preclinical findings, SDF-1 has been proposed as therapeutic target for stem cell-mediated cardiac regeneration. This even led to the initiation of phase I clinical trials in patients suffering from ischemic cardiac diseases. Juventas Therapeutics Inc. examines the effects of SDF-1 overexpression in patients with class III chronic heart failure via the delivery of a DNA plasmid encoding SDF-1 (JVS-100).[150] Bioheart Inc. is going to use skeletal myoblasts that overexpress SDF-1 (MyoCell® SDF-1) in patients suffering from congestive heart failure in the REGEN trial. Furthermore, a phase III clinical trial was conducted that combines G-CSF administration and the use of the CD26/DPPIV inhibitor Sitagliptin in AMI patients (SITAGRAMI trial). Theiss *et al*. recently reported the safety of the approach that might be a novel therapeutic option with the aim to increase the mobilization (by G-CSF) and homing (by increased SDF-1 levels) of stem cells.[151]

1.2.4 Platelet-derived SDF-1 and its Role in Cardiac Repair

After tissue injury such as myocardial infarction, subendothelium and ECM proteins become exposed. This in turn leads to extensive adhesion and activation of platelets that subsequently initiate vascular thrombosis. As reported by Massberg *et al*., platelets are moreover essential for the direction of BM-derived stem/progenitor cells to the site of endothelial disruption.[152] The finding that platelets (as well as their megakaryocytic precursors) contain SDF-1α in their α-granules and release the chemokine upon activation suggested that platelet-derived SDF-1 could mediate this cell recruitment. Indeed, it was reported that the secretion of SDF-1α from platelets promotes the recruitment of $CD34^+$ and Lin^- $Sca\text{-}1^+$ $c\text{-}Kit^+$ (LSK) stem/progenitor cells from the BM to the site of vascular injury and in the microcirculation of ischemic tissue, where the cells can adhere to platelets via P-selectin and GPIIb integrin[152]. In line with this, SDF-1 plasma elevation and mobilization of $CXCR4^+$ hematopoietic progenitor cells was found to be severely impaired in thrombocytopenic mice, which results in profound reduction of neovascularization.[153] Moreover, platelet-derived SDF-1 has been documented to mediate the firm adhesion of $CD34^+$ progenitor cells on immobilized platelets and to promote the differentiation of these cells towards an endothelial phenotype[154] or into macrophages and then foam cells.[155] In support to this, another study by Stellos *et al*. revealed enhanced levels of SDF-1 on circulating platelets in patients suffering

from acute coronary syndrome compared to those with stable angina pectoris.[156] In addition, platelet-bound SDF-1 expression positively correlated with the number of circulating $CD34^+$ progenitor cells. Besides endothelial progenitors, platelet-derived SDF-1 was also shown to be involved in the regulation of mobilization and homing of BM-derived vascular smooth muscle progenitor cells.[157] In summary, these findings indicate that platelets are a major source of SDF-1 during vascular or tissue injury. Since platelets are the first cells that adhere to damaged tissue and healing depends on the recruitment, accumulation and differentiation of stem/progenitor cells, platelet-derived SDF-1 might play a central role in vascular and tissue regeneration.

1.2.5 Negative Impact of SDF-1/CXCR4-Based Therapy in Myocardial Infarction

In contrast to the beneficial effects of the SDF-1/CXCR4 axis observed in most studies, there are several recent reports that demonstrate deleterious effects of the chemokine and its receptor on cardiac regeneration (see also Fig. 4). First hints emerged from an *in vitro* study by Pyo and colleagues who reported negative inotropic effects of CXCL12 treatment or CXCR4 overexpression on cardiomyocyte function by changing the calcium channel activity.[158] The observed results might be due to a direct effect of SDF-1 on cardiomyocytes, suggesting that the local delivery of the chemokine may diminish the function of the heart. Moreover, the trans-endocardial injection of SDF-1α in a porcine model of myocardial infarction surprisingly failed to improve myocardial perfusion and even impaired left ventricular function despite increased vessel density in the peri-infarct region and less collagen deposition.[159] One explanation for these results could be related to the delayed SDF-1α injection two weeks after infarction. Another study by Chen *et al.* used an adenovirus-mediated gene therapy approach and reported that the overexpression of CXCR4 in infarcted rat hearts one week before MI induction led to increased infarct areas and impaired cardiac function.[160] This was accompanied by enhanced cardiomyocyte apoptosis. These data suggest that the overexpression of CXCR4 worsens cardiac dysfunction by increasing the influx of inflammatory cells and activating pro-apoptotic pathways.

The pharmacologic inhibition of the SDF-1/CXCR4 axis via AMD3100 (Plerixafor), a selective CXCR4 antagonist, has also produced conflicting results.[149] Whereas long-term AMD3100 treatment after chronic coronary artery ligation was shown to worsen left ventricular remodeling and cardiac function despite increased levels of c-Kit^+ progenitor cells[161], other studies reported beneficial effects of CXCR4 inhibition on cardiac contractility and infarct expansion in rats.[162] An explanation for these controversial results might be related to the timing of CXCR4 inhibition. On the one hand, early AMD3100 administration might preserve cardiac function by attracting EPCs, thereby enhancing neovascularization and cell survival.

On the other hand, continuous CXCR4 blockade might worsen the outcome due to impaired incorporation of EPCs in the peri-infarct region.[163]

Recently, gene targeting approaches have also been used to clarify the role of endogenous CXCR4 in myocardial repair. Congenital and conditional cardiomyocyte-specific $CXCR4^{-/-}$ mice have been developed.[164] Analysis of these mice revealed normal cardiac development and function despite congenital ablation of CXCR4 in cardiomyocytes. Surprisingly, induction of AMI revealed no differences in cardiac function and infarct size, vascular density, collagen content or hypertrophy in conditional $CXCR4^{-/-}$ mice compared to controls. Based on these findings, CXCR4 seems to be not essential for cardiac development and remodeling after myocardial infarction. Another study by Liehn *et al*. analyzed heterozygous $CXCR4^{+/-}$ animals (since homozygous CXCR4-null mice die perinatally).[165] These mice showed significantly reduced baseline coronary flow and impaired neoangiogenesis upon induction of myocardial infarction. However, no differences in cardiac function and cardiomyocyte apoptosis were seen in $CXCR4^{+/-}$ animals post-MI compared to wild type mice. Furthermore, scar sizes were smaller in heterozygous knockouts and this was associated with altered inflammatory cell recruitment. The infiltrate in the infarcted heart in $CXCR4^{+/-}$ mice contained fewer neutrophils and pro-inflammatory $Gr1^{high}$ monocytes as well as an increased number of reparative $Gr1^{low}$ monocytic cells in comparison to controls. The authors concluded from these results that CXCR4 plays an important role in LV remodeling after AMI by influencing the recruitment of inflammatory/progenitor cells and neoangiogenesis. The contradictory observations of decreased infarct sizes and an adaptation to hypoxic stress in heterozygous mice despite reduced baseline coronary flow and neoangiogenesis highlight the pleiotropic effects of CXCR4.

In order to elucidate the role of cardiomyocyte-specific SDF-1 in cardiac repair, we generated conditional knockout mice lacking the chemokine specifically in this cell type. The phenotypic analysis of these animals revealed normal development and function of the heart at baseline, but significantly improved cardiac function upon experimental myocardial infarction.[166] Moreover, the development of fibrosis was diminished and we found a tendency towards lower numbers of infiltrating macrophages in hearts of SDF-1 conditional knockout mice compared to controls. On the other hand, no effect on stem/progenitor cell recruitment was observable. Thus, our results indicate that cardiomyocyte-derived SDF-1 has a negative impact on cardiac healing after ischemic injury by modulating inflammatory and fibrotic processes rather than influencing the recruitment of stem/progenitor cells.

In summary, studies investigating the role of the SDF-1/CXCR4 axis in the heart after ischemic injury revealed conflicting results. Despite much evidence for beneficial effects of the chemokine and its receptor on neovascularization, cardiomyocyte function and survival, there are studies that show a negative impact of the SDF-1/CXCR4 axis on myocardial repair.

The use of diverse experimental models, variable time points and methods of delivery in combination with multiple cell types might cause different outcomes. In addition, dose-dependent effects of SDF-1 can influence the balance between reparative and pro-inflammatory actions. Future studies and conditionally targeted mouse models that allow the investigation of cell type- and time-specific effects are needed to evaluate the therapeutic potential of the SDF-1/CXCR4 axis in myocardial infarction. However, the observed multifunctional effects of the chemokine and its receptor should advise caution for using SDF-1 as therapeutic target in clinical trials.

1.3 GPNMB/Osteoactivin

1.3.1 Biology of the Glycoprotein GPNMB/Osteoactivin

Glycoprotein (transmembrane) nmb (GPNMB), also named hematopoietic growth factor inducible neurokinin-1 type (HGFIN), dendritic cell-associated heparin sulfate proteoglycan-integrin ligand (DC-HIL) or osteoactivin, is a highly glycosylated type I transmembrane protein of 572 amino acids. It was first described in 1995 as a protein that shares significant sequence homology to several melanosomal proteins.[167] The human GPNMB gene was localized to chromosome 7p15.1 (a locus involved in the human inherited disease cystoid macular dystrophy)[168], whereas the mouse GPNMB was mapped to chromosome 6.[169] The highly conserved GPNMB gene consists of 11 exons and encodes a protein with three major structural domains: the extracellular, the transmembrane and the cytoplasmic domain (Fig. 5).[170,171] The extracellular domain contains a signal peptide and a cleavage site at position 23 as well as a polycystic kidney disease (PKD) domain. Furthermore, GPNMB consists of 13 predicted N-linked glycosylation sites and an Arg-Gly-Asp (RGD) motif as integrin-binding site at position 556.[172] The cytoplasmic domain of GPNMB also includes a conserved di-leucin-based endosomal/melanosomal-sorting signal.

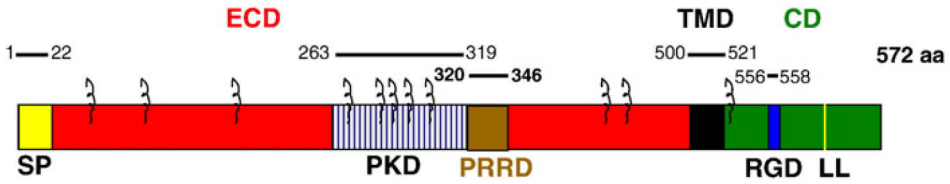

Fig. 5: Schematic structure of the GPNMB protein. The protein consists of the extracellular domain (ECD), the transmembrane domain (TMD) and the cytoplasmic domain (CD). SP: signal peptide; PKD: polycystic kidney disease domain; PRRD: proline-rich repeat domain; RGD: integrin binding domain; LL: di-leucine sorting sequence.[170]

GPNMB/osteoactivin is expressed in a wide variety of human and mouse tissues[169] and cell types such as pigment-producing melanocytes[170,173], endothelial cells as well as antigen-presenting cells (e.g. dendritic cells and macrophages).[174-176] Within a cell, GPNMB is localized to the cell surface as well as to vesicular, endosomal- or lysosomal-like

structures.[168,174,177] In macrophages, the glycoprotein is present in the Golgi apparatus and was shown to translocate to the cell periphery following interferon (IFN)-γ or lipopolysaccharide (LPS) treatment.[178] In addition, GPNMB can also be secreted from cells via ectodomain shedding.[170,172] This process is regulated by protein kinase C as well as intracellular Ca^{2+}-dependent pathways (including calmodulin) and it is mediated by MMPs and a disintegrin and metalloproteinase (ADAM)-10.[179-181] Based on the existence of different isoforms of GPNMB, several functions and modes of action have been predicted.[171] Transmembrane-bound GPNMB could function as receptor for extracellular ligands, whereas the secreted isoform could function as ligand. In support to this, it has been demonstrated that the cleaved GPNMB, which possesses the heparin-binding RGD motif, actually binds to a heparin sulfate proteoglycan-type receptor similar to the FGF receptor.[171] It was furthermore shown that GPNMB on the surface of dendritic cells can bind to endothelial cells via its RGD motif[174] as well as to T cells via the PKD domain.[182] The interaction between dendritic cells and T cells is actually mediated by the binding of GPNMB to syndecan-4 on T cells, which in turn leads to an inhibition of T cell responses. On the other hand, the binding of soluble GPNMB after shedding to syndecan-4 on activated T-cells inhibits the binding of GPNMB on the antigen-presenting cells and boosts the T-cell activation.[183] A recent study by Schwarzbich *et al*. confirmed the role of GPNMB as immune inhibitory molecule.[184] The upregulation of GPNMB in monocyte-derived dendritic cells upon treatment with tyrosine kinase inhibitors resulted in significantly reduced stimulatory capacity of these cells in mixed lymphocyte reactions. In addition, it was reported that GPNMB can act as negative regulator of macrophage pro-inflammatory responses.[178] Apart from these findings, little is known about the signaling pathways and potential interaction partners or receptors of GPNMB. The expression of GPNMB in osteoclasts and melanocytes was shown to be regulated by microphthalmia transcription factor (MITF) via a MITF-binding site (M-box) that is present in the GPNMB promoter.[173,185] In skeletal muscle cells after denervation, basic fibroblast growth factor (bFGF) and platelet-derived growth factor (PDGF) have been shown to regulate the expression of GPNMB.[186]

Functionally, GPNMB plays an important role in bone homeostasis. First evidence came from a study by Safadi *et al*. that reported a high expression of GPNMB in bones from osteopetrotic mutant rats.[172] GPNMB expression was furthermore found in osteoblasts and osteoclasts at all stages of differentiation[169,185,187] and it was shown that GPNMB is important for the maturation and function of both cell types.[170,188] BMP-2 has been demonstrated to regulate the expression of GPNMB through the Smad1 signaling pathway[189] and the homeodomain transcription factors Dlx3, Dlx5 and Msx2.[190] Thus, GPNMB acts as downstream mediator of BMP-2 to regulate osteoblast differentiation and function.[189] These findings suggest that GPNMB is a key player in the regulation of bone remodeling and recent

studies even suggest its function as potential osteogenic growth factor, which could be beneficial for repair of fractures and bone defects.[191,192]

GPNMB is furthermore essential for normal eye function. It is highly expressed in retinal pigment epithelium and iris during embryonic development.[168] Studies using DBA/2J mice revealed that the premature stop codon mutation in the GPNMB gene ($GPNMB^{R150X}$) in these mice causes a pigment dispersing iris disease and subsequent age-related pigmentary glaucoma.[193-195] It was suggested that BM-derived cells, e.g. F4/80-positive antigen-presenting cells, contribute to this phenotype by altering the innate ocular immune privilege.[196,197] The absence of GPNMB likely mediates a melanosomal defect associated with cellular debris shedding in the eye chamber. The GPNMB-dependent BM cells react abnormally to this debris, which causes an inflammatory attack to the iris, atrophy and finally glaucoma.

1.3.2 Functional Role of GPNMB/Osteoactivin in Disease Processes

GPNMB is upregulated in several types of cancer. First, it was described to be expressed in low-metastatic human melanoma cell lines.[167] However, later studies suggested that GPNMB is induced in highly malignant tumors and actually induces invasion and metastasis (partly via increased expression of MMP-2/9 and MMP-3).[198,199] Thereby, p53 seems to play a central role in the upregulation of GPNMB in cancer cells.[200] Several studies also reported a high expression of GPNMB in cutaneous melanomas.[201,202] Other authors described GPNMB as a protein that is expressed in aggressive human breast cancers and other malignant tumors and is capable of promoting cancer metastasis to bone.[199,201,203,204] In addition, GPNMB expression in breast cancer cells increased tumor angiogenesis partially mediated by its soluble form.[180] These findings even led to the development of CDX-011 (glembatumumab vedotin), a fully human monoclonal antibody against the extracellular domain of GPNMB conjugated to the cytotoxic microtubule toxin monomethylauristatin E.[201,205] Ongoing phase I/II trials suggest that CDX-011 has antitumor activity in patients with breast cancer or melanoma by inducing apoptosis of GPNMB-expressing tumor cells.[206,207]

In addition, a number of studies demonstrated a pathophysiological role of GPNMB in various disease models associated with fibrosis and inflammation.[172,199] In skeletal muscle, GPNMB was found to be upregulated in myofibers after denervation and might function as a key regulator for ECM regeneration and fibrosis.[186] Highly expressed GPNMB interacts with infiltrated fibroblasts, which in turn stimulates the expression of matrix-related genes such as MMP-3, MMP-9 and collagen I. These actions can be blocked by addition of heparin, suggesting that the heparin-binding motif of GPNMB is crucial for the regulation of fibroblast function. Another study by the same group demonstrated that the overexpression of GPNMB protects skeletal muscle from severe degeneration caused by long-term denervation in

mice.[208] This was accompanied by decreased infiltration of fibroblast-like cells, upregulation of anti-fibrotic genes and lower levels of collagen deposition. In support of this view it was reported that the extracellular fragments of GPNMB, which result from ectodomain shedding, induce MMP-3 expression in mouse fibroblasts via activation of the ERK pathway.

A first hint that GPNMB plays a significant role in liver pathophysiology was the finding that it is strongly induced in inflammatory macrophages after acute liver injury in rats.[176] In humans, GPNMB is not detectable in normal liver tissue, but was found to be increased during hepatitis and paracetamol intoxication. Moreover, the transgenic expression of GPNMB in the liver was shown to attenuate the development of hepatic fibrosis in a rat model of chronic liver disease.[209] No apparent changes in matrix-related gene expression (e.g. MMP-3) were found in this model, but the overexpression of GPNMB in the liver was linked to suppression of PDGFR-α and -β, suppressor of cytokine signaling (SOCS)-2, latent TGF-β binding protein (LTBP)-1, prostaglandin E receptor 1 and fibrillin 1. In fibroblasts, a GPNMB-mediated activation of ERK1/2 and p38 in the MAPK pathway was detected that may be involved in the attenuation of fibrosis.

In kidney, GPNMB might also regulate regenerative processes and fibrosis upon injury since its expression was found to be strongly induced in tubular endothelium and interstitial fibroblasts after unilateral ureteral obstruction in rats.[210] Moreover, GPNMB was upregulated in monocytes and macrophages of mice after ischemic kidney disease and of patients with end-stage renal disease.[211,212] This even led to the suggestion of GPNMB as novel biomarker of progressive kidney disease.[181,213] A recent study using DBA/2J mice revealed that the absence of functional GPNMB results in impaired phagocytosis and autophagy responsible for the degradation of internal debris and apoptotic cells.[211] As a consequence of this, DBA/2J mice demonstrated higher mortality rates accompanied by increased apoptosis rates and prevention of normal organ repair. These results suggest that GPNMB is involved in the repair after kidney damage by affecting macrophage function.

In summary, these studies indicate that GPNMB plays an important role in inflammatory, fibrotic and degenerative processes after injury in skeletal muscle, liver and kidney. Based on these findings, GPNMB was even used as anti-fibrotic marker gene in a recent study.[214] However, the function of GPNMB in pathophysiological processes in the heart remains largely unknown. It was reported that GPNMB is not detectable in resident macrophages of the heart[211] but is expressed by cells that infiltrate the myocardium of desmin-deficient (des-/-) mice, a model for dilated cardiomyopathy and heart failure with myocardial degeneration and fibrosis.[215] Thereby, GPNMB was found to colocalize with a subset of infiltrating $CD11b^+$ cells. Strikingly, the putative GPNMB receptor syndecan-4 has recently been described as biomarker in chronic heart failure.[216] It is expressed on cardiomyocytes and is involved in apoptosis and hypertrophy after myocardial infarction or pressure

overload[217]. But still, there are conflicting data whether it confers pro- or anti-hypertrophic actions.[218,219] Nevertheless, there is consensus that the lack of syndecan-4 in knockout mice leads to increased myocardial damage after ischemia.[220] However, GPNMB is only one of several possible ligands of syndecan-4 and it probably also uses other signaling pathways or modes of action. Thus, these findings are not predictive for the cardiac actions of GPNMB and future investigation is needed to clarify the role and therapeutic potential of GPNMB in the heart.

2 Aim of the Study

The prognosis for patients suffering from ischemic heart diseases remains poor due to the limited reparative capacity of heart tissue. Over the last decade, a number of studies focused on cell therapy approaches in order to improve myocardial function and clinical outcome by using stem and progenitor cells. The chemokine SDF-1/CXCL12 has been described as a key player for cardiac repair processes by recruiting inflammatory and stem/progenitor cells to the site of injury. Most studies using pharmacological targeting of SDF-1 and gain-of-function experiments revealed beneficial effects of the chemokine and its receptor CXCR4 on cardiac remodeling. However, a number of recent reports demonstrated detrimental effects of the SDF-1/CXCR4 axis on cardiac repair and thus questioned the role of the chemokine and its receptor in regenerative processes after ischemic injury of the heart. In support to this, a previous study in our laboratory revealed that the conditional knockout of SDF-1 in hearts of mice results in improved cardiac healing and remodeling upon myocardial infarction. Due to the conflicting results regarding the role of the SDF-1/CXCR4 axis in cardiac repair processes, one objective of this project was the generation of a transgenic rat line with overexpression of SDF-1 exclusively in cardiomyocytes. The cardiac function and morphology of these animals should be analyzed at basal levels as well as upon experimental induction of myocardial infarction. Histological methods, expression studies and flow cytometry analysis of blood composition will help to clarify the importance of cardiomyocyte-specific SDF-1 for cell recruitment, fibrosis development and neoangiogenesis after MI. SDF-1 transgenic rats should therefore shed light on the therapeutic potential of the chemokine *in vivo*. Furthermore, conditional knockout mice should be generated that lack SDF-1 only in platelets. The analysis of these mice should contribute to the understanding which cell types in the heart in addition to cardiomyocytes are important for the SDF-1-mediated effects on cardiac repair.

Another aim of the study is the identification of novel candidates that might be involved in myocardial healing upon injury and could therefore constitute new targets for treating ischemic cardiac diseases. For this purpose, a microarray screening should be performed using cardiac tissue of rats after myocardial infarction and molecules that are upregulated as early as 24 hours after coronary artery occlusion should be further analyzed. Subsequent *in vitro* and *in vivo* studies will be conducted in order to characterize the impact of selected molecules, e.g. GPNMB/osteoactivin, on cardiac repair processes. Measurements in plasma samples of human patients after acute myocardial infarction should furthermore help to evaluate the potential of the identified candidate as cardiac biomarker.

3 Material and Methods

3.1 Material

3.1.1 Chemicals and Reagents

Table 1: Chemicals and Reagents.

Chemical	Manufacturer (Location)
[α-^{32}P] dCTP (9,25 MBq)	PerkinElmer (Rodgau)
Acetic acid (glacial)	Roth (Karlsruhe)
Acetone	Roth (Karlsruhe)
Agarose	Biozym (San Diego, USA)
Bovine Serum Albumin (BSA)	Sigma-Aldrich (Steinheim)
β-mercaptoethanol	Sigma-Aldrich (Steinheim)
Bromphenol blue	Sigma-Aldrich (Steinheim)
Chloroform	Merck (Darmstadt)
Citric acid	Merck (Darmstadt)
Complete Protease Inhibitor Cocktail Tablets	Roche (Mannheim)
Creatine	Sigma-Aldrich (Steinheim)
Cytosin-D-arabinofuranoside	Serva (Heidelberg)
DAPI (4',6-Diamidino-2-pheyindole)	Sigma-Aldrich (Steinheim)
DEPC	Sigma-Aldrich (Steinheim)
DMEM (1g/l glucose, L-glutamine, pyruvate)	Gibco (Darmstadt)
Dextran sulfate	Sigma-Aldrich (Steinheim)
dNTPs	Bioline (Luckenwalde)
DTT	Invitrogen (Darmstadt)
EDTA	Serva (Heidelberg)
Ethanol	Berkel AHK (Berlin)
Ethidium bromide	Invitrogen (Darmstadt)
FBS	Sigma-Aldrich (Steinheim)
Ficoll 400	Serva (Heidelberg)
Gentamicin	Invitrogen (Darmstadt)
Glucose	Sigma-Aldrich (Steinheim)
Glycine	Roth (Karlsruhe)
H_3PO_4	Sigma-Aldrich (Steinheim)
HCl	Roth (Karlsruhe)
Hepes	Sigma-Aldrich (Steinheim)
IFN-γ (recombinant, murine)	PeproTech (Hamburg)
IL-4 (recombinant, murine)	PeproTech (Hamburg)
Isoflurane	Abott (Wiesbaden)
Isoprenaline	Sigma-Aldrich (Steinheim)
Isopropanol	Roth (Karlsruhe)
KCl	Sigma-Aldrich (Steinheim)
KH_2PO_4	Sigma-Aldrich (Steinheim)
Laminin	Sigma-Aldrich (Steinheim)
L-Carnitin	Sigma-Aldrich (Steinheim)
Lysing Buffer Pharm Lyse™	BD (Heidelberg)
M 199 medium	Sigma-Aldrich (Steinheim)

M-CSF (recombinant, murine)	PeproTech (Hamburg)
Methanol	Roth (Karlsruhe)
$MgCl_2$	Sigma-Aldrich (Steinheim)
Skim Milk Powder	Fluka (Steinheim)
NaCl	Roth (Karlsruhe)
NaF	Sigma-Aldrich (Steinheim)
$NaHCO_3$	Roth (Karlsruhe)
Na_2HPO_4	Sigma-Aldrich (Steinheim)
Odyssey® Blocking Buffer	LI-COR GmbH (Bad Homburg)
Paraffin	Roth (Karlsruhe)
Paraformaldehyde	Otto Fischar GmbH (Saarbrücken)
Penicillin-streptomycin (100x)	Gibco (Darmstadt)
Picric acid (aqueous solution)	Applichem (Darmstadt)
Polyvinylpyrrolidone (PVP)	Serva (Heidelberg)
Random Hexamer Primer	Roche (Mannheim)
Rat Serum	AbD Serotec (Düsseldorf)
Roti®-Block	Roth (Karlsruhe)
Roti®-Load	Roth (Karlsruhe)
Rotiphorese® Gel 30 (37.5:1)	Roth (Karlsruhe)
SDS	Serva (Heidelberg)
Sirius red F3B (Direct Red 80)	Sigma-Aldrich (Steinheim)
Sodium acetate	Sigma-Aldrich (Steinheim)
Sodium citrate	Merck (Darmstadt)
Sodium deoxycholate	Merck (Darmstadt)
Sucrose	Merck (Darmstadt)
Taurin	Sigma-Aldrich (Steinheim)
TEMED	Roth (Karlsruhe)
Tergitol type NP-40	Sigma-Aldrich (Steinheim)
Tissue-Tek® OCT™ Compound	Sakura (Staufen)
TMB Microwell Peroxidase Substrate	KPL (Gaithersburg, USA)
TripLE™ Express	Gibco (Darmstadt)
Tris	Roth (Karlsruhe)
Triton X-100	Fluka (Steinheim)
Trizol®	Invitrogen (Darmstadt)
Trypsin tablet	Sigma-Aldrich (Steinheim)
Tween-20	Sigma-Aldrich (Steinheim)
Vectashield® Mounting Medium with DAPI	Vector Laboratories (CA, USA)
Xylol	Roth (Karlsruhe)
β-Mercaptoethanol	Sigma-Aldrich (Steinheim)

3.1.2 Enzymes, Markers and Kits

Table 2: Enzymes, Markers and Kits.

Product	Manufacturer (Location)
Collagenase type 2	Worthington Biochemical (NJ, USA)
DNase I	Roche (Mannheim)
GoTaq® qPCR Master Mix	Promega (WI, USA)

M-MLV Reverse Transcriptase	Invitrogen (Darmstadt)
Proteinase K	Invitrogen (Darmstadt)
Restriction Enzymes	NEB (Frankfurt/Main)
RNase A	Applichem (Darmstadt)
RNase inhibitor	EURx (Gdansk, Poland)
Taq DNA Polymerase	Invitrogen (Darmstadt)
TaqMan© PCR Master Mix	Applied Biosystems (Darmstadt)
Hyperladder 1	Bioline (Luckenwalde)
Lambda DNA/EcoRI+HindIII (EH) marker	Fermentas (St. Leon-Rot)
Quick-Load© 100bp DNA ladder	NEB (Frankfurt/Main)
Quick-Load© 1kb DNA ladder	NEB (Frankfurt/Main)
PhiX174 DNA/BsuRI (Phi) marker	Fermentas (St. Leon-Rot)
Precision Blue Protein™ Standard All Blue	BioRad Laboratories (München)
Bicinchoninic Acid (BCA) Protein Assay Kit	Sigma-Aldrich (Steinheim)
Expand Long Template PCR Kit	Roche (Mannheim)
FirstChoice® RLM-RACE Kit	Ambion (Darmstadt)
GeneChip® WT Sense Target Labeling Kit	Affymetrix (CA, USA)
GeneChip® Eukaryot. Poly-A RNA Control Kit	Affymetrix (CA, USA)
GeneChip® Hybridization, Wash and Stain Kit	Affymetrix (CA, USA)
Human Osteoactivin/GPNMB DuoSet® ELISA	R&D Systems (Wiesbaden-Nordenstadt)
Mouse CXCL12/SDF-1 DuoSet® ELISA	R&D Systems (Wiesbaden-Nordenstadt)
Mouse IL-6 ELISA kit	PeproTech (NJ, USA)
Mouse IL-10 ELISA kit	PeproTech (NJ, USA)
Mouse IL-12 ELISA kit	PeproTech (NJ, USA)
Mouse Osteoactivin/GPNMB DuoSet® ELISA	R&D Systems (Wiesbaden-Nordenstadt)
Prime-It® RmT Random Primer Labeling Kit	Stratagene (Waldbronn)
RNeasy® Mini Kit	Qiagen (Hilden)
SuperSignaling™ West Dura Substrate	Thermo Scientific (Rockford, USA)
Trichrom Stain (Masson) Kit	Sigma-Aldrich (Steinheim)
Wizard® SV Gel and PCR Clean-Up System	Roche (Mannheim)

3.1.3 Antibodies

Table 3: Antibodies used for flow cytometry (FC) or immunofluorescence (IF).

Antibody	Method	Dilution in	Manufacturer (Location)
CD3 Alexa® 647 anti-rat	FC	1/200, FC buffer	BioLegend (CA, USA)
CD3 PB® anti-mouse	FC	1/500, FC buffer	BioLegend (CA, USA)
CD4 PE anti-mouse	FC	1/500, FC buffer	BioLegend (CA, USA)
CD8 APC anti-mouse	FC	1/500, FC buffer	BioLegend (CA, USA)
CD11b/c APC anti-rat	FC	1/4000, FC buffer	BioLegend (CA, USA)
CD11b APC anti-mouse	FC	1/4000, FC buffer	BioLegend (CA, USA)
CD11b PB® anti-mouse	FC	1/5000, FC buffer	BioLegend (CA, USA)
CD16/32 anti-mouse	FC	1/1000, FC buffer	BioLegend (CA, USA)
CD31 anti-rat	IF	1/100, PBS	BD (Heidelberg)
CD34 FITC anti-mouse	FC	1/200, FC buffer	eBioscience (CA, USA)

CD41 FITC anti-mouse	FC	1/1000, FC buffer	BioLegend (CA, USA)
CD45 APC/Cy7 anti-rat	FC	1/400, FC buffer	BioLegend (CA, USA)
CD45 PB® anti-mouse	FC	1/2000, FC buffer	BioLegend (CA, USA)
CD68 anti-rat	IF	1/100, PBS	AbD Serotec (Düsseldorf)
CD115 PE anti-mouse	FC	1/1000, FC buffer	BioLegend (CA, USA)
CD117 (c-Kit) PE anti-mouse	FC	1/1000, FC buffer	BioLegend (CA, USA)
Collagen 1 anti-rat	IF	1/500, PBS	Southern Biotech (AL, USA)
B220 PE anti-rat	FC	1/200, FC buffer	eBioscience (CA, USA)
B220 PB® anti-mouse	FC	1/500, FC buffer	BioLegend (CA, USA)
B220 PE/Cy7 anti-mouse	FC	1/1000, FC buffer	BioLegend (CA, USA)
GPNMB monoclonal anti-mouse	IF	1/100, PBS	R&D Systems (Wiesbaden-Nordenstadt)
Gr-1 (Ly-6G/6C) PB® anti-mouse	FC	1/2000, FC buffer	BioLegend (CA, USA)
Gr-1 PE anti-rat	FC	1/3000, FC buffer	eBioscience (CA, USA)
Ly-6C Alexa® 700 anti-mouse	FC	1/1000, FC buffer	BioLegend (CA, USA)
Ly-6G FITC anti-mouse	FC	1/1000, FC buffer	BioLegend (CA, USA)
Mac-2 (Galectin-3) anti-mouse	IF	1/100, PBS	Acris (Herford)
Sca-1 (Ly-6A/E) PE anti-rat	FC	1/400, FC buffer	Antibodies-online (GA, USA)
Sca-1 (Ly-6A/E) APC anti-mouse	FC	1/800, FC buffer	BioLegend (CA, USA)
TER-119 PB® anti-mouse	FC	1/200, FC buffer	BioLegend (CA, USA)

3.1.4 Oligonucleotides

All oligonucleotides were synthetized by Biotez Berlin Buch GmbH and delivered in a lyophilized state. The primers were diluted in water to a concentration of 50 pmol/µl and stored at -20°C. For PCR reactions, primers were diluted to a final concentration of 5 pmol/µl. Table 4 lists all oligonucleotides used for genotyping and quantitative RT-PCR. All probes used for Taqman© qRT-PCRs were labeled with FAM (F) as reporter and TAMRA (T) as quencher.

Table 4: Primers (forward f, reverse r) and probe (p) used for genotyping and quantitative RT-PCRs. F: FAM; T: TAMRA.

Primer	Sequence (5´-3´)	Gene	Species	Method
m28S f	GGATGGCGAGAAATACCAGA	Mrp S28	mouse	qRT-PCR
m28S r	AGCGCAGTCCATTACTTGCT	Mrp S28	mouse	qRT-PCR
m28S p	F-ACTGGAGGCTGATGCAGTTC-T	Mrp S28	mouse	qRT-PCR
r28S f	GCAAGGTGTTCTTCACCACAAA	Mrps 28	rat	qRT-PCR
r28S r	CAGTTTCTTACGGCGTCTGTGAT	Mrps 28	rat	qRT-PCR
r28S p	F-CATCGCTGGTACCCACACGGACAG-T	Mrps 28	rat	qRT-PCR
mABC1 f	CCCAGAGCAAAAAGCGACTC	Abca1	mouse	qRT-PCR
mABC1 r	GGTCATCATCACTTTGGTCCTTG	Abca1	mouse	qRT-PCR
mANP f	GAGAAGATGCCGGTAGAAGA	Nppa	mouse	qRT-PCR
mANP r	AAGCACTGCCGTCTCTCAGA	Nppa	mouse	qRT-PCR
mANP p	F-ATGCCCCCGCAGGCCCGG-T	Nppa	mouse	qRT-PCR

rANP f	CTTCTTCTTCTTGGCCTTTTG	Nppa	rat	qRT-PCR
rANP r	GTGTTGGACACCGCACTGTATAC	Nppa	rat	qRT-PCR
rANP p	F-TCCCAGGCCATATTGGAGCAAATCC-T	Nppa	rat	qRT-PCR
mArg f	CTCCAAGCCAAAGTCCTTAGAG	Arg1	mouse	qRT-PCR
mArg r	AGGAGCTGTCATTAGGGACATC	Arg1	mouse	qRT-PCR
mBNP f	CTGCTGGAGCTGATAAGAGA	Nppb	mouse	qRT-PCR
mBNP r	TGCCCAAAGCAGCTTGAGAT	Nppb	mouse	qRT-PCR
mBNP p	F-CTCAAGGCAGCACCCTCCGGG-T	Nppb	mouse	qRT-PCR
rBNP f	CAAGCTGCTTTGGGCAGAAG	Nppb	rat	qRT-PCR
rBNP r	AAACAACCTCAGCCCGTCAC	Nppb	rat	qRT-PCR
rBNP p	F-AGACCGGATCGGCGCAGTCAGTCGCT-T	Nppb	rat	qRT-PCR
rCcl2 f	CACTCACCTGCTGCTACTC	Ccl2	rat	qRT-PCR
rCcl2 r	TGGTGACAAATACTACAGCTTC	Ccl2	rat	qRT-PCR
mCCL17 f	TGGTATAAGACCTCAGTGGAGTGTTC	Ccl17	mouse	qRT-PCR
mCCL17 r	GCTTGCCCTGGACAGTCAGA	Ccl17	mouse	qRT-PCR
mCCL22 f	GAGTTCTTCTGGACCTCAAAATCC	Ccl22	mouse	qRT-PCR
mCCL22 r	TCTCGGTTCTTGACGGTTATCA	Ccl22	mouse	qRT-PCR
rCD68 f	CGGACAAGGGACACTTCG	CD68	rat	qRT-PCR
rCD68 r	GATTGTCGTCTCCGGGTAAC	CD68	rat	qRT-PCR
rCD68 p	F-GACCAATCTCTCTTGCTGCC-T	CD68	rat	qRT-PCR
mColl1a1 f	CTTCACCTACAGCACCCTTGTG	Col1a1	mouse	qRT-PCR
mColl1a1 r	GATGACTGTCTTGCCCCAAGTT	Col1a1	mouse	qRT-PCR
mColl1a1 p	F-ACGGCTGCACGAGTCACACCG-T	Col1a1	mouse	qRT-PCR
rColl1a1 f	ATTCACCTACAGCACGCTTGTG	Col1a1	rat	qRT-PCR
rColl1a1 r	GATGACTGTCTTGCCCCAAGTT	Col1a1	rat	qRT-PCR
rColl1a1 p	F-ATGGCTGCACGAGTCACACCG-T	Col1a1	rat	qRT-PCR
mColl3 f	GGTGGTTTTCAGTTCAGCTATGG	Col3	mouse	qRT-PCR
mColl3 r	CTGGAAAGAAGTCTGAGGAATGC	Col3	mouse	qRT-PCR
mColl3 p	F-TTCCTGAAGATGTCGTTGATGTGCAGCT-T	Col3	mouse	qRT-PCR
rColl 3 f	GCTGGCCTTCCTCAGACTTCT	Col3	rat	qRT-PCR
rColl 3 r	GCTGTTTTTGCAGTGGTATGTAATG	Col3	rat	qRT-PCR
rColl 3 p	F-TCCAGCCGGGCCTCCCAG-T	Col3	rat	qRT-PCR
mCXCL9 f	CCCAATTGCAACAAAACTGA	Cxcl9	mouse	qRT-PCR
mCXCL9 r	TCCCATTCTTTCATCAGCTTC	Cxcl9	mouse	qRT-PCR
mCXCL10 f	TCCTTGTCCTCCCTAGCTCA	Cxcl10	mouse	qRT-PCR
mCXCL10 r	ATAACCCCTTGGGAAGATGG	Cxcl10	mouse	qRT-PCR
mCXCL11 f	GATGAAAGCCGTCAAAATGG	Cxcl11	mouse	qRT-PCR
mCXCL11 r	CCAGGCACCTTTGTCGTTTA	Cxcl11	mouse	qRT-PCR
mCXCR4 f	TGGAACCGATCAGTGTGAGT	Cxcr4	mouse	qRT-PCR
mCXCR4 r	GTAGATGGTGGGCAGGAAGA	Cxcr4	mouse	qRT-PCR
mCXCR4 p	F-GACTCCAACAAGGAACCCTG-T	Cxcr4	mouse	qRT-PCR
rCXCR4 f	CCGAAGAAGTAGGGTCTGGA	Cxcr4	rat	qRT-PCR
rCXCR4 r	GCCCACTATGCCAGTCAAGA	Cxcr4	rat	qRT-PCR

mF4/80 f	CATCCAGCCAAAGCAGAAGT	Emr1	mouse	qRT-PCR
mF4/80 r	CAGCTGCAGACTGTGTGTGT	Emr1	mouse	qRT-PCR
mF4/80 p	F-GATGTGGAGGATGGGAGATG-T	Emr1	mouse	qRT-PCR
mFibron f	TCGCACTGGTAGAAGTTCCA	Fibronectin	mouse	qRT-PCR
mFibron r	ATCATTTCATGCCAACCAGTT	Fibronectin	mouse	qRT-PCR
mFibron p	F-CCGACGAAGAGCCCTTACAGTTCCA-T	Fibronectin	mouse	qRT-PCR
rFibron f	GGCAACAAATGATCTTTGAGGAA	Fibronectin	rat	qRT-PCR
rFibron r	CATCTACATTCGGCAGGTATGGT	Fibronectin	rat	qRT-PCR
rFibron p	F-CACCCCCGTCAGGCTTAGGCCA-T	Fibronectin	rat	qRT-PCR
mGpnmb f	GAAGCCAGCATCTCAGGTTC	GPNMB	mouse	qRT-PCR
mGpnmb r	CTGAACACCGACCCAGTTTT	GPNMB	mouse	qRT-PCR
mGpnmb p	F-TCTTTCACACACTTGGCCAG-T	GPNMB	mouse	qRT-PCR
rHbegf f	TACTGCATCCACGGAGAGTG	Hbegf	rat	qRT-PCR
rHbegf r	AGCCAAGACGGTAGTGTGGT	Hbegf	rat	qRT-PCR
mHPRT f	GCTCGAGATGTCATGAAGGAGAT	Hprt	mouse	qRT-PCR
mHPRT r	AAAGAACTTATAGCCCCCCTTGA	Hprt	mouse	qRT-PCR
mHPRT p	F-CCATCACATTGTGGCCCTCTGTGTG-T	Hprt	mouse	qRT-PCR
mIL-6 f	CTGCAAGAGACTTCCATCCAGTT	IL6	mouse	qRT-PCR
mIL-6 r	GAAGTAGGGAAGGCCGTGG	IL6	mouse	qRT-PCR
mIL-10 f	TTGCCAAGCCTTATCGGA	IL10	mouse	qRT-PCR
mIL-10 r	TTCTGGGCCATGCTTCTCT	IL10	mouse	qRT-PCR
mIL-12 f	CATCGATGAGCTGATGCAGT	IL12a	mouse	qRT-PCR
mIL-12 r	CAGATAGCCCATCACCCTGT	IL12a	mouse	qRT-PCR
miNOS f	CCAAGCCCTCACCTACTTCC	Nos2	mouse	qRT-PCR
miNOS r	CTCTGAGGGCTGACACAAGG	Nos2	mouse	qRT-PCR
rITGAM f	GCGTCCAAAGCTTGGTTTTA	Itgam	rat	qRT-PCR
rITGAM r	CGTCCATGTCCACAGAACAG	Itgam	rat	qRT-PCR
mMHCa f	GGAGAAAGTGTCCCGGACACT	Myh6	mouse	qRT-PCR
mMHCa r	TGGGCTTCTTCCAGCTTCA	Myh6	mouse	qRT-PCR
mMHCa p	F-AGGACCAGGCCAATGAGTACCGC-T	Myh6	mouse	qRT-PCR
rMHCa f	CAGAAAATGCACGATGAGGA	Myh6	rat	qRT-PCR
rMHCa r	TCAAGCATTCATATTTATTGTGGG	Myh6	rat	qRT-PCR
rMHCa p	F-AGCAGAAAGAGCCTCGCTGTTG-T	Myh6	rat	qRT-PCR
mMHCb f	AGTTTGTCAAGGCCAAGATCGT	Myh7	mouse	qRT-PCR
mMHCb r	GTCTTGCCATTCTCCGTCTCA	Myh7	mouse	qRT-PCR
mMHCb p	F-TCCCGAGAGGGTGGCAAAGTCACTG-T	Myh7	mouse	qRT-PCR
rMHCb f	GGGCCTGAATGAAGAGTAGAT	Myh7	rat	qRT-PCR
rMHCb r	GTGTTTCTGCCTAAGGTGCT	Myh7	rat	qRT-PCR
rMHCb p	F-TTGTGCTACCCAACCCTAAGGAT-T	Myh7	rat	qRT-PCR
rMSR1 f	GCGTGCAGGAATATCAACCT	Msr1	rat	qRT-PCR
rMSR1 r	ATCACAGATTGTGCCCCACT	Msr1	rat	qRT-PCR
mPecam f	AAGCAGCACTCTTGCAGTCA	Pecam1	mouse	qRT-PCR
mPecam r	CGATGACCACTCCAATGACA	Pecam1	mouse	qRT-PCR

mPecam p	F-ATGGAAGAAAGGGCTCATTG-T	Pecam1	mouse	qRT-PCR
rPecam1 f	CATCGAGGAGCAAGACCACC	Pecam1	rat	qRT-PCR
rPecam1 r	GCATTTTGATTCCGGACAGG	Pecam1	rat	qRT-PCR
SDF-1 f4	ATCTCTGGGAGACCTGTTTGG	Cxcl12	mouse	PCR
SDF-1 r4	GGACTGCTAGGCTTAGGGCAA	Cxcl12	mouse	PCR
SDF-1 r5	CAGCGCGAGTTCAAGAGCT	Cxcl12	mouse	PCR
SDF-1 r7	CGCTATGACGGCAATAAAAAG	Cxcl12	mouse	PCR
SDF Tg f4	TCACAGCCTCTGGCAAGTTA	Cxcl12	rat	PCR
SDF Tg r4	ACCAGGGGTCCATTCAATCT	Cxcl12	rat	PCR
r/m SDF1 f	GAGCCAACGTCAAGCATCTG	Cxcl12	rat/mouse	qRT-PCR
r/m SDF1 r	CAGCCGTGCAACAATCTGA	Cxcl12	rat/mouse	qRT-PCR
r/m SDF1 p	F-AAATCCTCAACACTCCAAACTGTGCCC-T	Cxcl12	rat/mouse	qRT-PCR
rTgfb2 f	GCAGAGTTCAGGGTCTTTCG	Tgfb2	mouse	qRT-PCR
rTgfb2 r	GCTGGGTTGGAGATGTTAGG	Tgfb2	mouse	qRT-PCR
mVEGF f	CATCTTCAAGCCGTCCTGTGT	Vegfa	mouse	qRT-PCR
mVEGF r	CTCCAGGGCTTCATCGTTACA	Vegfa	mouse	qRT-PCR
mVEGF p	F- CGCTGATGCGCTGTGCAGGCT-T	Vegfa	mouse	qRT-PCR
rVEGFa f	AACGAAAGCGCAAGAAATCCC	Vegfa	rat	PCR
rVEGFa r	GTCTGCGGATCTTGGACAAAC	Vegfa	rat	PCR

3.1.5 Mouse and Rat Strains

Both SDF-1 mouse and rat lines were generated and maintained in the group of Prof. Michael Bader at the Max Delbrueck Center for Molecular Medicine (MDC). The inbred strain C57BL/6N (purchased from Charles River) was used for the generation and backcrossing of SDF-1 conditional knockout mouse strains. Mx1-Cre mice[221] were provided from Prof. Dr. Carmen Birchmeier-Kohler at the MDC and Pf4-Cre[222] mice were purchased from the Jackson Laboratories. SDF-1 transgenic rats were generated using Sprague Dawley® (SD) rats (RjHAN:SD; from JANVIER), which were also used as wild type (WT) controls in all experiments. For the microarray screening, 15 Wistar Kyoto (WKY) rats were ordered from Charles River. Both DBA/2J-Gpnmb+ (GPNMB WT) and DBA/2J (GPNMB Mut) mouse strains were ordered from The Jackson Laboratory and kept as inbred strains in the animal core facility of the MDC.

3.1.6 Lab Equipment and Expendable Material

Table 5: Lab Equipment and Expendable Material.

Equipment and Material	Manufacturer (Location)
8 - channel - pipette M300	Biohit (Rosbach v.d. Höhe)
96-well clear microplates	R&D Systems (Wiesbaden-Nordenstadt)
384-well optical plate MicroAmp®	Applied Biosystems (Darmstadt)
Agarose gel electrophoresis chamber	Biometra (Göttingen)
Alzet© osmotic pumps	Durect (CA, USA)
Centrifuge 5415C	Eppendorf (Hamburg)
Centrifuge G5-6R	Beckman Coulter (Krefeld)
Cell culture incubator Heracell	GFL (Burgwedel)
Cell culture dishes and plates Cellstar®	Greiner bio-one (Frickenhausen)
Cell strainer	BD Falcons (Heidelberg)
Cryostat CM3050 S	Leica (Wetzlar)
Disposable pipettes Cellstar®	Greiner bio-one (Frickenhausen)
EDTA tubes MiniCollect®	Greiner bio-one (Frickenhausen)
Electronic pipette Xplorer©	Eppendorf (Hamburg)
Falcon tubes	Greiner bio-one (Frickenhausen)
FastPrep™-24 instrument	MP Biomedicals (Illkirch, France)
FastPrep™ lysing matrix tubes	MP Biomedicals (Illkirch, France)
Filter tips	Biozym (San Diego, USA)
Fluorescence microscope BZ-9000	Keyence (Neu-Isenburg)
Fuji imaging plate BAS-III	Fujifilm (Willich)
GeneChip® Rat Gene 1.0 ST Array	Affymetrix (CA, USA)
Hybond™ ECL nitrocellulose membrane	Amersham Biosciences (Little Chalfon, UK)
Hybond™ XL nylon membrane	Amersham Biosciences (Little Chalfon, UK)
Inverted microscope DMI6000B	Leica (Wetzlar)
Laminar Flow SAFE 2020	Thermo Scientific (Rockford, USA)
Luminescent image analyzer LAS-1000	Fujifilm (Willich)
Membrane filter	Millipore (Morlsheim)
Microbalance	Sartorius (Göttingen)
Microplate Reader Infinite® M200	Tecan (Crailsheim)
MicroSpin™ G-50 columns	Amersham Biosciences (Little Chalfon, UK)
Microwave 8020	Privileg (Fürth)
Multipette® plus	Eppendorf (Hamburg)
NanoDrop™ 1000 spectrophotometer	Peqlab (Erlangen)
Odyssey©	Li-Cor Bioscience GmbH (Bad Homburg)
PCR tubes	Biozym (San Diego, USA)
Pasteur pipettes	Roth (Karlsruhe)
pH Meter pH Level 1	WTW (Weilheim)
Pipetboy acu	Integra Biosciences (Zizers, Switzerland)
Power supply PowerPac™ HC	BioRad Laboratories (München)
Precision balance 440-43N	Kern & Sohn GmbH (Balingen)
PVDF membranes	Amersham Biosciences (Little Chalfon, UK)
Radioluminography Laser Scanner CR 35	Dürr Medical (Bietigheim Bissingen)
Real time PCR system 7900HT AbiPrism	Applied Biosystems (Darmstadt)
Roller mixer SRT1	Snijders (Tilburg, NL)

Rotable platform Polymax 1040	Heidolph Instruments (Schwabach)
Rotary microtome HM 355 S	Microm (Walldorf)
Save-Lock Tubes	Eppendorf (Hamburg)
Scintillation counter LS600SC	Beckman Coulter (Krefeld)
Scil Vet abc	Scil GmbH (Viernheim)
SDS-PAGE gel electrophoresis chamber	BioRad Laboratories (München)
Serological pipettes	Sarstedt (Nümbrecht)
Single pipettes Discovery	Abimed (Langenfeld)
SpeedVac SVC100	Savant Instruments (NY, USA)
SuperFrost® Plus slides	Menzel Gläser (Braunschweig)
Syringe filter	Sartorius (Göttingen)
Tank blotter	BioRad Laboratories (München)
Thermocycler PTC-200	BioRad Laboratories (München)
Thermomixer 5437	Eppendorf (Hamburg)
Tri-Carb Liquid Scintillation Analyzer	PerkinElmer (Rodgau)
Ultrasound Sonoplus	Bandelin electronic (Berlin)
UV transilluminator MultiImage®	Alpha Innotech (CA, USA)
UV Stratalinker 1800	Stratagene (La Jolla, USA)
Vacuum pump Vacusafe comfort	Integra Biosciences (Zizers, Switzerland)
Vevo 700 In Vivo Micro-Imaging System	Visual Sonics (Amsterdam, NL)
Vortex Genie 2	Bender & Hobein AG (Zürich, Switzerland)
Water bath	GFL (Burgwedel)
Whatman paper (3 mm)	Whatman (Madison, USA)
X-ray films	Fotochemische Werke GmbH (Berlin)

3.2 Methods

3.2.1 DNA Analysis

3.2.1.1 DNA Isolation for Genotyping

Ear or tail biopsies from mice and rats were used for the isolation of genomic DNA by incubating them with 100 µl Ear buffer containing 1 mg/ml proteinase K overnight at 55°C using a thermomixer. Enzyme activity was inactivated by incubation at 95°C for 10 min and 750 µl TE buffer containing 20 µg/ml RNase A were added. Samples were mixed vigorously and stored at -20°C until usage.

Ear buffer	
NaCl	200 mM
Tris-HCL	100 mM
EDTA	0.1 mM
SDS	1%
pH 7.0	

TE buffer (1x)	
Tris-HCL	10 mM
EDTA	1 mM
pH 8.0	

3.2.1.2 DNA Isolation for Southern Blot

In order to isolate DNA for Southern blot analysis, rat tail cuts (approx. 1 cm) were incubated with 700 µl Tail buffer containing 0.5 mg/ml proteinase K overnight at 55°C using a

thermomixer. Then, samples were left 10 min on ice, 300 µl 6 M NaCl solution were added and they were incubated on ice again for 5 min. After centrifugation at 16,000 g for 30 min at 4°C, supernatants were transferred into new tubes and 5 µl RNase A (10 mg/ml) were added. Samples were incubated for 15 min at 37°C using a thermomixer, 1 ml isopropanol was added and suspensions were centrifuged at 16,000 g for 25 min at 4°C. The resulting pellet was washed with 1 ml 75% ethanol and dried for 10-20 min at room temperature (RT). Finally, the DNA pellets were resuspended in 50 µl nuclease-free water, incubated for 1 h at 37°C using a thermomixer and stored at -20°C until further use.

Tail buffer	
NaCl	100 mM
EDTA	100 mM
Tris	50 mM
SDS	1%

3.2.1.3 Determination of Nucleic Acid Concentration

Nucleic acid concentration was measured based on absorbance at 260 nm using the NanoDrop™ spectrophotometer (Peqlab). Purity of nucleic acid samples was determined via the ratio of sample absorbance at 260 and 280 nm as well as 260 and 230 nm. A 260/280 ratio of 1.8 is generally accepted as “pure” for DNA, a ratio of 2.0 as “pure” for RNA. The 260/230 values for “pure” nucleic acid are often higher than the respective 260/280 ratios and are commonly in the range of 1.8 - 2.2.

3.2.1.4 DNA Extraction from Agarose Gels

The Wizard® SV Gel and PCR Clean-up System (Promega) was utilized in order to extract and purify DNA fragments from agarose gels or to purify PCR products directly from a PCR reaction. The manufacturer’s instructions were followed.

3.2.1.5 Sequencing

Sequencing of DNA samples was performed by the company Invitek (Berlin Buch) using the BigDye® Terminator v1.1 Cycle Sequencing Kit (Invitrogen) and the 3130 Genetic Analyzer (Applied Biosystems).

3.2.1.6 Polymerase Chain Reaction (PCR)

Polymerase Chain Reaction (PCR) was performed according to the manufacturer’s guidelines (Invitrogen). The typical reaction mix is shown in Tab. 6. Concentrations of primers, dNTPs, $MgCl_2$ and template DNA were adjusted for each reaction.

Table 6: PCR reaction mix.

Component	Volume
10x PCR buffer (-$MgCl_2$)	3 µl
dNTP mixture (5 mM)	2 µl
$MgCl_2$ (50 mM)	1.5 µl
Primer forward (5 µM)	1 µl
Primer reverse (5 µM)	1 µl
Template DNA	2 µl
Taq DNA polymerase (5 U/µl)	0.3 µl
Autoclaved distilled water	19.2 µl

Table 7 depicts the basic PCR protocol. Optimal reaction conditions (e.g. duration and temperatures for annealing and elongation steps) varied and were optimized for each reaction.

Table 7: Basic PCR program.

PCR step	Time	Temperature	Cycles
Initial denaturation	2 min	94°C	1
Denaturation	20 sec	94°C	
Annealing	30 sec	55-65°C	35
Elongation	30-45 sec	72°C	
Final elongation	4 min	72°C	1

For visualization of PCR results, 2-5 µl of each reaction were mixed with DNA loading buffer (4 g sucrose, 2.5 mg bromphenol blue in 10 ml 1x TE solution) and loaded on agarose gels containing 1% - 3% agarose (depending on the product size) and 0.5 µg/ml ethidium bromide dissolved in 1x TAE buffer (484 g Tris, 136 g sodium acetate, 37 g EDTA in 2 l H_2O).

3.2.1.7 Long Template PCR

The Expand Long Template (ELT) PCR System (Roche) was used for amplification of large genomic DNA fragments. Tables 8 and 9 depict the reaction mix and thermal cycling steps applied.

Table 8: Long template PCR reaction mix.

Component	Volume
Buffer 1	5 µl
dNTP mixture (5 mM)	2 µl
Primer forward (5 µM)	1 µl

Primer reverse (5 µM)	1 µl
Template DNA	1 µl
ELT enzyme mix	0.75 µl
Autoclaved distilled water	39.25 µl

Table 9: Long template PCR program.

PCR step	Time	Temperature	Cycles
Initial denaturation	2 min	94°C	1
Denaturation	10 sec	94°C	
Annealing	30 sec	60°C	10
Elongation	2 min	68°C	
Denaturation	15 sec	94°C	
Annealing	30 sec	60°C	25
Elongation	2 min*	68°C	
Final elongation	7 min	68°C	1

*2 min + 20 sec cycle elongation for each successive cycle

3.2.1.8 Southern Blot

10 µg of genomic DNA were digested overnight at 37°C using appropriate restriction enzymes and buffers (e.g. Xho I, New England Biolabs) in a final volume of 50 µl. Digested DNA was loaded on 1% agarose gels (as described above) using Hyperladder 1 (Bioline) as marker. After 2h of electrophoresis at 80 V, a picture was taken, the gel was transferred into a plastic box containing denaturing buffer and shaken for 45 min at room temperature. The DNA was blotted overnight onto Hybond™ XL nylon membranes (Amersham) using 10% SSC buffer via the capillary transfer method.[223] The membrane was air-dried and the DNA cross-linked by exposing it to UV light for 30 sec using the UV Stratalinker 1800 (Stratagene). The membrane was then pre-hybridized for 2 h at 62°C with 10 ml pre-hybridization buffer containing (pre-boiled) salm sperm (ss) DNA.

20x SSC	
NaCl	3 M
NaCitrate	300 mM

Denaturing buffer	
NaCl	1.5 M
NaOH	0.5 M

100x Denhardts solution	
BSA	2%
Ficoll 400	2%
Polyvinylpyrrolidone	2%
Keep at -20°C	

Pre-hybridization buffer	
Tris pH 8.0	50 mM
EDTA pH 8.0	10 mM
SSC	5x
Denhardts	5x
SDS	0.5%
ssDNA	100 µg/ml

In parallel, 40 µg of the probe, which spans the MLC-2 promoter and exon 1 of the murine SDF-1 gene (Tab. 10), was digested with restriction enzymes Sac I and Sac II (and appropriate buffers) overnight at 37°C in a volume of 30 µl.

Table 10: Southern blot probe used to analyze DNA from SDF-1 transgenic rats.

Name	Sequence
MLC-2SDF-1	CAGCCACTGTCTCTTTAACCTTGAAGGCATTTTTGGGTCTCACGTG TCCACCAGGCGGGTGTCGGACTTTGAACGGCTCTTACTTCAGAAG AACGGCATGGGTGGGGGGGGCTTAGGTGGCCTCTGCCTCACCTACA ACTGCCAAAAGTGGTCATGGGGTTATTTTTAACCCCAGGGAAGAGG TATTTATTGTTCCACACAGGGGCCGGCCAGCAGGCTCCTTGAATTC GATAAGCTCGATACCTCGGTGTCCTCTTGCTGTCCAGCTCTGCAGC CTCCGGCGCGCCCTCCCGCCCACGCCATGGACGCCAAGGTCGTC GCCGTGCTGGCCCTGGTGCTGGCCGCGCTCTGCATCAGTGA

The following day, the digested DNA was loaded on 1% agarose gels and the linearized probe (~ 350 bp) was extracted from the gel and labeled with the Prime-It® RmT Random Labeling Kit (Stratagene) that uses random 9-mer oligonucleotides for labeling DNA to produce highly sensitive hybridization probes. For this purpose, 25-50 ng template DNA were mixed with distilled water to a final volume of 42 µl in single-use reaction tubes, boiled at 95°C for 5 min and centrifuged briefly at RT to collect condensed liquid. 5 µl of radioactively labeled nucleotide [α-32P] dCTP (10 µCi/µl) and 3 µl of magenta DNA polymerase (4 U/µl) were added and the mixture was incubated at 37°C for 10 min. The reaction was stopped by adding 2 µl of stop mix per reaction tube. The reaction mix was purified by using MicroSpin™ G-50 columns and 1 µl of purified solution was used to measure the radioactivity of the sample with the Tri-Carb Liquid Scintillation Analyzer (PerkinElmer). The membrane was hybridized overnight at 62°C using 10 ml of hybridization buffer containing ssDNA. The next day, the membrane was washed twice briefly with pre-warmed wash buffer W1 followed by two 30 min washing steps with wash buffer W2 and W3 at 62°C. Finally, the membrane was dried on Whatman paper, sealed in plastic foil and exposed to the imaging plate BAS-III (Fujifilm) overnight. Signals were detected using the Radioluminography Laser Scanner CR 35 (Dürr Medical).

Hybridization buffer	
Tris pH 8.0	50 mM
EDTA pH 8.0	10 mM
SSC	5x
Denhardts	1x
Dextran sulfate	10%
SDS	0.5%
ssDNA	100 µg/ml

Wash buffer W1	
SSC	2x
SDS	0.5%
Keep at RT	

Wash buffer W2	
SSC	0.5x
SDS	0.5%
Keep at 62°C	

Wash buffer W3	
SSC	0.1x
SDS	0.5%
Keep at 62°C	

3.2.2 RNA Analysis

3.2.2.1 RNA Extraction from Tissue

Tissue samples were collected in FastPrep™ lysing matrix tubes containing matrix beads (MP Biomedicals), immediately frozen in liquid nitrogen and stored at -80°C until further use. For RNA extraction, 1 ml Trizol® reagent was added per 100 mg of tissue and samples were homogenized one or two times for 40 sec at speed level 4 using the FastPrep™-24 instrument. After 5 min incubation at room temperature for complete dissociation of the nucleoprotein complex, 200 µl of chloroform were added per 1 ml of Trizol® reagent, samples were shaken vigorously for 15 min and incubated for 2-3 min at room temperature. After centrifugation at 12,000 g for 15 min at 4°C, the upper aqueous phase was transferred into new tubes and 500 µl of 100% isopropanol were added. Samples were incubated at RT for 10 min and then centrifuged at 12,000 g for 10 min at 4°C. RNA pellets were washed with 1 ml of 75% ethanol per 1 ml of Trizol® reagent, centrifuged at 7,500 g for 5 min at 4°C and air-dried for 5-10 min. Finally, RNA pellets were resuspended in DEPC-treated H_2O and incubated in a heat block at 55°C for 10 min. RNA concentration was measured using the NanoDrop™ spectrophotometer (Peqlab) as described in chapter 3.2.1.3 and samples were stored at -80°C until use.

3.2.2.2 RNA Extraction from Cells

RNA from cultured cells was purified using the RNeasy® Mini Kit (Qiagen) and manufacturer's instructions were followed. In detail, cells grown in a monolayer (< 5 x 10^6) were lysed by resuspending them in 350 µl buffer RLT (containing 10 µl β-mercaptoethanol per 1 ml of buffer) using a pipette. 350 µl of 75% ethanol were added, lysates were homogenized by passing them 5 times through a 20-gauge needle and transferred into QIAshredder spin columns placed in 2 ml collection tubes. After centrifugation for 15 sec at 8,000 g, flow-through was discarded and columns were washed with 700 µl buffer RW1, followed by another two washes with 500 µl buffer RPE. Columns were then placed in new collection tubes, dried by centrifugation for 1 min at full speed and placed in new 1.5 ml collection tubes. 30-50 µl RNase-free water were added directly to the spin column membrane and samples were centrifuged again for 1 min at 8,000 g to elute the RNA. RNA concentration was measured using the NanoDrop™ spectrophotometer (Peqlab) and samples were stored at -80°C.

3.2.2.3 Reverse Transcription

2 µg total RNA were digested by incubation with 1 µl DNase I (Roche) and 1 µl 10x PCR buffer (-$MgCl_2$) for 30 min at 37°C followed by incubation for 10 min at 75°C in order to inactivate enzyme activity. Digested RNA was then mixed with 2 µl of random hexamer

primers (5 U/ml) and 19 µl of DEPC-treated H_2O. The mixture was incubated at 65°C for 5 min to avoid formation of secondary structures of the RNA and quickly chilled on ice. After adding 19 µl of RT master mix (Tab. 11), the reaction was incubated for 1 h at 37°C followed by 10 min at 80°C for enzyme inactivation.

Table 11: Reverse transcription reaction mix.

Component	Volume
5x First-Strand Buffer	10 µl
dNTPs (5 mM)	4 µl
DTT (0.1 M)	2 µl
M-MLV	2 µl
RNase inhibitor	1 µl

3.2.2.4 Quantitative Real Time PCR (qRT-PCR)

Quantitative real time PCR (qRT-PCR) was used to amplify and simultaneously quantify cDNA and thereby determine mRNA levels in cells or tissues. Both SYBR© green and Taqman© protocols were applied in a 384-well plate format by using the Real time PCR system 7900HT (Applied Biosystems). For each reaction, optimal primer concentrations, cDNA dilutions and most suitable housekeeping genes were tested in advance. For Taqman© qRT-PCRs, 2 µl primer mix (10 mM), 1 µl TAMRA/FAM probe (5 mM), 10 µl master mix (2x), 5 µl ddH_2O and 2 µl cDNA (10-40 ng/µl) were mixed. The typical thermal profile is depicted in Table 12. For SYBR© green reactions, 1 µl primer mix (5 mM), 10 µl GoTaq® qPCR master mix (2x), 0.2 µl CXR reference dye (100x) and 6.8 µl ddH_2O were mixed with 2 µl cDNA. In contrast to Taqman qPCR reactions, a melting curve analysis was carried out at the end of the PCR program. Gene expression was calculated using the $\Delta\Delta C_t$-method.[224] Glyceraldehyde-3-phoshate (GAPDH), 28S ribosomal protein (Mrps28) as well as hypoxanthin-phosphoribosyl-transferase (HPRT) were used as reference genes.

Table 12: qRT-PCR program.

qRT-PCR step	Time	Temperature	Cycles
Initial denaturation	10 min	95°C	1
Denaturation	15 sec	95°C	40
Annealing & elongation	60 sec	60°C	

3.2.2.5 5´ RLM-RACE

FirstChoice® RNA Ligase Mediated Rapid Amplification of cDNA Ends (RLM-RACE; Roche) was used to amplify cDNA from full-length, capped mRNA. Manufacturer's instructions were

followed. In brief, 10 µg of total RNA were treated with Calf Intestine Alkaline Phosphatase (CIP) for 1 h at 37°C followed by phenol:chloroform extraction. CIP'd RNA was treated with Tobacco Acid Pyrophosphate (TAP) for 1 h at 37°C, then the 5`RACE adapter was ligated by incubating the CIP/TAP-treated RNA for 1 h at 37°C with T4 RNA ligase. Reverse transcription of ligated RNA was applied using M-MLV Reverse Transcriptase for 1 h at 42°C followed by outer and inner 5`RLM-RACE PCR (Tables 13 and 14).

Table 13: Primers used for outer and inner 5`RLM-RACE PCR.

Primer name	Sequence (5`-3`)
Outer+inner 5`RACE F	GAG CCA ACG TCA AGC ATC TG
Outer 5`RACE R r+m	GAT CCA CTT TAA TTT CGG GTC A
Inner 5`RACE R rat	TGT CTG TTG TTG CTT TTC AGC CT
Inner 5`RACE R mouse	TGT CTG TTG TTG TTC TTC AGC CG

Table 14: Program for outer and inner 5`RLM-RACE PCR.

PCR step	Time	Temperature	Cycles
Initial denaturation	3 min	94°C	1
Denaturation	15 sec	94°C	
Annealing	10 sec	68-60°C*	40
Elongation	30 sec	72°C	
Final elongation	7 min	72°C	1

*3x 68°C, 3x 66°C, 3x 64°C, 3x 62°C, 3x 60°C

Finally, inner 5`RLM-RACE PCR products were analyzed on 2% agarose gels, extracted from the gels as described in 3.2.1.4 and sequenced.

3.2.2.6 Microarray

Total RNA was extracted from rat hearts using the Trizol protocol described in chapter 3.2.2.1. 200 ng of isolated RNA were applied to the GeneChip® Whole Transcript Sense Target Labeling Assay (Affymetrix) and manufacturer's instructions were followed in order to generate amplified and biotinylated sense-strand DNA. This fragmented and labeled DNA was used for hybridization on probe arrays that were scanned at the MDC core facility under technical assistance of Gabriele Born (group of Prof. Norbert Hübner). The GeneChip® Scanner 3000 7G and the GeneChip® operating software (GCOS) were used. Data were analyzed with the help of Dr. Herbert Schulz (group of Prof. Norbert Hübner) by using the Partek® Genomic Suite™ 6.4 software.

3.2.3 Protein Biochemistry

3.2.3.1 Protein Isolation from Cells and Organs

To isolate proteins from cells, culture plates were washed twice with cold PBS and cells were scraped off the plate with RIPA buffer (for Western Blot) or with Protein extraction buffer (for ELISA). Then, cells were sonicated for 30 sec and centrifuged for 10 min at 13,000 g and 4°C. The supernatants containing protein were transferred into new tubes and stored at -80°C. To isolate proteins from organs, 100 mg tissue were homogenized in 1 ml RIPA or Protein extraction buffer using the FastPrep™-24 instrument. The homogenate was sonicated, centrifuged and finally stored as described above.

RIPA buffer	
NaCl	150 mM
Tris (pH 8.0)	50 mM
Tergitol type NP-40	1%
Sodium deoxycholate	0.5%
SDS	0.1%
Complete cocktail*	1 tablet

Protein extraction buffer	
NaCl	150 mM
Tris (pH 7.5	25 mM
NaF	10 mM
EDTA	0.5 mM
Triton X-100	1%
Complete cocktail*	1 tablet

*Complete protease inhibitor cocktail: 1 tablet in 25 ml buffer

3.2.3.2 Measurement of Protein Concentration

The quantity of proteins was measured using the BCA Protein Assay. In principle, the assay is based on the Lowry procedure that uses Cu^{2+} reduction to Cu^{1+} under alkaline conditions.[225] The amount of reduction is proportional to the protein present. BCA forms a purple-blue complex with Cu^{2+} that can be measured spectrophotometrically. Samples containing either no protein or known concentrations of bovine serum albumin (BSA) were used to calculate the protein concentration. Protein samples were diluted in PBS (from 1:2 to 1:50) and 5 µl of each sample or standard (0.1 - 1.4 µg/µl BSA) were mixed with 200 µl of BCA solution (a 1:50 mixture of Reagent A and Reagent B). After 30 min incubation at 37°C, samples were measured at 562 nm using a microplate reader (Tecan). Protein concentrations were calculated using the standard curve prepared from the BSA protein standards.

3.2.3.3 SDS Polyacrylamide Gel Electrophoresis (SDS-PAGE)

For separation of proteins according to their molecular weight, samples were mixed with 4x Roti®-Load and denatured by incubation at 95°C for 5 min. Proteins were separated by electrophoresis in SDS-PAGE running buffer on gradient gels (8-15% acrylamide/bisacrylamide 37.5:1) at 100 V. Gels were subjected to Western Blotting afterwards.

SDS-PAGE running buffer	
Glycine	196 mM
Tris-HCl	20 mM pH8.4
SDS	0.1%

3.2.3.4 Western Blot

Proteins were blotted to PVDF membranes (pre-activated with methanol) for 1-2 hours at 80-100 V using a tank blotter filled with transfer buffer. The membranes were then incubated with different blocking buffers (2.5% milk; 5% BSA; Odyssey® blocking buffer) for 1 hour at room temperature, followed by an overnight incubation with primary antibody dilution (1:200 - 1:1000 in TBST) on a roller mixer at 4°C. This was followed by three washing steps in order to remove unspecifically bound antibody. Depending on the detection system, the membranes were afterwards incubated with peroxidase-conjugated (diluted 1:2000 in TBST) or with Odyssey® infrared dye-labeled (diluted 1:10,000 in TBST) secondary antibodies for 1 hour at room temperature. Upon another three washing steps, the membranes were either incubated with peroxidase substrate (SuperSignaling™ West Dura Substrate) and signals were detected by a luminescent image analyzer (LAS-1000) or signals were recorded directly using the Odyssey® infrared imaging system.

Transfer buffer	
Glycine	200 mM
Tris	20 mM
Methanol	20%

Wash buffer (TBST)	
NaCl	150 mM
Tris	50 mM
Tween-20	0.5%

3.2.3.5 Enzyme-linked Immunosorbent Assay (ELISA)

Commercially available ELISA kits were used to detect SDF-1, GPNMB and chemokines IL-10 and IL-12 in tissue or cell culture lysates according to the manufacturer's protocols. In brief, 96-well microplates were coated with 100 µl diluted capture antibody (usually 1:180 in PBS) per well overnight at RT. The next day, plates were washed three times with wash buffer (0.05% Tween-20 in PBS) and blocked by incubation with 300 µl reagent diluent (1% BSA in PBS) per well for 1 h at room temperature. After another three washing steps, 100 µl of sample or standards (seven 2-fold serial dilutions in reagent diluent) were added per well and plates were incubated for 2 h at room temperature. The three washing steps were repeated and 100 µl detection antibody (usually 1:180 in reagent diluent) were added per well. After 2 h of incubation at room temperature, plates were washed again three times and samples were incubated with 100 µl Streptavidin-HRP (usually 1:200 in reagent diluent) for 20 min at room temperature. Plates were washed three times and incubated with 100 µl TMB substrate solution (1:1 mixture of TMB Peroxidase Substrate and Peroxidase Substrate Solution B) per well for 10-20 min at room temperature. Then, the reaction was stopped by addition of 100 µl stop solution (1M H_3PO_4) per well and optical density of each well was

measured at 450 nm (with wavelength correction at 540 nm) using the microplate reader M200 (Tecan). Protein concentrations were calculated using the seven point standard curve obtained from the protein standards.

3.2.4 Isolation and Culture of Adult Rat Cardiomyocytes

12 weeks old SDF-1 transgenic and SD control rats were used for isolation of adult cardiomyocytes (CM) that was performed under technical assistance of Petra Domaing from the group of Prof. Dr. Ingo Morano at the MDC. In brief, hearts were retrogradely rinsed with a CM perfusion solution containing 0.1 M $CaCl_2$ and collagenase type 2 (125 U/mg) for 20 min at RT and afterwards minced using scissors in a perfusion solution with 0.1 M $CaCl_2$ and 1 mg/ml BSA. Dissociated cells were filtered, sedimented for 10 min at RT, dissolved in CM medium and plated in laminin-coated cell culture plates at a density of 2.5 x 10^5 cells/ml. 2 hours after plating, medium was exchanged. After 24 h of incubation at 37°C and 5% CO_2, supernatants were harvested, centrifuged for 3 minutes at 1000 rpm and frozen at -80°C until subsequent analysis. Cardiomyocytes were trypsinized by incubating them with TripLE™ Express for 5 min at 37°C. After addition of an equal amount of CM medium and centrifugation for 3 min at 1000 rpm, cell pellets were washed with 1xPBS and used for protein isolation as described in chapter 3.2.3.1.

CM perfusion solution	
NaCl	117 mM
Hepes	10 mM
KCl	4 mM
$NaHCO_3$	4 mM
$MgCl_2$	1.7 mM
KH_2PO_4	1 mM
Glucose	1.8 mg/ml
pH 7.4	

CM medium	
Medium M199	
Creatine	5 mM
Taurin	5 mM
L-Carnitin	2 mM
Cytosin-D-arabinofuranoside	10 µM
FBS	5%
BSA	0.2%
Gentamycin	10 mg/l
$NaHCO_3$	2.2 g/l
pH 7.4	

3.2.5 Isolation and Culture of Murine Macrophages

Murine bone marrow-derived macrophages were isolated as described previously.[226] Briefly, 10-12 weeks old mice were euthanized by cervical dislocation, skin was peeled from each hind leg and excess muscle was removed. Leg bones (femur and tibia) were carefully cut proximal to each joint with sharp scissors and flushed with 2 ml cold sterile PBS using a 10 ml-syringe and 25-G needle until bone cavity appeared white. Cells were centrifuged for 10 min at 500 g and RT, supernatants were discarded and cell pellets were resuspended in macrophage complete medium (DMEM low glucose with 10% FBS and 100 U/ml penicillin-streptomycin). Cells were counted and a total of 4 x 10^5 cells were plated per well of 6-well

plates with 2 ml macrophage complete medium containing 20 ng/ml recombinant murine macrophage colony stimulating factor (M-CSF) per well. Cells were incubated at 37°C and 5% CO_2. On day 3, another 1 ml of macrophage complete medium with 20 ng/ml M-CSF was added per well. On day 7, culture supernatants were removed, cells were washed once with macrophage complete medium and 2 ml of serum-low macrophage complete medium (containing 1% FBS) were added per well. The following day, supernatants were discarded and 2 ml serum-low medium containing 10 ng/ml recombinant murine interferon (IFN)-γ, 10 ng/ml recombinant murine interleukin (IL)-4 or without cytokine supplement (Ø) were added to each well. Cells and supernatants were harvested after 4 or 24 h of incubation at 37°C and 5% CO_2 and frozen at -20°C until further use.

3.2.6 Animal Work

3.2.6.1 Animal Husbandry

Mice and rats were kept at pathogen-free conditions in the animal core facility of the MDC according to the German Animal Protection Law. Animals were housed at a constant temperature of 21 ± 2°C with a humidity of 65 ± 5% and a 12 h/12 h light/dark cycle in individually ventilated cages (Tecniplast) with free excess to standard chow (0.25% sodium; Ssniff) and drinking water. The offspring was weaned and genotyped at the age of 3 weeks and unless otherwise specified, male animals at an age of 10 - 16 weeks were used for experiments. All procedures were carried out in accordance with the guidelines provided and approved by the *Landesamt für Gesundheit und Soziales* (LAGeSo). All efforts were made to minimize suffering.

3.2.6.2 Generation of SDF-1 Transgenic Rats

Transgenic rats were generated in the group of Prof. Michael Bader at the MDC with the help of Dr. Elena Popova as described previously.[227] Briefly, immature SD rats were superovulated by intraperitoneal (i.p.) injection of gonadotropin followed by injection of human chorionic gonadotropin and mating of male and female SD rats 48 h later. One-cell rat embryos were recovered on day 1 after superovulation. The linear DNA construct (3 µg/ml dissolved in microinjection buffer containing 8 mM Tris-HCl and 0.15 mM EDTA, pH 7.4) was microinjected into the male or female pronucleus of zygotes by using a pair of manipulators (Eppendorf). Eggs were subsequently cultured for 2 h and then transferred into pseudo-pregnant recipients. Integration of the transgene was determined by transgene-specific PCRs and Southern blot with genomic DNA.

3.2.6.3 Generation of SDF-1 Conditional Knockout Mice

SDF-1 “floxed” mice (SDF-1^{flox}) were generated in the group of Prof. Michael Bader at the MDC by Dr. Santhosh Ghadge with the aim to create an animal model that allows tissue- and

time- specific deletion of SDF-1. For this purpose, two loxP sites were introduced upstream and downstream of exon 1 of the SDF-1 gene by homologous recombination upon electroporation of the knockout (KO) vector into embryonic stem (ES) cells. Positive clones were selected by ganciclovir and G418 treatment due to the neomycin resistance cassette of the KO vector and used for microinjection into blastocysts. Resulting offspring was genotyped using Southern blot and PCR and positive mice were backcrossed for several generations using C57BL/6N mice. Finally, SDF-1^{flox} animals were bred with Mx1-Cre or Pf4-Cre mice in order to achieve hematopoietic cell- or platelet-specific knockouts of SDF-1.

3.2.6.4 Echocardiography

Echocardiographic measurements were performed at the MDC core facility under technical assistance of Martin Taube and Stefanie Schelenz. Mice and rats were anesthetized with isoflurane (1.6 vol% isoflurane/air), the chest was depilated, covered with ultrasound transmission gel and adhesive electrodes were attached to the extremities of the animal. Two-dimensional images were recorded using the Visual Sonics Vevo® 700 and a 45 MHz ultrasound linear probe suitable for small animals. Measurements of interventricular septum (IVS) and posterior wall thickness (PWT) as well as inner left ventricular diastolic (D) and systolic (S) diameters (LVEDD, LVESD) were conducted in parasternal long- and short-axis projections with guided M-mode recordings at the midventricular level in both views. These data were used to calculate LV volumes, cardiac output, ejection fraction (EF) and fractional shortening (FS) (Vevo® 2100 Imaging System). In addition, the ratios of LV posterior wall thickness to LV diameter in diastole and systole (PWTD/LVEDD and PWTS/LVESD) were determined that indicate hypertrophic and dilative changes of the left ventricle. In animals after myocardial infarction, a Simpson measurement was conducted additionally that measures the LV at multiple planes (e.g. one near the cardiac apex, one at the mid-section near the papillary muscle and one under the base of the aorta) in systole and diastole. For each level, the endocardial borders were traced and resulting data were used to calculate Simpson´s EF.

3.2.6.5 Cardiac MRI

Cardiac MRI measurements were conducted by the group of Prof. Dr. Thoralf Niendorf at the MDC. All imaging experiments were carried out under isoflurane anesthesia on a 9.4T small animal MR system (Biospec 94/20, Bruker Biospin, Ettlingen, Germany). A curved four channel receive only rat heart surface coil array (Bruker Biospin, Ettlingen, Germany) was used in conjunction with a linear polarized birdcage resonator for transmission (Bruker Biospin, Ettlingen, Germany). For the imaging experiments, rats were anesthetized in a warmed anesthetic chamber using 3.5% isoflurane in an oxygen/air mixture (2:1) with a flow rate of 1500 ml/min for induction and then maintained at 2.0%. A body temperature of 37°C

was maintained by warming the animal beds using a circulating heated water system (Thermo Haake GmbH, Karlsruhe, Germany) and monitoring by a rectal temperature probe throughout the measurements. Respiratory signals were continuously monitored using a commercial monitoring and gating system (SA Instruments, Inc., New York, USA) and kept between 50-70 respiration cycles per minute by regulating the isoflurane dose. Pulse rate, pulse length and peripheral oxygen saturation were determined via a pulse oximeter sensor (SA Instruments, Inc., New York, USA) attached to the foot. To obtain a stack of cardiac short axis (SAX) views covering the whole heart, 7x2 slices were consecutively acquired using a self-gated black-blood cine fast low angle shot technique (IntraGate-FLASH). Imaging parameters were as follows: TE/TR=2.1ms/17.8ms, field of view=50 mm, matrix size=192x128, spatial resolution=260 x 390 x 1200 μm^3, α=20°, number of repetitions=70, cardiac frames=20, acquisition time ~ 2.5 min. Additionally, four chamber views were acquired with following imaging parameters: TE/TR=3.0ms/6.1ms, field of view=50 mm, matrix size=192x192, spatial resolution=260 x 260 x 800 μm^3, α=10°, number of repetitions=150, cardiac frames=20, acquisition time ~ 3 min. For delayed contrast enhancement, the short axis scans were repeated after administration of a contrast agent: 0.3 mmol/kg Gd-DTPA (Magnevist, Schering AG, Germany) was injected i.p. 25 minutes prior to MRI.

Cardiac function assessment was performed by an experienced observer in a blinded manner using CMR42 (Circle CVI, Calgary, Canada). For this purpose, endo- and epicardial borders were contoured in end-systole and end-diastole using a stack of non-contrast-enhanced short axis cine views. Stroke volumes (SV), end-diastolic volumes (EDV), end-systolic volumes (ESV), ejection fraction (EF), and myocardial masses (EDM) were calculated for the left ventricle. Infarct sizes were calculated based on the manual segmentation of the infarcted myocardium using the images with delayed enhancement contrast.

3.2.6.6 Isoprenaline Infusion via Minipumps

In order to apply isoprenaline subcutaneously in mice at a constant dose of 30 mg/kg/day, Alzet® micro-osmotic pumps (model # 1002) were used with a volume capacity of 102 µl and a flow rate of 0.24 µl/h. The appropriate amount of isoprenaline was dissolved in sterile 0.9% NaCl (saline) solution according to the body weight of the mice and pumps were filled by using a syringe and a provided 27 gauge filling tube. To ensure correct loading, pumps were weighted before and after filling. Pumps were placed in saline and incubated at 37°C for 24 h. For implantation, mice were anesthetized via isoflurane inhalation and pumps were introduced under the skin of the neck through a 0.5 cm-long incision.

3.2.6.7 Induction of Myocardial Infarction

Permanent ligation of the left anterior descending artery (LAD) was used for experimental induction of myocardial infarction and was performed under technical assistance of Astrid Schiche. For this purpose, 12-16 weeks old mice and 8-10 weeks old rats were anesthetized with isoflurane and artificially ventilated with a respirator. The animals were constantly kept at 37°C and monitored via ECG during the surgery. LAD ligation was produced by using a 7-0 nylon surgical suture and a dissecting microscope. Efficiency of the procedure was verified visually by color change of the ischemic area and by ECG. In addition, mice and rats were subjected to echocardiographic measurements at different time points after MI induction.

3.2.6.8 Collection of Organs and Blood Composition Analysis

Mice and rats were anesthetized via isoflurane inhalation and blood was collected from the abdominal aorta and directly transferred into MiniCollect® EDTA tubes placed on ice. 12 µl of each blood sample were used for automated blood composition analysis with the Scil Vet abc hematology analyzer. The blood samples were afterwards centrifuged for 10 min at 3000 rpm and 4°C and supernatants were immediately frozen at -80°C. In parallel, hearts and lungs (and additional organs if required) were dissected, washed in PBS, weighed and frozen in liquid nitrogen. Organs were kept at -80°C until use.

3.2.6.9 Preparation of Thrombocytes from Mice

Mice were anesthetized using isoflurane and blood (~ 900 µl) was collected from the abdominal aorta and transferred into tubes containing 100 µl sodium citrate (3.8%). 500 µl Tyrode hepes buffer were added and samples were centrifuged for 8 min at 210 g (without brake). The resulting upper phase (platelet-rich plasma) was transferred into new tubes and centrifuged again for 5 min at 1020 g (without brake). The upper phase (platelet-poor plasma) was removed and the platelet pellet frozen in liquid nitrogen and kept at -80°C until use.

Tyrode hepes buffer	
NaCl	134 mM
Hepes	20 mM
$NaHCO_3$	12 mM
Glucose	5 mM
KCl	2.9 mM
$MgCl_2$	1 mM
Na_2HPO_4	0.34 mM
ddH_2O	

3.2.7 Flow Cytometry

3.2.7.1 Preparation of Cells for Flow Cytometry

Peripheral blood (~ 1ml) was incubated 1-2x with 2 ml 1x BD™ Pharm Lyse™ reagent for 5 min at RT in order to lyse red blood cells. The reaction was stopped by addition of an equal amount of FACS buffer (5% FBS in PBS) and centrifuged for 2 min at 1200 rpm. The supernatant was discarded, cells were resuspended in blocking buffer (rat: rat serum 1:100 in FACS buffer; mouse: CD16/CD32 1:1000 in FACS buffer) and kept at 4°C for 15 min.

Both femur and tibia were dissected and carefully cleaned from adherent tissue. The tip of each bone was removed with scissors and the bones were flushed with 2 ml PBS by using a 23 G needle and a 1 ml syringe. Red blood cells were lysed as described above and cell suspensions were filtered using 40 µm nylon filters followed by blocking at RT for 15 min.

Splenic tissue was homogenized using scissors and cells were resuspended in 2 ml PBS and filtered using 100 µm nylon filters. Red blood cell lysis and blocking was performed as described above.

3.2.7.2 Antibody Staining and Measurement

Upon blocking, cells were centrifuged for 2 min at 1200 rpm, resuspended with fluorescence-labeled antibody dilution (usually 1:500 - 1:4000 in FACS buffer) and incubated at 4°C for 30 min. Samples were centrifuged for 2 min at 1200 rpm, washed twice with FACS buffer and fixed by incubation with 2% PFA (diluted in FACS buffer) for 5 min at RT. After another centrifugation step, cells were resuspended in FACS buffer and stored at 4°C until use. For flow cytometry, 250 µl of PBS were added and between 50,000 - 600,000 cells were analyzed per sample using the BD™ LSR II or LSRFortessa™ benchtop cell analyzers as well as the BD FACSDiva™ software. Data were analyzed with the FlowJo software (Tree Star Inc., OR, USA).

3.2.8 Histology

3.2.8.1 Preparation of Paraffin Sections

In order to prepare paraffin sections, tissue samples were fixed for 48 h in 4% PFA (diluted in PBS) at 4°C. After fixation, specimen were washed twice with PBS and dehydrated by incubating them in a series of ethanol solutions (2x 70%, 2x 80%, 2x 96%, 2x isopropanol and 2x xylene) for 1 h each step. Following dehydration, the samples were incubated twice for 90 min in paraffin and finally embedded in paraffin at 67°C. The embedded tissue was stored at 4°C until use. Sections (3-5 µm) were produced with a rotary microtome (Microm), placed on SuperFrost® Plus slides and stored at 4°C.

3.2.8.2 Preparation of Cryosections

To produce cryosections, freshly dissected organs were rinsed with PBS and slowly frozen using pre-cooled 2-methylbutane. The frozen samples were kept at -80°C. Before cutting, the organs were embedded with Tissue-Tek® O.C.T.™ Compound and 6-10 µm thick sections were produced using the cryostat CM3050 S (Leica). They were mounted on SuperFrost® Plus slides, air-dried and subsequently stored at -20°C.

3.2.8.3 Sirius Red Staining of Cryosections

Cryosections were incubated in 4% PFA solution at 4°C for 24 to 48 hours, followed by two washes in PBS. Sections were stained by incubation with picro-sirius red solution (0.1% sirius red F3B in saturated aqueous solution of picric acid) for one hour at RT. After two washes with acidified water (0.5% glacial acetic acid in tap water), sections were dehydrated in three changes of 100% ethanol, cleared using xylene and mounted in a resinous medium.

3.2.8.4 Immunofluorescence Staining

Paraffin sections were incubated three times with xylol in order to remove the paraffin followed by a series of alcohol solutions (2x 100%, 95%, 80%, 70%, 50%, 30%) for 5 min each step for rehydration. After two final washes with water and PBS, paraffin sections were treated either with citrate puffer for 10 min at 95°C or with trypsin solution (1 mg/ml trypsin in H_2O) for 15 min at 37°C for antigen retrieval followed by two washes with PBS. Cryosections were fixed by incubating them for 10 min with pre-cooled acetone on dry ice and then air-dried for 30 min at RT. They were incubated in PBS (pH 7.4) for 20 min for swelling and afterwards in PBST (0.1% Triton-X 100 in 1x PBS) for 30 min for permeabilization.

Citrate buffer	
Citric acid	9.5 mM
Sodium citrate	41.5 mM
ddH_2O	
pH 6.0	

Pre-treated paraffin or cryosections were blocked for 30 min with 10% normal donkey serum in PBS followed by incubation with the 1st antibody solution (diluted in PBS) overnight at 4°C in a humified chamber. The next day, sections were washed with PBS three times for 15 min and incubated with the 2nd antibody solution (diluted in PBS) for 2 h at room temperature in the humified chamber. Sections were washed again three times with PBS and mounted using Vectashield® mounting medium (containing 1.5 µg/ml DAPI). Pictures were taken using the inverted microscope DMI6000B (Leica) as well as the fluorescence microscope BZ-9000 (Keyence). Stainings were quantified using the BZ-II Analyzer software (Keyence). If not specified otherwise, three sections per animal were analyzed in a blinded manner.

3.2.9 Patient Population

Plasma samples of 20 controls (5 females, 15 males) with preserved ejection fraction (EF>55%) and of 20 patients (10 females, 10 males) with systolic heart failure (EF<35%), which had been used in a study by Posch *et al.*[228], were used for GPNMB ELISA measurements. All plasma samples of myocardial infarct patients (1 female, 35 males) were collected at different time points during the first week after acute MI between March and May 2000 under the direction of Prof. Dr. med. Rainer Dietz. Patients were grouped according to their blood CK or CK-MB levels. The project was approved by the ethics commission committee of the Charité-Universitätsmedizin Berlin.

3.2.10 Statistics

Results are presented as mean ± SEM. Data were analyzed statistically using the GraphPad Prism 5 software (GraphPad Software, CA, USA). The Student's t-test was applied for comparisons between individual pairs of means. Three or more groups were analyzed using one-way ANOVA with Bonferroni post-test. Differences with a p-value of $p<0.05$ were considered to be significant.

4 Results

4.1 Generation and Basic Characterization of SDF-1α Transgenic Rats

The objective of this part of the project was the generation of a SDF-1 overexpressing rat line that can be helpful to clarify the importance and therapeutic potential of cardiomyocyte-derived SDF-1 on myocardial regeneration after injury.

4.1.1 Generation of SDF-1α Transgenic Rats

The DNA construct used for the generation of a transgenic (Tg) rat line overexpressing SDF-1α exclusively in the heart was generated by Dr. Santhosh Ghadge in the laboratory of Prof. Michael Bader. The construct consists of the cardiomyocyte-specific promoter myosin light chain-2 (MLC-2) and the murine SDF-1α gene (Fig. 6A) that were both cloned into the pBluescript SK+ vector (Fermentas). For microinjection, the construct was digested with the restriction enzymes Kpn I and Not I, loaded on an agarose gel and the resulting 9 kb fragment was extracted from the gel. The eluted fragment was diluted with microinjection buffer (8 mM Tris-HCl, 0.15 mM EDTA) and filtered (0.2 µm). The linear DNA construct was used for microinjection into pronuclei of SD rat zygotes, which were subsequently re-implanted into pseudo-pregnant rats.

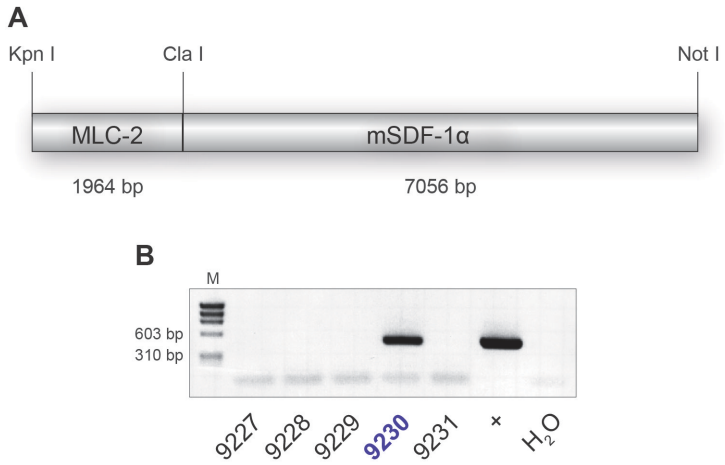

Fig. 6: Transgenic DNA construct and genotyping PCR. A DNA construct that was used for microinjection consists of the cardiomyocyte-specific MLC-2 promoter and the murine SDF-1α gene. **B** PCR-based genotyping revealed one positive founder animal # 9230. MLC-2: myosin light chain-2; bp: base pairs; M: Phi marker (Fermentas); + positive control (diluted construct DNA).

PCR-based genotyping revealed one positive founder (# 9230; Fig. 6B) that was used for further breeding with SD rats in order to achieve heterozygous first filial (F1) offspring. These heterozygous animals were interbred to achieve homozygous progeny for long-term maintenance of the line.

4.1.2 Transgene Insertion and Expression Analysis

Genomic DNA isolated from tail biopsies of heterozygous rats of the F1 generation was used for Southern blot analysis. As shown in Fig. 7, different patterns were found on the blot revealing possible different integration sites of the transgene into the genome. The three

labeled animals 3, 7 and 15 were used for further breeding, however offspring was only achieved from male rat # 7 and thus one transgenic sub-line could be established.

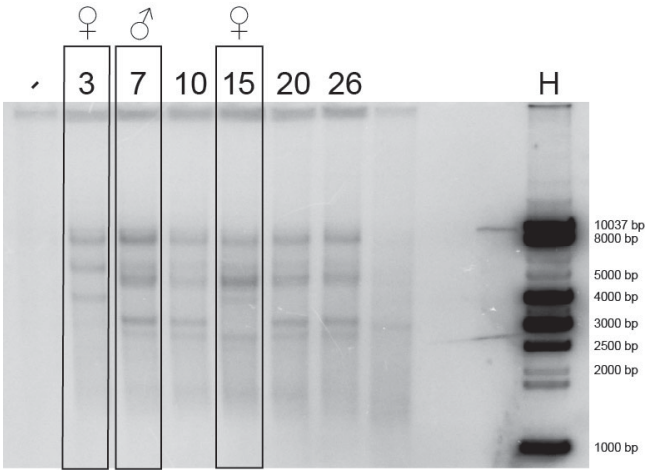

Fig. 7: Southern blot analysis of DNA from SDF-1 transgenic rats. Genomic DNA of six heterozygous transgenic rats out of the F1 generation was analyzed by Southern blot. Labeled animals were used for further breeding. H: hyperladder 1 (Bioline); bp: base pairs; - negative control.

RNA was extracted from transgenic rat hearts and used for 5´ RLM-RACE. This method is applied to amplify cDNA from full-length, capped mRNA. This cDNA usually produces a single band after PCR and can be further used for sequencing in order to confirm the correct expression of the transgenic DNA. Here, cDNA was produced from transgenic cardiac RNA and analyzed using primers specific for murine (transgenic) as well as rat (endogenous) SDF-1. As expected, PCR reactions revealed a single band for mouse and rat SDF-1 (Fig. 8A). Both fragments were extracted from the agarose gel and subsequently sequenced. As shown in Fig. 8B, the BLAST comparison of the murine SDF-1 (CXCL12) mRNA (NCBI reference NM_021704.3) and the inner mouse 5´RACE PCR revealed one G → A mutation (labeled in red) that does not alter the final amino acid sequence. Apart from this silent mutation, the open reading frame of SDF-1 including sequenced exons 1, 2 and partially exon 3 appears correct.

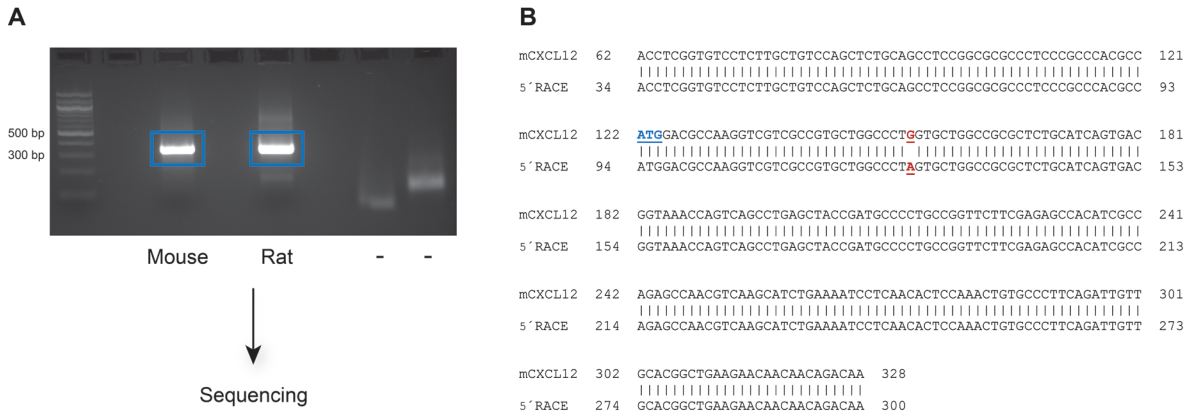

Fig. 8: 5´ RLM-RACE of RNA from SDF-1α transgenic rat hearts. A Agarose gel electrophoresis result of the inner 5´ RLM-RACE PCR using primers specific for mouse or rat SDF-1. **B** BLAST search result comparing murine SDF-1/CXLC12 mRNA (NM_021704.3) and the mouse 5´ RLM-RACE inner PCR product. Start codon in blue; one silent G → A mutation in red; bp: base pairs; - negative control.

4.1.3 SDF-1 mRNA Levels and Protein Content in Rat Tissues

In order to analyze the expression levels of SDF-1, RNA was extracted from different organs of transgenic as well as wild type (WT) rats and analyzed via qRT-PCR (Fig. 9). 28S ribosomal protein (Mrps28) and GAPDH were used as reference ("housekeeping") genes. SDF-1 expression was found to be significantly and specifically induced in hearts of transgenic rats.

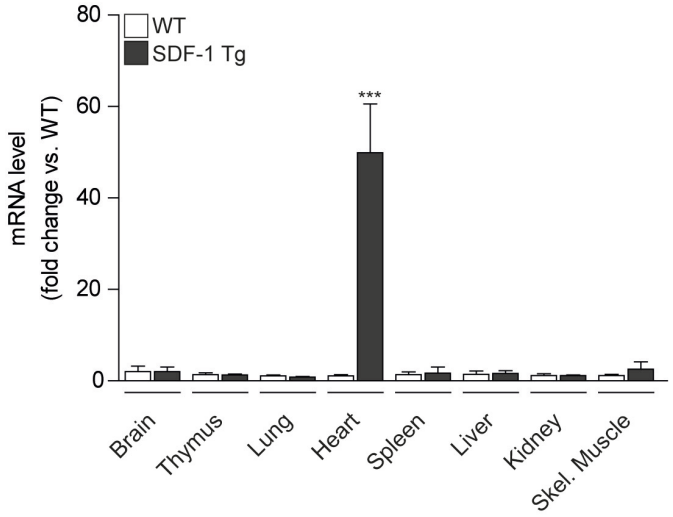

Fig. 9: SDF-1 mRNA levels in different organs of WT and Tg rats. Quantitative RT-PCR of SDF-1 in different organs of wild type (WT) and SDF-1 transgenic (Tg) rats. *** p<0.001; WT n=4, Tg n=4.

Furthermore, SDF-1 protein expression was analyzed in heart lysates of WT and transgenic rats via Western blot using several commercially available SDF-1 antibodies and different blocking solutions (milk powder, BSA, Odyssey® Blocking). However, none of the tested antibodies was able to produce a specific band in heart tissue of transgenic animals (data not shown). In order to clarify if the SDF-1 transgene results in higher protein levels in hearts of SDF-1 Tg rats, cardiomyocytes were isolated from 12 weeks old WT and transgenic animals with the help of Petra Domaing (group of Prof. Ingo Morano at the MDC). After culture for 24 h, cells and supernatants were harvested and analyzed via ELISA. SDF-1 protein levels were calculated as pg/mg total protein (measured in the BCA assay) and found to be significantly higher in transgenic cardiomyocyte lysates compared to WT controls (Fig. 10A).

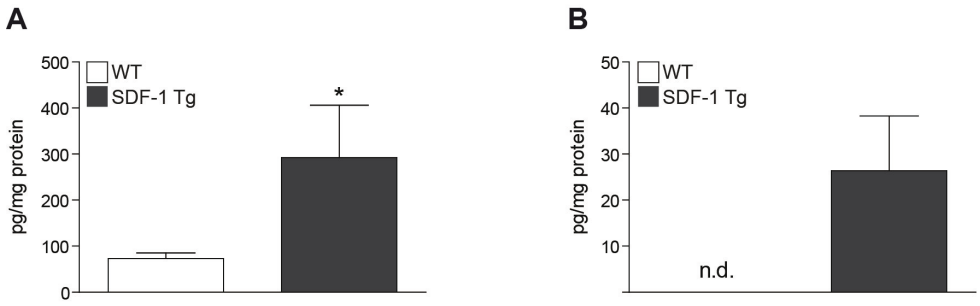

Fig. 10: SDF-1 protein levels in cardiomyocytes isolated from WT and Tg rats. Cardiomyocytes were isolated from adult wild type (WT) and SDF-1 transgenic (Tg) rat hearts. After 24 h of culture, SDF-1 protein levels were determined in cardiomyocyte lysates (**A**) and supernatants (**B**) via ELISA. n.d.: not detected; * p<0.05 vs. WT; WT n=4, Tg n=4.

In addition, SDF-1 protein was present in the supernatant of cardiomyocytes from transgenic hearts, whereas it was not detectable in the medium of WT cardiomyocytes (Fig. 10B). This finding suggests that the transgenic cells are capable of secreting SDF-1.

4.1.4 Basic Phenotyping of SDF-1α Transgenic Rats

Cardiac function and morphology of 10-12 weeks old WT and SDF-1 transgenic rats were assessed by 2-dimensional echocardiography performed at the MDC core facility. Fig. 11A depicts functional parameters calculated from the recordings, e.g. ejection fraction (EF), fractional shortening (FS), stroke volume and cardiac output. In parallel, left ventricular (LV) dimensions were measured such as thickness of the interventricular septum (IVS) and the posterior wall (PWT) as well as left ventricular end-diastolic diameter (LVEDD) (Fig. 11B). All parameters shown were recorded in diastole (D). None of these values was significantly different between WT and SDF-1 Tg rats. The same applies to all parameters recorded in systole (data not shown).

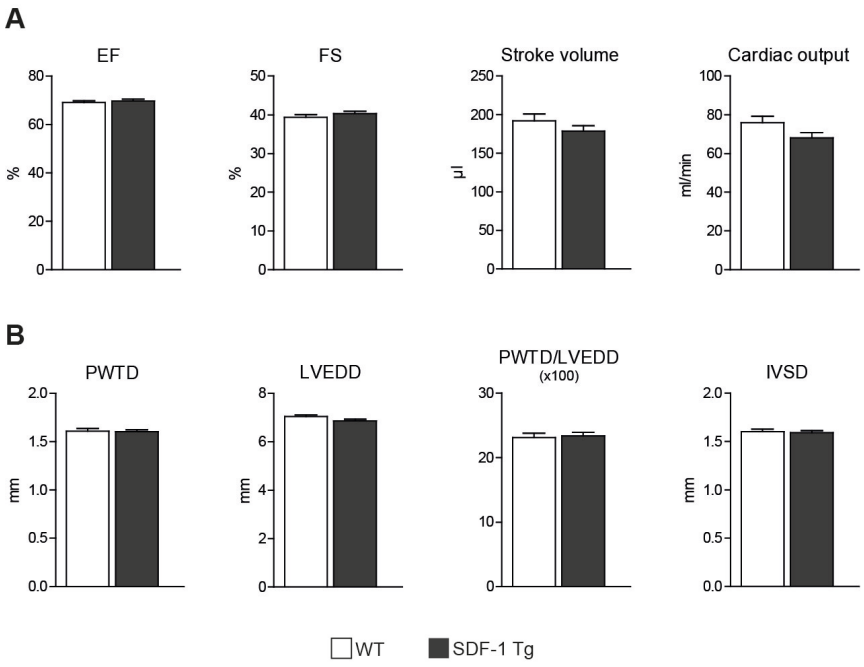

Fig. 11: Basic characterization of WT and SDF-1 Tg rats by 2-dimensional echocardiography. A Calculated parameters of cardiac function in 10-12 weeks old wild type (WT) and SDF-1 transgenic (Tg) rats. **B** Measurements of LV dimensions. EF: ejection fraction, FS: fractional shortening, PWTD: posterior wall thickness (diastole), LVEDD: left ventricular end-diastolic diameter, IVSD: interventricular septum (diastole); WT n=28, Tg n=27.

In summary, the transgenic murine SDF-1α gene is correctly and specifically expressed in the rat hearts resulting in significantly higher mRNA and protein levels of the chemokine. Furthermore, the cardiac function and morphology was found to be normal in SDF-1 Tg animals compared to controls. Thus, the transgenic rats can be used as model to investigate the curative potential of cardiomyocyte-specific SDF-1α.

4.2 Myocardial Regeneration in SDF-1α Transgenic Rats

In order to examine the functional consequence of SDF-1 overexpression in the heart, myocardial infarction (MI) was induced in 8-10 weeks old WT and homozygous SDF-1 Tg rats by permanent ligation of the left anterior descending (LAD) artery. Sham-operated rats of each genotype were used as controls. Rats were monitored via echocardiography before as well as 7, 14 and 28 days (d) after surgery. Some animals were sacrificed 3 and 7 days after surgery in order to analyze their cell composition in blood, bone marrow and spleen via flow cytometry measurements. One final magnet resonance imaging (MRI) measurement was conducted 28 days after MI induction for assessment of cardiac function and infarct sizes in addition to echocardiography. The entire experimental outline is depicted in Fig. 12.

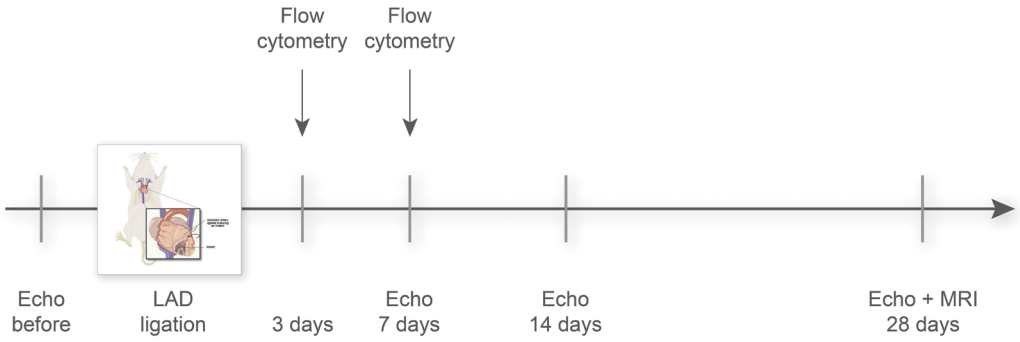

Fig. 12: Survey of myocardial infarct experiments in SDF-1 Tg rats. Myocardial infarction was induced by ligation of the left anterior descending (LAD) artery (picture © 2001 Terese Winslow, Lydia Kibiuk). Animals were monitored via echocardiography (echo) before as well as 7, 14 and 28 days after MI. In addition, flow cytometry measurements were conducted 3 and 7 days after surgery. Finally, one magnet resonance imaging (MRI) measurement was carried out 28 days after infarction.

4.2.1 Impaired Cardiac Function in SDF-1α Transgenic Rats after MI

Mortality rates upon induction of MI were 31.6% for WT and 7.2% for SDF-1 Tg rats. However, these rats died during the first 48 h after MI induction as a direct effect of anesthesia and surgery. Thus, no difference between both genotypes was found regarding long-term survival after myocardial infarction. Also, analysis of relative heart weights as parameter for cardiac hypertrophy revealed higher levels in both groups 28 days after MI surgery, but no significant difference between WT and SDF-1 Tg rats (Fig. 13).

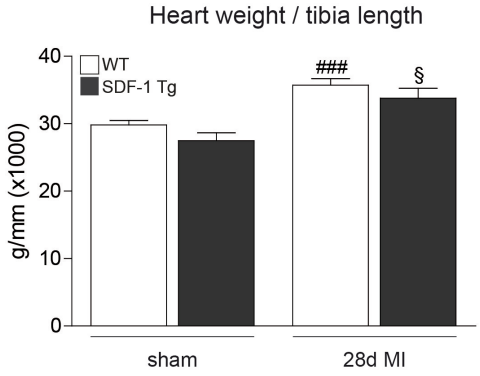

Fig. 13: Analysis of relative heart weight 28 days after MI. Comparison of heart weight / tibia length ratios as indicator of cardiac hypertrophy in WT and SDF-1 transgenic (Tg) rats 28 days (d) after induction of myocardial infarction (MI) or after sham operation. ### $p<0.001$ vs. WT sham, § $p<0.05$ vs. SDF-1 Tg sham; WT sham n=20, SDF-1 Tg sham n=15, WT MI n=13, SDF-1 Tg MI n=15.

All functional parameters of the hearts were recorded via echocardiography. During the first 2 weeks after AMI, cardiac function declined in both WT and SDF-1 transgenic rats as expected without significant differences between the groups (Fig. 14). The final measurement 4 weeks after operation revealed significantly lower Simpson's ejection fraction and fractional shortening in SDF-1 transgenic animals compared to WT controls. Also, stroke volume and cardiac output were significantly decreased in Tg rats. There were no differences between the sham groups at any time.

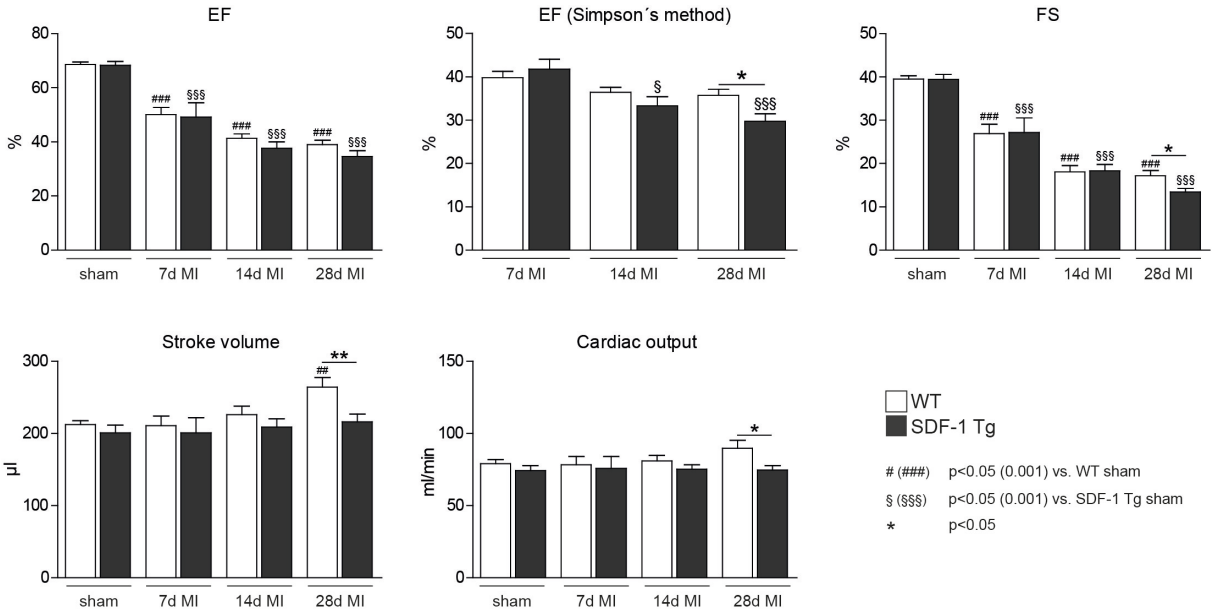

Fig. 14: Cardiac function in WT and SDF-1 Tg rats after MI. 2-dimensional echocardiographic measurements after sham surgery as well as 7, 14 and 28 days (d) after experimental induction of myocardial infarction (MI) in wild type (WT) and SDF-1 transgenic (Tg) rats. EF: ejection fraction, FS: fractional shortening; WT sham n=20, SDF-1 Tg sham n=15, WT after MI n=13, SDF-1 Tg after MI n=15.

Furthermore, alterations of cardiac geometry, which indicate remodeling processes of the heart, were analyzed in both groups after MI (Fig. 15). Inner left ventricular diastolic and systolic diameters (LVEDD, LVESD) increased during 28 days after infarct induction as a sign of dilatation of the LV in all animals, but both parameters showed no difference between WT and SDF-1 Tg animals. In contrast, measures of cardiac hypertrophy such as thickness of posterior wall and interventricular septum in diastole and systole (PWTD, PWTS and IVSD, IVSS) did not change in both groups early (7d and 14d) after MI, but were significantly decreased in SDF-1 transgenic rats later (28d) after MI. Consequently, the ratios PWTD/LVEDD and PWTS/LVESD were smaller in SDF-1 transgenic animals in comparison to WT rats 28 days after MI.

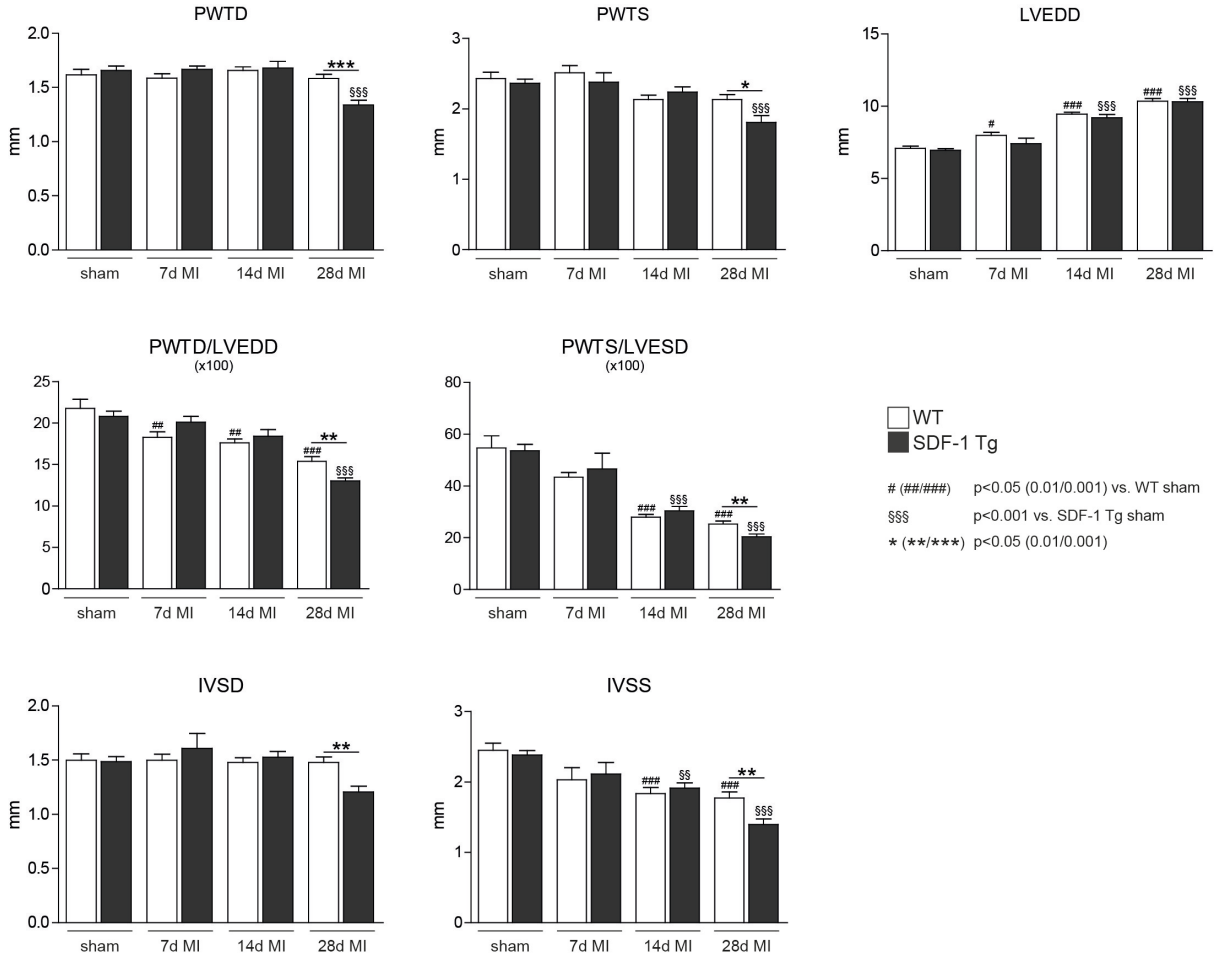

Fig. 15: Cardiac morphology in WT and SDF-1 Tg rats after MI. 2-dimensional echocardiographic measurements after sham surgery as well as 7, 14 and 28 days (d) after experimental induction of myocardial infarction (MI) in wild type (WT) and SDF-1 transgenic (Tg) rats. PWTD/S: posterior wall thickness in diastole/systole, LVED(S)D: left ventricular end-diastolic (/-systolic) diameter, IVSD/S: interventricular septum thickness in diastole/systole; WT sham n=20, SDF-1 Tg sham n=15, WT after MI n=13, SDF-1 Tg after MI n=15.

Figure 16 depicts representative M-mode recordings at the midventricular level of a wild type and a transgenic rat 4 weeks after surgery with plotted contours that have been used to determine the left ventricular diastolic and systolic diameters as well as interventricular septum and posterior wall thickness.

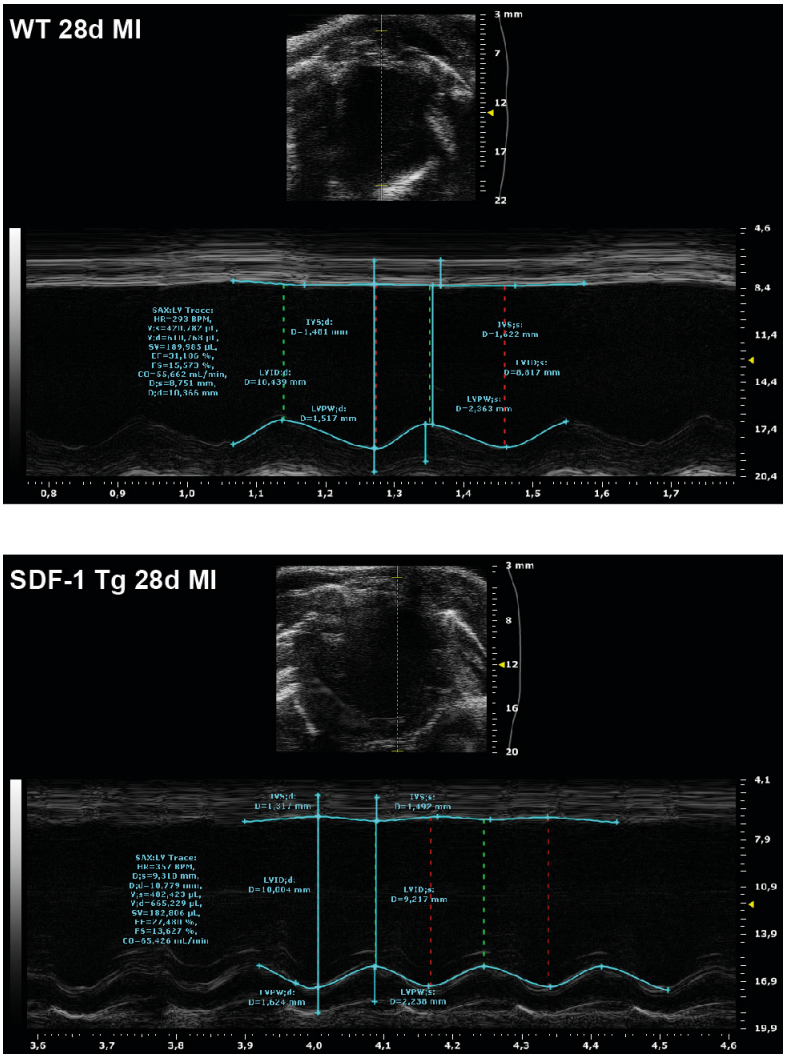

Fig. 16: Representative pictures of M-mode recordings 28 days after MI. M-mode echocardiographic recordings of a wild type (WT) and a SDF-1 transgenic (Tg) rat 28 days (d) after induction of myocardial infarction (MI).

In addition to echocardiography, rats were monitored via magnetic resonance imaging that was performed 28 days after MI induction by the group of Prof. Dr. Thoralf Niendorf at the MDC core facility. As depicted in Fig. 17, these measurements confirmed the deterioration of cardiac function in SDF-1 Tg rats compared to WT controls at this late time point. Furthermore, the MRI measurements revealed no alteration of LV end-diastolic volume (LVEDV) between both groups, but a significantly decreased LV mass in transgenic rats. Therefore, these measurements confirm the results obtained from echocardiography.

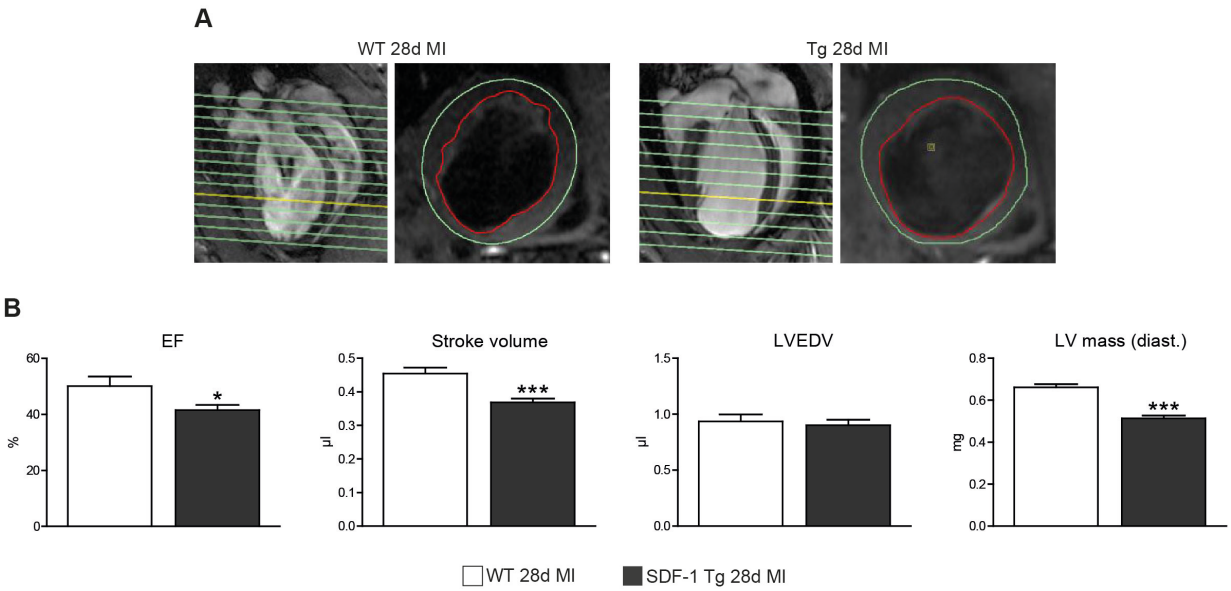

Fig. 17: MRI measurement of cardiac function and morphology 28 days after MI. A Pictures of the mid-ventricular layer position (# 5, in yellow) used to record the end-diastolic parameters of the left ventricle of wild type (WT) and SDF-1 transgenic (Tg) rats 28 days (d) after induction of myocardial infarction (MI). Short axis slices from that position were used to trace contours (green: epicardial border; red: endocardial border) of the left ventricle. **B** Measures of cardiac function (EF, stroke volume) and remodeling (LVEDV, LV mass) in WT and SDF-1 Tg rats. LV: left ventricle, EF: ejection fraction, LVEDV: left ventricular end-diastolic volume, diast.: diastolic; * $p<0.05$, *** $p<0.001$; WT MI n=13, SDF-1 Tg MI n=15.

MRI was furthermore used to determine myocardial infarct sizes in WT and SDF-1 Tg rats 28 days after surgery. For this purpose, contrast agent was injected into the animals and infarct borders were contoured subsequently (Fig. 18A). MI sizes were analyzed by using two different methods. One the one hand, infarct sizes were calculated as % infarct = (infarct area / LV area) x 100%. On the other hand, the angle of the infarct was determined and infarct sizes were calculated as % infarct = (angle infarct / 360°) x100%. As shown in Fig. 18B, both methods revealed no significant difference of MI sizes between both groups.

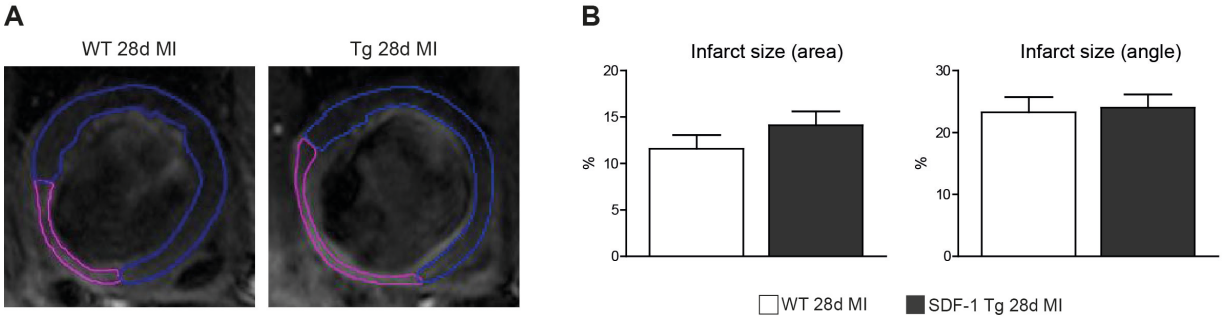

Fig. 18: MRI measurement of infarct sizes 28 days after MI. A End-diastolic (mid-ventricular) short axis images of the LV that were used to contour the infarct zone (in pink) in wild type (WT) and SDF-1 transgenic (Tg) rats after injection of contrast agent. **B** Calculations of infarct sizes based on infarct area (left) and infarct angle (right) determination. MI: myocardial infarction, d: day(s); WT MI n=13, SDF-1 Tg MI n=15.

In summary, the overexpression of SDF-1α in transgenic rats influenced the remodeling of the heart post-MI resulting in impaired cardiac function accompanied by alterations of the geometry of the heart despite no effect on infarct sizes.

4.2.2 Gene Expression Analysis in SDF-1α Transgenic Rats after MI

Rats were sacrificed and RNA was extracted from cardiac tissue at three different time points (3, 7 and 28 days) after MI induction and subsequently used to study the expression levels of hypertrophy, fibrosis, macrophage and neovascularization marker genes via qRT-PCR. As expected, levels of the hypertrophy marker genes ANP and BNP were found to be increased in both groups at all three time points after MI peaking at 7 days post-MI (Fig. 19). In contrast, levels of α-MHC decreased over time with lowest expression levels 28 days after infarction. No difference was observed between wild type and transgenic animals for these three genes. In contrast, β-MHC mRNA levels, which were found to be increased 3 and 7 d after MI as a sign of reactivation of cardiac fetal gene expression, were significantly increased in SDF-1 Tg rats compared to WT animals 28 days after MI.

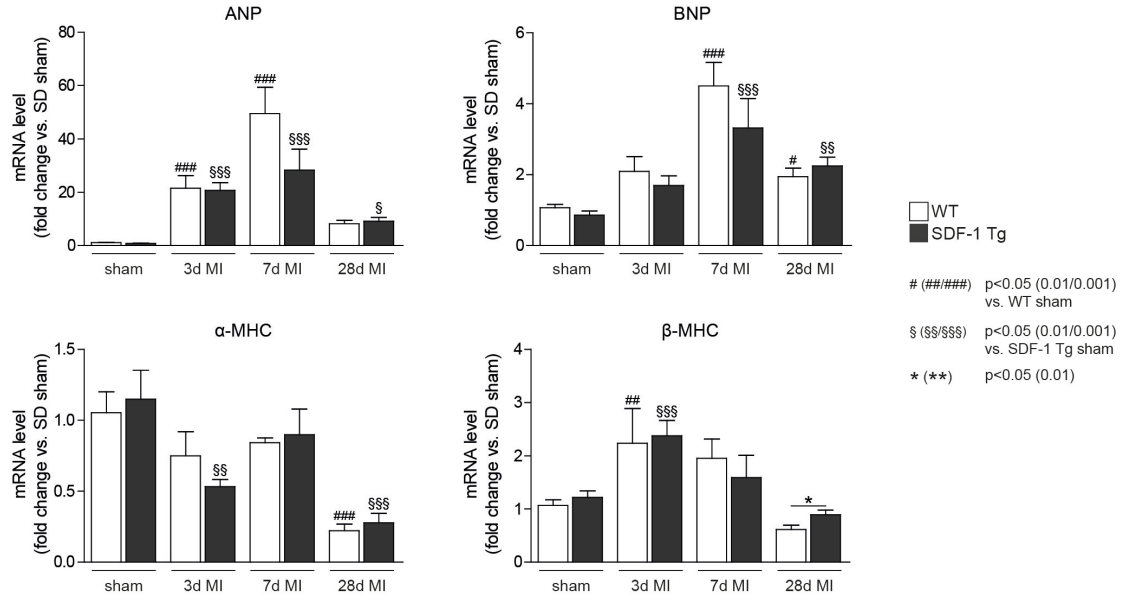

Fig. 19: Quantitative RT-PCR analysis of hypertrophy genes in WT and SDF-1 Tg rats after MI. Expression levels of hypertrophy genes ANP, BNP, α-MHC and β-MHC in cardiac tissue of wild type (WT) and SDF-1 transgenic (Tg) rats after sham surgery as well as 3, 7 and 28 days (d) after myocardial infarct (MI) induction. WT sham n=11, SDF-1 Tg sham n=9, WT 3d MI n=8, SDF-1 Tg 3d MI n=18, WT 7d MI n=9, SDF-1 Tg 7d MI n=8, WT 28d n=13, SDF-1 28d Tg n=15.

Also, relative quantification of fibrosis genes revealed higher levels in both groups after MI compared to sham controls (Fig. 20). However, WT and SDF-1 transgenic animals showed no significant difference regarding collagen 1a1 and fibronectin levels, whereas expression of collagen 3 was less induced in Tg rats resulting in significantly decreased levels of this marker gene in SDF-1 Tg animals 3d after MI. Accordingly, the ratio of collagen 1a1 / collagen 3 expression levels was significantly increased in SDF-1 Tg rats 3d and even more pronounced 28d after MI.

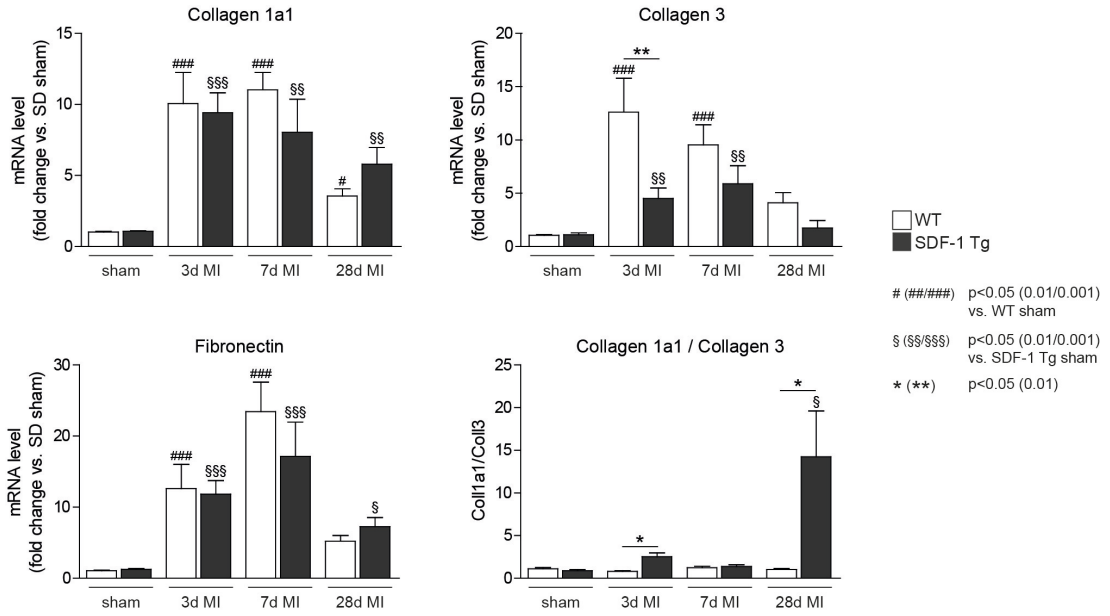

Fig. 20: Quantitative RT-PCR analysis of fibrosis genes in WT and SDF-1 Tg rats after MI. mRNA levels of fibrosis genes collagen 1a1, collagen 3 and fibronectin in cardiac tissue of wild type (WT) and SDF-1 transgenic (Tg) rats after sham surgery as well as 3, 7 and 28 days (d) after myocardial infarct (MI) induction. WT sham n=11, SDF-1 Tg sham n=9, WT 3d MI n=8, SDF-1 Tg 3d MI n=18, WT 7d MI n=9, SDF-1 Tg 7d MI n=8, WT 28d n=13, SDF-1 28d Tg n=15.

Quantitative RT-PCR studies were furthermore applied to investigate if the cardiac overexpression of SDF-1 results in differences of monocyte/macrophage recruitment, neovascularization and CXCR4 expression after MI. As depicted in Fig. 21A, all monocyte/macrophage markers (CD68, ITGAM, CCL2, MSR1) were significantly induced as early as 3 days after MI induction and the levels of these markers remained increased at 7 and 28 days after MI. However, the expression of the general macrophage marker CD68 was significantly higher in SDF-1 transgenic rats compared to WT controls 28 days after infarction. This difference might be due to higher numbers of pro-inflammatory macrophages in SDF-1 Tg rat hearts since the expression level of CCL2, a chemokine predominantly expressed in this monocyte/macrophage subset, was found to be significantly higher in transgenic rats at that time point. In contrast, expression of macrophage scavenger receptor (MSR) 1, which is mostly present in reparative macrophages, was not altered between Tg and WT rats. The vascularization marker vascular endothelial growth factor (VEGF)-A is the only gene with higher levels in hearts of SDF-1 transgenic rats at baseline. After MI, expression of VEGF-A increased in WT animals 7d after MI, whereas it was not changed in Tg rats at that time point and was even decreased 3d and 28d after MI induction (Fig. 21B). A similar result was found for the second vascularization marker platelet endothelial cell adhesion molecule (PECAM)-1 (also named CD31), which showed higher levels in WT rats 7d after MI, but was not induced in SDF-1 transgenic animals at all time points tested. The analysis of CXCR4 levels in heart tissue revealed no difference between WT and transgenic rats early (3 and 7 days) after MI, but slightly higher CXCR4 expression in SDF-1 Tg rats 28 days post-MI (Fig. 21C).

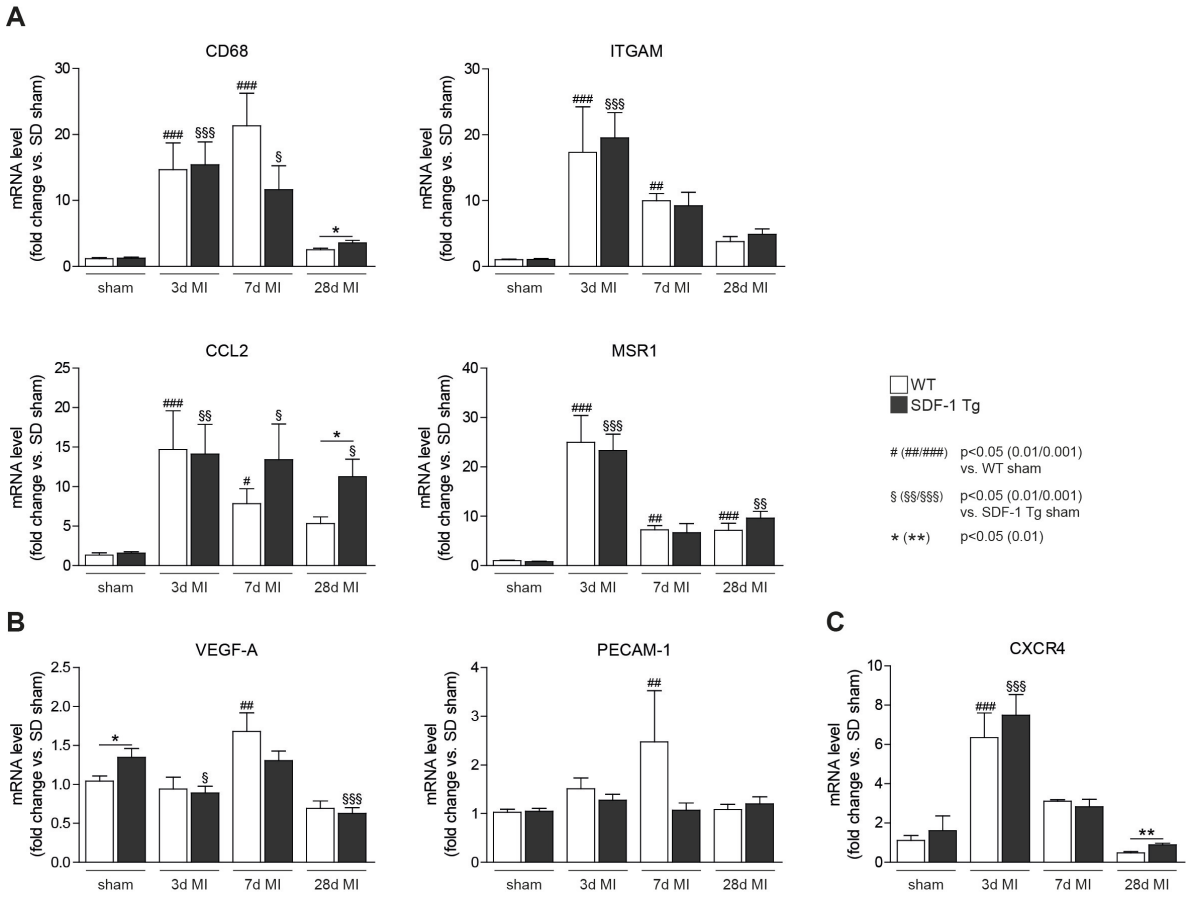

Fig. 21: Quantitative RT-PCR analysis of macrophage and neovascularization genes and CXCR4 in WT and SDF-1 Tg rats after MI. mRNA levels of macrophage-related genes (**A**), neovascularization genes (**B**) and CXCR4 (**C**) in cardiac tissue of wild type (WT) and SDF-1 transgenic (Tg) rats after sham surgery as well as 3, 7 and 28 days (d) after myocardial infarct (MI) induction. WT sham n=11, SDF-1 Tg sham n=9, WT 3d MI n=8, SDF-1 Tg 3d MI n=18, WT 7d MI n=9, SDF-1 Tg 7d MI n=8, WT 28d n=13, SDF-1 28d Tg n=15.

In summary, the overexpression of SDF-1 in transgenic animals seems to alter the remodeling process after cardiac damage as measured by higher levels of the hypertrophy marker β-MHC and decreased expression of collagen 3 and higher collagen 1 / collagen 3 ratios. In addition, SDF-1 might influence myeloid cell recruitment and infiltration into the heart since CD68 as a general monocyte/macrophage marker and CCL2 as pro-inflammatory marker were found to be higher in SDF-1 Tg rats. On the other hand, levels of vascularization markers were not dramatically changed in transgenic hearts. Moreover, CXCR4 expression as an indicator of cell infiltration was not changed early after infarction.

4.2.3 Histological Analysis in SDF-1α Transgenic Rats after MI

In order to confirm the qRT-PCR results that indicated alterations of fibrosis in Tg rats after MI, immunofluorescence stainings were conducted. Figure 22A depicts representative pictures of heart sections stained with an anti-collagen 1 antibody. Quantification of the staining revealed higher collagen 1 levels in Tg rats compared to WT controls in the peri-infarct (PI) zone of the injured heart seven days after MI (Fig. 22B).

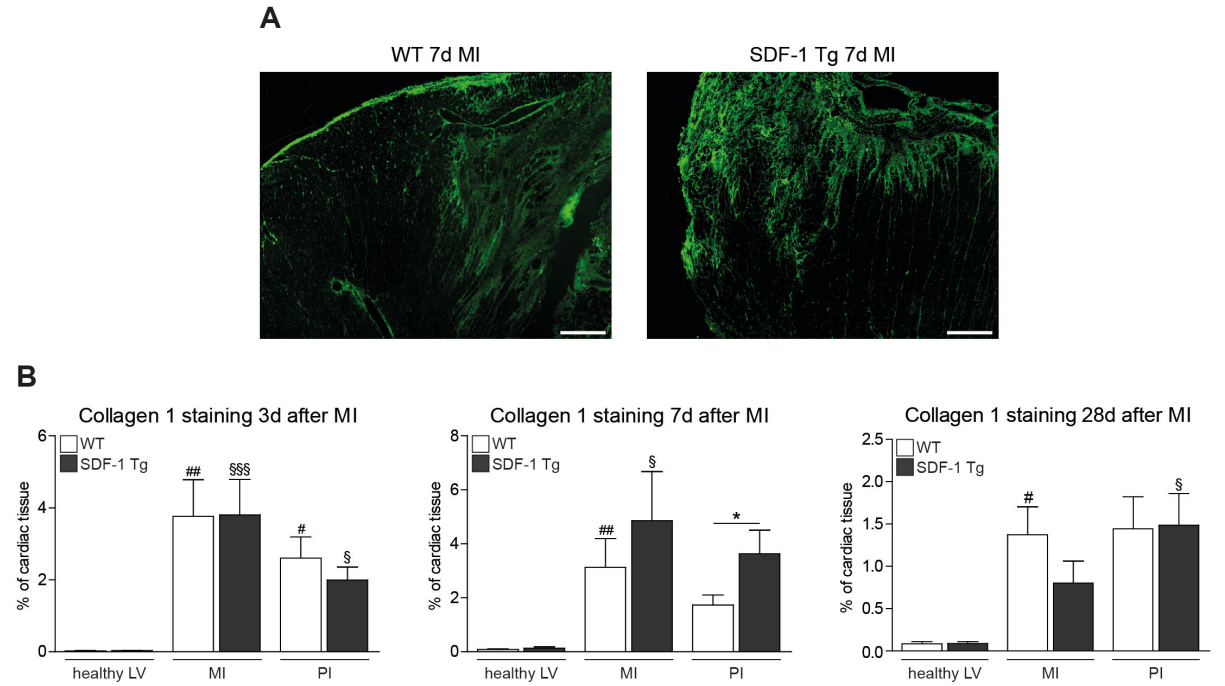

Fig. 22: Collagen 1 levels in WT and SDF-1 Tg rat hearts after MI. A Collagen 1 staining in the peri-infarct region of wild type (WT) and SDF-1 transgenic (Tg) rats 7 days (d) after myocardial infarction (MI) used for quantification. Scale bar=300 µm; 10x magnification. **B** Quantified collagen 1 levels in healthy left ventricle (LV), MI and peri-infarct (PI) region at 3d (left), 7d (middle) and 28d (right) after MI. # (##) $p<0.05$ (0.01) vs. WT LV, § (§§, §§§) $p<0.05$ (0.01, 0.001) vs. SDF-1 Tg LV, * $p<0.05$; 3 sections per animal were analyzed; WT 3d n=4, Tg 3d n=8, WT 7d n=4, Tg 7d n=3, WT 28d n=5, Tg 28d n=5.

In addition, heart sections were stained using sirius red in order to visualize and quantify the complete collagen content. Fig. 23 includes representative pictures of WT and Tg rat hearts (Fig. 23A) and quantification of the staining (Fig. 23B). Transgenic hearts displayed significantly more fibrosis compared to WT rats 7 days after MI.

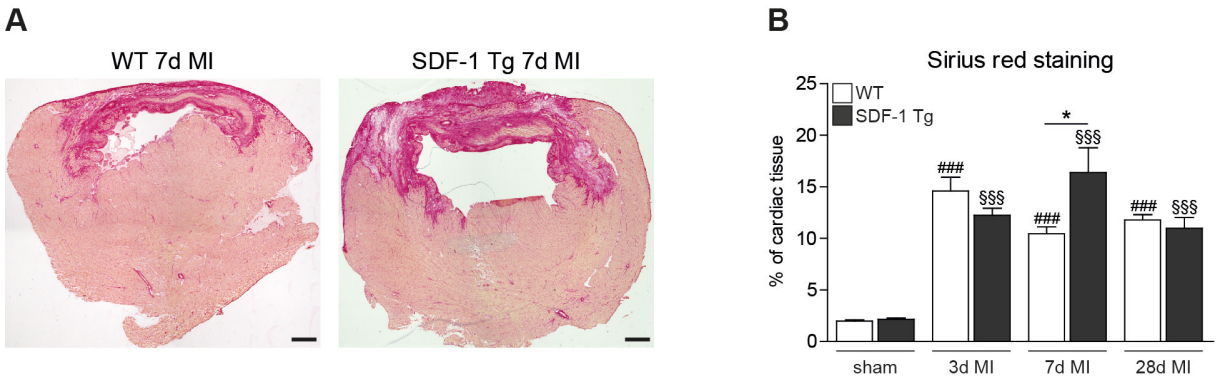

Fig. 23: Sirius red staining of WT and SDF-1 Tg rat hearts after MI. A Representative pictures of sirius red-stained transverse heart sections of wild type (WT) and SDF-1 transgenic (Tg) rats 7 days (d) after experimental myocardial infarction (MI). Scale bar=800 µm; 2x magnification. **B** Quantification of sirius red staining after sham surgery as well as 3, 7 and 28 d after MI induction. ### $p<0.001$ vs. WT sham, §§§ $p<0.001$ vs. SDF-1 Tg sham, * $p<0.05$; 3 sections per animals were analyzed; WT sham n=6, Tg sham n=5, WT 3d n=4, Tg 3d n=9, WT 7d n=4, Tg 7d n=4, WT 28d n=6, Tg 28d n=5.

In addition, immunofluorescence stainings using an anti-CD31 antibody were conducted. CD31 (PECAM-1) is a marker of endothelial cells and thus the quantification of this staining in cardiac sections can be used as a measure of neovascularization. As depicted in Fig. 24, CD31 staining revealed comparable levels of vascularization at basal levels in sham-operated

rats. Moreover, no differences of vessel formation were found between SDF-1 transgenic and wild type rats at all three time points after myocardial infarction. Thus, the overexpression of SDF-1α in cardiomyocytes does not seem to have a major impact on basal and post-MI vascularization of the heart.

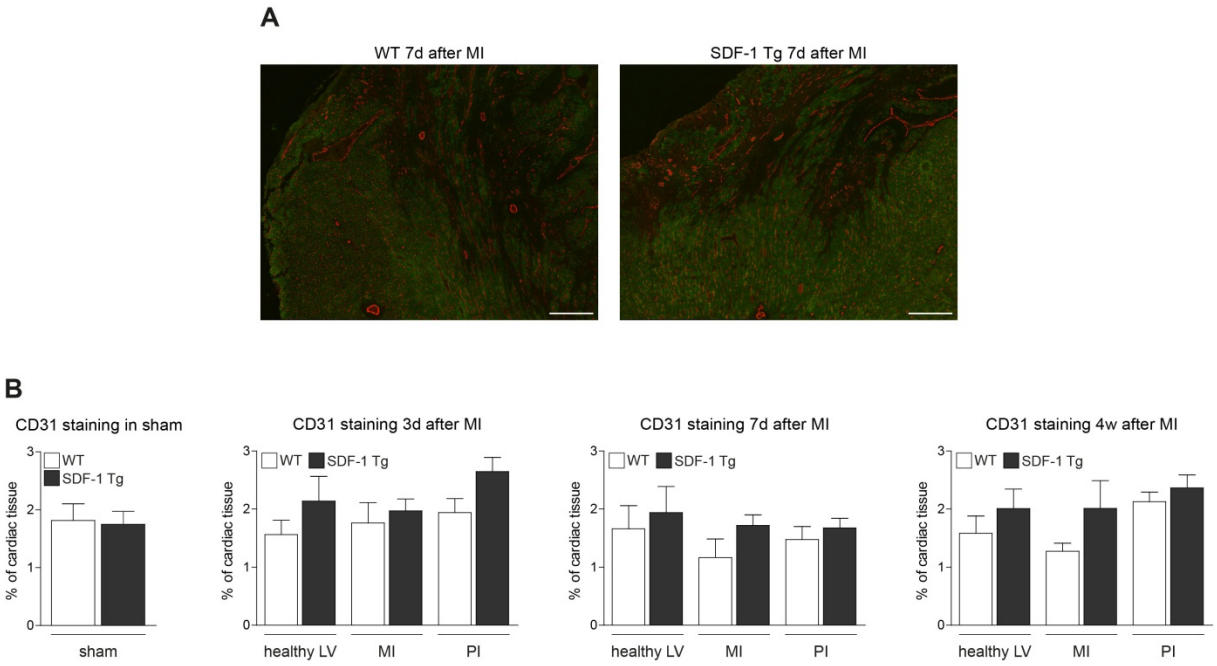

Fig. 24: Levels of neovascularization in WT and SDF-1 Tg rats after MI. A Representative pictures of transverse heart sections of wild type (WT) and SDF-1 transgenic (Tg) rats 7 days (d) after myocardial infarction (MI) stained using an anti-CD31 antibody. Scale bar=300µm; 10x magnification. **B** Quantification of CD31 signal in left ventricle (LV) of sham-operated animals as well as in healthy LV, MI and peri-infarct (PI) region 3, 7 and 28 d after MI induction. 2 sections per animals were analyzed; WT sham n=6, Tg sham n=5, WT 3d n=4, Tg 3d n=9, WT 7d n=4, Tg 7d n=4, WT 28d n=6, Tg 28d n=5.

In order to validate the qRT-PCR results regarding monocyte/macrophage infiltration into the hearts after MI, cardiac sections of wild type and transgenic rats were stained using a rat-specific anti-CD68 antibody. As depicted in Fig. 25, quantification of this staining revealed significantly higher levels of CD68-positive cells in the peri-infarct region of SDF-1 transgenic rats compared to WT controls three days after infarction. At later time points (7d and 28d after MI), levels of infiltrating cells were found to be similar between WT and transgenic rats. Thus, higher levels of cardiomyocyte-derived SDF-1 seem to affect the early infiltration of myeloid cells that are major regulators of the post-MI healing process.

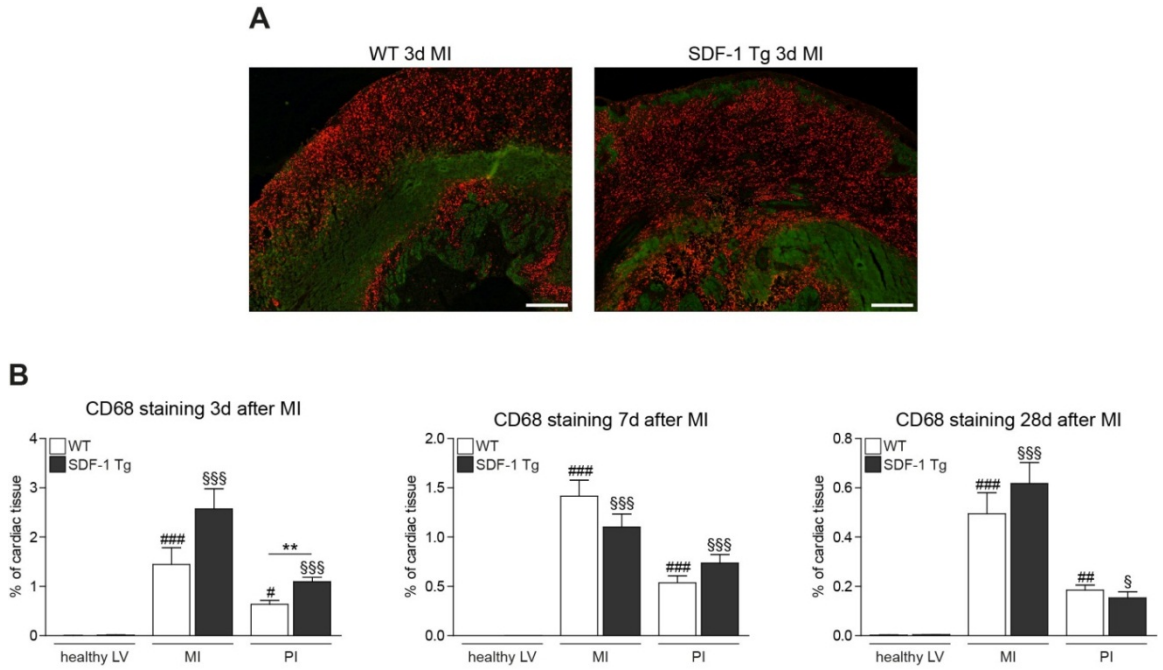

Fig. 25: Levels of macrophages in WT and SDF-1 Tg rats after MI. A Representative pictures of transverse heart sections of wild type (WT) and SDF-1 transgenic (Tg) rats 3 days (d) after myocardial infarction (MI) stained using an anti-CD68 antibody. Scale bar=300 µm; 10x magnification. **B** Quantification of CD68 signal in healthy left ventricle (LV), MI and peri-infarct (PI) region 3, 7 and 28 d after MI induction. # (##, ###) $p<0.05$ (0.01, 0.001) vs. WT sham, § (§§§) $p<0.05$ ($p<0.001$) vs. SDF-1 Tg sham, ** $p<0.01$; 3 sections per animal were analyzed; WT sham n=6, Tg sham n=5, WT 3d n=4, Tg 3d n=9, WT 7d n=4, Tg 7d n=4, WT 28d n=6, Tg 28d n=5.

4.2.4 Altered Cell Recruitment in SDF-1α Transgenic Rats after MI

In order to find a mechanism that might explain the observed effects on cardiac regeneration in SDF-1α Tg rats, numbers of cell types that are capable of influencing repair processes (e.g. progenitor cells, lymphocytes and myeloid cells) and that are known to be recruited in a SDF-1-dependent manner were determined. For this purpose, flow cytometry measurements were conducted in blood, bone marrow (BM) and spleen of WT and transgenic rats 3 and 7 days after MI induction. Fig. 26 depicts the gating strategy and numbers of progenitor cells ($CD11b/c^-$ $CD3^-$ $CD45^+$ stem cell antigen (Sca)-1^+) in blood and BM. No significant difference regarding cell numbers was found in sham-operated controls as well as in WT and SDF-1 Tg rats at both time points after MI.

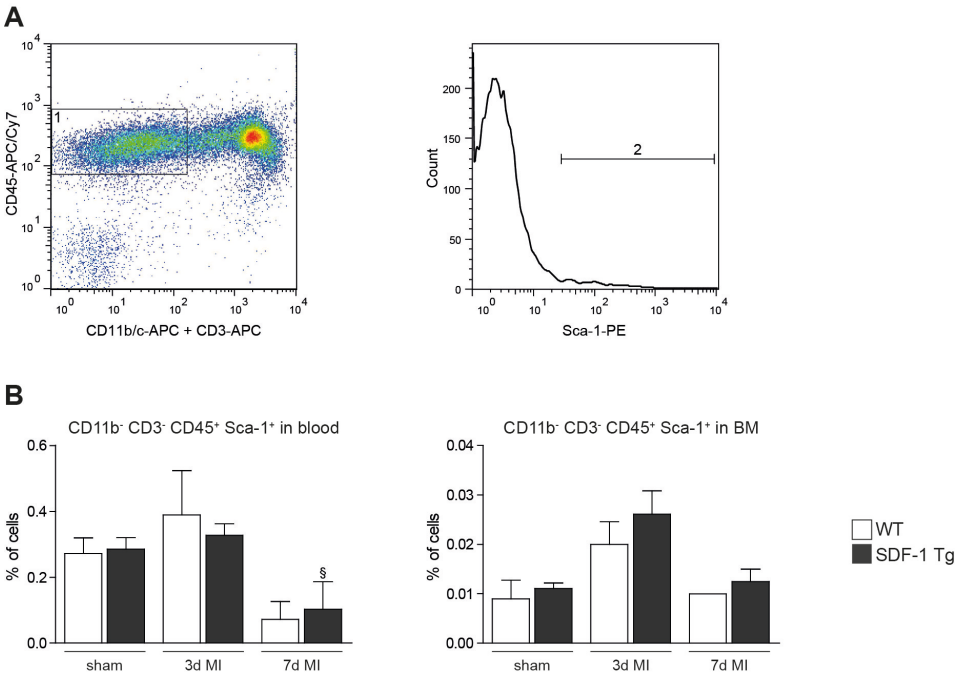

Fig. 26: Progenitor cell numbers in blood and BM after MI. A Gating strategy of flow cytometry data used to define CD11b/c$^-$ CD3$^-$ CD45$^+$ (1) and Sca-1$^+$ (2) progenitor cells. **B** Progenitor cell numbers in blood and bone marrow (BM) of wild type (WT) and SDF-1 transgenic (Tg) rats 3 and 7 days (d) after myocardial infarction (MI) and in sham controls. § p<0.05 vs. SDF-1 Tg sham; WT sham n=11, SDF-1 Tg sham n=9, WT 3d MI n=8, SDF-1 Tg 3d MI n=18, WT 7d MI n=9, SDF-1 Tg 7d MI n=8.

Furthermore, blood, BM and spleen of WT and SDF-1 transgenic animals were analyzed in order to quantify B (CD45$^+$ CD3$^-$ B220$^+$) and T (CD45$^+$ CD3$^+$ B220$^-$) lymphocytes. As shown in Fig. 27, numbers of both cell types declined in blood of WT and SDF-1 Tg rats after MI compared to sham controls. Despite lower levels of B cells in blood and T cells in BM of sham-operated SDF-1 transgenic rats compared to wild type sham controls, percentages of B and T cells at both time points after MI were not significantly different between transgenic and wild type animals. Thus, the alterations of lymphocyte counts in SDF-1 Tg animals at basal levels are not sufficient to give rise to altered levels of B and T cells after MI.

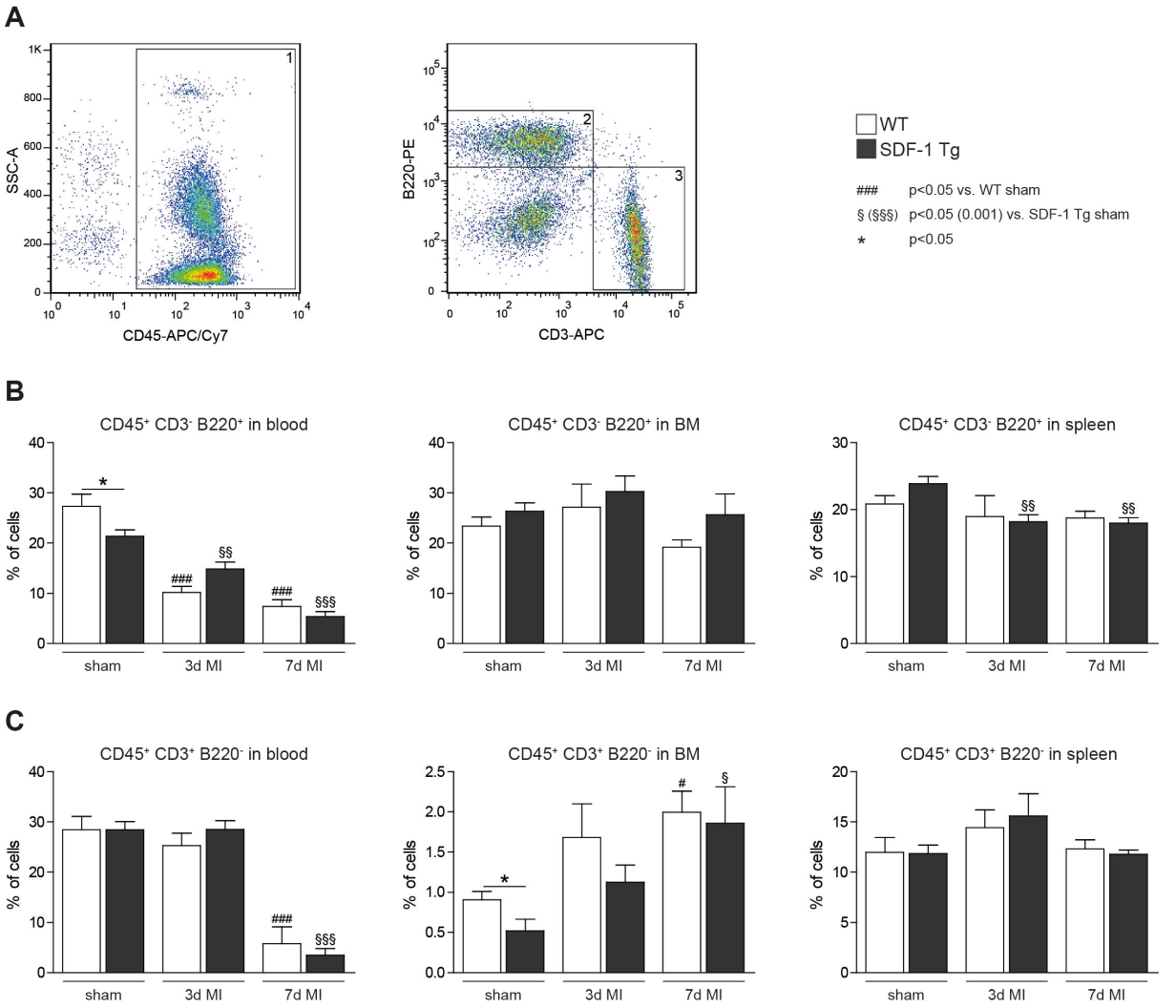

Fig. 27: Lymphocyte numbers in blood, BM and spleen after MI. A Gating strategy of flow cytometry results used to distinguish $CD45^+$ (1) $CD3^-$ $B220^+$ (2) B and $CD3^+$ $B220^-$ (3) T lymphocytes. **B** Numbers of B cells in blood, bone marrow (BM) and spleen of wild type (WT) and SDF-1 transgenic (Tg) rats 3 and 7 days (d) after myocardial infarction (MI) as well as in sham controls. **C** Numbers of T cells in blood, BM and spleen of WT and SDF-1 Tg rats 3d and 7d after MI as well as in sham controls. WT sham n=11, SDF-1 Tg sham n=9, WT 3d MI n=8, SDF-1 Tg 3d MI n=18, WT 7d MI n=9, SDF-1 Tg 7d MI n=8.

Also, myeloid cell numbers were analyzed by flow cytometry. As depicted in Fig. 28, two cell populations were defined based on their expression of the granulocyte marker Gr-1 (high, low) that possibly refers to functional differences of the subpopulations. Hence, $CD11b/c^+$ $Gr\text{-}1^{high}$ cells are thought to be pro-inflammatory neutrophils, whereas $CD11b/c^+$ $Gr\text{-}1^{low}$ cells are described as monocytes and dendritic cells with pro-reparative potential. The only significant differences between WT and SDF-1 transgenic rats were found regarding the $CD11b/c^+$ $Gr\text{-}1^{high}$ subpopulation. One the one hand, numbers of these cells were higher in blood of Tg animals compared to WT controls 7d after MI. On the other hand, $CD11b/c^+$ $Gr\text{-}1^{high}$ cell numbers were lower in BM of SDF-1 transgenic sham-operated controls than in WT sham rats as well as in BM of SDF-1 Tg animals 3 days after infarction compared to WT rats at the same time point. $CD11b/c^+$ $Gr\text{-}1^{low}$ cell counts were not different between wild type and transgenic rats in all organs and at all time points analyzed.

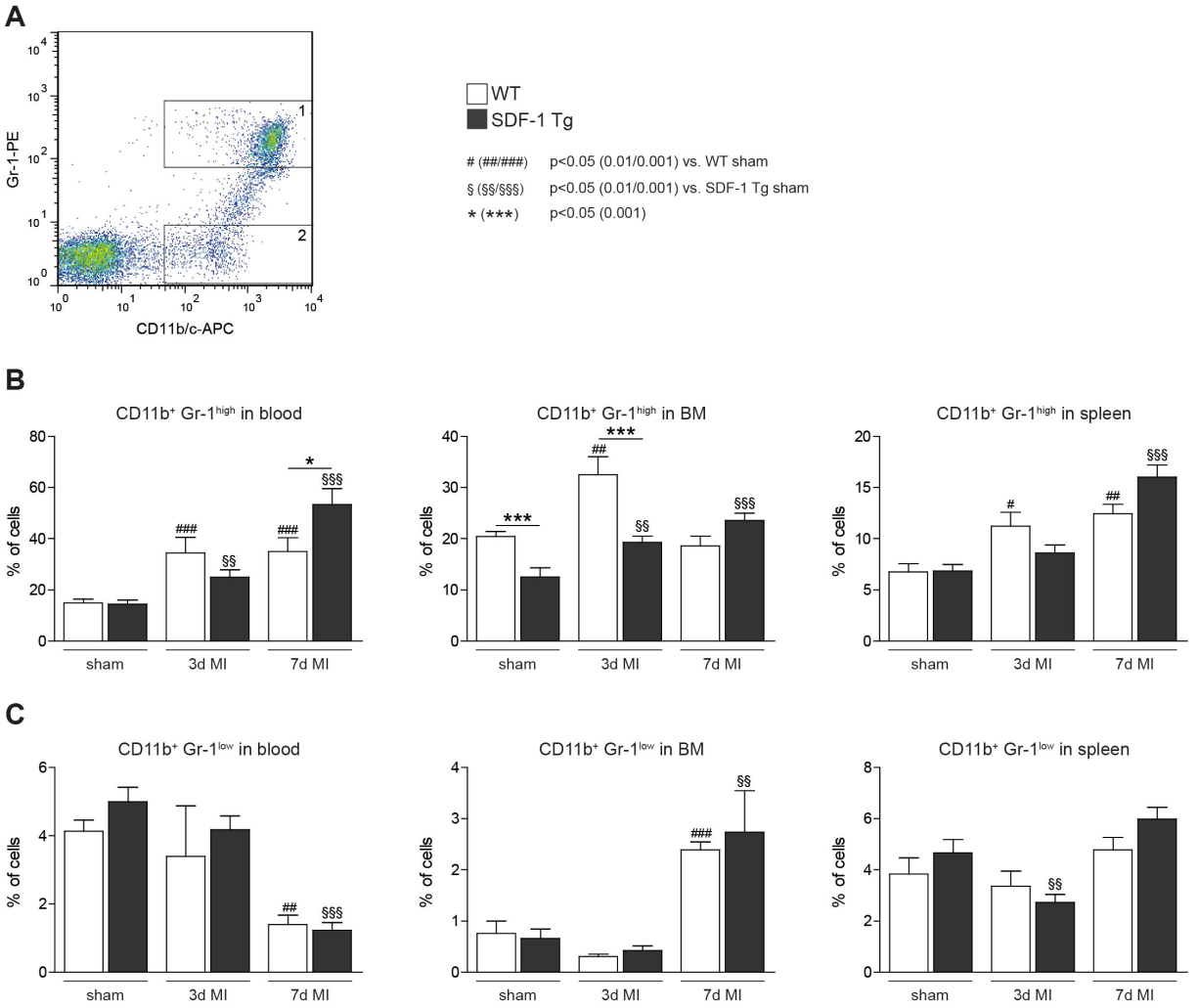

Fig. 28: Myeloid cell numbers in blood, BM and spleen after MI. A Gating strategy used to define myeloid subpopulations based on their Gr-1 expression levels. **B** Percentages of CD11b/c^{+} Gr-1^{high} (1) cells in blood, bone marrow (BM) and spleen of wild type (WT) and SDF-1 transgenic (Tg) rats 3 and 7 days (d) after myocardial infarction (MI) and in sham controls. **C** Percentages of CD11b/c^{+} Gr-1^{low} (2) cells. WT sham n=11, SDF-1 Tg sham n=9, WT 3d MI n=8, SDF-1 Tg 3d MI n=18, WT 7d MI n=9, SDF-1 Tg 7d MI n=8.

In conclusion, flow cytometry analysis in blood, bone marrow and spleen revealed no differences in terms of progenitor cell, B and T lymphocyte numbers between SDF-1 Tg and WT rats 3 and 7 days after infarction. Also, numbers of CD11b^{+} Gr-1^{low} myeloid cells were similar in transgenic and wild type rats. Only CD11b^{+} Gr-1^{high} neutrophil numbers were significantly higher in blood and lower in BM of SDF-1 transgenic rats after MI. This finding could be explained by a higher release of these cells from BM early (3d) after MI that may result in higher CD11b^{+} Gr-1^{high} numbers in blood 7d after MI. This alteration of cell composition in SDF-1 Tg rats might influence myocardial repair processes since neutrophils are recruited to the site of injury where they implement pro-inflammatory actions.

4.2.5 Higher SDF-1 Plasma Levels in Transgenic Rats after MI

Observed changes of cell counts in the circulation and bone marrow of SDF-1α transgenic rats might be due to altered SDF-1 concentrations in the blood of these animals. In order to elucidate this possibility, protein levels of the chemokine were measured in plasma samples of WT and SDF-1α Tg rats 3 days and 7 days after infarction and compared to sham-operated controls. As depicted in Fig. 29, the ELISA measurement revealed similar SDF-1 levels in WT and transgenic rats at basal levels. After infarction, the amount of plasma SDF-1 is slightly decreased in WT animals 3 days after MI. In contrast, plasma levels of the chemokine remain significantly higher in SDF-1 Tg rats at this time point. 7 days after infarction, SDF-1 concentrations are comparably low in both WT and transgenic animals.

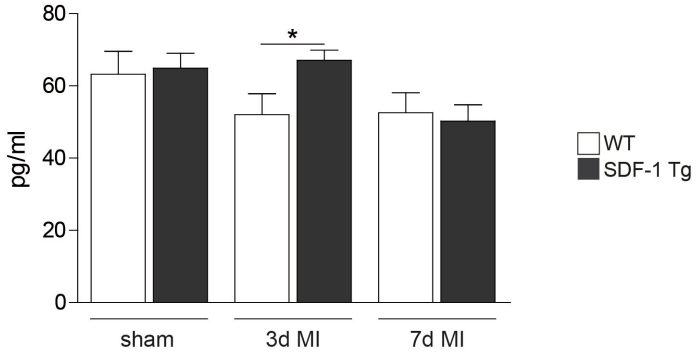

Fig. 29: SDF-1 protein levels in plasma of WT and SDF-1 Tg rats. SDF-1 levels were measured via ELISA in plasma samples of wild type (WT) and SDF-1 transgenic (Tg) rats 3 and 7 days (d) after MI and compared to sham controls. * $p<0.05$; WT sham n=9, SDF-1 Tg sham n=9; WT 3d MI n=5, SDF-1 Tg 3d MI n=5; WT 7d MI n=5, SDF-1 Tg 7d MI n=5.

In summary, experimental induction of myocardial infarction in SDF-1α-overexpressing rats resulted in altered cardiac regeneration with effects on cardiac function, remodeling and fibrosis. Furthermore, the recruitment of neutrophils and macrophages to the heart was altered in transgenic rats, which might have a direct influence on the inflammation and healing of the injured heart. On the other hand, lymphocyte and stem/progenitor cell counts and neoangiogenesis levels were found to be similar in SDF-1α Tg and WT rats after MI and might therefore not account for the observed phenotype.

4.3 Generation and Basic Characterization of Platelet-Specific SDF-1 Knockout Mice

The aim of this part of the project was to investigate the importance of platelet-derived SDF-1 for myocardial repair processes. For this purpose, a platelet-specific SDF-1 conditional knockout mouse (cKO) line was generated.

4.3.1 Generation of Platelet-Specific SDF-1 cKO Mice

SDF-1 “floxed” (SDF-1^{flox}) mice were generated by Dr. Santhosh Ghadge in the laboratory of Prof. Dr. Michael Bader at the MDC. In brief, two loxP sites were introduced upstream and downstream of exon 1 of the SDF-1 gene by homologous recombination upon electroporation of the knockout vector into embryonic stem (ES) cells. Positive ES cells were selected based

on the neomycin resistance cassette of the KO vector and microinjected into blastocysts. Offspring was genotyped and positive animals were backcrossed using C57BL/6N mice. SDF-1$^{flox/flox}$ animals were finally bred with CMV-Cre mice in order to obtain a complete knockout of one SDF-1 allele (SDF-1$^{flox/-}$). For the generation of platelet-specific SDF-1 knockout mice, SDF-1$^{flox/-}$ mice were first bred with animals of the inducible Mx1-Cre line[221] that were provided by the group of Prof. Dr. Carmen Birchmeier-Kohler at the MDC. In these mice, the Cre recombinase is expressed in all hematopoietic cells (including platelets) upon injection of interferon alpha and beta or synthetic double-stranded RNA (poly(I):(C)). SDF-1$^{flox/-}$ controls and SDF-1$^{flox/-}$/Mx1-Cre^{+} cKO mice were analyzed at two time points (7 days and 7 weeks) after i.p. poly(I):(C) injection. PCR and qRT-PCR analysis showed significantly decreased SDF-1 levels in all organs tested (bone marrow, thymus, lung, heart, liver, spleen and kidney) at both time points (data not shown). This finding is due to the expression of Cre in various hematopoietic cell types besides platelets. Furthermore, flow cytometry and colony forming unit (CFU) assays revealed significantly higher hematopoietic stem cell counts in the blood of cKO mice compared to controls at basal levels (data not shown). Due to these basal alterations, which might critically influence repair processes after ischemic cardiac injury, mice of this line were not used further. Instead, SDF-1$^{flox/-}$ mice were bred with Pf4-Cre mice that were purchased from The Jackson Laboratories. Mice of this strain express the Cre recombinase under the control of the platelet factor 4 (Pf4 or CXCL4) promoter, which results in Cre expression only in megakaryocytes and platelets.[222] Resulting SDF-1$^{flox/flox}$ and SDF-1$^{flox/flox}$/Pf4-Cre^{+} offspring were analyzed via PCR with primers that amplify the “floxed” SDF-1 gene (containing loxP sites) as well as the deleted SDF-1 locus (after excision of exon 1 due the presence of a Cre recombinase). As expected, the amplified floxed SDF-1 allele was present in all organs of SDF-1$^{flox/flox}$ and SDF-1$^{flox/flox}$/Pf4-Cre^{+} mice (Fig. 30A). In addition, the knockout band was detected in all organs of SDF-1$^{flox/flox}$/Pf4-Cre^{+} animals at different intensities but was absent in SDF-1$^{flox/flox}$ mice. This finding indicates the expression of the Cre recombinase and subsequent excision of exon 1 of SDF-1 in the organs of Pf4-Cre^{+} mice due to the presence of megakaryocytes and platelets. The weakest bands and therefore lowest Cre expression was found in brain, skeletal muscle and testis, whereas the strongest band was detected in bone marrow. This finding is a first hint that the Pf4-Cre expression is specific based on the high levels of megakaryocytes in the BM. SDF-1$^{flox/flox}$/Pf4-Cre^{+} were further bred to contain one knockout allele. Resulting SDF-1$^{flox/-}$ and SDF-1$^{flox/-}$/Pf4-Cre^{+} mice were used to determine SDF-1 mRNA levels in order to confirm the specificity of the conditional knockout. Quantitative RT-PCR using 28S protein (Mrps28) as well as hypoxanthin-phosphoribosyl-transferase (HPRT) as reference genes revealed similar SDF-1 levels in all organs of control and cKO mice (Fig. 30B). Thus, there was no

unspecific Cre expression in other cell types and tissues detected and SDF-1$^{flox/-}$ and SDF-1$^{flox/-}$/Pf4-Cre^{+} were used as controls and cKO mice in all subsequent experiments.

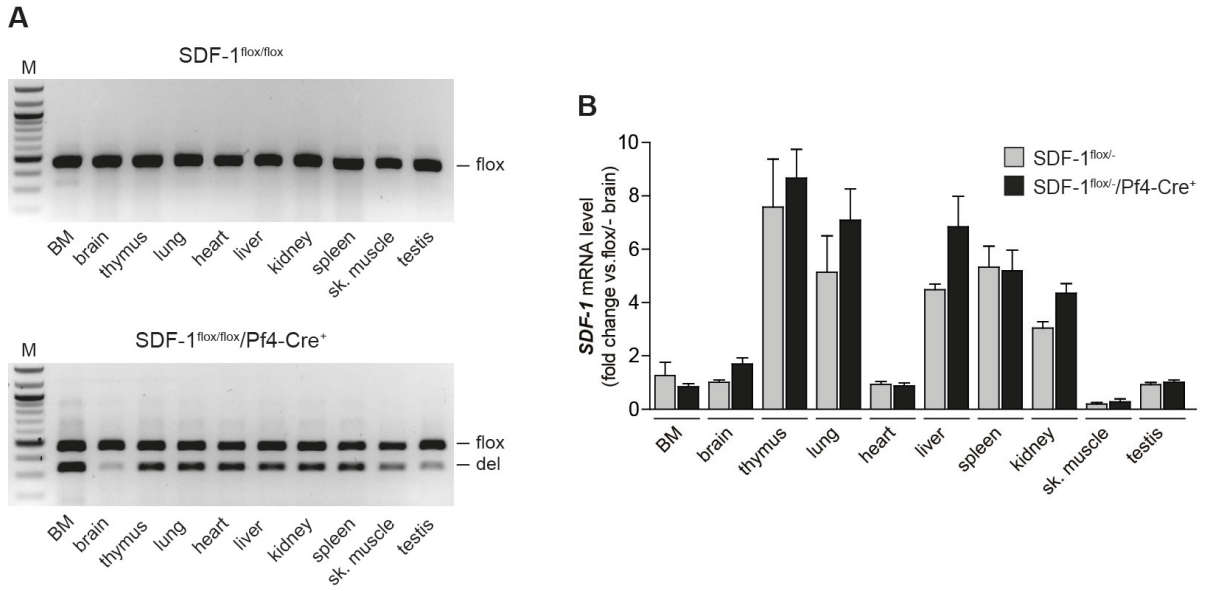

Fig. 30: SDF-1 expression in various organs of platelet cKO mice. A Agarose gel picture of a PCR in various organs of SDF-1$^{flox/flox}$ and SDF-1$^{flox/flox}$/Pf4-Cre^{+} mice using primers that detect the floxed allele ("flox") as well as the knockout allele ("del"). **B** Quantitative RT-PCR analysis of SDF-1 in various organs of SDF-1$^{flox/-}$ (controls) and SDF-1$^{flox/-}$/Pf4-Cre^{+} (cKO) mice. M: 100bp DNA ladder (NEB); BM: bone marrow, Sk. muscle: skeletal muscle.

In order to prove the platelet specificity of the conditional knockout of SDF-1 in these mice, the peripheral blood of the animals was analyzed via flow cytometry. Platelets were labeled via surface expression of CD41, followed by permeabilization of the cells and counterstaining against intracellular SDF-1. This experiment revealed a trend towards less CD41^{+} SDF-1^{+} cell counts in cKO animals in comparison to SDF-1$^{flox/flox}$ and SDF-1$^{flox/-}$ controls (Fig. 31A).

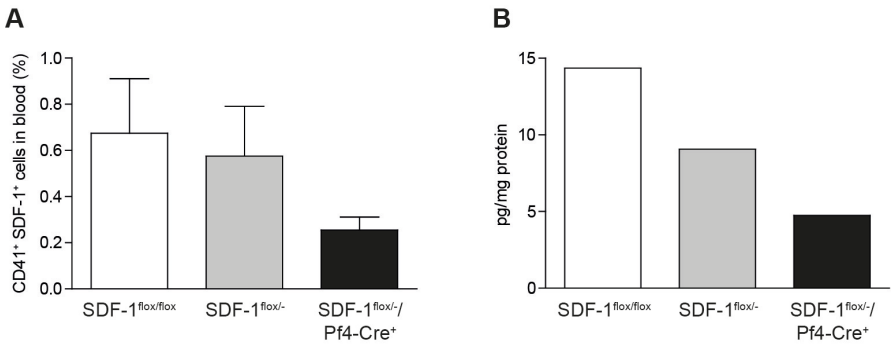

Fig. 31: Confirmation of conditional KO of SDF-1 via flow cytometry and ELISA. A Blood of SDF-1$^{flox/flox}$, SDF-1$^{flox/-}$ and SDF-1$^{flox/-}$/Pf4-Cre^{+} mice was stained for CD41^{+} platelets that also contain intracellular SDF-1. SDF-1$^{flox/flox}$ n=9, SDF-1$^{flox/-}$ n=7, SDF-1$^{flox/-}$/Pf4-Cre^{+} n=9. **B** SDF-1 protein content was measured as pg/mg of complete protein in platelets isolated and pooled from peripheral blood of SDF-1$^{flox/flox}$, SDF-1$^{flox/-}$ and SDF-1$^{flox/-}$/Pf4-Cre^{+} mice. n=5 mice per genotype.

As another approach to confirm the efficacy of the conditional knockout, platelets were isolated from the peripheral blood of the animals and used for RNA or protein extraction. However, the RNA and protein quantities were insufficient to perform qRT-PCR or Western blot analysis. Thus, protein lysates of five animals per genotype were pooled and used for

SDF-1 ELISA measurements. As illustrated in Fig. 31B, SDF-1 levels were highest in SDF-1$^{flox/flox}$ mice, tended to be lower in SDF-1$^{flox/-}$ and were even further decreased in SDF-1$^{flox/-}$/Pf4-Cre^{+} animals. Thus, the conditional knockout of SDF-1 via Pf4-Cre appears to be effective and specific.

4.3.2 Basic Phenotyping of Platelet-Specific SDF-1 cKO Mice

An automated blood composition analysis was carried out in the animals to investigate if the conditional knockout of SDF-1 in platelets alters cell counts or other blood variables at basal levels. As depicted in Fig. 32A, all parameters measured such as levels of white and red blood cells, hemoglobin and hematocrit as well as numbers of lymphocytes, monocytes and granulocytes were not significantly different between SDF-1$^{flox/flox}$, SDF-1$^{flox/-}$ and SDF-1$^{flox/-}$/Pf4-Cre^{+} mice. Also, levels of platelets and the mean platelet volume were not changed between the groups (Fig. 32B).

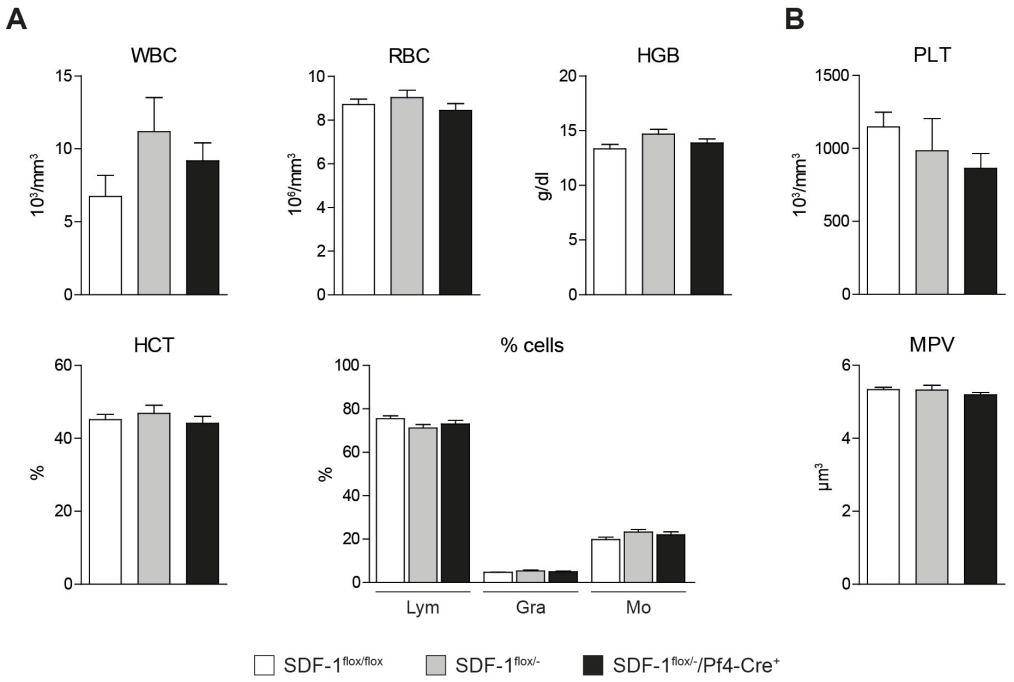

Fig. 32: Basic blood composition analysis in platelet-specific SDF-1 cKO mice. A Levels of white and red blood cells (WBC, RBC), hemoglobin (HGB), hematocrit (HCT) and percentages of lymphocytes (Lym), granulocytes (Gra) and monocytes (Mo) in peripheral blood of SDF-1$^{flox/flox}$, SDF-1$^{flox/-}$ and SDF-1$^{flox/-}$/Pf4-Cre^{+} mice. **B** Platelet (PLT) counts and mean platelet volume (MPV) in blood of all three groups of mice. SDF-1$^{flox/flox}$ n=22, SDF-1$^{flox/-}$ n=10, SDF-1$^{flox/-}$/Pf4-Cre^{+} n=19.

Echocardiography analysis furthermore demonstrated normal cardiac function and morphology in platelet-specific SDF-1 cKO mice compared to controls (Fig. 33).

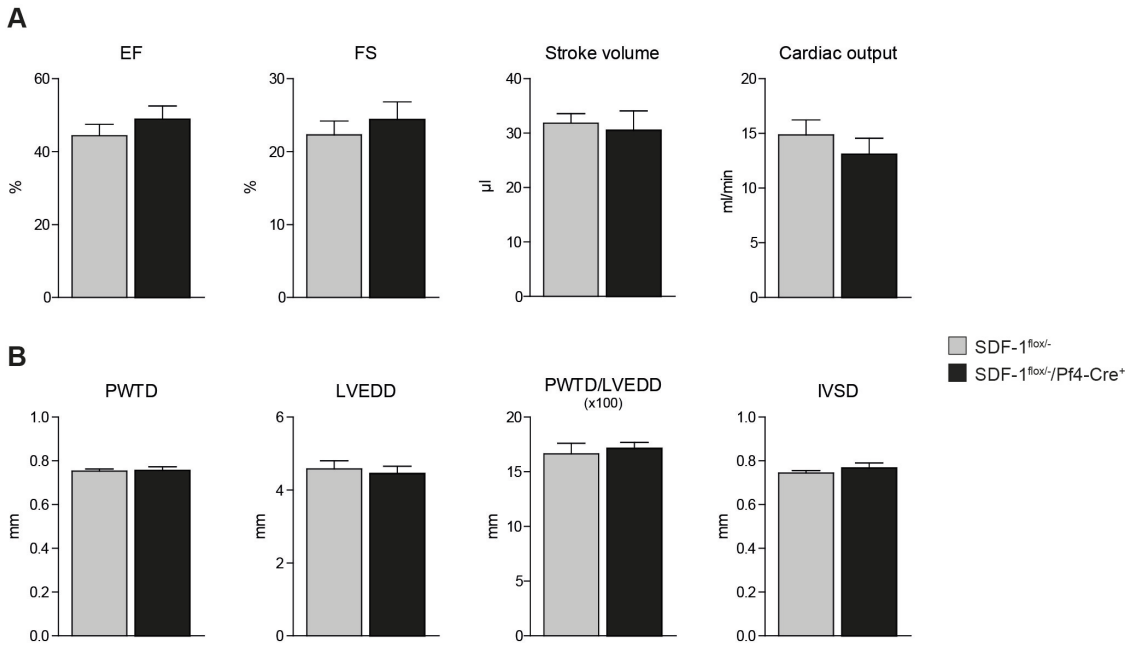

Fig. 33: Characterization of SDF-1 cKO mice by 2-dimensional echocardiography. A Calculated parameters of cardiac function in 10-12 weeks old control (SDF-$1^{flox/-}$) and SDF-1 cKO (SDF-$1^{flox/-}$/Pf4-Cre^{+}) mice. **B** Measurements of LV dimensions. EF: ejection fraction, FS: fractional shortening, PWTD: posterior wall thickness (diastole), LVEDD: left ventricular end-diastolic diameter, IVSD: interventricular septum (diastole); control n=5, SDF-1 cKO n=6.

In summary, the conditional knockout of SDF-1 appears effective and specific in megakaryocytes and platelets and is not sufficient to alter the basal blood composition, cell counts or platelet numbers in these mice. Also, the cardiac function and morphology is normal at basal levels. Thus, the mouse model is suitable to study the functional relevance of platelet-derived SDF-1 on cardiac repair upon ischemic cardiac disease induction.

4.4 A Screening for Novel Factors in the Pathophysiology of Myocardial Infarction

All existing therapeutic options to treat patients with ischemic cardiac diseases are not sufficient to prevent or reverse the persistent cardiac damage after injury and progression to end-stage disease. Furthermore, specific and reliable biomarkers are needed in order to evaluate the disease state of a patient (diagnosis) and to validate its future progression and the success of different treatment options (prognosis). Thus, a microarray study was carried out with the aim to identify new molecules that are involved in the pathophysiology of myocardial infarction and might therefore function as novel therapeutic targets as well as markers for the disease.

4.4.1 Design and Evaluation of the Microarray Study

For the microarray study, myocardial infarction was induced in 10 Wistar Kyoto (WKY) rats by ligation of the LAD. 24 hours later, the hearts were collected and five rats were selected to be used for the screening (subsequently named as “case”) due to a clearly visible, pale infarct area (Fig. 34A). The cardiac tissue was subsequently divided into three parts: healthy left

ventricle (case LV), peri-infarct area (case PI) and myocardial infarct region (case MI). In addition, hearts of five sham-operated WKY rats were dissected and used as controls in the study (control LV).

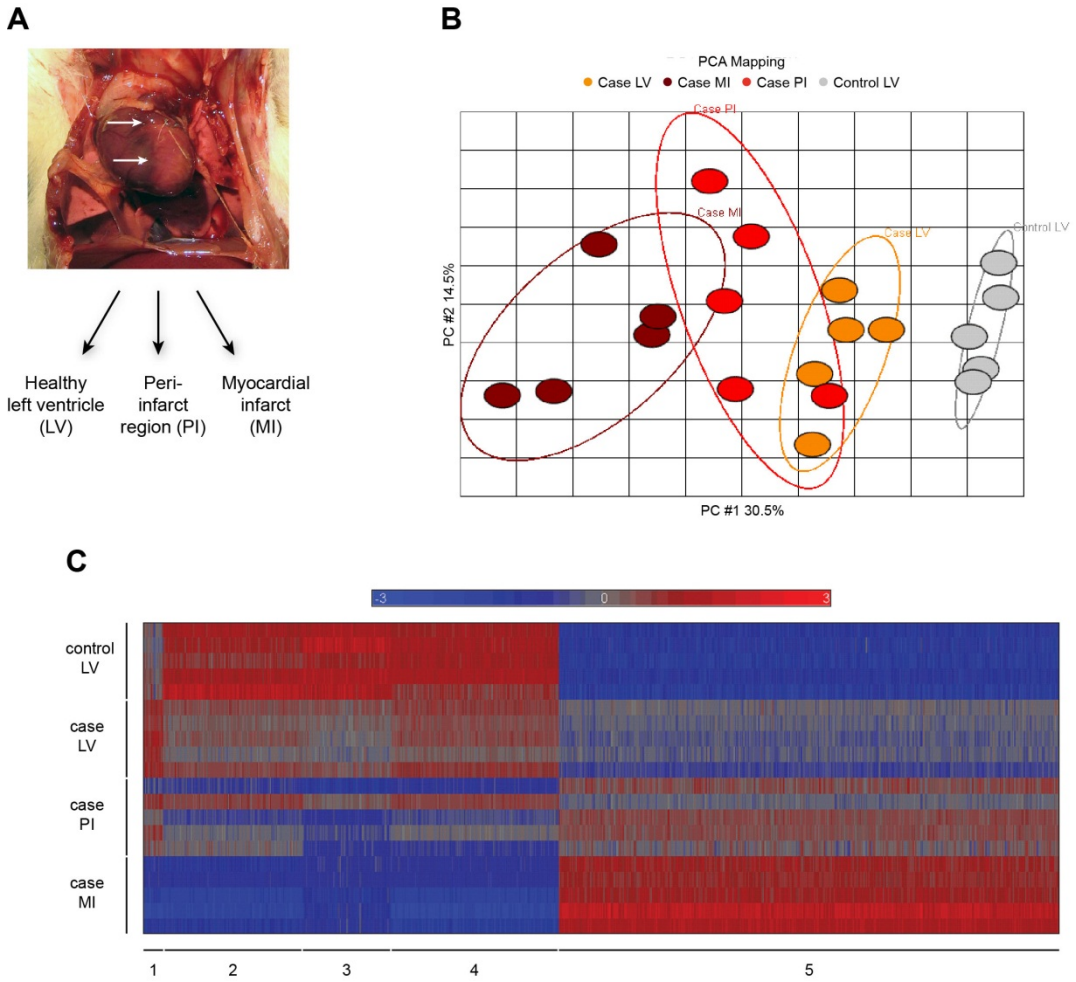

Fig. 34: Microarray screening of cardiac tissue from WKY rats 24 hours after MI. A WKY rat 24 h after myocardial infarct (MI) induction with a clearly visible ischemic infarct region (arrows). Hearts were dissected and subdivided into healthy left ventricle (LV), peri-infarct (PI) and MI region for subsequent microarray analysis. **B** Principle component analysis (PCA) mapping of all 20 arrays from MI rats (case) as well as sham-operated controls. **C** κ-means clustering of all upregulated (red) and downregulated (blue) genes.

Total RNA was isolated from these samples and 200 ng of RNA were used to generate amplified and biotinylated sense-strand DNA for hybridization to a single array and subsequent scanning. GeneChip® Rat Gene 1.0 ST (“sense target”) arrays (Affymetrix) were used that comprise probes for 27,342 genes and therefore allow a gene-level expression profiling of the complete rat genome. Resulting data were analyzed with the help of Dr. Herbert Schulz (group of Prof. Norbert Hübner, MDC) by using the Partek® Genomics Suite™ 6.4 software. This analysis included the removal of ~ 12,000 genes with no detectable or very low expression levels, the Nalimov test to identify and exclude outliers as well as a principle component analysis (PCA) of all arrays. The PCA, which allows the visualization of the microarray data, is depicted in Fig. 34B. It confirms that the healthy part of the infarcted

hearts (case LV) predominantly resembles the pattern of sham-operated animals (control LV), whereas the myocardial infarct region (case MI) displays the greatest difference to the controls. The peri-infarct area is as expected the most heterogeneous group and thus takes an intermediate position. An ANOVA test was applied thereafter in order to compare the means of all genes, followed by the false discovery rate (FDR) control and the Fisher's least significant difference (LSD) post-test. The outcome of this analysis was a list of 4,940 significantly regulated genes that was further classified by a κ-means clustering. As shown in Fig. 34C, this method yielded 5 different clusters. Most genes with expression levels more than 1.5-fold different from case LV were found in the myocardial infarct region (21.23% up- and 25.30% downregulated genes). In contrast, in the peri-infarct area only 1.87% of genes were up- and 3.29% downregulated ≥ 1.5-fold vs. case LV. This difference might be at least partially explained by the severe ischemia in the MI region resulting in many gene expression alterations due to hypoxia and dying cardiomyocytes.

4.4.2 Identification of the Most Promising Candidate

Subsequent analysis of the microarray data focused on genes that were found to be upregulated in the peri-infarct region (mainly represented in cluster # 5). Those candidates with expression levels of case PI / case LV ≥ 1.5-fold were further analyzed by using the SignalP 3.0 server (www.cbs.dtu.dk/services/SignalP/). This server predicts the presence of signal peptides in amino acid sequences and thus allows the identification of transmembrane and/or secreted proteins. By this method, 34 candidates were identified that code for potential membrane and secretory proteins and also possess significantly higher expression levels in the peri-infarct region compared to healthy parts of the LV (Tab. 18). These genes were further analyzed via qRT-PCR in order to confirm the expression pattern obtained from the microarray study.

Table 18: List of candidates analyzed via qRT-PCR. 34 candidate genes with expression levels of case PI / case LV ≥ 1.5-fold were identified that code for potential membrane and secretory proteins. These candidates were further analyzed via qRT-PCR.

Gene symbol	Accession number	Fold-change case PI / case LV
Mmp12	NM_053963	2.79350
RGD1561778	XR_009487	2.01461
Hbegf	NM_012945	1.91036
Lilrb4	NM_001013894	1.89540
Il1rn	NM_022194	1.89153
Emb	NM_053719	1.86550
Ccl12	NM_001105822	1.84690
Itgam	NM_012711	1.82868
Ccl7	NM_001007612	1.82434

Cd53	NM_012523	1.82023
Tgfb2	NM_031131	1.81907
PVR	NM_017076	1.81384
Olr1	NM_133306	1.78594
Serpine1	NM_012620	1.77141
Adamts4	AB042272	1.76835
Cd180	NM_001106405	1.74990
Scn3b	NM_139097	1.73648
Ccl2	NM_031530	1.72872
Msr1	ENSRNOT00000017339	1.72761
Glipr1	NM_001011987	1.71755
Adam12	ENSRNOT00000024974	1.71583
Sele	NM_138879	1.71513
Plau	NM_013085	1.71419
MGC105649	BC086337	1.71202
Gpnmb	NM_133298	1.70431
Gprc5a	NM_001079890	1.68093
Clec5a	NM_001109377	1.65373
Anpep	NM_031012	1.57614
Lrrc25	ENSRNOT00000031692	1.53947
Tfpi2	NM_173141	1.53817
Col12a1	ENSRNOT00000051159	1.53540
Mpeg1	NM_022617	1.52340
Csf2rb	NM_133555	1.51957
Selp	NM_013114	1.50759

The subsequent SYBR© green qRT-PCR studies could validate significantly higher expression levels in the peri-infarct region compared to remote myocardium for 3 out of the 34 genes analyzed: Hbegf, Tgfb2 and GPNMB (Fig. 35). The expression levels of both Hbegf and Tgfb2 were increased approximately 6-fold in the peri-infarct region in relation to control LV, whereas GPNMB was found ~ 17-fold higher in PI compared to control LV.

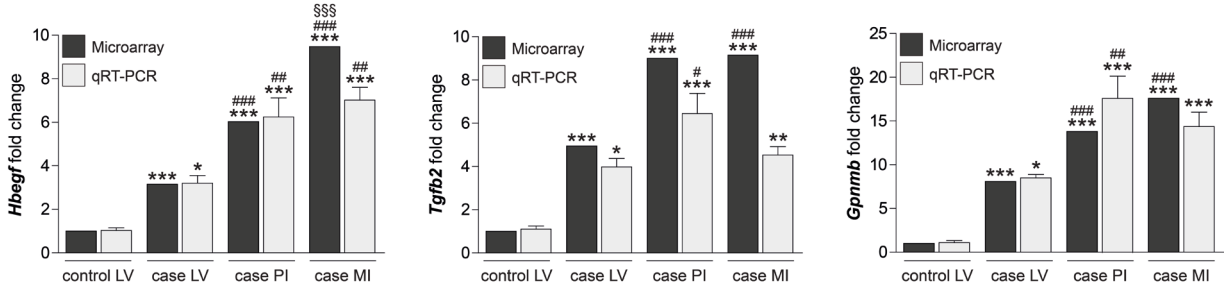

Fig. 35: Quantitative RT-PCR analysis of selected candidates from the microarray study. Expression levels of 3 selected candidates in the left ventricle (LV) of sham controls (control LV) as well as remote LV (case LV), peri-infarct (case PI) and infarct (case MI) region of rats 24 hours after MI and analyzed via qRT-PCR. * (**/***) p<0.05 (0.01/0.001) vs. control LV, # (##/###) p<0.05 (0.01/0.001) vs. case LV, §§§ p<0.001 vs. case PI.

Transforming growth factor beta 2 (Tgfb2) is a cytokine known to be induced after myocardial infarction.[229] It has been further reported that Tgfb2 plays an important role as regulator of cardiac fibrosis and ventricular remodeling.[230] In addition, Tgfb2 knockout mice have been

generated and display embryonic or postnatal lethality due to multiple developmental defects including structural malformations of both ventricles and the ventricular septum of the heart.[231] Heparin-binding EGF-like growth factor (Hbegf), a member of the EGF protein family, is described to be rapidly increased after myocardial infarction.[232,233] Furthermore, its overexpression in the MI border area in rabbit hearts exacerbated remodeling by inducing apoptosis, fibrosis and LV hypertrophy.[234] Hbegf$^{-/-}$ mice mostly die in the first postnatal week and the survivors develop severe heart failure with dilated ventricular chambers and impaired cardiac function.[235] In summary, Tgfb2 and Hbegf have already been described to be involved in cardiac development and pathophysiology. The third candidate gene, glycoprotein (transmembrane) nmb (GPNMB), is a protein first described in 1995 that exists in several isoforms (intracellular, transmembrane and secreted).[167] It has been demonstrated that GPNMB is important for bone remodeling and normal eye function. Furthermore, the glycoprotein is involved in progression of certain types of cancers as well as in fibrotic and regenerative processes after injury in skeletal muscle, liver and kidney. However, the role of GPNMB in cardiac pathophysiology remained unknown. Thus, GPNMB was chosen as an interesting candidate for further *in vitro* and *in vivo* studies in order to clarify its function in the heart.

4.5 Basic Characterization of the Selected Candidate GPNMB

As a first approach to investigate the role of GPNMB in cardiac pathophysiology, its expression pattern in several cardiac disease models was analyzed via qRT-PCR and histological methods. This was followed by the search for a suitable model to study GPNMB *in vivo*, which revealed DBA/2J inbred mice that bear a point mutation in the GPNMB gene.

4.5.1 GPNMB Expression Studies

In order to investigate if GPNMB is involved in cardiac repair processes, its expression levels in experimental models of cardiac hypertrophy (after angiotensin II or isoprenaline infusion) and myocardial infarction were analyzed. Angiotensin II is a peptide hormone that functions as potent vasoconstrictor and thus leads to increased blood pressure. Furthermore, it is an important stimulator of cardiac cell growth upon activation of the G_q protein and protein kinase C. As shown in Fig. 36A, GPNMB mRNA levels are slightly (~ 1.5-fold) but significantly higher in cardiac tissue of wild type mice treated with angiotensin II for two weeks in comparison to sham-treated controls. Isoprenaline (or isoproterenol) is a non-selective beta-adrenergic agonist. It exerts its pro-hypertrophic actions by stimulating β_1-adrenoreceptors in the heart, which results in positive chronotropic, inotropic and dromotropic effects. In WT mice treated with isoprenaline for two weeks, GPNMB levels are ~ 2-fold higher compared to sham controls. Furthermore, cardiac tissue of WT mice before as well as 2, 7 and 28 days after induction of myocardial infarction was analyzed. GPNMB levels were highly (~ 25-fold)

upregulated already 2 days after MI (Fig. 36B). This effect was even further augmented 7 days after infarct revealing ~ 300-fold higher GPNMB expression compared to controls.

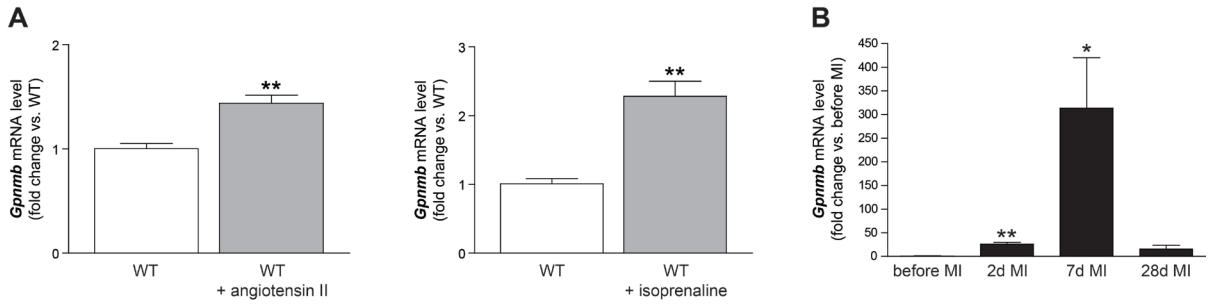

Fig. 36: GPNMB expression in cardiac disease models. A GPNMB mRNA levels in cardiac tissue of wild type (WT) mice treated for 2 weeks with angiotensin II or isoprenaline. **B** GPNMB expression in cardiac tissue of WT mice before and 2, 7 or 28 days (d) after induction of myocardial infarction (MI). * p<0.05, ** p<0.01; WT n=4, WT + angiotensin II n=4, WT + isoprenaline n=5, MI n=3 per group.

To identify cell types in the heart that express GPNMB as well as the source of the upregulation of the protein after ischemic injury, immunofluorescence stainings were performed. As shown in Fig. 37, no GPNMB staining was visible in heart sections of healthy (sham-operated) animals as well as early (two days) after MI induction.

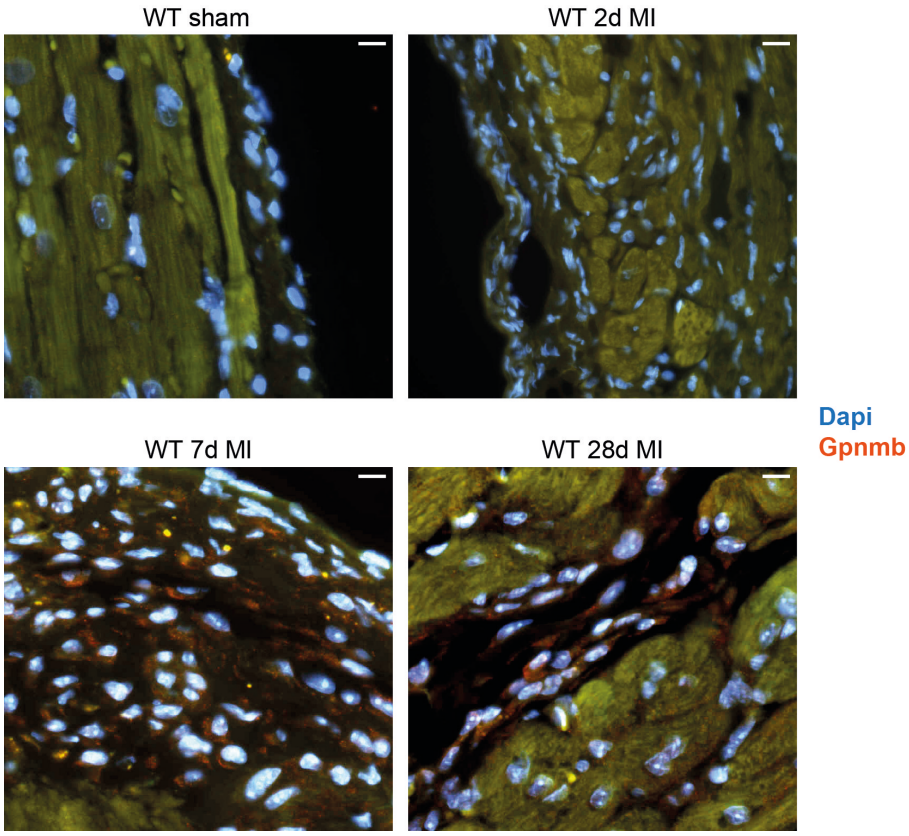

Fig. 37: GPNMB immunostaining in WT hearts after MI. Immunofluorescence staining of GPNMB (red) in cardiac tissue sections of wild type (WT) mice 2, 7 and 28 days (d) after myocardial infarction (MI) as well as of sham-operated controls. Scale bar=50 µm; 40x magnification; Dapi: nuclear stain (blue).

However, there were GPNMB-positive cells detectable at later time points (7 and 28 days) after MI. These cells appeared small and were predominantly found in the border zone and

the infarct region itself. In summary, the basal expression of GPNMB in the heart seems to be marginal. The strong induction of GPNMB, which was detected after myocardial infarction, might be due to immune cells (e.g. macrophages) that express high amounts of the protein and infiltrate the ischemically injured areas of the heart. This process might be part of the inflammatory and repair processes after cardiac injury.

4.5.2 DBA/2J Mice as Model to Study GPNMB *in vivo*

For further functional characterization of GPNMB *in vivo*, DBA/2J inbred mice were selected due to a naturally occurring point mutation (R150X) in the GPNMB gene.[193] This nonsense mutation leads to significantly reduced GPNMB mRNA levels and absent protein. As controls, DBA/2J-Gpnmb+ mice were chosen that had been bred to carry a wild type version of the GPNMB allele (Fig. 38).[195]

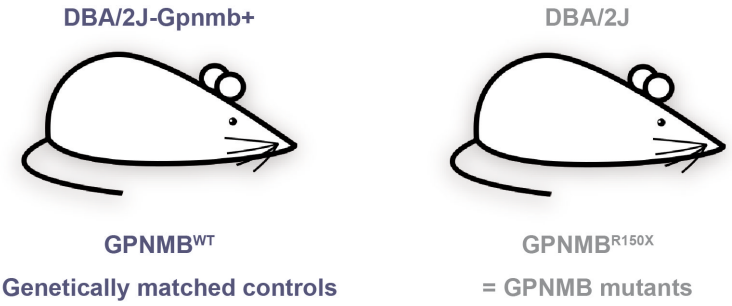

Fig. 38: DBA/2J mouse strains used to study GPNMB *in vivo*. DBA/2J mice were selected due to a naturally occurring point mutation (R150X) of GPNMB resulting in absent protein (=GPNMB mutants). DBA/2J-Gpnmb+ mice that carry a wild type version of the GPNMB allele were used as controls.

Both DBA/2J mouse strains were purchased from the Jackson Laboratories. After establishing breeding colonies, an expression analysis was performed in various organs of mice from both strains. As depicted in Fig. 39, GPNMB mRNA levels were drastically reduced in all organs of DBA/2J mice compared to DBA/2J-Gpnmb+ animals. This finding is likely due to nonsense-mediated mRNA decay.[197,236]

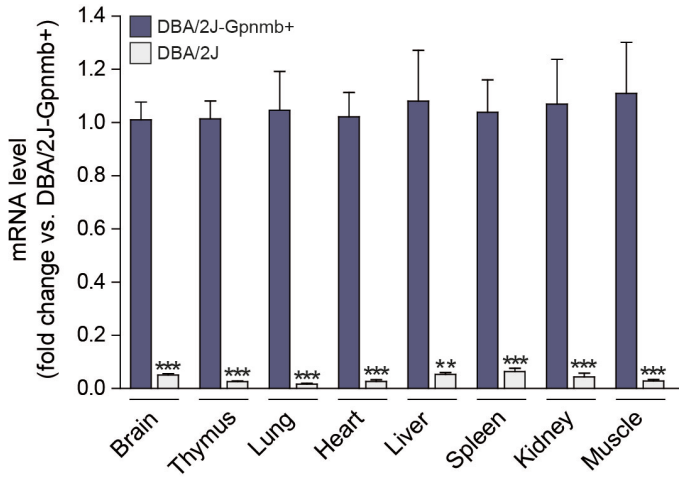

Fig. 39: GPNMB expression in different organs of both DBA/2J strains. GPNMB mRNA levels in different organs of DBA/2J-Gpnmb+ (WT) and DBA/2J (Mut) mice. ** (***) p<0.01 (0.001) vs. WT; WT and Mut mice n=6.

4.5.3 Basic Characterization of DBA/2J Mouse Strains

The cardiovascular phenotype of both DBA/2J strains is poorly described despite the finding that the mutant mice possess a low susceptibility to develop atherosclerotic lesions in the aorta.[237] Thus, two-dimensional echocardiographic measurements were performed in DBA/2J-Gpnmb+ and DBA/2J mice at different ages in order to examine if the absence of functional GPNMB affects parameters of cardiac function and LV dimensions. As shown in Fig. 40, animals of both strains revealed no difference of functional and morphological parameters at 3, 7 and 11 months of age. In conclusion, the mutation of GPNMB in DBA/2J mice alone is not sufficient to alter the cardiac physiology under basal conditions.

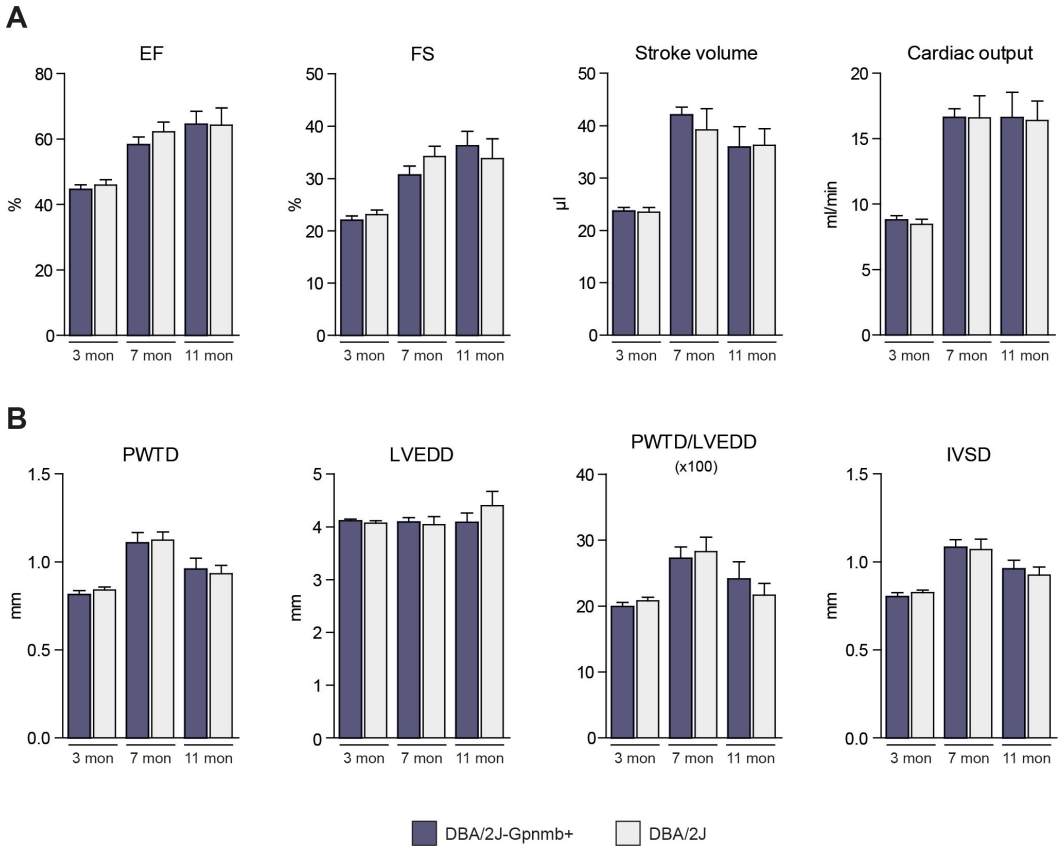

Fig. 40: Basic cardiac function and morphology in aging DBA/2J mouse strains. Parameters of cardiac function (**A**) and LV dimensions (**B**) in 3, 7 and 11 months (mon) old DBA/2J-Gpnmb+ (WT) and DBA/2J (Mut) mice. EF: ejection fraction, FS: fractional shortening, PWTD: posterior wall thickness (diastole), LVEDD: left ventricular end-diastolic diameter, IVSD: interventricular septum (diastole); 3 mon WT n=44, 3 mon Mut n=46, 7 and 11 mon n=7 per group.

4.5.4 Altered Macrophage Phenotype in DBA/2J Mice

GPNMB expression was found to be marginal in hearts at basal levels, but strongly induced in cardiac disease models such as myocardial infarction. Thereby, GPNMB staining was detected in small cells in the MI and PI region of ischemically injured hearts. These GPNMB-positive cells may represent infiltrating leukocytes such as monocytes/macrophages that actively participate in repair processes after injury.[215] In line with this, it was shown that GPNMB is highly upregulated in macrophages after ischemic kidney injury and that the

glycoprotein is necessary for proper function of the cells.[211] A study by Li *et al*. furthermore demonstrated that the stimulation of BM-derived macrophages with interferon (IFN)-γ or treatment with LPS downregulated GPNMB expression. In order to test if the mutation of GPNMB in DBA/2J mice influences the differentiation and function of macrophages and might thereby affect tissue repair after injury, BM cells were isolated from DBA/2J-Gpnmb+ and DBA/2J mice, cultured for one week in the presence of M-CSF for macrophage differentiation followed by treatment with either IFN-γ (that leads to maturation of pro-inflammatory macrophages) or interleukin (IL)-4 (that results in maturation of reparative macrophages). GPNMB expression was determined in whole cell lysates after 4 hours of treatment. As expected, this analysis revealed almost no detectable GPNMB levels in macrophages from DBA/2J mutant mice and confirmed previous findings of significantly lower GPNMB levels in macrophages from DBA/2J-Gpnmb+ WT mice treated with IFN-γ.[211] In contrast, IL-4 treatment did not alter GPNMB expression compared to unstimulated cells (Fig. 41).

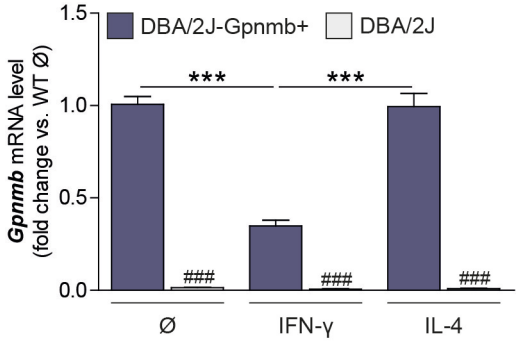

Fig. 41: GPNMB expression in BM-derived macrophages of DBA/2J mouse strains. qRT-PCR analysis of GPNMB mRNA levels in bone marrow (BM)-derived macrophages after one week of culture with M-CSF and 4 hours of treatment with interferon (IFN)-γ, interleukin (IL)-4 or without stimulation (Ø). *** p<0.001; both genotypes n=9.

Furthermore, expression levels of marker genes and chemokines that are differentially expressed in macrophage subpopulations were analyzed in cell lysates after 4 hours of treatment. As depicted in Fig. 42, iNOS as M1 marker gene was only detected in macrophages treated with IFN-γ, whereas the M2 marker arginase-1 was expressed exclusively in cells after treatment with IL-4. These findings confirm the efficacy of IFN-γ or IL-4 treatment for differentiation of both macrophage subsets. In addition, levels of the chemokines CXCL9, CXCL10 and CXCL11 that are typically secreted by pro-inflammatory macrophages were examined. No difference of expression was observed between macrophages from DBA/2J-Gpnmb+ and DBA/2J mice (Fig. 42A). In contrast, levels of CCL17 and CCL22, which are known to be produced and secreted by patrolling or reparative macrophages, were higher in DBA/2J mice compared to DBA/2J-Gpnmb+ controls (Fig. 42B).

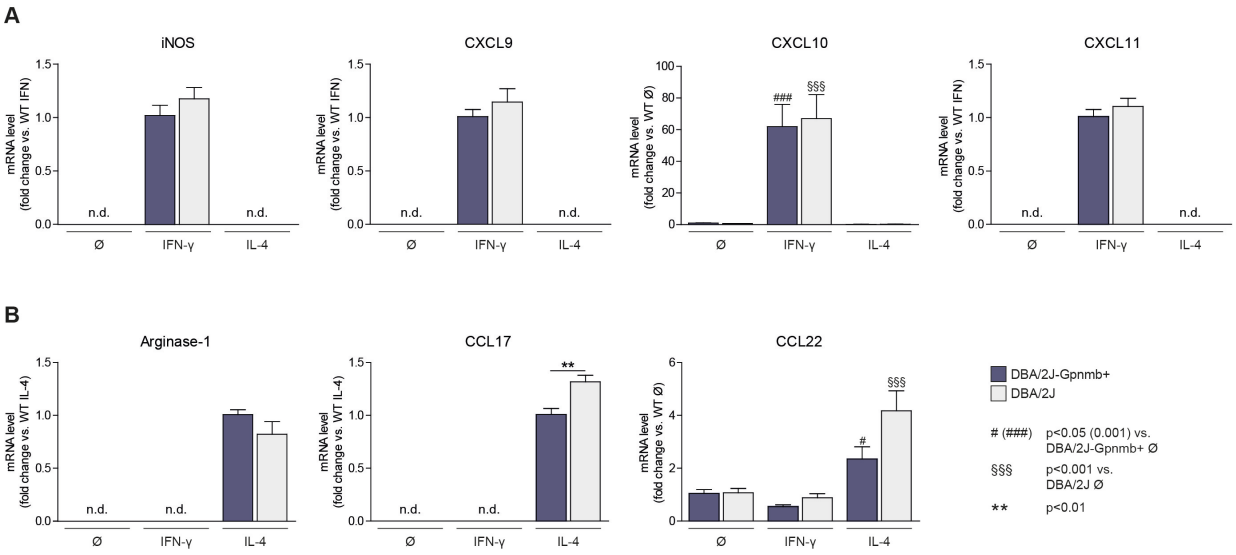

Fig. 42: Expression of M1 and M2 marker genes in macrophages from DBA/2J mouse strains. mRNA levels of M1 (**A**) and M2 (**B**) markers in BM-derived macrophages from DBA/2J-Gpnmb+ (WT) and DBA/2J (Mut) mice treated for 4 hours with interferon (IFN)-γ, interleukin (IL)-4 or without stimulation (Ø). iNOS, CXCL9 and CXCL11 expression was only detected in IFN-γ-treated cell lysates and calculated as fold change of WT cells treated with IFN-γ. Expression of arginase-1 and CCL17 was only detected in IL-4-treated macrophages and calculated as fold change of WT cells treated with IL-4. n.d.: not detected; WT and Mut n=9.

24 hours after treatment with IFN-γ or IL-4, supernatants of macrophages were collected and used to determine IL-10 and IL-12 levels via ELISA. IL-12 is secreted by pro-inflammatory macrophages and IL-10 is known to be produced by patrolling or reparative macrophages. Similar levels of both interleukins were found in supernatants of macrophages from DBA/2J-Gpnmb+ and DBA/2J animals (Fig. 43).

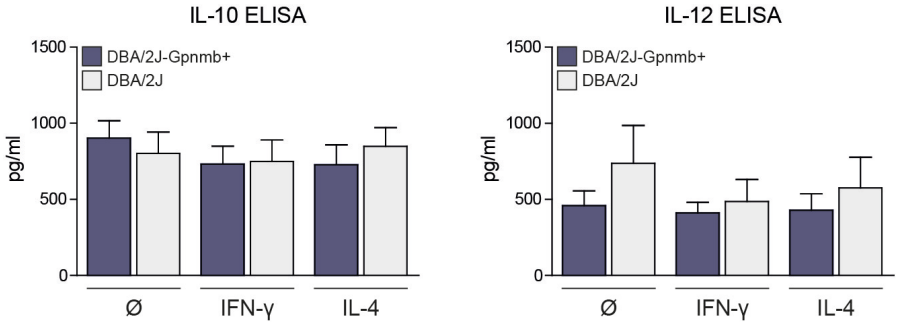

Fig. 43: IL-10 and IL-12 levels in supernatants of macrophages from DBA/2J mouse strains. ELISA measurements of IL-10 and IL-12 in supernatants of macrophages from DBA/2J-Gpnmb+ (WT) and DBA/2J (Mut) macrophages after 24 hours of treatment with interferon (IFN)-γ, interleukin (IL)-4 or without stimulation (Ø). WT and Mut n=9.

In summary, the *in vitro* studies of BM-derived macrophages from both DBA/2J mouse strains confirmed lower GPNMB levels in pro-inflammatory M1 macrophages after treatment with interferon-γ. Moreover, no phenotypic difference was found for this subset regarding production and secretion of chemokines and cytokines. On the other hand, macrophages isolated from DBA/2J mice and stimulated with IL-4 expressed higher levels of the chemokine CCL17 and showed a trend towards higher expression of CCL22 compared to cells from

DBA/2J-Gpnmb+ controls. Thus, the phenotype of reparative M2 macrophages seems to be altered in the absence of GPNMB.

4.6 GPNMB as Novel Therapeutic Target and Biomarker of Ischemic Cardiac Diseases

In order to study the functional relevance of GPNMB in cardiac pathophysiology *in vivo*, DBA/2J-Gpnmb+ and DBA/2J mice were subjected to models of cardiac hypertrophy (via infusion of isoprenaline for two weeks) and myocardial infarction (via coronary artery ligation for four weeks).

4.6.1 Cardiac Function and Morphology in DBA/2J Mouse Strains after Isoprenaline Treatment

Since there was no difference of cardiac function and dimensions of the left ventricle between DBA/2J-Gpnmb+ and DBA/2J mice under basal conditions, animals of both strains were treated with the β-adrenergic agonist isoprenaline in order to induce a hypertrophic change of the heart. This approach was chosen because the expression levels of GPNMB were found to be higher after isoprenaline infusion in comparison to treatment with angiotensin II in WT mice (see chapter 4.5.1). This observation suggests that GPNMB might be of relevance upon cardiac hypertrophy induction via isoprenaline. To test this hypothesis, mice were treated with 30 mg/kg/day isoprenaline for two weeks via micro-osmotic pumps (Alzet®) that had been implanted subcutaneously. The outcome of this experiment was monitored via blood composition analysis, echocardiography, qPCR and histological methods. In order to prove the efficiency of the approach, heart weight / tibia length ratios were determined in wild type and mutant mice after two weeks of sham or isoprenaline treatment. DBA/2J-Gpnmb+ and DBA/2J mice developed significantly higher relative heart weights under isoprenaline infusion indicating hypertrophic changes of the organ (Fig. 44). However, no difference was found between both genotypes.

Fig. 44: Relative heart weights in DBA/2J mouse strains after isoprenaline infusion. Heart weight / tibia length ratios were determined in DBA/2J-Gpnmb+ (WT) and DBA/2J (Mut) mice after two weeks of sham or isoprenaline treatment. ### p<0.001 vs. WT sham, § p<0.05 vs. Mut sham; sham n=3 per group, WT 2w iso n=8, Mut 2w iso n=6.

The functional outcome of the treatment was examined via echocardiography. Measurements were carried out before and after one as well as two weeks of isoprenaline treatment. As illustrated in Fig. 45, parameters of cardiac function such as fractional shortening, ejection fraction, stroke volume and cardiac output were similar between both groups at basal levels and increased significantly as a result of the β-adrenergic stimulation. However, the responses of DBA/2J-Gpnmb+ and DBA/2J hearts to the treatment were indistinguishable.

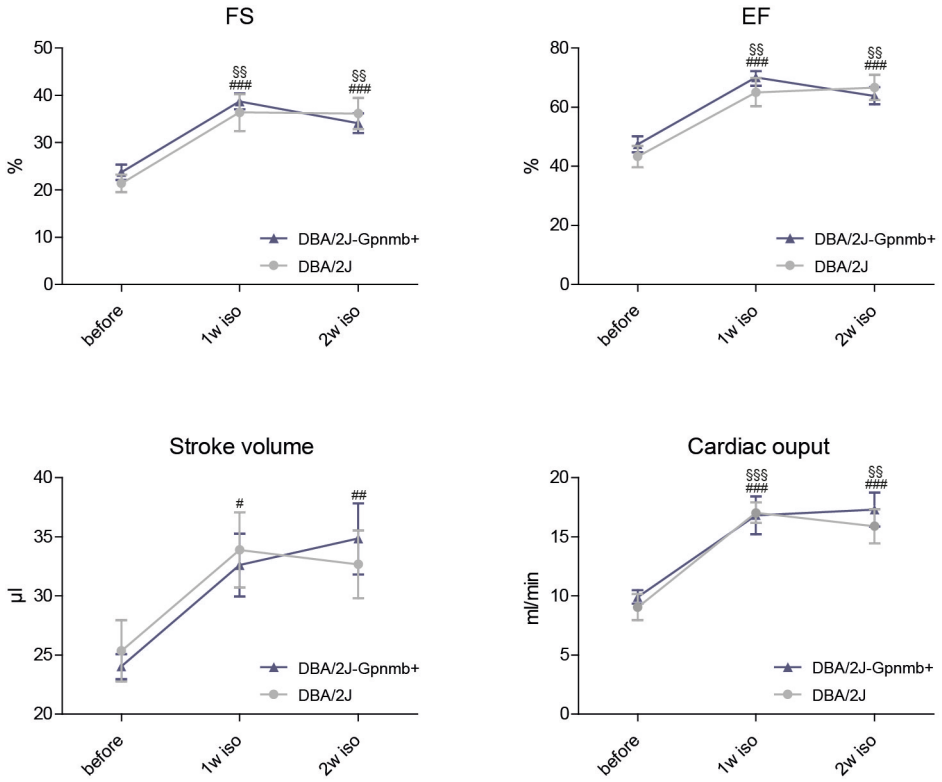

Fig. 45: Cardiac function in DBA/2J mouse strains after isoprenaline treatment. Measures of fractional shortening (FS), ejection fraction (EF), stroke volume and cardiac output before as well as after one and two weeks (w) of sham or isoprenaline (iso) treatment. # (##, ###) p<0.05 (0.01, 0.001) vs. DBA/2J-Gpnmb+ before, §§ (§§§) p<0.01 (0.001) vs. DBA/2J before; sham n=3 per group, DBA/2J-Gpnmb+ 2w iso n=8, DBA/2J 2w iso n=6.

The dimensions of the left ventricle such as posterior wall (PWT) and interventricular septum thickness (IVS) or left ventricular diameter (LVEDD, LVESD) were also recorded via echocardiography in diastole and systole. Changes of these parameters indicate hypertrophic and/or dilative remodeling of the heart. The measurements revealed an expected increase of PWTD and IVSD in DBA/2J-Gpnmb+ wild type animals as result of the isoprenaline treatment (Fig. 46). In contrast, the hypertrophic response was less pronounced in DBA/2J mutant mice and thus PWTD and IVSD were not significantly altered by the treatment in these animals compared to sham controls. Both groups showed no change of LVEDD. As a consequence, the PWTD/LVEDD ratio was slightly, but not significantly higher in DBA/2J-Gpnmb+ mice at one and two weeks of treatment. All depicted results were recorded in diastole. The same tendencies were found in systole (data not shown).

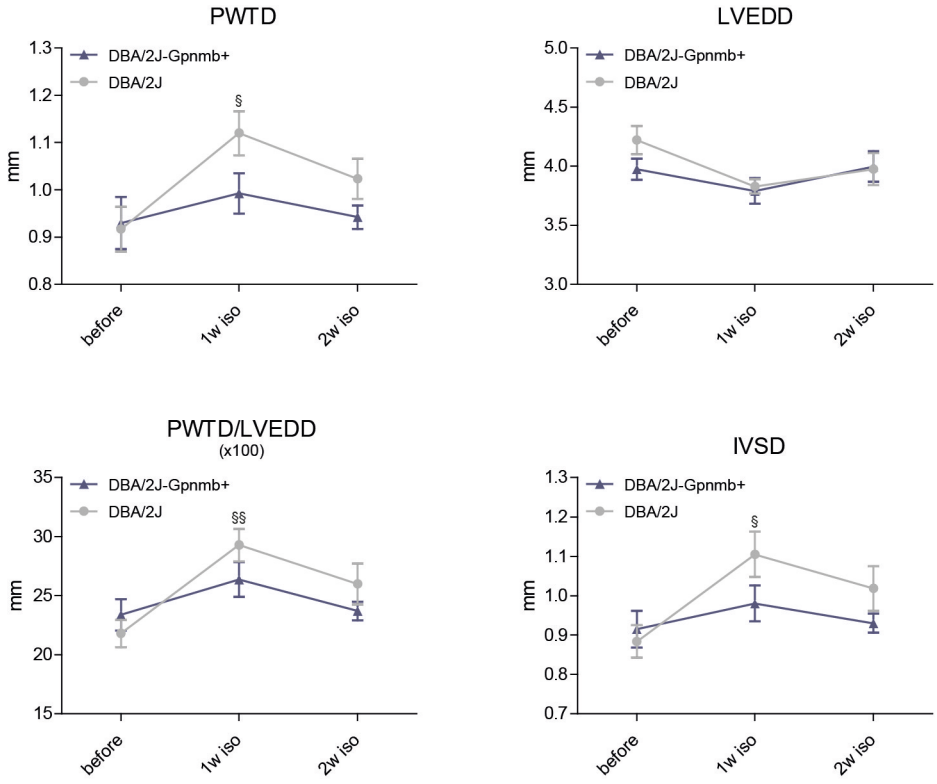

Fig. 46: Cardiac dimensions in DBA/2J mouse strains after isoprenaline treatment. Measures of posterior wall thickness (PWTD), LV end-diastolic diameter (LVEDD), interventricular septum (IVSD) and PWTD/LVEDD ratio in diastole before as well as after one and two weeks (w) of sham or isoprenaline (iso) treatment. § (§§) p<0.05 (0.01) vs. DBA/2J before; sham n=3 per group, DBA/2J-Gpnmb+ 2w iso n=8, DBA/2J 2w iso n=6.

4.6.2 Blood Composition in DBA/2J Mouse Strains after Isoprenaline Treatment

The blood composition of all four groups of animals was analyzed. The automated measurement yields information about levels of white and red blood cells (WBC and RBC), platelets (PLT), hemoglobin (HGB) and hematocrit (HCT). All these parameters did not differ significantly between DBA/2J-Gpnmb+ and DBA/2J mice after sham and/or isoprenaline treatment (Fig. 47A). In addition, numbers of lymphocytes (Lym), monocytes (Mo) and granulocytes (Gra) were determined. Whereas lymphocyte and granulocyte levels were not changed between the groups, monocyte numbers were found to be significantly lower in DBA/2J mice after 2 weeks of isoprenaline infusion compared to treated DBA/2J-Gpnmb+ controls (Fig. 47B).

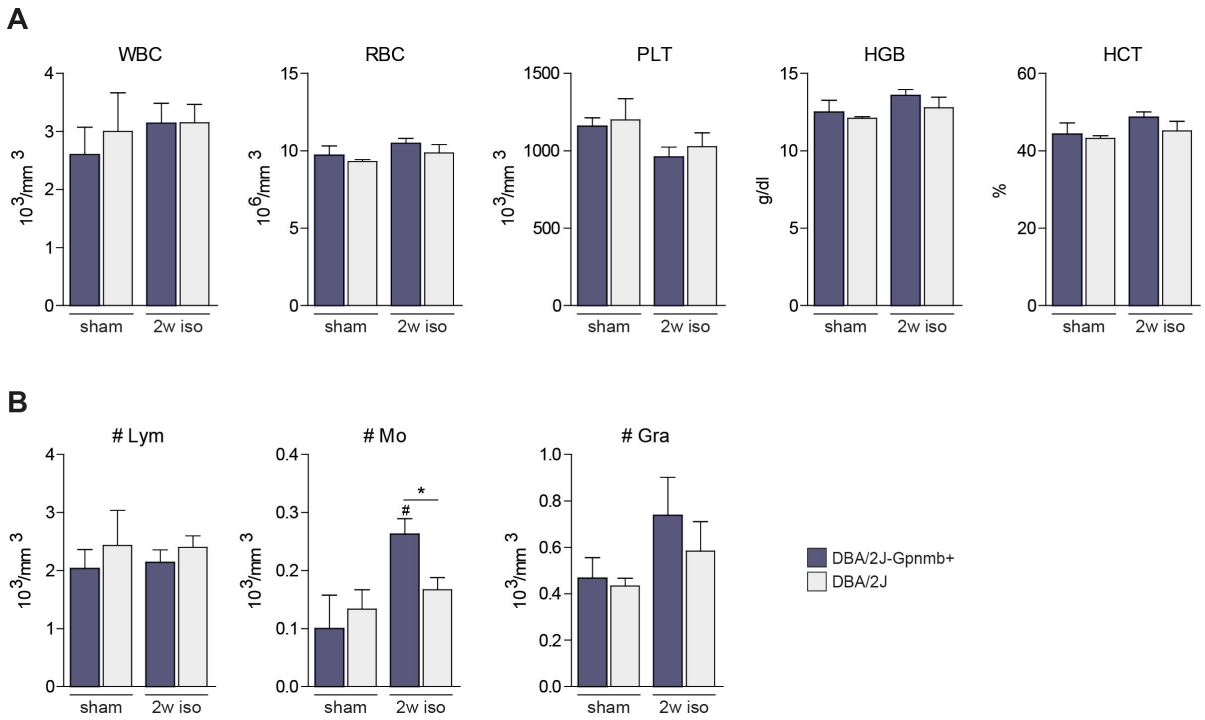

Fig. 47: Blood composition analysis in DBA/2J mouse strains after isoprenaline treatment. A Numbers of white and red blood cells (WBC and RBC), platelets (PLT), hemoglobin (HGB) and hematocrit (HCT) in blood samples of DBA/2J-Gpnmb+ and DBA/2J mice after 2 weeks (w) of sham or isoprenaline (iso) treatment. **B** Numbers of lymphocytes (Lym), monocytes (Mo) and granulocytes (Gra). # p<0.05 vs. DBA/2J-Gpnmb+ sham, * p<0.05; sham n=3 per group, DBA/2J-Gpnmb+ 2w iso n=8, DBA/2J 2w iso n=6.

4.6.3 Expression and Histological Analysis in DBA/2J Mouse Strains after Isoprenaline Treatment

Cardiac RNA was extracted from sham- and isoprenaline-treated animals and used for gene expression studies via qRT-PCR. Levels of ANP and BNP were slightly increased in DBA/2J-Gpnmb+ mice and not significantly different from DBA/2J mice (Fig. 48). On the other hand, the fibrosis markers collagen 1a1, collagen 3 and fibronectin were clearly induced in mice of both genotypes as a consequence of isoprenaline treatment. Collagen levels were found to be similar in both groups, whereas fibronectin was significantly decreased in DBA/2J mutant mice in comparison to WT controls.

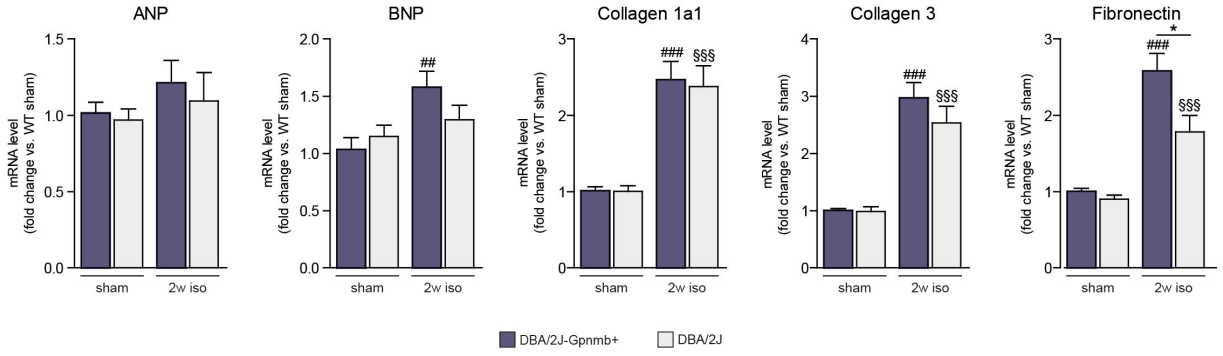

Fig. 48: Expression of hypertrophy and fibrosis genes in DBA/2J mouse strains after isoprenaline treatment. qRT-PCR analysis in heart tissue of DBA/2J-Gpnmb+ (WT) and DBA/2J (Mut) mice after two weeks (w) of sham or isoprenaline (iso) treatment. The hypertrophy markers ANP and BNP as well as the fibrosis genes collagen 1a1, collagen 3 and fibronectin were analyzed. ## (###) p<0.01 (0.001) vs. WT sham, §§§ p<0.001 vs. Mut sham, * p<0.05; sham n=3 per group, DBA/2J-Gpnmb+ 2w iso n=8, DBA/2J 2w iso n=6.

Sirius red stainings were carried out in cardiac sections of DBA/2J-Gpnmb+ and DBA/2J mice in order to quantify the collagen content of the hearts. This analysis revealed similar collagen levels in the sham groups and in both DBA/2J groups after 2 weeks of isoprenaline treatment thus confirming the qRT-PCR results (Fig. 49).

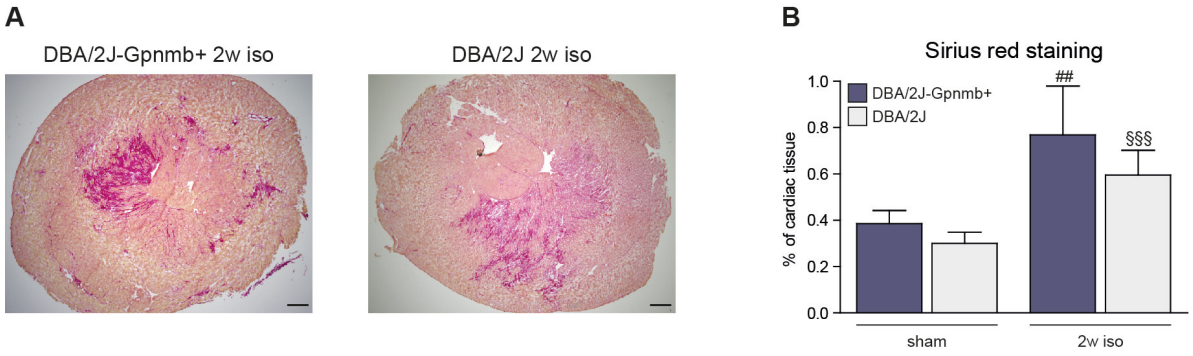

Fig. 49: Sirius red staining in DBA/2J mouse strains after isoprenaline treatment. A Representative pictures of sirius red-stained transverse heart sections from DBA/2J-Gpnmb+ (WT) and DBA/2J (Mut) mice after 2 weeks (w) of isoprenaline (iso) treatment. Scale bar=500 µm; 2x magnification. **B** Quantification of sirius red staining in sham- or isoprenaline-treated mice. ## p<0.01 vs. WT sham, §§§ p<0.001 vs. Mut sham; 3 sections per animal were analyzed; sham n=3 per group, DBA/2J-Gpnmb+ 2w iso n=8, DBA/2J 2w iso n=6.

The blood composition analysis had revealed significantly lower monocyte numbers in blood of DBA/2J mice compared to WT controls. This difference suggests the possibility of altered monocyte infiltration to and macrophage composition in the heart. Therefore, heart lysates were used to determine levels of general macrophage markers as well as genes specifically expressed in pro-inflammatory (iNOS, IL-6, IL-12) or reparative (arginase-1, ABCA1, IL-10) macrophages. As shown in Fig. 50, the expression of the general macrophage marker F4/80 was similarly increased in both groups after two weeks of treatment. Furthermore, IL-6 was significantly increased, whereas IL-12 was not changed and iNOS was slightly decreased in both groups compared to sham controls. None of these M1 genes was differentially expressed between DBA/2J-Gpnmb+ and DBA/2J mice. The M2 markers arginase-1 (Arg), ABCA1 and IL-10 were significantly induced under cardiac hypertrophy. Levels of Arg and ABCA1 were not different in both treated groups, whereas IL-10 expression was found to be significantly higher in DBA/2J mutant mice compared to DBA/2J-Gpnmb+ controls.

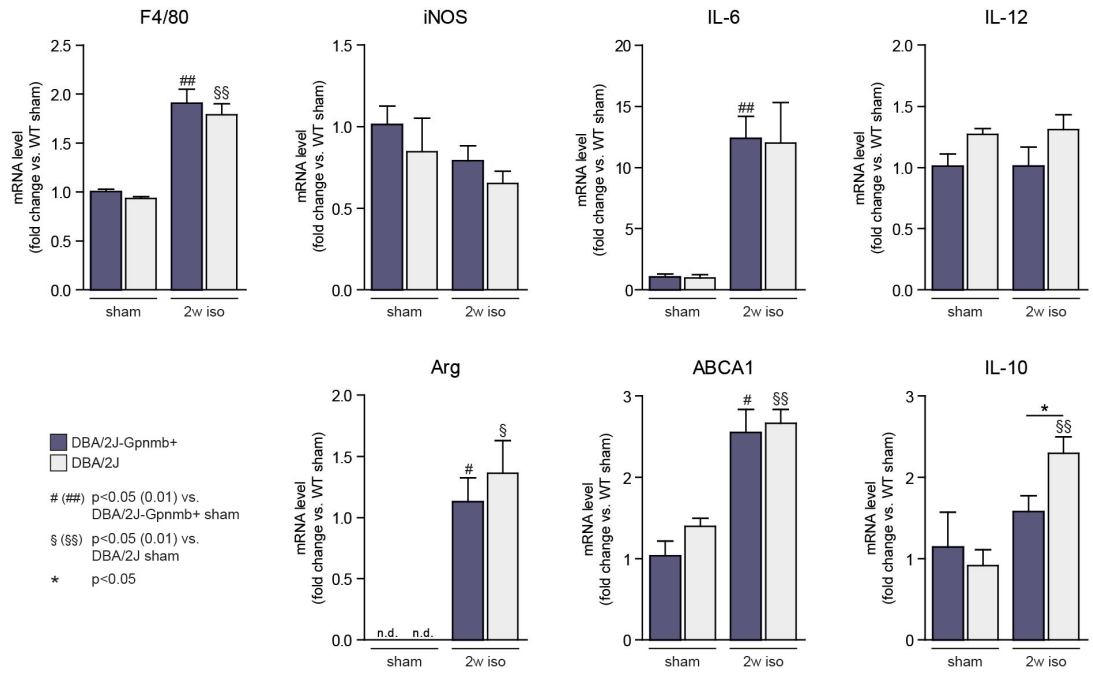

Fig. 50: Expression of macrophage marker genes in DBA/2J mouse strains after isoprenaline treatment. qRT-PCR analysis in heart tissue of DBA/2J-Gpnmb+ (WT) and DBA/2J (Mut) mice after two weeks (w) of sham or isoprenaline (iso) treatment. The general macrophage marker F4/80, the M1 markers iNOS, IL-6 and IL-12 (upper panel) as well as the M2 markers arginase-1 (Arg), ABCA1 and IL-10 (lower panel) were analyzed. Sham n=3 per group, WT 2w iso n=8, Mut 2w iso n=6.

Moreover, macrophage numbers were analyzed via immunofluorescent stainings using an anti-mac-2 (-galectin-3) antibody. As illustrated in Fig.51, levels of mac-2-positive cells were significantly increased in both DBA/2J mouse after 2 weeks of isoprenaline treatment compared to sham controls. However, no difference of macrophage numbers was found between treated DBA/2J-Gpnmb+ WT and DBA/2J mutant mice.

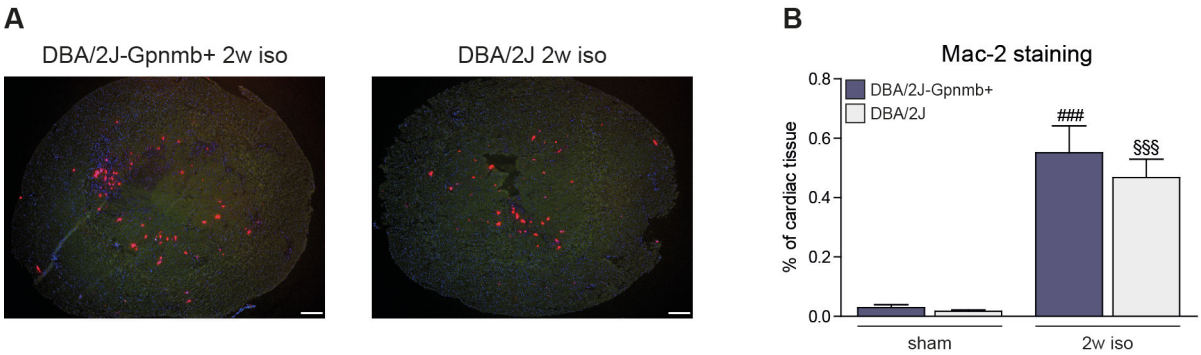

Fig. 51: Macrophage numbers in DBA/2J mouse strains after isoprenaline treatment. A Representative pictures of transverse heart sections from DBA/2J-Gpnmb+ (WT) and DBA/2J (Mut) mice after immunofluorescence staining using an anti-mac-2 antibody. Scale bar=500 µm; 2x magnification. **B** Quantification of mac-2 staining after 2 weeks (w) of sham or isoprenaline (iso) treatment. 3 sections per animal were analyzed; sham n=3 per group, WT 2w iso n=8, Mut 2w iso n=6.

In conclusion, the treatment of DBA/2J-Gpnmb+ and DBA2J mice with isoprenaline (30mg/kg/day) for two weeks was sufficient to induce a hypertrophic response of the heart with increased heart weight / tibia length ratios, thicker posterior wall and interventricular septum of the heart and higher expression levels of hypertrophic marker genes. Furthermore, the function of the heart (measured as fractional shortening and ejection fraction) was

improved in mice of both strains under isoprenaline infusion. This finding might be due to the development of compensatory hypertrophy as response to the β-adrenergic stimulus. The only significant differences between DBA/2J-Gpnmb+ and DBA/2J mice upon isoprenaline treatment were related to fibrosis and monocyte/macrophage infiltration. Whereas sirius red stainings revealed similar levels of collagen deposition in both DBA/2J strains, the mRNA level of fibronectin was lower in DBA/2J mutant mice. Also, monocyte numbers were decreased in the blood of these mice. On the other hand, the general macrophage marker F4/80 and all M1 macrophage genes tested were not differently expressed in the hearts of both groups. Moreover, immunostainings revealed no difference in macrophage numbers in the heart. Only the expression of the M2 macrophage marker IL-10 was significantly higher in treated DBA/2J mice compared to WT controls.

4.6.4 Cardiac Function and Morphology in DBA/2J Strains after MI

GPNMB was found to be upregulated approximately 300-fold in hearts of wild type mice seven days after induction of myocardial infarction (see chapter 4.5.1). This finding strongly suggests an involvement of the protein in repair processes of the heart after ischemic injury. To look into this hypothesis and examine if the absence of GPNMB in DBA/2J mice is beneficial or detrimental for cardiac regeneration, myocardial infarction was induced in DBA/2J-Gpnmb+ and DBA/2J mice. The animals were subsequently followed for 4 weeks after surgery and the outcome was monitored via echocardiography, qPCR and histology. Additionally, a group of mice was sacrificed 7 days after MI and the blood composition was analyzed. Moreover, flow cytometry measurements were conducted in order to investigate levels of lymphocytes, progenitor and myeloid cells in blood, bone marrow and spleen of the animals. The first observation was a similar mortality rate of 48.28% in DBA/2J-Gpnmb+ (14 out of 29 died) and of 50.0% in DBA/2J (13 out of 26 died). Furthermore, relative heart weights were similarly increased in both mouse strains 4 weeks after infarct induction (Fig. 52).

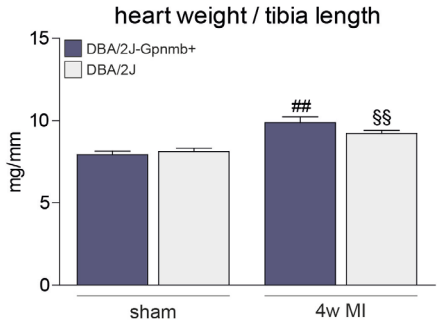

Fig. 52: Relative heart weights in DBA/2J mouse strains after MI. Heart weight / tibia length ratios were determined in DBA/2J-Gpnmb+ (WT) and DBA/2J (Mut) mice 28 days after sham operation or myocardial infarct (MI) induction. ## p<0.01 vs. WT sham, §§ p<0.01 vs. Mut sham; WT sham n=5, Mut sham n=11, WT 28d MI n=15, Mut 28d MI n=13.

Echocardiographic analysis before as well as 1 and 4 weeks after MI revealed significantly better Simpson's ejection fraction and fractional shortening in DBA/2J mice despite no

difference in stroke volume and cardiac output between both strains (Fig. 53). Thus, the absence of GPNMB in DBA/2J mice results in preserved cardiac function after MI.

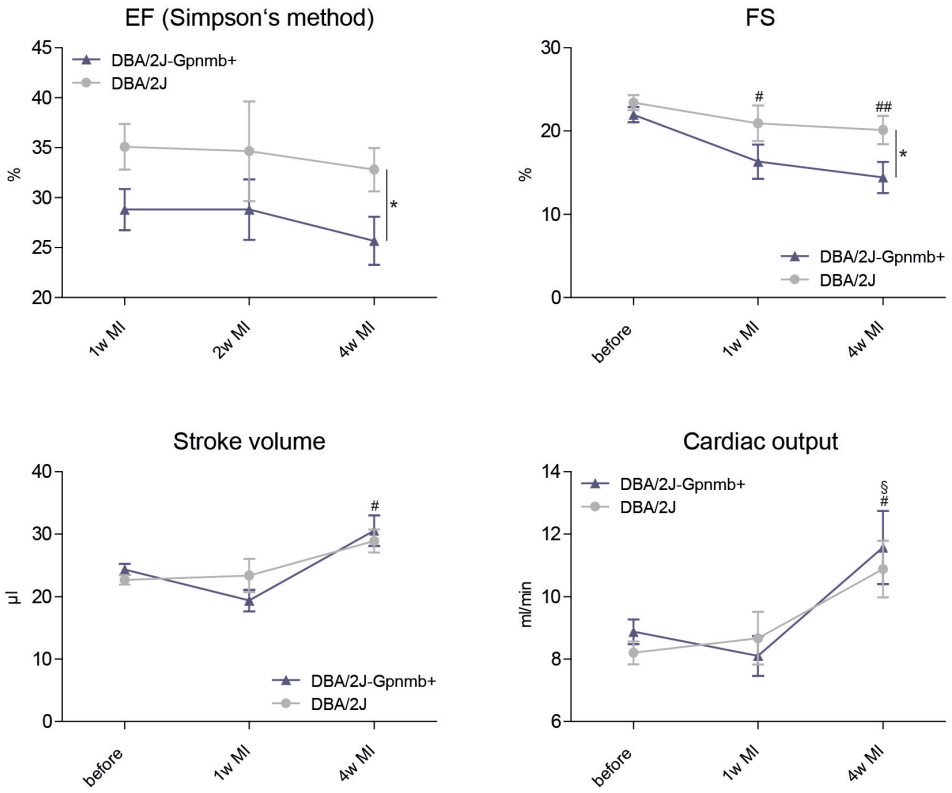

Fig. 53: Cardiac function in DBA/2J mouse strains after MI. Functional parameters such as Simpson's ejection fraction (EF), fractional shortening (FS), stroke volume and cardiac output were determined via two-dimensional echocardiography in DBA/2J-Gpnmb+ (WT) and DBA/2J mice (Mut) before as well as 1 and 4 weeks after experimental induction of MI. Simpson's EF was additionally measured 2 weeks after MI. # (##) $p<0.05$ (0.01) vs. WT before, § $p<0.05$ vs. Mut before, * $p<0.05$; WT before n=41, Mut before n=45, WT after MI n=17, Mut after MI n=16.

Furthermore, echocardiography was applied to analyze the dimensions of the left ventricle in both strains that could indicate differences of cardiac remodeling. On the one hand, diastolic posterior wall thickness (PWTD) and interventricular septum thickness (IVSD) were not different between DBA/2J-Gpnmb+ and DBA/2J mice pointing to similar levels of hypertrophy in both strains (Fig. 54). On the other hand, LV end-diastolic diameter (LVEDD) was significantly lower in DBA/2J mice 4 weeks after MI, which resulted in slightly higher PWTD/LVEDD ratios in these mice compared to DBA/2J-Gpnmb+ controls. These observations suggest less dilatation development after MI in GPNMB mutants.

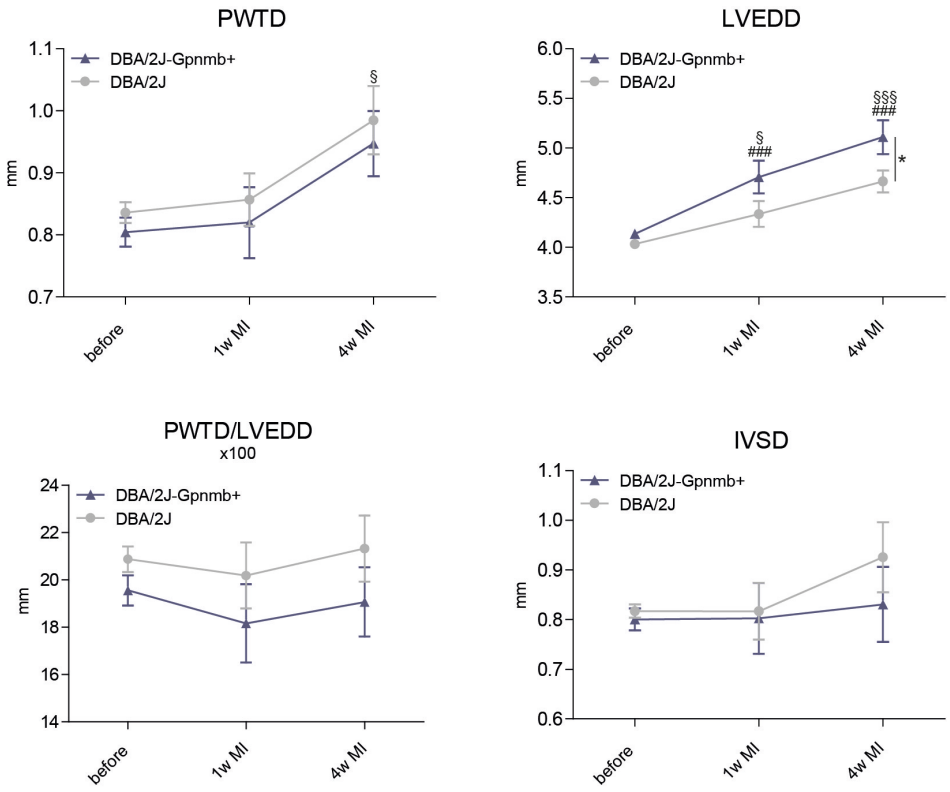

Fig. 54: LV dimensions in DBA/2J mouse strains after MI. Two-dimensional echocardiographic measurements of posterior wall thickness (PWTD), LV diameter (LVEDD), interventricular septum thickness (IVSD) and calculated ratio of PWTD/LVEDD (x100) in DBA/2J-Gpnmb+ (WT) as well as DBA/2J (Mut) mice in diastole. ### p<0.001 vs. WT before, § (§§§) p<0.05 (0.001) vs. Mut before, * p<0.05; WT before n=41, Mut before n=45, WT after MI n=16, Mut after MI n=12.

In summary, the virtual absence of functional GPNMB in DBA/2J mice influenced the cardiac remodeling after ischemic injury. The function of the heart was found to be preserved in the mutant mice accompanied by less dilatation of the left ventricle.

4.6.5 Blood Composition and Cell Recruitment in DBA/2J Strains after MI

After treatment with isoprenaline, DBA/2J mice revealed decreased blood monocyte levels compared to wild type controls. In order to examine if myocardial infarction also triggers alterations of monocyte numbers in blood of GPNMB mutant mice, both DBA/2J strains were subjected to automated blood composition analysis 7 days after MI. As depicted in Fig. 55, monocyte counts were not significantly changed between both genotypes after MI despite a stronger increase in DBA/2J mice compared to sham controls. Also, levels of lymphocytes, granulocytes, WBCs and platelets as well as hematocrit were similar in both strains. Nevertheless, red blood cell levels were significantly higher in DBA/2J mice compared to DBA/2J-Gpnmb+ controls. In line with this, the concentration of hemoglobin was found to be higher in mutant mice.

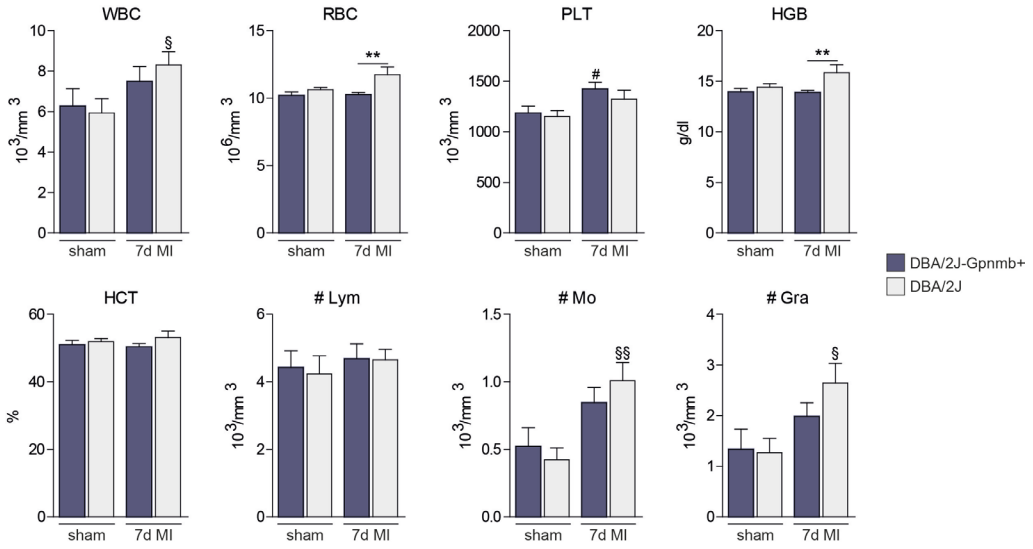

Fig. 55: Blood composition in DBA/2J mouse strains 7 days after AMI. Numbers of white and red blood cells (WBC and RBC), platelets (PLT), hemoglobin (HGB), hematocrit (HCT), lymphocytes (Lym), monocytes (Mo) and granulocytes (Gra) in blood of DBA/2J-Gpnmb+ (WT) and DBA/2J (Mut) mice 7 days (d) after sham or MI surgery. # p<0.05 vs. WT sham, § (§§) p<0.05 (0.01) vs. Mut sham, ** p<0.01; sham n=9 per group, WT 7d MI n=19, Mut 7d MI n=13.

In addition to automated blood composition analysis, flow cytometry measurements were conducted in blood, BM and spleen of the two DBA/2J mouse strains 7 days after MI in order to analyze levels of progenitor cells, lymphocytes and also myeloid cells. Figure 56 contains the levels of Lin$^-$ Sca-1$^+$ c-Kit$^+$ (LSK) and Lin$^-$ CD34$^+$ stem/progenitor cells, which were found to be similar in blood and bone marrow of wild type and mutant animals.

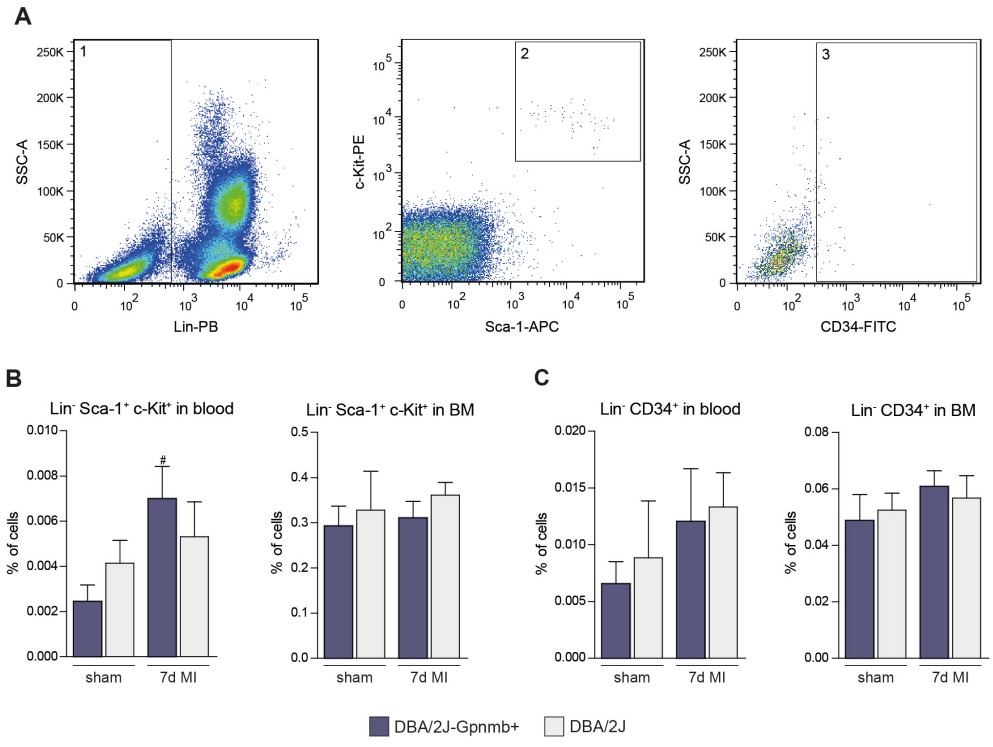

Fig. 56: Progenitor cell numbers in blood and BM of DBA/2J mouse strains after MI. A Gating strategy of flow cytometry data used to define Lin$^-$ (1) and Sca-1$^+$ c-Kit$^+$ (2) (LSK) or CD34$^+$ (3) progenitor cells. **B** Numbers of LSK cells in blood and bone marrow (BM) of DBA/2J-Gpnmb+ (WT) and DBA/2J (Mut) mice 7 days (d) after myocardial infarction (MI) and in sham controls. **C** Number of Lin$^-$ CD34$^+$ cells in blood and BM of WT and Mut mice 7d after sham or MI surgery. # p<0.05 vs. WT sham; sham n=9 per group, WT 7d MI n=19, Mut 7d MI n=13.

Moreover, lymphocyte numbers were determined in blood, BM and spleen. Neither B lymphocytes ($CD4^-$ $CD8^-$ $B220^+$) nor $CD4^+$ ($CD4^+$ $CD8^-$ $B220^-$) or $CD8^+$ ($CD4^-$ $CD8^+$ $B220^-$) T lymphocytes were significantly different between DBA/2J-Gpnmb+ and DBA/2J mice in all tissues analyzed (Fig. 57).

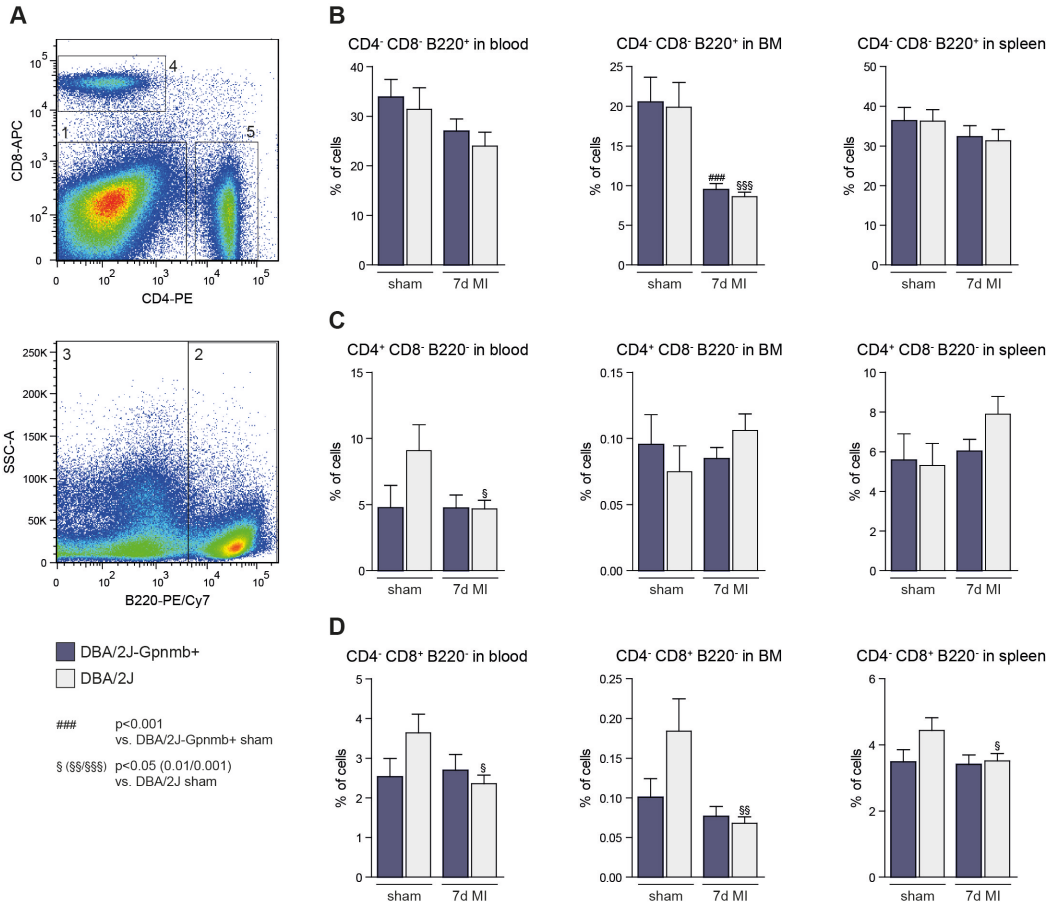

Fig. 57: Lymphocyte numbers in blood, BM and spleen of DBA/2J mouse strains after MI. A Gating strategy of flow cytometry data used to define $CD4^-$ $CD8^-$ (1) $B220^+$ (2) B lymphocytes as well as $B220^-$ (3) $CD4^+$ (5) or $CD8^+$ (4) T lymphocytes. **B** Numbers of B lymphycytes in blood, bone marrow (BM) and spleen of DBA/2J-Gpnmb+ (WT) and DBA/2J (Mut) mice 7 days (d) after myocardial infarction (MI) and in sham controls. **C** $CD4^+$ $CD8^-$ T lymphocyte counts in blood, BM and spleen. **D** Numbers of $CD4^-$ $CD8^+$ T lymphocytes in blood, BM and spleen. Sham n=9 per group, WT 7d MI n=19, Mut 7d MI n=13.

Finally, myeloid cell numbers were measured. Whereas neutrophil ($CD11b^+$ $Gr\text{-}1^+$ $CD115^-$) numbers were not changed in blood samples of both groups, monocyte ($CD11b^+$ $Gr\text{-}1^-$ $CD115^+$) levels were found to be higher in DBA/2J mutant mice compared to wild type controls (Fig. 58).

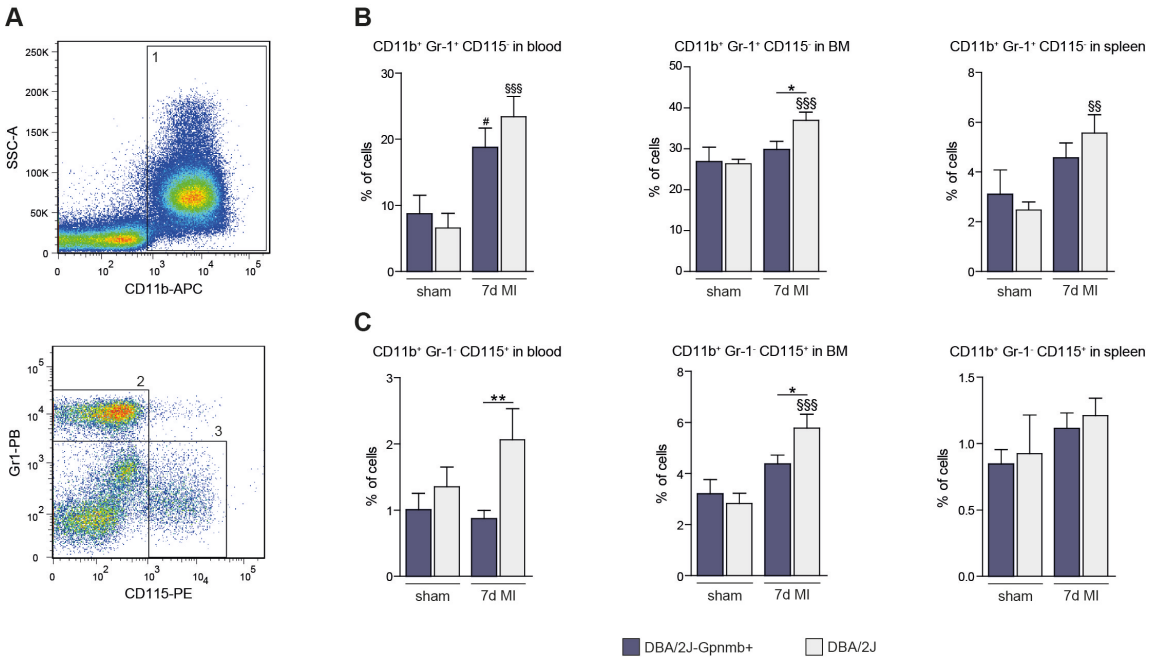

Fig. 58: Levels of neutrophils and monocytes in blood, BM and spleen of DBA/2J mouse strains after MI. **A** Gating strategy of flow cytometry data used to define $CD11b^+$ (1) $Gr\text{-}1^+$ $CD115^-$ (2) neutrophils as well as $CD11b^+$ (1) $Gr\text{-}1^-$ $CD115^+$ (3) monocytes. **B** Numbers of neutrophils in blood, bone marrow (BM) and spleen of DBA/2J-Gpnmb+ (WT) and DBA/2J (Mut) mice 7 days (d) after myocardial infarction (MI) and in sham controls. **C** Number of monocytes in blood, BM and spleen. # p<0.05 vs. WT sham, §§ (§§§) p<0.01 (0.001) vs. Mut sham, * (**) p<0.05 (0.01); sham n=9 per group, WT 7d MI n=19, Mut 7d MI n=13.

Flow cytometry measurements were furthermore applied to determine the levels of different monocyte/macrophage subsets based on their expression of Ly6C (Fig. 59A). As illustrated in Fig. 59B, levels of pro-inflammatory $CD11b^+$ $Gr\text{-}1^-$ $CD115^+$ $Ly6C^{high}$ monocytes that give rise to M1 macrophages were found to be higher in blood and BM of DBA/2J mice compared to wild type controls. On the other hand, $CD11b^+$ $Gr\text{-}1^-$ $CD115^+$ $Ly6C^{low}$ cell counts that refer to reparative M2 macrophages were not different in blood of both DBA/2J strains but were significantly increased in BM of GPNMB mutant mice 7 days post-MI (Fig. 59C).

In summary, blood composition and flow cytometry analysis revealed higher red blood cell and hemoglobin counts in blood of GPNMB mutant mice compared to controls 7 days after MI. Also, numbers of monocytes were significantly increased in DBA/2J mice, which might be due to higher levels of pro-inflammatory monocytes in these mice, whereas the counts of reparative monocytes were found to be similar in both groups. Numbers of stem/progenitor cells as well as B and T lymphocytes were not altered in GPNMB mutant mice compared to wild type controls.

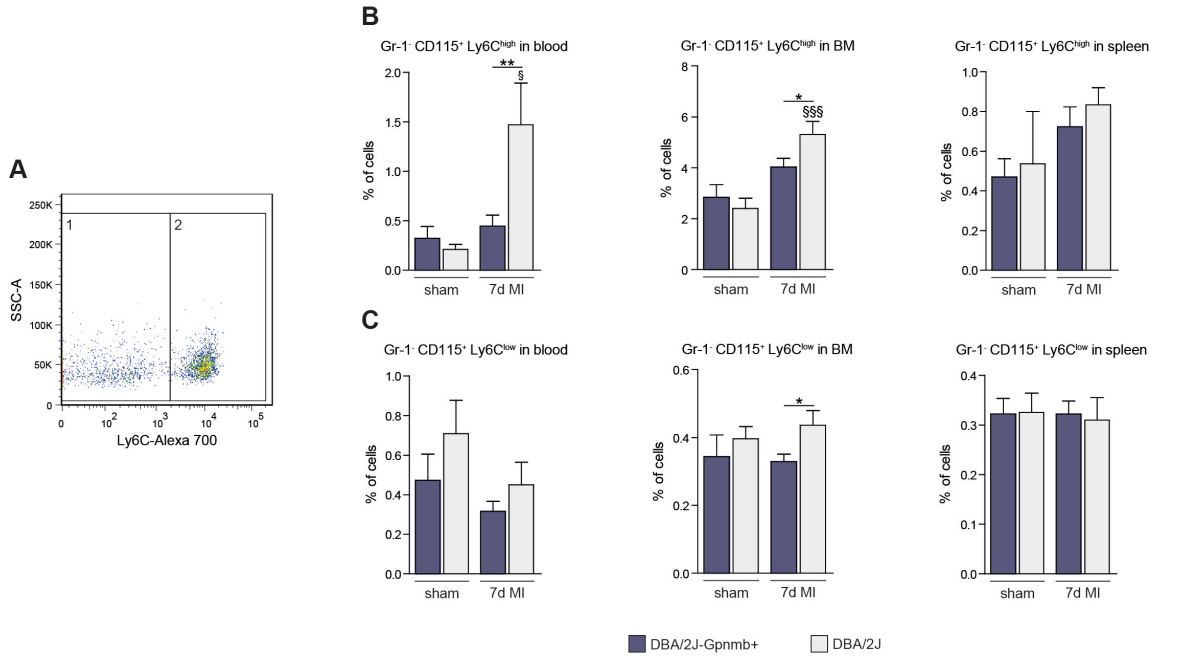

Fig. 59: Numbers of monocyte/macrophage subsets in blood, BM and spleen of DBA/2J mouse strains after MI. A Gating strategy of flow cytometry data used to define CD11b^{+} Gr-1^{-} CD115^{+} Ly6C^{high} (1) as well as CD11b^{+} Gr-1^{-} CD115^{+} Ly6C^{low} (2) cells. **B** Numbers of Ly6C^{high} monocytes/macrophages in blood, bone marrow (BM) and spleen of DBA/2J-Gpnmb+ (WT) and DBA/2J (Mut) mice 7 days (d) after myocardial infarction (MI) and in sham controls. **C** Number of Ly6C^{low} monocytes/macrophages in blood, BM and spleen. § (§§§) p<0.05 (0.001) vs. Mut sham, * (**) p<0.05 (0.01); sham n=9 per group, WT 7d MI n=19, Mut 7d MI n=13.

4.6.6 Expression and Histological Analysis in DBA/2J Strains after MI

Quantitative RT-PCR was applied to analyze the relative expression of hypertrophy, fibrosis and macrophage genes 7 days as well as 4 weeks after the induction of myocardial infarction. As depicted in Fig. 60, levels of the hypertrophy markers ANP and BNP were found to be higher in both groups post-MI and were significantly decreased in DBA/2J mutant mice 4 weeks after infarction in comparison to DBA/2J-Gpnmb+ controls. α-MHC levels were decreased in both groups compared to sham-operated animals but were not different between wild type and mutant mice. In contrast, β-MHC expression was found to be significantly lower in DBA/2J mice 4 weeks post-MI. The analysis of fibrosis markers revealed similar expression levels of collagen 1a1, collagen 3 and fibronectin.

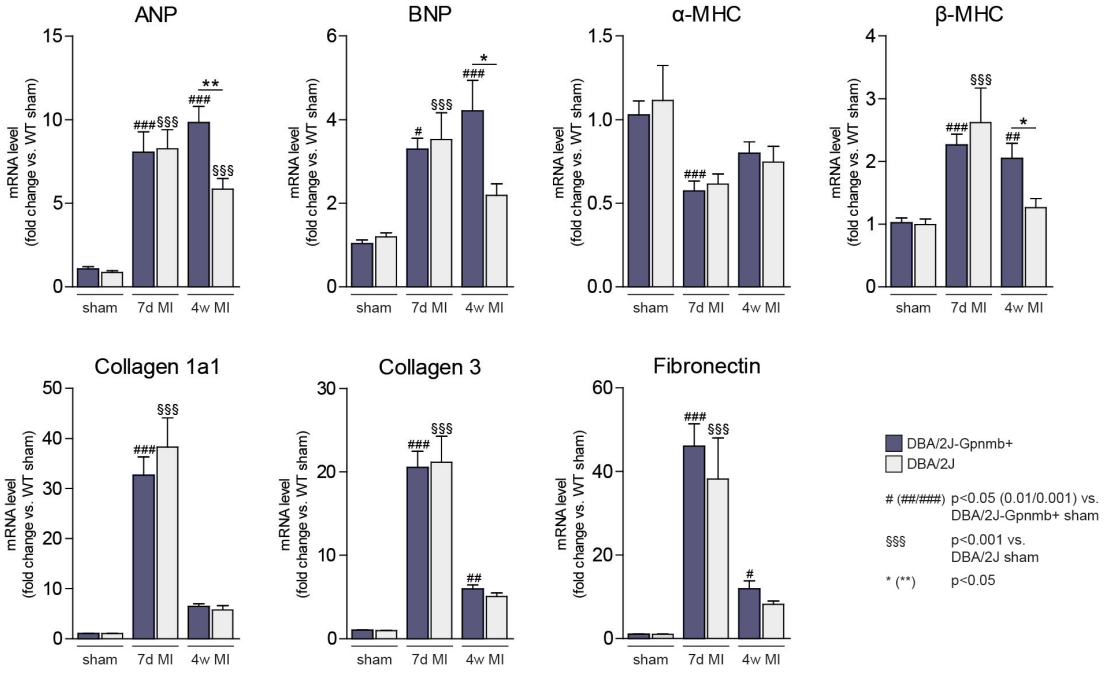

Fig. 60: Expression of hypertrophy and fibrosis genes in DBA/2J mouse strains after MI. qRT-PCR analysis in heart tissue of DBA/2J-Gpnmb+ (WT) and DBA/2J (Mut) mice 7 days (d) and 4 weeks (w) after myocardial infarction (MI) or sham operation. The hypertrophy markers ANP, BNP, α-MHC and β-MHC (upper panel) as well as the fibrosis genes collagen 1a1, collagen 3 and fibronectin (lower panel) were analyzed. WT sham n=9, Mut sham n=10, WT 7d MI n=8, Mut 7d MI n=6, WT 4w MI n=10, Mut 4w MI n=9.

In line with the qRT-PCR data, quantification of sirius red stainings of cardiac tissue revealed similar collagen levels in DBA/2J-Gpnmb+ and DBA/2J mice 7 days and 4 weeks after myocardial infarction (Fig. 61).

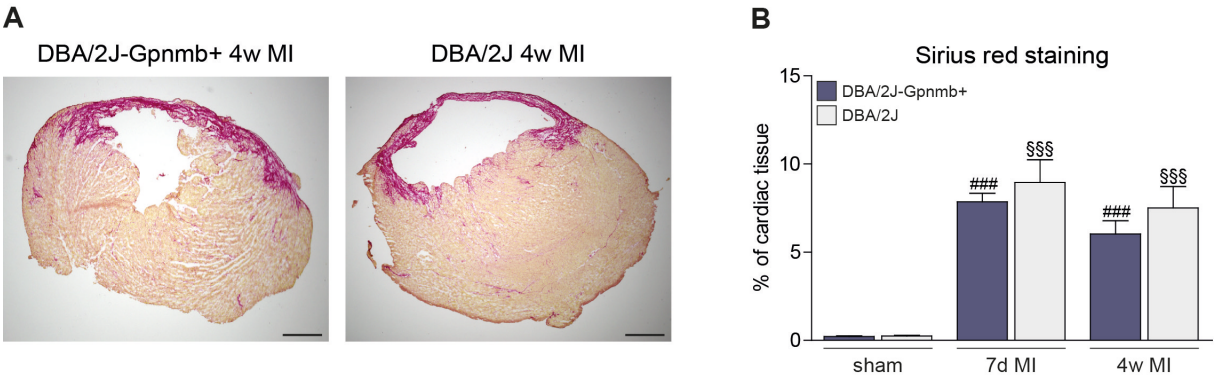

Fig. 61: Sirius red staining in DBA/2J mouse strains after MI. A Representative pictures of sirius red-stained transverse heart sections from DBA/2J-Gpnmb+ (WT) and DBA/2J (Mut) mice 4 weeks (w) after myocardial infarction (MI). Scale bar=800 µm; 2x magnification. **B** Quantification of sirius red staining 7 days (d) and 4 weeks after MI as well as in sham controls. ### p<0.001 vs. WT sham, §§§ p<0.001 vs. Mut sham; 3 sections per animal were analyzed; WT sham n=10, Mut sham n=11, WT 7d MI n=9, Mut 7d MI n=9, WT 4w MI n=6, Mut 4w MI n=5.

Relative quantification of macrophage-related genes revealed similar expression levels of the general macrophage marker F4/80 as well as the M1 genes iNOS and IL-12 and the M2 markers Arg, IL-10 and CCL17 in wild type and mutant mice post-MI (Fig. 62). Solely the M1 markers CXCL9 and CXCL10 tended to be higher in DBA/2J mutant mice in comparison to DBA/2J-Gpnmb+ controls. However, this difference did not reach statistical significance.

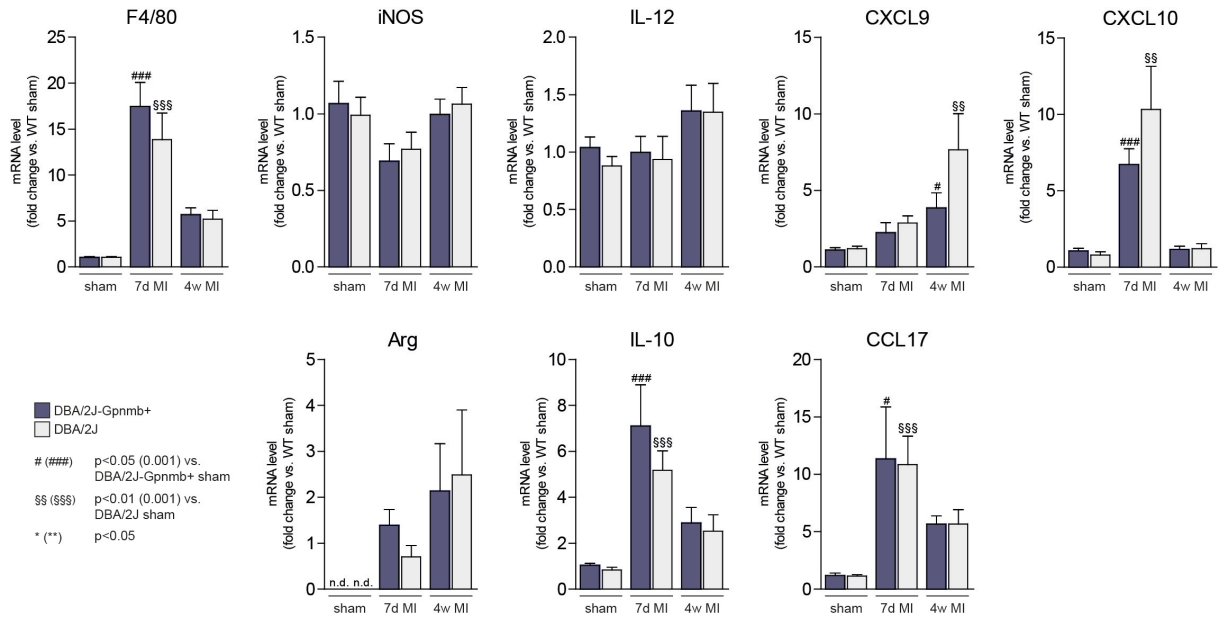

Fig. 62: Expression of macrophage-related genes in DBA/2J mouse strains after MI. qRT-PCR analysis in heart tissue of DBA/2J-Gpnmb+ (WT) and DBA/2J (Mut) mice 7 days (d) and 4 weeks (w) after myocardial infarction (MI) or sham operation. The general macrophage marker F4/80 as well as the M1 genes iNOS, IL-12, CXCL9, CXCL10 (upper panel) and the M2 genes Arg, IL-10 and CCL17 (lower panel) were analyzed. WT sham n=9, Mut sham n=10, WT 7d MI n=8, Mut 7d MI n=6, WT 4w MI n=10, Mut 4w MI n=9.

In order to validate the qRT-PCR results, immunostainings of cardiac sections from both DBA/2J strains were accomplished using an anti-mac-2 antibody that binds all macrophages. Quantification of this staining revealed similar levels of mac-2-positive cells in wild type and GPNMB mutant mice after MI, thus confirming the finding of similar F4/80 expression levels in both strains after cardiac injury (Fig. 63).

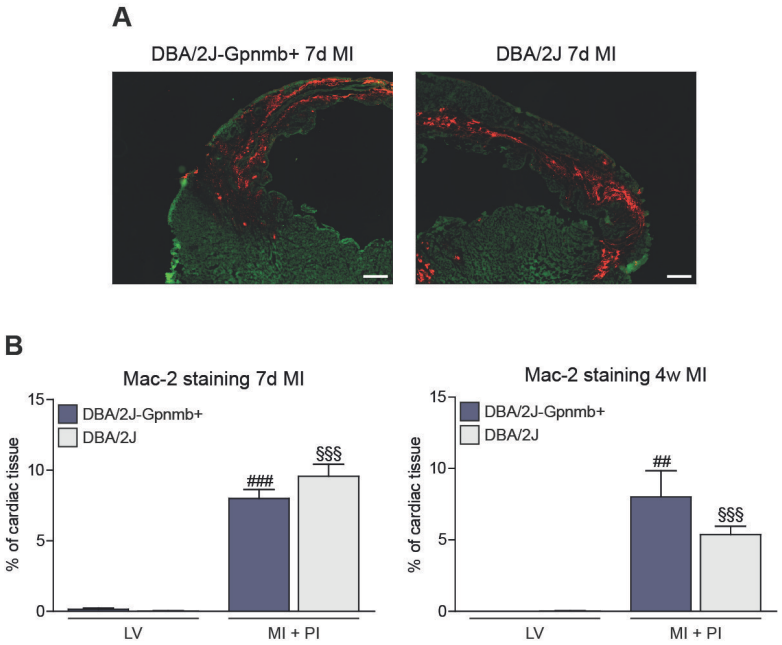

Fig. 63: Macrophage numbers in DBA/2J mouse strains after MI. A Representative pictures of transverse heart sections from DBA/2J-Gpnmb+ (WT) and DBA/2J (Mut) mice 7 days (d) after myocardial infarction (MI) stained using an anti-mac-2 antibody. Scale bar=300 µm; 10x magnification. **B** Quantification of mac-2 staining 7d and 4 weeks (w) after MI in the remote healthy myocardium (LV) as well as in the infarct and per-infarct region (MI+PI). ## (###) p<0.01 (0.001) vs. WT sham, §§§ p<0.001 vs. Mut sham; 3 sections per animal were analyzed; WT sham n=10, Mut sham n=11, WT 7d MI n=9, Mut 7d MI n=9, WT 4w MI n=6, Mut 4w MI n=5.

In summary, the induction of experimental infarction in both DBA/2J mouse strains revealed preserved cardiac functional parameters in GPNMB mutant mice accompanied by less dilatation and significantly lower expression of hypertrophy markers ANP, BNP and β-MHC. Underlying mechanisms might be related to changes of red blood cell counts and hemoglobin concentrations in these mice accompanied by changes of the function and distribution of monocyte/macrophage subsets. However, the absence of GPNMB in DBA/2J did neither affect post-MI fibrosis development nor levels of stem/progenitor cells, lymphocytes or neutrophils.

4.6.7 GPNMB Levels in Plasma of Cardiac Disease Patients

Our studies using GPNMB mutant mice revealed a functional relevance of the glycoprotein after ischemic injury of the heart. Moreover, GPNMB levels were strongly upregulated in cardiac tissue after experimental MI. It is therefore tempting to speculate that the induction of GPNMB in cardiac tissue might be paralleled by higher levels of the glycoprotein in plasma. In order to investigate this hypothesis, an ELISA measurement in human plasma samples of patients suffering from acute or chronic ischemic cardiac diseases was conducted. No difference of GPNMB levels was found in plasma of patients suffering from chronic coronary artery disease in comparison to healthy donors (Fig. 64A). Nevertheless, GPNMB was significantly increased in samples from patients after acute myocardial infarction (Fig. 64B and C). Thereby, GPNMB levels did not correlate with CK or CK-MB levels.

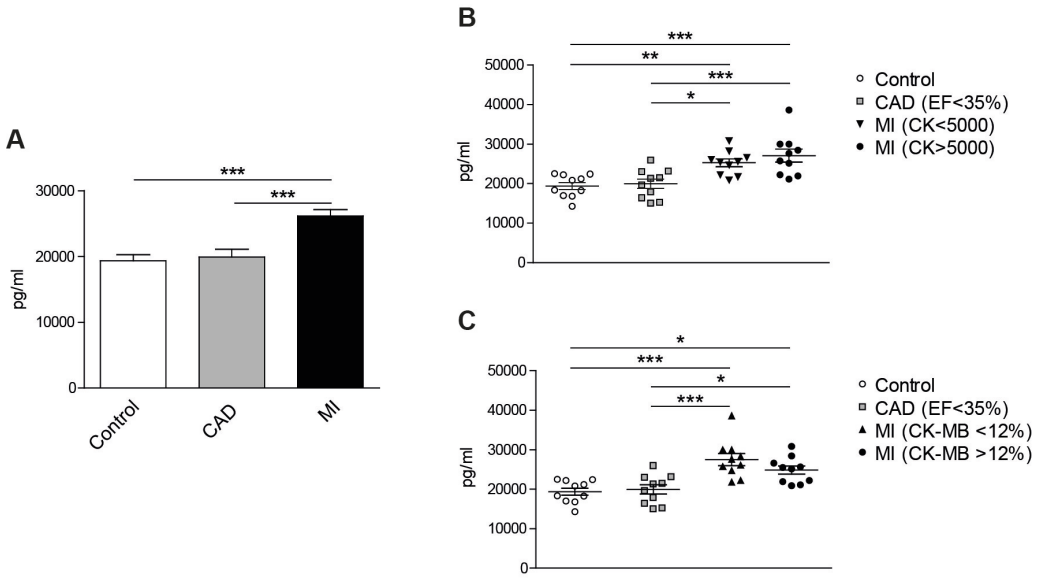

Fig. 64: GPNMB levels in human plasma samples. A ELISA measurement of GPNMB protein levels in plasma samples of healthy donors (control), patients suffering from coronary artery disease (CAD) and after acute myocardial infarction (MI). MI plasma samples were subdivided according to the creatine kinase (CK) levels (± 5000) (**B**) or the levels of the heart-specific CK-MB (± 12%) (**C**). * (**/***) p<0.05 (0.01/0.001); control n=10, CAD n=10, MI n=10.

In conclusion, GPNMB levels are not altered in chronic cardiac diseases such as CAD but are significantly higher in human plasma after acute ischemic injury, e.g. myocardial infarction. Therefore, our findings suggest the possibility that GPNMB might not only constitute a novel therapeutic target but might also represent a promising candidate as biomarker of acute ischemic cardiac diseases.

5 Discussion

The analysis of two proteins, SDF-1 and GPNMB, and their involvement in pathophysiological processes of the heart were in the focus of the present study. The chemokine SDF-1/CXCL12 has been intensively investigated in the last decade. The characterization of SDF-1 knockout mice revealed its involvement in embryogenesis and organ development and a number of reports furthermore demonstrated the importance of the chemokine in tissue repair processes in adults. Due to the embryonic lethality of SDF-1 knockout animals, these studies made use of pharmacological targeting of SDF-1 or gain-of-function studies. The majority of these experiments demonstrated positive effects of the chemokine and its receptor on myocardial regeneration. However, several recent reports actually questioned the benefit of the chemokine by showing opposite effects of the SDF-1/CXCR4 axis in the heart. This controversy might be partially due to a complex system of cell type- and disease- dependent actions of SDF-1 and the lack of a genetically engineered rodent model to specifically examine the role of cell type-specific SDF-1 in cardiac repair processes during adult life. Therefore, SDF-1α transgenic rats and platelet-specific SDF-1 knockout mice were generated and analyzed in the present study in order to clarify the relevance of cardiomyocyte- and platelet-derived SDF-1 for cardiac repair processes.

The glycoprotein GPNMB/osteoactivin plays a role in fibrotic and inflammatory processes after injury of several organs such as skeletal muscle, liver and kidney. However, the functional importance of GPNMB in the heart remains largely unknown. We identified the protein to be upregulated in the heart 24 hours after myocardial infarct induction in a microarray-based screening approach. Subsequent *in vitro* and *in vivo* experiments were conducted in order to characterize the role of GPNMB in the heart at basal levels as well as in pathophysiological processes.

5.1 Effect of Overexpression of SDF-1α in a Transgenic Rat Model

Transgenic rats were generated by microinjection of construct DNA, which includes the cardiomyocyte-specific promoter MLC-2 and the murine SDF-1α gene, into rat zygotes. The murine SDF-1 gene was selected based on the high homology between human, mouse and rat SDF-1. At the same time, the overexpression of murine SDF-1 in a transgenic rat model allows the differentiation between endogenous (rat) and exogenous (mouse) SDF-1 by using specific primers and antibodies. One founder rat was obtained that was crossed with SD rats to establish a transgenic line. Quantitative RT-PCR analysis demonstrated a robust overexpression of SDF-1 exclusively in the heart of these transgenic rats. Furthermore, 5'-RACE analysis revealed correct transcription of the transgenic DNA with appearance of one silent mutation. ELISA measurements using cardiomyocytes isolated from adult rats demonstrated significantly higher SDF-1 protein levels in cell lysates from transgenic rats

compared to wild type controls. Moreover, SDF-1 was detected in cell supernatants from transgenic rats whereas the chemokine was not detected in supernatants from non-transgenic animals. This finding indicates that cardiomyocytes from transgenic rats are capable of secreting reasonable amounts of SDF-1, a process that is necessary to fulfill its chemoattractant properties. In summary, a transgenic rat line could be established with cardiomyocyte-specific overexpression of SDF-1α.

Early analysis of homozygous SDF-1α transgenic rats revealed regular breeding performance, birth rates and a normal lifespan without altered mortality rates in comparison to SD controls. Furthermore, transgenic animals displayed no signs of cardiac abnormalities at basal levels. Measurements of heart weight / tibia lengths ratios were conducted for quantification of cardiac hypertrophy independent of body weight fluctuations[238] and revealed similar relative heart weights of transgenic and wild type rats. In line with this, relative quantification of hypertrophy and fibrosis markers revealed no change of expression in SDF-1 Tg animals. Histological analysis confirmed the observation of normal cardiac morphology and fibrosis content in transgenic animals. Moreover, two-dimensional echocardiographic measurements were performed as noninvasive tool to assess changes of cardiac function and structure.[239] Echocardiography revealed normal diastolic and systolic cardiac function and no signs of remodeling in SDF-1α Tg rats compared to SD controls. All together, the overexpression of SDF-1α was not sufficient to alter the development, function and structure of the heart at basal levels. The observation of normal cardiac development is consistent with studies that demonstrated that the expression of SDF-1 in the cardiac outflow tract and the endocardium as well as the presence of the chemokine and its receptors CXCR4 and CXCR7 in the myocardial microvasculature rather than in cardiomyocytes is essential for guidance of cells during embryogenesis and normal cardiac development.[113,240,241] In line with this, the deletion of CXCR7 specifically in endothelial cells recapitulated the cardiac phenotype of complete knockout animals[242], whereas the loss of CXCR4 in cardiomyocytes resulted in normal cardiac development and function.[164] Moreover, studies in our laboratory demonstrated that the conditional knockout of SDF-1 in cardiomyocytes does not alter the development of the heart during embryogenesis or the basal cardiac function in adult mice.[166] Therefore, induced expression of SDF-1α in cardiomyocytes of the transgenic rats might have no effect on proper development of the heart since the expression of SDF-1 in the endocardium, outflow tract and microvasculature and thus the signaling that is necessary to direct progenitor cells into appropriate microenvironments during embryogenesis is intact. Conditional knockout or overexpression of the chemokine in endothelial cells would be necessary to definitely clarify the role of this cell type in cell guidance and cardiac development during embryogenesis. The observation of normal cardiac function and structure in SDF-1α transgenic rats at basal levels is surprising regarding the study by Pyo *et al*. that

reported direct negative inotropic effects of SDF-1 on cardiomyocytes in association with decreased calcium transients.[158] However, these experiments were conducted in isolated adult cardiomyocytes. In SDF-1α Tg rats, the preserved cardiac function might be explained by the absence of additional signals that are generated upon inflammation and tissue injury. As hypothesized in the danger model[243], higher levels of SDF-1 alone might be not sufficient to induce recruitment of leukocytes and stem/progenitor cells that could potentially influence cardiac healing because an alarm signal, which is released from damaged and stressed tissue, is missing.

To confirm this hypothesis, SDF-1α transgenic rats were subjected to experimental myocardial infarction and parameters of cardiac function and remodeling, fibrosis, cell recruitment and angiogenesis were assessed. Echocardiographic measurements revealed an expected worsening of cardiac function during the first 2 weeks after surgery but no difference between wild type and transgenic animals. The final analysis 4 weeks after infarction yielded deteriorated function of the heart measured as lower Simpson's ejection fraction, fractional shortening, cardiac output and stroke volume in SDF-1α transgenic animals compared to controls. MRI measurements that were conducted thereafter confirmed these observations. Echocardiography and MRI were also applied to evaluate the remodeling of the heart upon AMI. This analysis demonstrated no difference of LV diameter and volume in diastole and systole between transgenic and wild type rats at any time after MI but significantly reduced posterior wall and interventricular septum thickness as well as decreased LV mass in SDF-1α Tg rats 4 weeks after infarction. Despite no alteration of heart weight / tibia length ratios between both groups after MI, our findings indicate that the overexpression of SDF-1α alters the remodeling of the hearts after ischemic injury towards worse cardiac function accompanied by less LV mass and hypertrophy. These findings could be due to a direct autocrine or paracrine effect of cardiomyocyte-derived SDF-1 in the heart since cardiomyocytes express CXCR4[128] and it was shown that the chemokine can have negative inotropic effects by changing calcium channel activities.[158] However, other studies reported a beneficial effect of direct intramyocardial or intraventricular injection of SDF-1 on cardiac function and infarct size.[128,136,142,244] Among all studies targeting the SDF-1/CXCR4 axis, the direct injection of the chemokine into cardiac tissue resembles best the situation in the transgenic rats. But still, the overexpression of SDF-1α in the transgenic rats is congenital and permanent, whereas the injection of the chemokine happens at the time or shortly before occlusion. Furthermore, different protein amounts were used for injection and due to diffusion effects and the short half-life of SDF-1 it is not clear how much protein stays in the heart and for how long it is available to exert its effects. MRI measurements revealed similar infarct sizes of SDF-1α transgenic animals and wild type controls. Therefore, the functional differences cannot be explained by a different degree of ischemic damage in both groups.

In order to further characterize the phenotypic alteration between transgenic and control rats, the expression of certain marker genes was quantified by qRT-PCR at 3, 7 and 28 days after myocardial infarction. The hypertrophy genes, ANP and BNP, were induced upon cardiac damage as expected but were not differentially expressed in transgenic animals in comparison to controls. Expression of α-MHC, the predominant MHC isoform in adult hearts, was decreased upon MI to a similar extent in both groups. On the other hand, levels of β-MHC were found to be increased after infarction with significantly higher expression in SDF-1α Tg rats compared to controls at 28 days post-MI. This increase of β-MHC levels is a sign of re-expression of a fetal gene program and is a common feature of biomechanical stress and remodeling of the heart. Besides its function as disease marker, higher expression levels of this MHC isoform can also have an impact on disease progression. A study using transgenic mice with replacement of the predominant α-MHC isoform with β-MHC revealed a disadvantageous effect to the mice under severe cardiac stress.[245] Thus, higher β-MHC / α-MHC ratios in SDF-1α transgenic rats 28 days after MI may be detrimental and contribute to the worsening of cardiac function that was observed at that late time point after MI possibly via alterations of mechanical stress sensors.

The relative quantification of fibrosis genes revealed an expected induction of all markers as early as 3 days after MI induction. The levels of fibronectin were found to be similar in hearts of transgenic and wild type rats, whereas collagen 3 expression was significantly decreased in SDF-1 transgenic rats 3 days post-MI. Levels of collagen 1a1 were not altered at 3 and 7 days after infarction, but tended to be higher in transgenic animals 4 weeks post-MI. As a result, collagen 1a1 / collagen 3 ratios were found to be significantly higher in SDF-1 transgenic rats compared to wild type controls early (3d) and later (28d) after MI. This finding was confirmed by immunofluorescence stainings of collagen 1 in heart sections that revealed significantly more deposition of collagen 1 in the peri-infarct region of SDF-1 Tg rats 7 days after MI. Furthermore, sirius red stainings were conducted in heart sections after MI and demonstrated higher levels of fibrosis in SDF-1 transgenic rats 7 days post-MI. In summary, the amount of collagen 3 was lower in the hearts of transgenic animals compared to wild type rats early (3d) after infarction, whereas fibronectin levels were similar between both groups and collagen 1 content was found to be higher in the peri-infarct region of SDF-1α Tg rats. Both fibrillar collagens (type 1 and 3) are major components of the ECM of the heart and changes in the amount or distribution of collagen can influence the function of the heart.[246,247]

In the early phase after myocardial damage, collagen 3 and fibronectin are produced by myofibroblasts in the infarct zone and are involved in the formation of the provisional matrix that is important to prevent further dilatation and rupture of the infarcted wall (early reparative fibrosis).[248] Fibronectin levels were not altered and no increased mortality rate was observed in SDF-1α Tg animals compared to controls indicating no increased incidence of cardiac

rupture and sudden cardiac death. Nevertheless, decreased collagen 3 levels in SDF-1α Tg rats early after MI might be a sign of impaired reparative fibrosis and might have detrimental effects via promotion of infarct expansion associated with dilatation and adverse LV remodeling. At later stages after MI, collagen is produced by fibroblasts in the remote myocardium, which is associated with disturbances in the conducting system and increased myocardial stiffness (late reactive fibrosis).[249,250] Thus, dense regions of post-MI reactive fibrosis and collagen 1 as seen in the SDF-1α transgenic animals can be accompanied by serious consequences including diastolic dysfunction and promotion of re-entry dysrhythmias[251] and might at least partially explain the worsening of cardiac function. Thereby, higher levels of the chemokine in the heart might be directly linked to the enhanced post-MI fibrosis in the transgenic rats since cardiac fibroblasts were shown to express CXCR4.[128] Thus, cardiomyocyte-derived SDF-1 might directly influence surrounding fibroblasts in a paracrine manner. Moreover, it was reported that SDF-1 is capable of recruiting bone marrow-derived mesenchymal progenitor cells (fibrocytes) that can enter the tissue and give rise to mature fibroblasts.[252-254] In support to this view, SDF-1 plasma levels were found to be higher in the transgenic rats three days after myocardial infarction, which could lead to stronger recruitment of fibroblast progenitors and more fibrosis development. Since cardiac fibrosis and regeneration constitute complementary processes, higher levels of fibrosis in the transgenic rats in association with impaired remodeling question the benefit of SDF-1 for cardiac repair.

SDF-1 is furthermore known to be able to recruit CXCR4-expressing circulating EPCs, hematopoietic cells and smooth muscle cell progenitors, which all can directly or indirectly contribute to ischemic revascularization.[255] Moreover, SDF-1 directly participates in new blood vessel formation in injured tissue by preventing apoptosis of EPCs and inducing proliferation and differentiation of endothelial cells. Therefore, qRT-PCR analysis and histological methods were applied to study the vessel density and amount of neovascularization in transgenic and wild type rats at basal levels as well as upon MI induction. Indeed, relative quantification of VEGF-A revealed higher levels in SDF-1α-overexpressing Tg rats at baseline. This finding confirms studies showing that the SDF-1/CXCR4 axis stimulates VEGF secretion[256] and may suggest higher levels of angiogenesis in sham-operated SDF-1α transgenic rats since VEGF is a main regulator of myocardial vessel formation.[257] However, mRNA levels of CD31 (PECAM-1) were found to be similar in both sham groups which was confirmed by immunofluorescence stainings using an anti-CD31 antibody. CD31 is primarily expressed by endothelial cells and its quantification can help to evaluate the degree of angiogenesis. Thus, the induction of VEGF alone in hearts of transgenic animals is not sufficient to alter the level of angiogenesis and vessel density at basal levels. After MI, no difference was found between transgenic and non-transgenic animals regarding VEGF-A and CD31 expression levels. In

support to this view, quantification of CD31 immunofluorescence demonstrated similar amounts of angiogenesis in SDF-1α Tg and wild type rats at all time points after MI. Therefore, higher levels of cardiomyocyte-derived SDF-1α in transgenic rats do not result in enhanced neovascularization after ischemic injury of the heart.

Besides the recruitment of pro-angiogenic progenitors, SDF-1 is known to be able to attract other CXCR4-positive stem/progenitor cell populations that might influence repair processes of the heart after injury. In order to examine if this recruitment is altered in SDF-1α transgenic rats, flow cytometry experiments were performed in blood and BM of these rats and wild type controls at basal levels and after MI induction. Thereby, progenitor cells were defined as CD11b/c$^-$ CD3$^-$ CD45$^+$ Sca-1$^+$. The negative selection of CD11b/c and CD3 was used to exclude mature myeloid cells and lymphocytes ("lineage (lin)-negative"). CD45 (leukocyte common antigen) is a protein tyrosine phosphatase that is present on the surface of all hematopoietic cells except erythrocytes and platelets.[258] However, it was also shown to be expressed by bone marrow-derived progenitor cells with multi-lineage differentiation potential.[259,260] Thus, progenitor cells positive for CD45 and the commonly used stem cell marker Sca-1 (Ly-6A/E)[261] were analyzed as described previously.[262,263] These measurements revealed no difference of progenitor cell numbers in blood and BM 3 and 7 days after MI. Nevertheless, infiltration of progenitor cells into the heart could be different despite similar cell counts in blood. In order to investigate this hypothesis, CXCR4 expression levels in heart tissue were analyzed, which revealed an expected induction of the receptor after MI but no difference between SDF-1α Tg and SD rats 3 and 7 days after MI. Only 28 days post-MI the CXCR4 expression was found to be slightly higher in transgenic rats. In summary, these findings indicate that the functional deterioration that we observed in the SDF-1α transgenic rats upon MI is not primarily due to alterations of the chemoattraction of Sca-1$^+$ CXCR4$^+$ progenitor cells to the heart. In accordance to these results, studies in our laboratory using cardiomyocyte-specific SDF-1 knockout mice revealed no evidence of altered stem cell recruitment at basal levels and after MI (unpublished data). Thus, cardiomyocyte-derived SDF-1 does not seem to play a major role in the homing of pro-angiogenic and other stem/progenitor cells in our models. SDF-1 from other cardiac cell types such as endothelial and perivascular cells might be more important for triggering arrest and extravasation as well as the maintenance of stem/progenitor cells at the site of injury.[255] In addition, SDF-1 might cooperate with other molecules and even build heterocomplexes to exert its chemoattractive actions as shown in a study by Salvucci *et al*. for endothelial cell movement and by Schiraldi *et al*. for recruitment of inflammatory cells and fibroblasts.[264,265] Higher and possibly suboptimal levels of SDF-1 in transgenic rats might interfere with this interaction and its stoichiometry and thus disturb the synergistic effects. A limitation of our study is the use of a small set of markers to define the stem/progenitor cell pool for flow

cytometry experiments. Thus, it cannot be ruled out that stem cell subsets expressing other markers are recruited differentially in transgenic rats compared to wild type controls. Furthermore, CXCR4 can be expressed by other cell types in the heart besides stem and progenitor cells[266] and therefore the relative quantification of receptor levels in the heart as parameter for cell recruitment is a rather indirect approach. Histological examinations of stem cell marker expression in the hearts post-MI are necessary to definitely evaluate the influence of SDF-1α overexpression on stem/progenitor cell recruitment to the injured heart.

Flow cytometry measurements were also applied to study the levels of lymphocytes and myeloid cells in blood, BM and spleen of transgenic and WT rats since SDF-1 is known to be a highly efficacious and potent chemoattractant for lymphocytes, monocytes/macrophages and neutrophils.[267-270] Despite some alterations of $CD45^+$ $CD3^-$ $B220^+$ B cells in blood and $CD45^+$ $CD3^+$ $B220^-$ T cells in BM of SDF-1α Tg sham-operated rats, no differences of T or B lymphocyte counts were found in blood, BM and spleen at both time points (3 and 7 days) after MI surgery. Thus, cardiomyocyte-derived SDF-1 does not seem to be critically involved in the regulation of post-MI lymphocyte recruitment. Different myeloid cell populations were analyzed based on their expression of CD11b/c and the granulocyte marker Gr-1.[271,272] $CD11b/c^+$ $Gr\text{-}1^{high}$ cells represent neutrophils whereas $CD11b/c^+$ $Gr\text{-}1^{low}$ cells comprise dendritic cells and monocytes/macrophages. In SDF-1α transgenic rats, $CD11b/c^+$ $Gr\text{-}1^{high}$ neutrophil numbers were found to be significantly lower in bone marrow at basal levels (after sham operation) as well as 3d after infarction and higher in blood 7d after MI induction. These findings could be due to a higher mobilization of $CD11b/c^+$ $Gr\text{-}1^{high}$ cells from the bone marrow of transgenic animals at basal levels and early after infarction, which might result in higher blood counts of these cells 7d after MI. This could lead to alterations of the inflammatory response in SDF-1α-overexpressing transgenic rats since neutrophils are important mediators of post-MI inflammation. Therefore, elevated levels of these cells accompanied by sustained pro-inflammatory signals might negatively affect the healing of the heart after ischemic injury. Nevertheless, increased neutrophil levels in blood do not necessarily result in increased infiltration of these cells into cardiac tissue. Immunofluorescence stainings using specific antibodies directed against neutrophil markers are needed to verify the effect of SDF-1 on recruitment of these cells to the injured heart. In contrast to the alterations of neutrophil counts, the number of $CD11b/c^+$ $Gr\text{-}1^{low}$ monocytes/macrophages and dendritic cells was found to be similar in blood, BM and spleen of SDF-1α Tg and WT rats at both time points after MI as well as in sham controls. Nevertheless, qRT-PCR analysis of heart tissue lysates revealed higher levels of the common macrophage marker CD68 in SDF-1α transgenic animals compared to wild type controls 28 days after MI induction. This was confirmed by immunofluorescence stainings of heart sections using an antibody against CD68 that demonstrated higher levels of macrophages in the peri-infarct region of SDF-1α Tg rats

3 days after MI. Given the multiple roles of these cells during all phases of post-MI healing, it can be assumed that the observed increase in infiltrated macrophages influences the remodeling of the heart in SDF-1α Tg rats. Higher levels of macrophages might also explain the increased accumulation of fibrosis in the hearts of transgenic rats. It has been demonstrated that infiltrating macrophages are important contributors to the development of cardiac fibrosis and that the balance of urokinase plasminogen activator and its inhibitor PAI-1 might mediate this effect.[273] However, there are several subsets of macrophages that exert diverse and even contrary functions. The quantification of CD68-positive staining cannot distinguish between these subpopulations. Immunofluorescence approaches with antibodies that bind specifically to different macrophage subsets are not yet available. Nevertheless, relative quantification of genes that are specific for both subsets in cardiac tissue of transgenic and wild type rats can be helpful to indicate alterations in macrophage subsets. Quantitative RT-PCR analysis revealed similar levels of markers specific for reparative macrophages but higher expression of genes which refer to pro-inflammatory cells in hearts of SDF-1α Tg rats. Increased levels of pro-inflammatory macrophages accompanied by higher levels of neutrophils might sustain and/or prolong the inflammatory phase of the heart after infarction and thus contribute to an impaired cardiac healing that was observed in SDF-1α transgenic animals.

In conclusion, the analysis of SDF-1α transgenic rats after experimental induction of myocardial infarction resulted in deteriorated cardiac function accompanied by altered remodeling, more fibrosis and higher numbers of neutrophils in the blood and infiltrated macrophages in the heart. The levels of stem/progenitor cells and lymphocytes were found to be similar between transgenic animals and controls. Also, there was no effect observable on post-MI neovascularization. These findings suggest that the cardiomyocyte-derived chemokine is predominantly involved in the regulation of the inflammatory response rather than influencing stem/progenitor cell levels or angiogenesis. This is in line with a recent report demonstrating that the overexpression of CXCR4 in hearts prior to MI induction leads to an increased recruitment of inflammatory cells and thus enhances the ischemic cardiac injury.[160] The differences between our findings compared to studies that described beneficial effects of the SDF-1/CXCR4 axis on cardiac regeneration might be due to several reasons. First, the overexpression of the chemokine in our transgenic model is congenital and permanent. Therefore, the elevation of SDF-1 that is normally occurring early after MI as signal to initiate repair processes is missing and the high quantity of the chemokine in heart and circulation at basal levels might prevent an additional effect on the recruitment of stem/progenitor cells and lymphocytes after cardiac injury. Second, SDF-1 might not act alone but in combination with other proteins in order to accomplish its complex functions. The overexpression of the chemokine could potentially interfere with these interactions and/or desensitize the involved

pathways. Third, the actions of SDF-1 are highly cell type- and context-specific. Different subsets of leukocytes and stem/progenitor cells might be recruited dependent on a certain concentration gradient and precise timing of SDF-1. The persistent overexpression of the chemokine in the transgenic rats might constitute a disturbance in the tight regulation of the system and therefore cause an imbalance between inflammatory and regenerative processes. Furthermore, other cell types such as endothelial cells and platelets that also express and secret SDF-1 might be important players in the post-MI healing process. The expression of the chemokine in these cells is not altered in our transgenic rats and thus conditional knockout and transgenic models targeting these cell types are needed to definitely clarify their relevance as source of SDF-1. Nevertheless, our data suggest that the therapeutic targeting of SDF-1 in clinical studies should be thoroughly reviewed due to its pleiotropic effects.

5.2 Generation of Platelet-Specific Conditional SDF-1 Knockout Mice

In a first attempt to generate a murine platelet-specific SDF-1 knockout model, SDF-1^{flox} mice were bred with transgenic animals that carry the Cre under the control of the interferon-inducible Mx1-Cre promoter.[221] In these mice, Cre is not expressed in healthy mice but it can be transiently activated upon application of interferon (IFN-α or IFN-β) or of synthetic double-stranded RNA (poly(I):(C)) that functions as IFN inducer. The Mx1-Cre transgene causes efficient recombination in bone marrow, liver, spleen and other hematopoietic tissues and Mx1-Cre-mediated excision of genes has been used as a tool to study the hematopoietic system.[274-276] However, the analysis of SDF-1$^{flox/-}$/Mx1-Cre^{+} cKO mice early (7 days) and later (7 weeks) after poly(I):(C) injection revealed lower expression of SDF-1 in all organs tested accompanied by altered levels of stem/progenitor cells in blood and bone marrow. These results indicate basal changes in the stem/progenitor cell pool in the bone marrow and blood of Mx1-Cre^{+} mice. Since these cells are described to be involved in cardiac repair processes after being recruited to the injured heart via SDF-1 gradients, the regeneration of the heart after MI might be different in the mice due to these basal alterations. Thus, the SDF-1$^{flox/-}$/Mx1-Cre^{+} cKO mice are not appropriate to examine the importance of the platelet-specific secretion of SDF-1 for cardiac repair and were not used further. Instead, SDF-1^{flox} animals were bred with transgenic Pf4-Cre mice that had been described as an effective tool for generating megakaryocyte lineage-restricted specifically targeted mutants.[222] Indeed, flow cytometry and ELISA measurements revealed lower levels of SDF-1-expressing platelets and decreased amounts of SDF-1 protein in platelets of SDF-1$^{flox/-}$/Pf4-Cre^{+} cKO mice compared to SDF-1$^{flox/-}$ controls. Furthermore, PCR analysis demonstrated highest Pf4-Cre activity in bone marrow and qRT-PCR studies showed similar SDF-1 mRNA levels of control and cKO mice in all organs tested. Thus, the deletion of the chemokine by the Pf4-Cre transgene

appears to be restricted to megakaryocytes and platelets without unspecific Cre activity in other cell types or organs.

At basal levels, blood composition was found to be similar in control and SDF-1 cKO mice. Furthermore, no difference was detected regarding platelet counts and mean platelet volume. These findings indicate that the generation of platelets in the bone marrow and their release into the circulation is not altered by the conditional KO of SDF-1 although it has been shown that megakaryocytes and platelets express CXCR4 and that SDF-1 can influence the development of megakaryocytic progenitor cells and platelet release.[277-280] Thus, other cell types in the bone marrow that express SDF-1 such as osteoblasts and endothelial cells seem to be important to ensure normal megakaryocyte development and migration as well as subsequent platelet shedding.[281,282] Echocardiographic measurements in conditional SDF-1 knockout mice moreover demonstrated normal cardiac function and morphology in these animals at baseline. Thus, the SDF-1/Pf4-Cre conditional mouse model is suitable to analyze the effect of platelet-derived SDF-1 on cardiac function and regeneration upon myocardial injury.

5.3 The Potential of GPNMB as Novel Therapeutic Target and Biomarker of Ischemic Heart Diseases

The function of GPNMB in the heart remains largely unknown. However, studies in other tissues such as liver, skeletal muscle and spleen demonstrated its involvement in inflammatory, fibrotic and repair processes after injury possibly by influencing macrophage and fibroblast function.[283] We identified the glycoprotein in a screening for factors that are significantly upregulated in the peri-infarct region of rat hearts 24 hours after MI induction. In line with this, we also found a strong (300-fold) upregulation of GPNMB in murine cardiac tissue 7 days after infarction. Another hint that the glycoprotein might be involved in cardiac pathophysiology was the finding that it is significantly induced in heart tissue of wild type mice after pharmacological induction of cardiac hypertrophy. Based on these initial results we decided to analyze GPNMB further using *in vitro* and *in vivo* approaches. Favorably, the classic DBA/2J inbred strain appeared as a suitable animal model to study the relevance of GPNMB *in vivo* due to the presence of a naturally occurring point mutation, which results in a premature stop codon. Quantitative RT-PCR analysis revealed negligible levels of GPNMB mRNA in all tissues tested due to nonsense-mediated mRNA decay, a process that degrades mRNAs that terminate translation more than 50 nucleotides upstream of an exon-exon junction.[236] Thus, DBA/2J mice can be seen as GPNMB knockouts. As controls, DBA/2J-Gpnmb+ mice, which had been bred to carry a wild type version of the GPNMB gene,[195] were selected. Surprisingly, DBA/2J did not show any sign of cardiac abnormalities at basal levels. The hearts of DBA/2J mutant mice were morphologically indistinguishable from DBA/2J-Gpnmb+ wild type controls. Also, echocardiographic analysis revealed normal cardiac

function and geometry in young (3 months old) but also in aging (up to 11 months old) GPNMB mutant mice. Furthermore, heart weight / body weight ratios demonstrated similar values for both DBA/2J mouse strains. Therefore, the virtual absence of GPNMB is not sufficient to cause defects of cardiac development or function at basal levels.

Based on the observation of higher GPNMB expression in heart tissue after angiotensin II or isoprenaline treatment, we hypothesized that the glycoprotein might play a role in cardiac hypertrophy. In order to investigate this possibility, both DBA/2J mouse strains were treated with the β-adrenergic agonist isoprenaline to induce cardiac hypertrophy.[284] The outcome of the treatment was examined via echocardiography, qRT-PCR and blood composition analysis as well as histological approaches. As expected, we found a strong increase in relative heart weights in DBA/2J-Gpnmb+ and DBA/2J after 2 weeks of infusion compared to sham-treated littermates. In addition, echocardiographic analysis revealed better cardiac function as measured by higher fractional shortening, ejection fraction, cardiac output and stroke volume in both groups. These findings suggest that the isoprenaline dose and treatment period were adequate in order to induce hypertrophic changes of the heart. The improved functional parameters moreover suggest that the hypertrophy was sufficient as a compensatory response to the chronic β-adrenergic stimulation. However, no difference regarding cardiac function was noticeable between wild type and mutant mice. Echocardiography furthermore displayed only slight alterations of cardiac geometry in wild type mice after isoprenaline treatment that were non-significant in comparison to their sham-treated controls. On the other hand, posterior wall and interventricular septum thickness were found to be significantly higher in mutant mice compared to the respective sham group after one week of isoprenaline infusion (the effect disappeared after two weeks of treatment). Despite the fact that the difference of both parameters between wild type and mutant mice did not reach statistical significance, the results indicate a modest trend towards more physiological hypertrophy development in DBA/2J mutant mice compared to DBA/2J-Gpnmb+ controls. In order to better characterize the phenotypic changes due to the chronic isoprenaline treatment, qRT-PCR analysis were conducted. Levels of both hypertrophy markers ANP and BNP were found to be not different between sham- or isoprenaline-treated mutant mice but tended to be higher in wild type mice after isoprenaline infusion compared to sham controls. Despite the lack of statistical significance between wild type and mutant mice, this result might be interpreted as a trend towards less remodeling in DBA/2J animals. Quantitative RT-PCR furthermore revealed a strong induction of several fibrosis markers. Among them, collagen 1a1 and collagen 3 were not different between treated wild type and mutant mice. This finding was confirmed by sirius red stainings of heart sections from both groups that revealed similar levels of collagen in both groups. In contrast, fibronectin levels were found to be significantly lower in DBA/2J mice compared to wild type controls. Thus, development and/or composition

of fibrosis might be altered in mutant mice after cardiac hypertrophy induction despite similar expression of collagens. Moreover, automated blood composition measurements were carried out and demonstrated similar levels of all parameters analyzed in treated DBA/2J-Gpnmb+ and DBA/2J mice apart from monocyte counts, which were found to be significantly lower in mutant mice. In order to analyze if altered monocyte levels in blood are accompanied by differences in macrophage infiltration into the heart, qRT-PCR and immunostainings were conducted using cardiac tissue. These methods revealed enhanced levels of macrophages in hearts from both DBA/2J strains due to the treatment with isoprenaline. However, expression levels of the general macrophage marker F4/80 and number of mac-2-positive cells were similar between treated wild type and mutant animals suggesting similar rates of macrophage infiltration in both genotypes. Also, expression levels of markers specific for different macrophage subsets appeared to be comparable between DBA/2J-Gpnmb+ and DBA/2J mice. Only the M2 marker gene IL-10 was found to be higher in mutants compared to controls. In conclusion, these results suggest that similar numbers of monocytes infiltrate the hearts of both groups, but the distribution and/or activity of macrophage subsets might be altered in DBA/2J mice resulting in more effective reparative M2 macrophages. This might positively affect remodeling processes, inflammation and fibrosis development in these animals. However, these changes were only marginal and therefore not sufficient to alter the cardiac function in GPNMB mutant mice in comparison to wild type controls.

Based on the results from the isoprenaline experiments and the dramatic upregulation of GPNMB in heart tissue of wild type mice after myocardial infarction, we hypothesized that the glycoprotein might be more important in acute ischemic injury of the heart than in chronic cardiac hypertrophy. To investigate this possibility, experimental myocardial infarction was induced in both DBA/2J strains and mice were examined for 4 weeks via echocardiography, blood composition as well as histological analysis, quantitative RT-PCR and flow cytometry. To our surprise, the function of the heart was improved in DBA/2J mutant mice compared to wild type animals 4 weeks post-MI as measured by increased Simpson's ejection fraction and fractional shortening. Parameters of hypertrophy such as heart weight / tibia length ratios or posterior wall and interventricular septum thickness were not different between wild type and mutant mice after MI indicating similar levels of cardiac hypertrophy in both DBA/2J mouse strains. On the other hand, the diameter of the left ventricle was found to be lower in mutant mice 4 weeks after infarction resulting in slightly higher PWTD/LVEDD ratios. Thus, the absence of GPNMB seems to preserve the cardiac function in DBA/2J mice after ischemic injury accompanied by less dilatation of the heart. In line with this, levels of β-MHC were reduced in mutant mice compared to wild type animals, which can by itself have a beneficial effect on the disease state of the heart as described previously.[245] Also, expression of ANP and BNP were significantly lower in DBA/2J mice compared to controls 4 weeks after MI.

Despite of possible anti-hypertrophic and anti-fibrotic actions of these peptides, it has been reported that levels of ANP and especially BNP positively correlate with infarct size, LV remodeling and the severity of heart failure.[285] Thus, the finding of lower ANP and BNP expression in DBA/2J mice may be considered of prognostic value and may thus reflect less cardiac damage in GPNMB mutant mice. Moreover, it has been reported that myofibroblasts within the infarct scar express ANP and BNP and that the peptides may act as regulators of post-MI fibroblast proliferation and collagen scar formation.[286-288] In order to investigate if reduced ANP and BNP levels in GPNMB mutant mice actually affect the development of fibrosis and might thereby also influence the healing of the hearts after injury, levels of collagen 1a1, collagen 3 and fibronectin were determined via qRT-PCR. However, no difference of expression of these genes was found between the two DBA/2J strains at both time points after MI induction. Also, quantification of sirius red stainings in cardiac sections demonstrated similar levels of post-MI fibrosis in both groups.

To further characterize the phenotype of GPNMB mutant mice upon ischemic cardiac injury, blood composition was measured 7 days post-MI. This analysis revealed similar levels of white blood cells, platelets, lymphocytes, monocytes and granulocytes as well as hematocrit in blood of wild type and mutant mice. But the number of red blood cells and the hemoglobin concentration were found to be significantly higher in GPNMB mutant mice compared to wild type controls after MI whereas these parameters were not different in sham-treated groups. It is known that a reduction in hemoglobin concentration after MI compromises oxygen supply to the myocardium, which might favor arrhythmias, worsen hypotension and increase infarct size.[289,290] Also, anemia increases myocardial oxygen demand by increasing the cardiac output. In support to this view, several studies reported that low hemoglobin levels and anemia in patients with AMI are strongly associated with adverse outcomes and increased mortality.[291-294] On the other hand, very high baseline hemoglobin was correlated with a greater risk for adverse cardiovascular events possibly by increasing blood viscosity, which in turn results in decreased coronary blood flow and increased myocardial work.[295] Therefore, normal levels of red blood cells and hemoglobin in DBA/2J mice at basal levels reflect no increased risk for adverse events, whereas a modest increase in these parameters after MI may result in better oxygen supply to the heart. This might help to reduce ischemia and may thus at least partially explain the preserved cardiac function in these animals. In addition, anemia had been shown to promote LV end-diastolic volume dilatation.[296] Hence, DBA/2J mice may be protected against dilatation due to their high red blood cell and hemoglobin counts. The exact mechanism that links GPNMB and red blood cell and hemoglobin levels needs further investigation. However, one possible explanation is related to the finding that GPNMB is expressed by $CD163^+$ macrophages in lymphoid organs.[211] This macrophage subpopulation is described to be anti-inflammatory and tissue-resident and plays a role in

plasma clearance of hemoglobin via CD163.[297] Thus, the clearance of hemoglobin was found to be slower in CD163-deficient mice.[297] The absence of GPNMB might interfere with the phagocytic properties of $CD163^+$ macrophages *in vivo* and thereby contribute to the increased levels of hemoglobin found in the circulation of DBA/2J mice.

Blood, bone marrow and spleen of DBA/2J-Gpnmb+ and DBA/2J mice were furthermore examined via flow cytometry measurements. In order to analyze stem and progenitor cell counts, two different populations were defined by their expression of Sca-1 and c-Kit (Lin^- $Sca\text{-}1^+$ $c\text{-}Kit^+$ or LSK) or CD34 (Lin^- $CD34^+$) as described previously.[298,299] The lineage-negative (Lin^-) selection was based on a set of antibodies that are capable of binding mature leukocytes and erythrocytes, namely CD45, B220, CD3, Ter119, CD11b and Gr-1. The evaluation of flow cytometry results revealed similar levels of LSK and Lin^- $CD34^+$ progenitor cells in blood and BM of both wild type and mutant mice 7 days after sham or MI surgery. In combination with results from a study by Bandari *et al*. demonstrating that GPNMB is not expressed in immature BM-derived cells[300], our findings suggest that the glycoprotein does not affect cardiac repair processes via alteration of the stem/progenitor cell pool. Additionally, levels of B lymphocytes as well as $CD4^+$ or $CD8^+$ T lymphocytes were found to be comparable between DBA/2J-Gpnmb+ and DBA/2J mice 7 days post-MI in all organs analyzed. Despite the finding that GPNMB can function as negative regulator of T lymphocytes[182], its virtual absence in DBA/2J mice does obviously not affect B and T cell populations that are involved in inflammatory processes after myocardial infarction. Flow cytometry was furthermore applied to determine levels of myeloid cell types in both DBA/2J strains 7 days after infarction. These measurements demonstrated similar neutrophil numbers in blood of both groups, which suggests that the initial neutrophil-mediated inflammatory phase after MI is similar in wild type and mutant animals. However, monocyte levels were found to be significantly higher in blood of mutant mice and this difference might be attributed to a shift of monocyte subsets since $Ly6C^{high}$ cells were also significantly increased in DBA/2J mice whereas $Ly6C^{low}$ monocyte levels were similar between wild type and mutant mice. In BM, all analyzed cell types were increased in GPNMB mutant mice whereas in spleen, no difference of neutrophil or monocyte cell counts was detected between DBA/2J-Gpnmb+ and DBA/2J mice. In summary, flow cytometry displayed similar levels of reparative monocytes in blood of both DBA/2J mouse strains but higher pro-inflammatory monocyte counts in blood of GPNMB mutant mice. Based on the various functions of the monocyte subsets during post-MI healing, these differences could have an effect on cardiac repair processes in these mice upon ischemic injury. A general limitation of the flow cytometry measurements is that cell counts in blood do not necessarily correlate with numbers of cells that infiltrate the injured cardiac tissue. For instance, higher levels of pro-inflammatory monocytes in blood of DBA/2J mice could give rise to higher rates of pro-inflammatory M1 macrophages in the heart since

more cells are available for tissue extravasation. On the other hand, higher cell counts in the blood could also be the consequence of less infiltration of this cell type into the heart. Also, monocytes might change their functional characteristics (e.g. receptor expression) in the course of myocardial infarction, which could alter their capacity to migrate into myocardium.[301] Immunostainings of cardiac sections using antibodies that specifically bind to the different macrophage subsets are needed to evaluate the distribution of these subpopulations in the heart. Nevertheless, relative quantification of genes specific for different macrophage subsets in cardiac tissue of both DBA/2J strains via qRT-PCR can be helpful to provide an indication of their infiltration into the heart. These measurements revealed similar levels of the general macrophage marker F4/80 in both DBA/2J strains, which was confirmed by immunostainings of cardiac sections using an anti-mac-2 antibody. Also, expression levels of Arg, IL-10 and CCL17, which are typically expressed by reparative M2 macrophages, were similar in both groups. Levels of both pro-inflammatory markers iNOS and IL-12 were also similar in hearts from wild type and mutant mice. Only CXCL9 and CXCL10 as two additional pro-inflammatory genes tended to be higher in DBA/2J mice compared to DBA/2J-Gpnmb+ controls. The different expression levels of both chemokines did not reach statistical significance but could nonetheless hint at higher levels of pro-inflammatory macrophages in hearts of GPNMB mutant mice. This might be a result of higher blood counts and increased extravasation of these cells into the heart. At the same time, levels of reparative M2 monocytes/macrophages in blood and heart tissue were not different between wild type and mutant mice. Given the multiple and even contrasting functions of different macrophage subsets during all phases of myocardial post-MI healing, different interpretations of the results are conceivable. First, cell counts were analyzed at 7 days after infarction in a phase that is dominated by the recruitment and functions of $Ly6C^{low}$ monocytes/macrophages. These cells contribute to granulation tissue formation by their attenuated inflammatory and proangiogenic properties.[12] Thus, depletion of this monocyte subset in phase II after MI results in decreased collagen deposition, reduced numbers of myofibroblasts and $CD31^{+}$ endothelial cells. Similar levels of $Ly6C^{low}$ monocytes in blood of DBA/2J-Gpnmb+ and DBA/2J accompanied by similar M2 marker expression in heart tissue of both strains after MI indicates that the reparative functions of this subset are not affected by the absence of GPNMB resulting in normal myocardial healing in DBA/2J mice. In line with this, relative quantification of CD31 and VEGF in cardiac tissue of wild type and mutant mice revealed similar expression of both factors, thus indicating comparable levels of post-MI angiogenesis in both strains (data not shown). On the other hand, blood counts of $Ly6C^{high}$ monocytes and cardiac expression of certain M1 marker genes were found to be higher in GPNMB mutant mice 7 days after infarction. This monocyte subset comprises proteolytic and phagocytic functions and increased numbers of these cells might impair cardiac healing by preventing or delaying the initiation of phase II.[12]

Nevertheless, these monocytes are important for removal of cell debris and their depletion during phase I results in large areas of debris and necrotic tissue. Furthermore, it was demonstrated that a population of these cells can contribute to neovascularization and restoration of LV function, indicating its functional diversity.[301,302,303] Thus, higher levels of M1 monocytes/macrophages in GPNMB mutant mice 7 days after infarction in combination with unchanged M2 monocyte/macrophage counts might have beneficial effects on cardiac repair due to more efficient removal of dead cells and debris (by more M1) accompanied by proper induction of angiogenesis and granulation tissue formation (by normal levels of M2). Nevertheless, pro-inflammatory monocytes normally dominate the first phase after infarction and our measurements 7 days post-MI cannot exclude the possibility of altered monocyte numbers and functions at an earlier time point after cardiac damage.

As a second hypothesis, the absence of GPNMB might alter the phenotype of monocytes/macrophages at basal levels and thereby also interfere with their various roles after myocardial infarction. Previous reports actually suggest that GPNMB is necessary for the proper function of monocytes/macrophages[18,84,85] and therefore, we analyzed the phenotype of macrophages from both DBA/2J strains *in vitro*. For this purpose, BM cell suspensions were isolated from DBA/2J-Gpnmb+ and DBA/2J mice, cells were cultured for one week in the presence of M-CSF for macrophage enrichment and subsequently treated with either IFN-γ or IL-4 in order to produce pro-inflammatory or reparative macrophages. Cells from both wild type and mutant mice appeared similar in their ability to differentiate into both macrophage subtypes. Quantitative RT-PCR and ELISA analysis furthermore displayed similar expression levels of the M1 markers iNOS, CXCL9, CXCL10 and CXCL11 as well as comparable secretion of IL-12 from macrophages treated with IFN-γ. Thus, the differentiation and behavior of pro-inflammatory M1 macrophages seems to be less dependent on GPNMB. In line with this, expression levels of the glycoprotein were found to be decreased in macrophages upon IFN-γ treatment in comparison to untreated or IL-4-treated cells. The analysis of M2 marker genes revealed similar levels of arginase-1 in macrophages derived from DBA/2J-Gpnmb+ and DBA/2J but significantly higher CCL17 and a trend towards enhanced CCL22 expression in mutant macrophages. In summary, the absence of GPNMB is not sufficient to alter the phenotype of pro-inflammatory M1 macrophages, but might change the differentiation and behavior of reparative M2 macrophages towards a more active phenotype characterized by higher chemokine production. These findings might explain the differences in cell counts that were observed via flow cytometry and qRT-PCR. In DBA/2J mutant mice, levels of M2 monocytes were not altered compared to wild type controls but the cells might be more active in the absence of GPNMB, which could lead to more ECM and fibrosis development. Therefore, numbers of M1 monocytes might be higher in DBA/2J mice as a counteraction to the higher and possible deleterious activity of M2 cells. Whereas

increased levels of pro-inflammatory M1 macrophages might normally impair the healing of the heart, they might be necessary in DBA/2J mice in order to balance the inflammatory and reparative actions of both monocyte subsets for proper myocardial repair.

In conclusion, we could for the first time describe a functional involvement of GPNMB in cardiac pathophysiology. Upon induction of cardiac hypertrophy, the virtual absence of the glycoprotein in DBA/2J mice resulted in modest changes of cardiac morphology, fibrosis and macrophage infiltration of the heart without affecting cardiac function or blood composition. In contrast to this, the induction of myocardial infarction in GPNMB mutant mice revealed a preserved cardiac function accompanied by less dilatation, higher red blood cell counts and hemoglobin concentration. Whereas the development of fibrosis was not affected, the levels and extravasation of different monocyte subsets was altered in DBA/2J animals, which could be due to an altered phenotype of these cells already at baseline. These results in combination with immunofluorescent stainings, which demonstrated GPNMB expression exclusively in small, infiltrating cells in the peri-infarct region, suggest that the glycoprotein mediates its beneficial actions by affecting the behavior and levels of macrophages. Due to the observations from these pre-clinical studies, it is tempting to speculate that GPNMB might be also of importance for cardiac diseases in humans. In order to investigate this possibility, we analyzed GPNMB protein levels in plasma samples from patients suffering from chronic coronary artery disease or acute myocardial infarction and compared them to samples from controls with preserved ejection fraction. These measurements revealed no alterations of GPNMB levels in coronary artery disease patients compared to healthy individuals, but a significant increase of GPNMB in plasma of patients after an acute myocardial infarction. Thereby, levels of the glycoprotein did not correlate with CK or CK-MB values. However, high sensitive-Troponin T (hs-TnT) is now the biomarker of preference after MI and future measurements are needed to examine the correlation between GPNMB and TnT levels. Also, the appearance of GPNMB in the blood and its time course in the hours and days after MI needs further investigation in order to assess its diagnostic and prognostic potential. Nevertheless, our results suggest GPNMB as potentially new therapeutic target and biomarker in ischemic cardiac diseases.[304] Unlike its functions after ischemic injury in other organs, it seems to be deleterious for cardiac repair processes. Thus, blocking the activity of GPNMB (e.g. by using the antibody glembatumumab) could be a promising therapeutic approach for future studies.

6 References

1. World Health Organization (WHO), Global Burden of Disease (2008).
2. European Heart Network (EHN), European Cardiovascular Disease Statistics (2008).
3. Fuster, V., Badimon, L., Badimon, J.J. & Chesebro, J.H. The pathogenesis of coronary artery disease and the acute coronary syndromes (2). *N Engl J Med* 326, 310-318 (1992).
4. Libby, P. Current concepts of the pathogenesis of the acute coronary syndromes. *Circulation* 104, 365-372 (2001).
5. Kumar, A. & Cannon, C.P. Acute coronary syndromes: diagnosis and management, part I. *Mayo Clin Proc* 84, 917-938 (2009).
6. Bonaca, M.P.*, et al.* American College of Cardiology/American Heart Association/European Society of Cardiology/World Heart Federation universal definition of myocardial infarction classification system and the risk of cardiovascular death: observations from the TRITON-TIMI 38 trial (Trial to Assess Improvement in Therapeutic Outcomes by Optimizing Platelet Inhibition With Prasugrel-Thrombolysis in Myocardial Infarction 38). *Circulation* 125, 577-583 (2012).
7. White, H.D. & Chew, D.P. Acute myocardial infarction. *Lancet* 372, 570-584 (2008).
8. Mill, J.G., Stefanon, I., dos Santos, L. & Baldo, M.P. Remodeling in the ischemic heart: the stepwise progression for heart failure. *Braz J Med Biol Res* 44, 890-898 (2011).
9. Olivetti, G.*, et al.* [Does apoptosis participate in heart failure?]. *Cardiologia* 44 Suppl 1, 859-861 (1999).
10. van Empel, V.P.*, et al.* Myocyte apoptosis in heart failure. *Cardiovasc Res* 67, 21-29 (2005).
11. Geissmann, F., Jung, S. & Littman, D.R. Blood monocytes consist of two principal subsets with distinct migratory properties. *Immunity* 19, 71-82 (2003).
12. Nahrendorf, M.*, et al.* The healing myocardium sequentially mobilizes two monocyte subsets with divergent and complementary functions. *J Exp Med* 204, 3037-3047 (2007).
13. Sun, Y. Myocardial repair/remodelling following infarction: roles of local factors. *Cardiovasc Res* 81, 482-490 (2009).
14. Frantz, S., Bauersachs, J. & Ertl, G. Post-infarct remodelling: contribution of wound healing and inflammation. *Cardiovasc Res* 81, 474-481 (2009).
15. Nahrendorf, M., Pittet, M.J. & Swirski, F.K. Monocytes: protagonists of infarct inflammation and repair after myocardial infarction. *Circulation* 121, 2437-2445 (2010).
16. Passlick, B., Flieger, D. & Ziegler-Heitbrock, H.W. Identification and characterization of a novel monocyte subpopulation in human peripheral blood. *Blood* 74, 2527-2534 (1989).
17. Grage-Griebenow, E., Flad, H.D. & Ernst, M. Heterogeneity of human peripheral blood monocyte subsets. *J Leukoc Biol* 69, 11-20 (2001).
18. Tsujioka, H.*, et al.* Impact of heterogeneity of human peripheral blood monocyte subsets on myocardial salvage in patients with primary acute myocardial infarction. *J Am Coll Cardiol* 54, 130-138 (2009).
19. Tapp, L.D., Shantsila, E., Wrigley, B.J., Pamukcu, B. & Lip, G.Y. The CD14++CD16+ monocyte subset and monocyte-platelet interactions in patients with ST-elevation myocardial infarction. *J Thromb Haemost* 10, 1231-1241 (2012).
20. Gajarsa, J.J. & Kloner, R.A. Left ventricular remodeling in the post-infarction heart: a review of cellular, molecular mechanisms, and therapeutic modalities. *Heart Fail Rev* 16, 13-21 (2011).
21. Sutton, M.G. & Sharpe, N. Left ventricular remodeling after myocardial infarction: pathophysiology and therapy. *Circulation* 101, 2981-2988 (2000).
22. Zimmerman, S.D., Criscione, J. & Covell, J.W. Remodeling in myocardium adjacent to an infarction in the pig left ventricle. *Am J Physiol Heart Circ Physiol* 287, H2697-2704 (2004).
23. Whittaker, P., Boughner, D.R. & Kloner, R.A. Role of collagen in acute myocardial infarct expansion. *Circulation* 84, 2123-2134 (1991).
24. Weisman, H.F. & Healy, B. Myocardial infarct expansion, infarct extension, and reinfarction: pathophysiologic concepts. *Prog Cardiovasc Dis* 30, 73-110 (1987).
25. Dobaczewski, M., Gonzalez-Quesada, C. & Frangogiannis, N.G. The extracellular matrix as a modulator of the inflammatory and reparative response following myocardial infarction. *J Mol Cell Cardiol* 48, 504-511 (2010).
26. Frey, N., McKinsey, T.A. & Olson, E.N. Decoding calcium signals involved in cardiac growth and function. *Nat Med* 6, 1221-1227 (2000).
27. Wright, G.A. & Struthers, A.D. Natriuretic peptides as a prognostic marker and therapeutic target in heart failure. *Heart* 92, 149-151 (2006).
28. Bers, D.M. Altered cardiac myocyte Ca regulation in heart failure. *Physiology (Bethesda)* 21, 380-387 (2006).
29. Chattington, P., Clarke, D. & Neithercut, W.D. Creatine kinase isoform electrophoresis for the early confirmation of myocardial infarction detected by timed sequential CK slope analysis. *Postgrad Med J* 70, 805-808 (1994).
30. Saenger, A.K. & Jaffe, A.S. The use of biomarkers for the evaluation and treatment of patients with acute coronary syndromes. *Med Clin North Am* 91, 657-681; xi (2007).
31. Wright, R.S.*, et al.* 2011 ACCF/AHA focused update of the Guidelines for the Management of Patients with Unstable Angina/Non-ST-Elevation Myocardial Infarction (updating the 2007 guideline): a report of the American College of Cardiology Foundation/American Heart Association Task Force on Practice Guidelines developed in collaboration with the American College of Emergency Physicians, Society for Cardiovascular Angiography and Interventions, and Society of Thoracic Surgeons. *J Am Coll Cardiol* 57, 1920-1959 (2011).
32. Wright, R.S.*, et al.* 2011 ACCF/AHA Focused Update of the Guidelines for the Management of Patients With Unstable Angina/ Non-ST-Elevation Myocardial Infarction (Updating the 2007 Guideline): a report of the American College of Cardiology Foundation/American Heart Association Task Force on Practice Guidelines. *Circulation* 123, 2022-2060 (2011).
33. Krause, E.G., Rabitzsch, G., Noll, F., Mair, J. & Puschendorf, B. Glycogen phosphorylase isoenzyme BB in diagnosis of myocardial ischaemic injury and infarction. *Mol Cell Biochem* 160-161, 289-295 (1996).
34. Hayashida, K.*, et al.* Serum soluble lectin-like oxidized low-density lipoprotein receptor-1 levels are elevated in acute coronary syndrome: a novel marker for early diagnosis. *Circulation* 112, 812-818 (2005).
35. Kobayashi, N.*, et al.* Matrix metalloproteinase-9 for the earliest stage acute coronary syndrome. *Circ J* 75, 2853-2861 (2011).
36. Arakawa, N., Nakamura, M., Aoki, H. & Hiramori, K. Relationship between plasma level of brain natriuretic peptide and myocardial infarct size. *Cardiology* 85, 334-340 (1994).

37. James, S.K., *et al.* N-terminal pro-brain natriuretic peptide and other risk markers for the separate prediction of mortality and subsequent myocardial infarction in patients with unstable coronary artery disease: a Global Utilization of Strategies To Open occluded arteries (GUSTO)-IV substudy. *Circulation* 108, 275-281 (2003).
38. Morrow, D.A., *et al.* C-reactive protein is a potent predictor of mortality independently of and in combination with troponin T in acute coronary syndromes: a TIMI 11A substudy. Thrombolysis in Myocardial Infarction. *J Am Coll Cardiol* 31, 1460-1465 (1998).
39. Tanaka, A., *et al.* Multiple plaque rupture and C-reactive protein in acute myocardial infarction. *J Am Coll Cardiol* 45, 1594-1599 (2005).
40. Sabatine, M.S., *et al.* Multimarker approach to risk stratification in non-ST elevation acute coronary syndromes: simultaneous assessment of troponin I, C-reactive protein, and B-type natriuretic peptide. *Circulation* 105, 1760-1763 (2002).
41. Pratap, P., Gupta, S. & Berlowtiz, M. Routine invasive versus conservative management strategies in acute coronary syndrome: time for a "hybrid" approach. *J Cardiovasc Transl Res* 5, 30-40 (2012).
42. Fajadet, J. & Chieffo, A. Current management of left main coronary artery disease. *Eur Heart J* 33, 36-50b (2012).
43. Mitsos, S., *et al.* Therapeutic angiogenesis for myocardial ischemia revisited: basic biological concepts and focus on latest clinical trials. *Angiogenesis* 15, 1-22 (2012).
44. Wojakowski, W., *et al.* Mobilization of CD34/CXCR4+, CD34/CD117+, c-met+ stem cells, and mononuclear cells expressing early cardiac, muscle, and endothelial markers into peripheral blood in patients with acute myocardial infarction. *Circulation* 110, 3213-3220 (2004).
45. Ghadge, S.K., Muhlstedt, S., Ozcelik, C. & Bader, M. SDF-1alpha as a therapeutic stem cell homing factor in myocardial infarction. *Pharmacol Ther* 129, 97-108 (2011).
46. Iwanaga, K., *et al.* Effects of G-CSF on cardiac remodeling after acute myocardial infarction in swine. *Biochem Biophys Res Commun* 325, 1353-1359 (2004).
47. Kuethe, F., *et al.* Treatment with granulocyte colony-stimulating factor for mobilization of bone marrow cells in patients with acute myocardial infarction. *Am Heart J* 150, 115 (2005).
48. Valgimigli, M., *et al.* Use of granulocyte-colony stimulating factor during acute myocardial infarction to enhance bone marrow stem cell mobilization in humans: clinical and angiographic safety profile. *Eur Heart J* 26, 1838-1845 (2005).
49. Ince, H., *et al.* Prevention of left ventricular remodeling with granulocyte colony-stimulating factor after acute myocardial infarction: final 1-year results of the Front-Integrated Revascularization and Stem Cell Liberation in Evolving Acute Myocardial Infarction by Granulocyte Colony-Stimulating Factor (FIRSTLINE-AMI) Trial. *Circulation* 112, I73-80 (2005).
50. Zohlnhofer, D., *et al.* Stem cell mobilization by granulocyte colony-stimulating factor in patients with acute myocardial infarction: a randomized controlled trial. *JAMA* 295, 1003-1010 (2006).
51. Ripa, R.S., *et al.* Bone marrow derived mesenchymal cell mobilization by granulocyte-colony stimulating factor after acute myocardial infarction: results from the Stem Cells in Myocardial Infarction (STEMMI) trial. *Circulation* 116, I24-30 (2007).
52. Engelmann, M.G., *et al.* Autologous bone marrow stem cell mobilization induced by granulocyte colony-stimulating factor after subacute ST-segment elevation myocardial infarction undergoing late revascularization: final results from the G-CSF-STEMI (Granulocyte Colony-Stimulating Factor ST-Segment Elevation Myocardial Infarction) trial. *J Am Coll Cardiol* 48, 1712-1721 (2006).
53. Gersh, B.J., Simari, R.D., Behfar, A., Terzic, C.M. & Terzic, A. Cardiac cell repair therapy: a clinical perspective. *Mayo Clin Proc* 84, 876-892 (2009).
54. Joggerst, S.J. & Hatzopoulos, A.K. Stem cell therapy for cardiac repair: benefits and barriers. *Expert Rev Mol Med* 11, e20 (2009).
55. Wei, H.M., Wong, P., Hsu, L.F. & Shim, W. Human bone marrow-derived adult stem cells for post-myocardial infarction cardiac repair: current status and future directions. *Singapore Med J* 50, 935-942 (2009).
56. George, J.C. Stem cell therapy in acute myocardial infarction: a review of clinical trials. *Transl Res* 155, 10-19 (2010).
57. Dixon, J.A. & Spinale, F.G. Myocardial remodeling: cellular and extracellular events and targets. *Annu Rev Physiol* 73, 47-68 (2011).
58. Menasche, P., *et al.* Autologous skeletal myoblast transplantation for severe postinfarction left ventricular dysfunction. *J Am Coll Cardiol* 41, 1078-1083 (2003).
59. Pagani, F.D., *et al.* Autologous skeletal myoblasts transplanted to ischemia-damaged myocardium in humans. Histological analysis of cell survival and differentiation. *J Am Coll Cardiol* 41, 879-888 (2003).
60. Siminiak, T., *et al.* Percutaneous trans-coronary-venous transplantation of autologous skeletal myoblasts in the treatment of post-infarction myocardial contractility impairment: the POZNAN trial. *Eur Heart J* 26, 1188-1195 (2005).
61. Smits, P.C., *et al.* Myocardial repair by percutaneous cell transplantation of autologous skeletal myoblast as a stand alone procedure in post myocardial infarction chronic heart failure patients. *EuroIntervention* 1, 417-424 (2006).
62. Herreros, J., *et al.* Autologous intramyocardial injection of cultured skeletal muscle-derived stem cells in patients with non-acute myocardial infarction. *Eur Heart J* 24, 2012-2020 (2003).
63. Dib, N., *et al.* One-year follow-up of feasibility and safety of the first U.S., randomized, controlled study using 3-dimensional guided catheter-based delivery of autologous skeletal myoblasts for ischemic cardiomyopathy (CAuSMIC study). *JACC Cardiovasc Interv* 2, 9-16 (2009).
64. Menasche, P., *et al.* The Myoblast Autologous Grafting in Ischemic Cardiomyopathy (MAGIC) trial: first randomized placebo-controlled study of myoblast transplantation. *Circulation* 117, 1189-1200 (2008).
65. Murry, C.E., Whitney, M.L. & Reinecke, H. Muscle cell grafting for the treatment and prevention of heart failure. *J Card Fail* 8, S532-541 (2002).
66. Leobon, B., *et al.* Myoblasts transplanted into rat infarcted myocardium are functionally isolated from their host. *Proc Natl Acad Sci U S A* 100, 7808-7811 (2003).
67. Giordano, A., Galderisi, U. & Marino, I.R. From the laboratory bench to the patient's bedside: an update on clinical trials with mesenchymal stem cells. *J Cell Physiol* 211, 27-35 (2007).
68. Chen, S.L., *et al.* Effect on left ventricular function of intracoronary transplantation of autologous bone marrow mesenchymal stem cell in patients with acute myocardial infarction. *Am J Cardiol* 94, 92-95 (2004).
69. Hare, J.M., *et al.* A randomized, double-blind, placebo-controlled, dose-escalation study of intravenous adult human mesenchymal stem cells (prochymal) after acute myocardial infarction. *J Am Coll Cardiol* 54, 2277-2286 (2009).
70. Chugh, A.R., Zuba-Surma, E.K. & Dawn, B. Bone marrow-derived mesenchymal stems cells and cardiac repair. *Minerva Cardioangiol* 57, 185-202 (2009).

71. Katritsis, D.G., *et al.* Transcoronary transplantation of autologous mesenchymal stem cells and endothelial progenitors into infarcted human myocardium. *Catheter Cardiovasc Interv* 65, 321-329 (2005).
72. Bartunek, J., *et al.* Intracoronary injection of CD133-positive enriched bone marrow progenitor cells promotes cardiac recovery after recent myocardial infarction: feasibility and safety. *Circulation* 112, I178-183 (2005).
73. Erbs, S., *et al.* Transplantation of blood-derived progenitor cells after recanalization of chronic coronary artery occlusion: first randomized and placebo-controlled study. *Circ Res* 97, 756-762 (2005).
74. Stamm, C., *et al.* Intramyocardial delivery of CD133+ bone marrow cells and coronary artery bypass grafting for chronic ischemic heart disease: safety and efficacy studies. *J Thorac Cardiovasc Surg* 133, 717-725 (2007).
75. Losordo, D.W., *et al.* Intramyocardial transplantation of autologous CD34+ stem cells for intractable angina: a phase I/IIa double-blind, randomized controlled trial. *Circulation* 115, 3165-3172 (2007).
76. Assmus, B., *et al.* Transplantation of Progenitor Cells and Regeneration Enhancement in Acute Myocardial Infarction (TOPCARE-AMI). *Circulation* 106, 3009-3017 (2002).
77. Strauer, B.E., *et al.* Repair of infarcted myocardium by autologous intracoronary mononuclear bone marrow cell transplantation in humans. *Circulation* 106, 1913-1918 (2002).
78. Schachinger, V., *et al.* Transplantation of progenitor cells and regeneration enhancement in acute myocardial infarction: final one-year results of the TOPCARE-AMI Trial. *J Am Coll Cardiol* 44, 1690-1699 (2004).
79. Schachinger, V., *et al.* Improved clinical outcome after intracoronary administration of bone-marrow-derived progenitor cells in acute myocardial infarction: final 1-year results of the REPAIR-AMI trial. *Eur Heart J* 27, 2775-2783 (2006).
80. Assmus, B., *et al.* Clinical outcome 2 years after intracoronary administration of bone marrow-derived progenitor cells in acute myocardial infarction. *Circ Heart Fail* 3, 89-96 (2010).
81. Miettinen, J.A., *et al.* Determinants of functional recovery after myocardial infarction of patients treated with bone marrow-derived stem cells after thrombolytic therapy. *Heart* 96, 362-367 (2010).
82. Wollert, K.C., *et al.* Intracoronary autologous bone-marrow cell transfer after myocardial infarction: the BOOST randomised controlled clinical trial. *Lancet* 364, 141-148 (2004).
83. Meyer, G.P., *et al.* Intracoronary bone marrow cell transfer after myocardial infarction: eighteen months' follow-up data from the randomized, controlled BOOST (BOne marrOw transfer to enhance ST-elevation infarct regeneration) trial. *Circulation* 113, 1287-1294 (2006).
84. Janssens, S., *et al.* Autologous bone marrow-derived stem-cell transfer in patients with ST-segment elevation myocardial infarction: double-blind, randomised controlled trial. *Lancet* 367, 113-121 (2006).
85. Lunde, K., *et al.* Intracoronary injection of mononuclear bone marrow cells in acute myocardial infarction. *N Engl J Med* 355, 1199-1209 (2006).
86. Penicka, M., *et al.* Intracoronary injection of autologous bone marrow-derived mononuclear cells in patients with large anterior acute myocardial infarction: a prematurely terminated randomized study. *J Am Coll Cardiol* 49, 2373-2374 (2007).
87. Kang, H.J., *et al.* Effects of intracoronary infusion of peripheral blood stem-cells mobilised with granulocyte-colony stimulating factor on left ventricular systolic function and restenosis after coronary stenting in myocardial infarction: the MAGIC cell randomised clinical trial. *Lancet* 363, 751-756 (2004).
88. Steinwender, C., *et al.* Effects of peripheral blood stem cell mobilization with granulocyte-colony stimulating factor and their transcoronary transplantation after primary stent implantation for acute myocardial infarction. *Am Heart J* 151, 1296 e1297-1213 (2006).
89. Kang, H.J., *et al.* Differential effect of intracoronary infusion of mobilized peripheral blood stem cells by granulocyte colony-stimulating factor on left ventricular function and remodeling in patients with acute myocardial infarction versus old myocardial infarction: the MAGIC Cell-3-DES randomized, controlled trial. *Circulation* 114, I145-151 (2006).
90. Pasquet, S., *et al.* Long-term benefit of intracardiac delivery of autologous granulocyte-colony-stimulating factor-mobilized blood CD34+ cells containing cardiac progenitors on regional heart structure and function after myocardial infarct. *Cytotherapy* 11, 1002-1015 (2009).
91. Zlotnik, A. & Yoshie, O. Chemokines: a new classification system and their role in immunity. *Immunity* 12, 121-127 (2000).
92. Frangogiannis, N.G. Chemokines in ischemia and reperfusion. *Thromb Haemost* 97, 738-747 (2007).
93. Frangogiannis, N.G. & Entman, M.L. Chemokines in myocardial ischemia. *Trends Cardiovasc Med* 15, 163-169 (2005).
94. Liehn, E.A., Postea, O., Curaj, A. & Marx, N. Repair after myocardial infarction, between fantasy and reality: the role of chemokines. *J Am Coll Cardiol* 58, 2357-2362 (2011).
95. Matsumori, A., *et al.* Plasma levels of the monocyte chemotactic and activating factor/monocyte chemoattractant protein-1 are elevated in patients with acute myocardial infarction. *J Mol Cell Cardiol* 29, 419-423 (1997).
96. Aukrust, P., *et al.* Elevated circulating levels of C-C chemokines in patients with congestive heart failure. *Circulation* 97, 1136-1143 (1998).
97. Damas, J.K., *et al.* Myocardial expression of CC- and CXC-chemokines and their receptors in human end-stage heart failure. *Cardiovasc Res* 47, 778-787 (2000).
98. Boyle, E.M., Jr., *et al.* Inhibition of interleukin-8 blocks myocardial ischemia-reperfusion injury. *J Thorac Cardiovasc Surg* 116, 114-121 (1998).
99. Dewald, O., *et al.* CCL2/Monocyte Chemoattractant Protein-1 regulates inflammatory responses critical to healing myocardial infarcts. *Circ Res* 96, 881-889 (2005).
100. Schenk, S., *et al.* Monocyte chemotactic protein-3 is a myocardial mesenchymal stem cell homing factor. *Stem Cells* 25, 245-251 (2007).
101. Bousquenaud, M., *et al.* Monocyte chemotactic protein 3 is a homing factor for circulating angiogenic cells. *Cardiovasc Res* 94, 519-525 (2012).
102. Oh, D.J., *et al.* Fractalkine receptor (CX3CR1) inhibition is protective against ischemic acute renal failure in mice. *Am J Physiol Renal Physiol* 294, F264-271 (2008).
103. Nishikawa, S., Ogawa, M., Kunisada, T. & Kodama, H. B lymphopoiesis on stromal cell clone: stromal cell clones acting on different stages of B cell differentiation. *Eur J Immunol* 18, 1767-1771 (1988).
104. Nagasawa, T., *et al.* Molecular cloning and characterization of a murine pre-B-cell growth-stimulating factor/stromal cell-derived factor 1 receptor, a murine homolog of the human immunodeficiency virus 1 entry coreceptor fusin. *Proc Natl Acad Sci U S A* 93, 14726-14729 (1996).
105. Shirozu, M., *et al.* Structure and chromosomal localization of the human stromal cell-derived factor 1 (SDF1) gene. *Genomics* 28, 495-500 (1995).

106. Gleichmann, M., *et al.* Cloning and characterization of SDF-1gamma, a novel SDF-1 chemokine transcript with developmentally regulated expression in the nervous system. *Eur J Neurosci* 12, 1857-1866 (2000).
107. Pillarisetti, K. & Gupta, S.K. Cloning and relative expression analysis of rat stromal cell derived factor-1 (SDF-1)1: SDF-1 alpha mRNA is selectively induced in rat model of myocardial infarction. *Inflammation* 25, 293-300 (2001).
108. Yu, L., *et al.* Identification and expression of novel isoforms of human stromal cell-derived factor 1. *Gene* 374, 174-179 (2006).
109. Busillo, J.M. & Benovic, J.L. Regulation of CXCR4 signaling. *Biochim Biophys Acta* 1768, 952-963 (2007).
110. Haribabu, B., *et al.* Regulation of human chemokine receptors CXCR4. Role of phosphorylation in desensitization and internalization. *J Biol Chem* 272, 28726-28731 (1997).
111. Balabanian, K., *et al.* The chemokine SDF-1/CXCL12 binds to and signals through the orphan receptor RDC1 in T lymphocytes. *J Biol Chem* 280, 35760-35766 (2005).
112. Burns, J.M., *et al.* A novel chemokine receptor for SDF-1 and I-TAC involved in cell survival, cell adhesion, and tumor development. *J Exp Med* 203, 2201-2213 (2006).
113. Sierro, F., *et al.* Disrupted cardiac development but normal hematopoiesis in mice deficient in the second CXCL12/SDF-1 receptor, CXCR7. *Proc Natl Acad Sci U S A* 104, 14759-14764 (2007).
114. Decaillot, F.M., *et al.* CXCR7/CXCR4 heterodimer constitutively recruits beta-arrestin to enhance cell migration. *J Biol Chem* 286, 32188-32197 (2011).
115. Nagasawa, T., *et al.* Defects of B-cell lymphopoiesis and bone-marrow myelopoiesis in mice lacking the CXC chemokine PBSF/SDF-1. *Nature* 382, 635-638 (1996).
116. Zou, Y.R., Kottmann, A.H., Kuroda, M., Taniuchi, I. & Littman, D.R. Function of the chemokine receptor CXCR4 in haematopoiesis and in cerebellar development. *Nature* 393, 595-599 (1998).
117. Ma, Q., *et al.* Impaired B-lymphopoiesis, myelopoiesis, and derailed cerebellar neuron migration in CXCR4- and SDF-1-deficient mice. *Proc Natl Acad Sci U S A* 95, 9448-9453 (1998).
118. Kucia, M., *et al.* Trafficking of normal stem cells and metastasis of cancer stem cells involve similar mechanisms: pivotal role of the SDF-1-CXCR4 axis. *Stem Cells* 23, 879-894 (2005).
119. Pituch-Noworolska, A., *et al.* Circulating CXCR4-positive stem/progenitor cells compete for SDF-1-positive niches in bone marrow, muscle and neural tissues: an alternative hypothesis to stem cell plasticity. *Folia Histochem Cytobiol* 41, 13-21 (2003).
120. Lazarini, F., Tham, T.N., Casanova, P., Arenzana-Seisdedos, F. & Dubois-Dalcq, M. Role of the alpha-chemokine stromal cell-derived factor (SDF-1) in the developing and mature central nervous system. *Glia* 42, 139-148 (2003).
121. Hatch, H.M., Zheng, D., Jorgensen, M.L. & Petersen, B.E. SDF-1alpha/CXCR4: a mechanism for hepatic oval cell activation and bone marrow stem cell recruitment to the injured liver of rats. *Cloning Stem Cells* 4, 339-351 (2002).
122. Tzeng, Y.S., *et al.* Loss of Cxcl12/Sdf-1 in adult mice decreases the quiescent state of hematopoietic stem/progenitor cells and alters the pattern of hematopoietic regeneration after myelosuppression. *Blood* 117, 429-439 (2011).
123. Sun, X., *et al.* CXCL12 / CXCR4 / CXCR7 chemokine axis and cancer progression. *Cancer Metastasis Rev* 29, 709-722 (2010).
124. Simmons, G., *et al.* Co-receptor use by HIV and inhibition of HIV infection by chemokine receptor ligands. *Immunol Rev* 177, 112-126 (2000).
125. Kucia, M., *et al.* CXCR4-SDF-1 signalling, locomotion, chemotaxis and adhesion. *J Mol Histol* 35, 233-245 (2004).
126. Askari, A.T., *et al.* Effect of stromal-cell-derived factor 1 on stem-cell homing and tissue regeneration in ischaemic cardiomyopathy. *Lancet* 362, 697-703 (2003).
127. Abbott, J.D., *et al.* Stromal cell-derived factor-1alpha plays a critical role in stem cell recruitment to the heart after myocardial infarction but is not sufficient to induce homing in the absence of injury. *Circulation* 110, 3300-3305 (2004).
128. Hu, X., *et al.* Stromal cell derived factor-1 alpha confers protection against myocardial ischemia/reperfusion injury: role of the cardiac stromal cell derived factor-1 alpha CXCR4 axis. *Circulation* 116, 654-663 (2007).
129. Yamani, M.H., *et al.* Peritransplant ischemic injury is associated with up-regulation of stromal cell-derived factor-1. *J Am Coll Cardiol* 46, 1029-1035 (2005).
130. Leone, A.M., *et al.* Endogenous G-CSF and CD34+ cell mobilization after acute myocardial infarction. *Int J Cardiol* 111, 202-208 (2006).
131. Chang, L.T., *et al.* Role of stromal cell-derived factor-1alpha, level and value of circulating interleukin-10 and endothelial progenitor cells in patients with acute myocardial infarction undergoing primary coronary angioplasty. *Circ J* 73, 1097-1104 (2009).
132. Ceradini, D.J., *et al.* Progenitor cell trafficking is regulated by hypoxic gradients through HIF-1 induction of SDF-1. *Nat Med* 10, 858-864 (2004).
133. Tang, Y.L., *et al.* Hypoxic preconditioning enhances the benefit of cardiac progenitor cell therapy for treatment of myocardial infarction by inducing CXCR4 expression. *Circ Res* 104, 1209-1216 (2009).
134. Tang, J., Wang, J., Yang, J. & Kong, X. Adenovirus-mediated stromal cell-derived- factor-1alpha gene transfer induces cardiac preservation after infarction via angiogenesis of CD133+ stem cells and anti-apoptosis. *Interact Cardiovasc Thorac Surg* 7, 767-770 (2008).
135. Tang, J., *et al.* Adenovirus-mediated stromal cell-derived factor-1 alpha gene transfer improves cardiac structure and function after experimental myocardial infarction through angiogenic and antifibrotic actions. *Mol Biol Rep* 37, 1957-1969 (2010).
136. Saxena, A., *et al.* Stromal cell-derived factor-1alpha is cardioprotective after myocardial infarction. *Circulation* 117, 2224-2231 (2008).
137. Sundararaman, S., *et al.* Plasmid-based transient human stromal cell-derived factor-1 gene transfer improves cardiac function in chronic heart failure. *Gene Ther* 18, 867-873 (2011).
138. Deglurkar, I., *et al.* Mechanical and electrical effects of cell-based gene therapy for ischemic cardiomyopathy are independent. *Hum Gene Ther* 17, 1144-1151 (2006).
139. Elmadbouh, I., *et al.* Ex vivo delivered stromal cell-derived factor-1alpha promotes stem cell homing and induces angiomyogenesis in the infarcted myocardium. *J Mol Cell Cardiol* 42, 792-803 (2007).
140. Zhao, T., Zhang, D., Millard, R.W., Ashraf, M. & Wang, Y. Stem cell homing and angiomyogenesis in transplanted hearts are enhanced by combined intramyocardial SDF-1alpha delivery and endogenous cytokine signaling. *Am J Physiol Heart Circ Physiol* 296, H976-986 (2009).
141. Petit, I., *et al.* G-CSF induces stem cell mobilization by decreasing bone marrow SDF-1 and up-regulating CXCR4. *Nat Immunol* 3, 687-694 (2002).
142. Segers, V.F., *et al.* Local delivery of protease-resistant stromal cell derived factor-1 for stem cell recruitment after myocardial infarction. *Circulation* 116, 1683-1692 (2007).

143. Zaruba, M.M., *et al.* Synergy between CD26/DPP-IV inhibition and G-CSF improves cardiac function after acute myocardial infarction. *Cell Stem Cell* 4, 313-323 (2009).
144. Huber, B.C., *et al.* Parathyroid hormone is a DPP-IV inhibitor and increases SDF-1-driven homing of CXCR4(+) stem cells into the ischaemic heart. *Cardiovasc Res* 90, 529-537 (2011).
145. Ziegler, M., *et al.* The bispecific SDF1-GPVI fusion protein preserves myocardial function after transient ischemia in mice. *Circulation* 125, 685-696 (2012).
146. Zhang, D., *et al.* Over-expression of CXCR4 on mesenchymal stem cells augments myoangiogenesis in the infarcted myocardium. *J Mol Cell Cardiol* 44, 281-292 (2008).
147. Cheng, Z., *et al.* Targeted migration of mesenchymal stem cells modified with CXCR4 gene to infarcted myocardium improves cardiac performance. *Mol Ther* 16, 571-579 (2008).
148. Shiba, Y., *et al.* Bone marrow CXCR4 induction by cultivation enhances therapeutic angiogenesis. *Cardiovasc Res* 81, 169-177 (2009).
149. Frangogiannis, N.G. The stromal cell-derived factor-1/CXCR4 axis in cardiac injury and repair. *J Am Coll Cardiol* 58, 2424-2426 (2011).
150. Penn, M.S., Pastore, J., Miller, T. & Aras, R. SDF-1 in myocardial repair. *Gene Ther* 19, 583-587 (2012).
151. Theiss, H.D., *et al.* Safety and efficacy of SITAgliptin plus GRanulocyte-colony-stimulating factor in patients suffering from Acute Myocardial Infarction (SITAGRAMI-Trial)--rationale, design and first interim analysis. *Int J Cardiol* 145, 282-284 (2010).
152. Massberg, S., *et al.* Platelets secrete stromal cell-derived factor 1alpha and recruit bone marrow-derived progenitor cells to arterial thrombi in vivo. *J Exp Med* 203, 1221-1233 (2006).
153. Jin, D.K., *et al.* Cytokine-mediated deployment of SDF-1 induces revascularization through recruitment of CXCR4+ hemangiocytes. *Nat Med* 12, 557-567 (2006).
154. Stellos, K., *et al.* Platelet-derived stromal cell-derived factor-1 regulates adhesion and promotes differentiation of human CD34+ cells to endothelial progenitor cells. *Circulation* 117, 206-215 (2008).
155. Stellos, K., *et al.* Platelets in regeneration. *Semin Thromb Hemost* 36, 175-184 (2010).
156. Stellos, K., *et al.* Expression of stromal-cell-derived factor-1 on circulating platelets is increased in patients with acute coronary syndrome and correlates with the number of CD34+ progenitor cells. *Eur Heart J* 30, 584-593 (2009).
157. Yokoi, H., *et al.* Bone marrow AT1 augments neointima formation by promoting mobilization of smooth muscle progenitors via platelet-derived SDF-1{alpha}. *Arterioscler Thromb Vasc Biol* 30, 60-67 (2010).
158. Pyo, R.T., *et al.* CXCR4 modulates contractility in adult cardiac myocytes. *J Mol Cell Cardiol* 41, 834-844 (2006).
159. Koch, K.C., *et al.* Effect of catheter-based transendocardial delivery of stromal cell-derived factor 1alpha on left ventricular function and perfusion in a porcine model of myocardial infarction. *Basic Res Cardiol* 101, 69-77 (2006).
160. Chen, J., *et al.* Effects of CXCR4 gene transfer on cardiac function after ischemia-reperfusion injury. *Am J Pathol* 176, 1705-1715 (2010).
161. Dai, S., *et al.* Chronic AMD3100 antagonism of SDF-1alpha-CXCR4 exacerbates cardiac dysfunction and remodeling after myocardial infarction. *J Mol Cell Cardiol* 49, 587-597 (2010).
162. Proulx, C., *et al.* Antagonism of stromal cell-derived factor-1alpha reduces infarct size and improves ventricular function after myocardial infarction. *Pflugers Arch* 455, 241-250 (2007).
163. Jujo, K., *et al.* CXCR4 blockade augments bone marrow progenitor cell recruitment to the neovasculature and reduces mortality after myocardial infarction. *Proc Natl Acad Sci U S A* 107, 11008-11013 (2010).
164. Agarwal, U., *et al.* Role of cardiac myocyte CXCR4 expression in development and left ventricular remodeling after acute myocardial infarction. *Circ Res* 107, 667-676 (2010).
165. Liehn, E.A., *et al.* Double-edged role of the CXCL12/CXCR4 axis in experimental myocardial infarction. *J Am Coll Cardiol* 58, 2415-2423 (2011).
166. Ghadge, S.K. Cardiomyocyte specific deletion of strom cell derived factor-1 (SDF-1/CXCL12) protects the heart from hypertrophic and ischemic damage (Thesis, Freie Universität Berlin, 2011).
167. Weterman, M.A., *et al.* nmb, a novel gene, is expressed in low-metastatic human melanoma cell lines and xenografts. *Int J Cancer* 60, 73-81 (1995).
168. Bachner, D., Schroder, D. & Gross, G. mRNA expression of the murine glycoprotein (transmembrane) nmb (Gpnmb) gene is linked to the developing retinal pigment epithelium and iris. *Brain Res Gene Expr Patterns* 1, 159-165 (2002).
169. Owen, T.A., *et al.* Identification and characterization of the genes encoding human and mouse osteoactivin. *Crit Rev Eukaryot Gene Expr* 13, 205-220 (2003).
170. Abdelmagid, S.M., *et al.* Osteoactivin, an anabolic factor that regulates osteoblast differentiation and function. *Exp Cell Res* 314, 2334-2351 (2008).
171. Selim, A.A. Osteoactivin bioinformatic analysis: prediction of novel functions, structural features, and modes of action. *Med Sci Monit* 15, MT19-33 (2009).
172. Safadi, F.F., *et al.* Cloning and characterization of osteoactivin, a novel cDNA expressed in osteoblasts. *J Cell Biochem* 84, 12-26 (2001).
173. Loftus, S.K., *et al.* Gpnmb is a melanoblast-expressed, MITF-dependent gene. *Pigment Cell Melanoma Res* 22, 99-110 (2009).
174. Shikano, S., Bonkobara, M., Zukas, P.K. & Ariizumi, K. Molecular cloning of a dendritic cell-associated transmembrane protein, DC-HIL, that promotes RGD-dependent adhesion of endothelial cells through recognition of heparan sulfate proteoglycans. *J Biol Chem* 276, 8125-8134 (2001).
175. Ahn, J.H., *et al.* Identification of the genes differentially expressed in human dendritic cell subsets by cDNA subtraction and microarray analysis. *Blood* 100, 1742-1754 (2002).
176. Haralanova-Ilieva, B., Ramadori, G. & Armbrust, T. Expression of osteoactivin in rat and human liver and isolated rat liver cells. *J Hepatol* 42, 565-572 (2005).
177. Tomihari, M., Hwang, S.H., Chung, J.S., Cruz, P.D., Jr. & Ariizumi, K. Gpnmb is a melanosome-associated glycoprotein that contributes to melanocyte/keratinocyte adhesion in a RGD-dependent fashion. *Exp Dermatol* 18, 586-595 (2009).
178. Ripoll, V.M., Irvine, K.M., Ravasi, T., Sweet, M.J. & Hume, D.A. Gpnmb is induced in macrophages by IFN-gamma and lipopolysaccharide and acts as a feedback regulator of proinflammatory responses. *J Immunol* 178, 6557-6566 (2007).
179. Hoashi, T., Tamaki, K. & Hearing, V.J. The secreted form of a melanocyte membrane-bound glycoprotein (Pmel17/gp100) is released by ectodomain shedding. *FASEB J* 24, 916-930 (2010).
180. Rose, A.A., *et al.* ADAM10 releases a soluble form of the GPNMB/Osteoactivin extracellular domain with angiogenic properties. *PLoS One* 5, e12093 (2010).

181. Patel-Chamberlin, M., *et al.* Hematopoietic growth factor inducible neurokinin-1 (Gpnmb/Osteoactivin) is a biomarker of progressive renal injury across species. *Kidney Int* 79, 1138-1148 (2011).
182. Chung, J.S., *et al.* Binding of DC-HIL to dermatophytic fungi induces tyrosine phosphorylation and potentiates antigen presenting cell function. *J Immunol* 183, 5190-5198 (2009).
183. Chung, J.S., Sato, K., Dougherty, II, Cruz, P.D., Jr. & Ariizumi, K. DC-HIL is a negative regulator of T lymphocyte activation. *Blood* 109, 4320-4327 (2007).
184. Schwarzbich, M.A., *et al.* The immune inhibitory receptor osteoactivin is upregulated in monocyte-derived dendritic cells by BCR-ABL tyrosine kinase inhibitors. *Cancer Immunol Immunother* 61, 193-202 (2012).
185. Ripoll, V.M., *et al.* Microphthalmia transcription factor regulates the expression of the novel osteoclast factor GPNMB. *Gene* 413, 32-41 (2008).
186. Ogawa, T., *et al.* Osteoactivin upregulates expression of MMP-3 and MMP-9 in fibroblasts infiltrated into denervated skeletal muscle in mice. *Am J Physiol Cell Physiol* 289, C697-707 (2005).
187. Selim, A.A., *et al.* Anti-osteoactivin antibody inhibits osteoblast differentiation and function in vitro. *Crit Rev Eukaryot Gene Expr* 13, 265-275 (2003).
188. Sheng, M.H., Wergedal, J.E., Mohan, S. & Lau, K.H. Osteoactivin is a novel osteoclastic protein and plays a key role in osteoclast differentiation and activity. *FEBS Lett* 582, 1451-1458 (2008).
189. Abdelmagid, S.M., *et al.* Osteoactivin acts as downstream mediator of BMP-2 effects on osteoblast function. *J Cell Physiol* 210, 26-37 (2007).
190. Singh, M., Del Carpio-Cano, F.E., Monroy, M.A., Popoff, S.N. & Safadi, F.F. Homeodomain transcription factors regulate BMP-2-induced osteoactivin transcription in osteoblasts. *J Cell Physiol* 227, 390-399 (2012).
191. Arosarena, O.A., *et al.* Comparison of bone morphogenetic protein-2 and osteoactivin for mesenchymal cell differentiation: effects of bolus and continuous administration. *J Cell Physiol* 226, 2943-2952 (2011).
192. Raynaud, C.M., *et al.* Comprehensive characterization of mesenchymal stem cells from human placenta and fetal membrane and their response to osteoactivin stimulation. *Stem Cells Int* 2012, 658356 (2012).
193. Anderson, M.G., *et al.* Mutations in genes encoding melanosomal proteins cause pigmentary glaucoma in DBA/2J mice. *Nat Genet* 30, 81-85 (2002).
194. Anderson, M.G., *et al.* Genetic context determines susceptibility to intraocular pressure elevation in a mouse pigmentary glaucoma. *BMC Biol* 4, 20 (2006).
195. Howell, G.R., *et al.* Absence of glaucoma in DBA/2J mice homozygous for wild-type versions of Gpnmb and Tyrp1. *BMC Genet* 8, 45 (2007).
196. Mo, J.S., *et al.* By altering ocular immune privilege, bone marrow-derived cells pathogenically contribute to DBA/2J pigmentary glaucoma. *J Exp Med* 197, 1335-1344 (2003).
197. Anderson, M.G., *et al.* GpnmbR150X allele must be present in bone marrow derived cells to mediate DBA/2J glaucoma. *BMC Genet* 9, 30 (2008).
198. Rich, J.N., *et al.* Bone-related genes expressed in advanced malignancies induce invasion and metastasis in a genetically defined human cancer model. *J Biol Chem* 278, 15951-15957 (2003).
199. Onaga, M., *et al.* Osteoactivin expressed during cirrhosis development in rats fed a choline-deficient, L-amino acid-defined diet, accelerates motility of hepatoma cells. *J Hepatol* 39, 779-785 (2003).
200. Metz, R.L., Patel, P.S., Hameed, M., Bryan, M. & Rameshwar, P. Role of human HGFIN/nmb in breast cancer. *Breast Cancer Res* 9, R58 (2007).
201. Tse, K.F., *et al.* CR011, a fully human monoclonal antibody-auristatin E conjugate, for the treatment of melanoma. *Clin Cancer Res* 12, 1373-1382 (2006).
202. Williams, M.D., *et al.* GPNMB expression in uveal melanoma: a potential for targeted therapy. *Melanoma Res* 20, 184-190 (2010).
203. Kuan, C.T., *et al.* Glycoprotein nonmetastatic melanoma protein B, a potential molecular therapeutic target in patients with glioblastoma multiforme. *Clin Cancer Res* 12, 1970-1982 (2006).
204. Rose, A.A., *et al.* Osteoactivin promotes breast cancer metastasis to bone. *Mol Cancer Res* 5, 1001-1014 (2007).
205. Qian, X., Mills, E., Torgov, M., LaRochelle, W.J. & Jeffers, M. Pharmacologically enhanced expression of GPNMB increases the sensitivity of melanoma cells to the CR011-vcMMAE antibody-drug conjugate. *Mol Oncol* 2, 81-93 (2008).
206. Naumovski, L. & Junutula, J.R. Glembatumumab vedotin, a conjugate of an anti-glycoprotein non-metastatic melanoma protein B mAb and monomethyl auristatin E for the treatment of melanoma and breast cancer. *Curr Opin Mol Ther* 12, 248-257 (2010).
207. Keir, C.H. & Vahdat, L.T. The use of an antibody drug conjugate, glembatumumab vedotin (CDX-011), for the treatment of breast cancer. *Expert Opin Biol Ther* 12, 259-263 (2012).
208. Furochi, H., *et al.* Osteoactivin fragments produced by ectodomain shedding induce MMP-3 expression via ERK pathway in mouse NIH-3T3 fibroblasts. *FEBS Lett* 581, 5743-5750 (2007).
209. Abe, H., *et al.* Transgenic expression of osteoactivin in the liver attenuates hepatic fibrosis in rats. *Biochem Biophys Res Commun* 356, 610-615 (2007).
210. Nakamura, A., Ishii, A., Ohata, C. & Komurasaki, T. Early induction of osteoactivin expression in rat renal tubular epithelial cells after unilateral ureteral obstruction. *Exp Toxicol Pathol* 59, 53-59 (2007).
211. Li, B., *et al.* The melanoma-associated transmembrane glycoprotein Gpnmb controls trafficking of cellular debris for degradation and is essential for tissue repair. *FASEB J* 24, 4767-4781 (2010).
212. Pahl, M.V., Vaziri, N.D., Yuan, J. & Adler, S.G. Upregulation of monocyte/macrophage HGFIN (Gpnmb/Osteoactivin) expression in end-stage renal disease. *Clin J Am Soc Nephrol* 5, 56-61 (2010).
213. Adler, S. Novel kidney injury biomarkers. *J Ren Nutr* 20, S15-18 (2010).
214. Pohjolainen, V., *et al.* Left ventricular periostin gene expression is associated with fibrogenesis in experimental renal insufficiency. *Nephrol Dial Transplant* (2011).
215. Psarras, S., *et al.* Regulation of adverse remodelling by osteopontin in a genetic heart failure model. *Eur Heart J* (2011).
216. Takahashi, R., *et al.* Serum syndecan-4 is a novel biomarker for patients with chronic heart failure. *J Cardiol* 57, 325-332 (2011).
217. Li, J., Brown, L.F., Laham, R.J., Volk, R. & Simons, M. Macrophage-dependent regulation of syndecan gene expression. *Circ Res* 81, 785-796 (1997).
218. Finsen, A.V., *et al.* Syndecan-4 is essential for development of concentric myocardial hypertrophy via stretch-induced activation of the calcineurin-NFAT pathway. *PLoS One* 6, e28302 (2011).

219. Echtermeyer, F.*, et al.* Syndecan-4 signalling inhibits apoptosis and controls NFAT activity during myocardial damage and remodelling. *Cardiovasc Res* 92, 123-131 (2011).
220. Matsui, Y.*, et al.* Syndecan-4 prevents cardiac rupture and dysfunction after myocardial infarction. *Circ Res* 108, 1328-1339 (2011).
221. Kuhn, R., Schwenk, F., Aguet, M. & Rajewsky, K. Inducible gene targeting in mice. *Science* 269, 1427-1429 (1995).
222. Tiedt, R., Schomber, T., Hao-Shen, H. & Skoda, R.C. Pf4-Cre transgenic mice allow the generation of lineage-restricted gene knockouts for studying megakaryocyte and platelet function in vivo. *Blood* 109, 1503-1506 (2007).
223. Sambrook, J. & Russell, D.W. Southern blotting: capillary transfer of DNA to membranes. *CSH Protoc* 2006(2006).
224. Livak, K.J. & Schmittgen, T.D. Analysis of relative gene expression data using real-time quantitative PCR and the 2(-Delta Delta C(T)) Method. *Methods* 25, 402-408 (2001).
225. Simpson, R.J. Quantifying protein by bicinchoninic Acid. *CSH Protoc* 2008, pdb prot4722 (2008).
226. Zhang, X., Goncalves, R. & Mosser, D.M. The isolation and characterization of murine macrophages. *Curr Protoc Immunol* Chapter 14, Unit 14 11 (2008).
227. Popova, E., Krivokharchenko, A., Ganten, D. & Bader, M. Efficiency of transgenic rat production is independent of transgene-construct and overnight embryo culture. *Theriogenology* 61, 1441-1453 (2004).
228. Posch, M.G.*, et al.* Plasma HER2 levels are not associated with cardiac function or hypertrophy in control subjects and heart failure patients. *Int J Cardiol* 145, 105-106 (2010).
229. Deten, A., Holzl, A., Leicht, M., Barth, W. & Zimmer, H.G. Changes in extracellular matrix and in transforming growth factor beta isoforms after coronary artery ligation in rats. *J Mol Cell Cardiol* 33, 1191-1207 (2001).
230. Azhar, M.*, et al.* Transforming growth factor beta in cardiovascular development and function. *Cytokine Growth Factor Rev* 14, 391-407 (2003).
231. Sanford, L.P.*, et al.* TGFbeta2 knockout mice have multiple developmental defects that are non-overlapping with other TGFbeta knockout phenotypes. *Development* 124, 2659-2670 (1997).
232. Iwabu, A.*, et al.* Concomitant expression of heparin-binding epidermal growth factor-like growth factor mRNA and basic fibroblast growth factor mRNA in myocardial infarction in rats. *Basic Res Cardiol* 97, 214-222 (2002).
233. Tanaka, N.*, et al.* A role of heparin-binding epidermal growth factor-like growth factor in cardiac remodeling after myocardial infarction. *Biochem Biophys Res Commun* 297, 375-381 (2002).
234. Ushikoshi, H.*, et al.* Local overexpression of HB-EGF exacerbates remodeling following myocardial infarction by activating noncardiomyocytes. *Lab Invest* 85, 862-873 (2005).
235. Iwamoto, R.*, et al.* Heparin-binding EGF-like growth factor and ErbB signaling is essential for heart function. *Proc Natl Acad Sci U S A* 100, 3221-3226 (2003).
236. Maquat, L.E. Nonsense-mediated mRNA decay in mammals. *J Cell Sci* 118, 1773-1776 (2005).
237. Kirk, E.A.*, et al.* Hyper- and hypo-responsiveness to dietary fat and cholesterol among inbred mice: searching for level and variability genes. *J Lipid Res* 36, 1522-1532 (1995).
238. Yin, F.C., Spurgeon, H.A., Rakusan, K., Weisfeldt, M.L. & Lakatta, E.G. Use of tibial length to quantify cardiac hypertrophy: application in the aging rat. *Am J Physiol* 243, H941-947 (1982).
239. Collins, K.A., Korcarz, C.E. & Lang, R.M. Use of echocardiography for the phenotypic assessment of genetically altered mice. *Physiol Genomics* 13, 227-239 (2003).
240. McGrath, K.E., Koniski, A.D., Maltby, K.M., McGann, J.K. & Palis, J. Embryonic expression and function of the chemokine SDF-1 and its receptor, CXCR4. *Dev Biol* 213, 442-456 (1999).
241. Smith, T.K. & Bader, D.M. Signals from both sides: Control of cardiac development by the endocardium and epicardium. *Semin Cell Dev Biol* 18, 84-89 (2007).
242. Yu, S., Crawford, D., Tsuchihashi, T., Behrens, T.W. & Srivastava, D. The chemokine receptor CXCR7 functions to regulate cardiac valve remodeling. *Dev Dyn* 240, 384-393 (2011).
243. Matzinger, P. The danger model: a renewed sense of self. *Science* 296, 301-305 (2002).
244. Sasaki, T.*, et al.* Stromal cell-derived factor-1alpha improves infarcted heart function through angiogenesis in mice. *Pediatr Int* 49, 966-971 (2007).
245. Krenz, M. & Robbins, J. Impact of beta-myosin heavy chain expression on cardiac function during stress. *J Am Coll Cardiol* 44, 2390-2397 (2004).
246. Caulfield, J.B. & Borg, T.K. The collagen network of the heart. *Lab Invest* 40, 364-372 (1979).
247. Cleutjens, J.P., Verluyten, M.J., Smiths, J.F. & Daemen, M.J. Collagen remodeling after myocardial infarction in the rat heart. *Am J Pathol* 147, 325-338 (1995).
248. Schulze, P.C. & Lee, R.T. Macrophage-mediated cardiac fibrosis. *Circ Res* 95, 552-553 (2004).
249. Litwin, S.E., Litwin, C.M., Raya, T.E., Warner, A.L. & Goldman, S. Contractility and stiffness of noninfarcted myocardium after coronary ligation in rats. Effects of chronic angiotensin converting enzyme inhibition. *Circulation* 83, 1028-1037 (1991).
250. Fraccarollo, D., Galuppo, P., Bauersachs, J. & Ertl, G. Collagen accumulation after myocardial infarction: effects of ETA receptor blockade and implications for early remodeling. *Cardiovasc Res* 54, 559-567 (2002).
251. Weber, K.T. Fibrosis in hypertensive heart disease: focus on cardiac fibroblasts. *J Hypertens* 22, 47-50 (2004).
252. Song, J.S.*, et al.* Inhibitory effect of CXC chemokine receptor 4 antagonist AMD3100 on bleomycin induced murine pulmonary fibrosis. *Exp Mol Med* 42, 465-472 (2010).
253. Chu, P.Y.*, et al.* Bone marrow-derived cells contribute to fibrosis in the chronically failing heart. *Am J Pathol* 176, 1735-1742 (2010).
254. Sopel, M.J., Rosin, N.L., Lee, T.D. & Legare, J.F. Myocardial fibrosis in response to Angiotensin II is preceded by the recruitment of mesenchymal progenitor cells. *Lab Invest* 91, 565-578 (2011).
255. Petit, I., Jin, D. & Rafii, S. The SDF-1-CXCR4 signaling pathway: a molecular hub modulating neo-angiogenesis. *Trends Immunol* 28, 299-307 (2007).
256. Kijowski, J.*, et al.* The SDF-1-CXCR4 axis stimulates VEGF secretion and activates integrins but does not affect proliferation and survival in lymphohematopoietic cells. *Stem Cells* 19, 453-466 (2001).
257. Claesson-Welsh, L. VEGF-B taken to our hearts: specific effect of VEGF-B in myocardial ischemia. *Arterioscler Thromb Vasc Biol* 28, 1575-1576 (2008).
258. Dahlke, M.H., Larsen, S.R., Rasko, J.E. & Schlitt, H.J. The biology of CD45 and its use as a therapeutic target. *Leuk Lymphoma* 45, 229-236 (2004).
259. Yeh, S.P.*, et al.* Induction of CD45 expression on bone marrow-derived mesenchymal stem cells. *Leukemia* 20, 894-896 (2006).
260. Shivtiel, S.*, et al.* CD45 regulates retention, motility, and numbers of hematopoietic progenitors, and affects osteoclast remodeling of metaphyseal trabecules. *J Exp Med* 205, 2381-2395 (2008).

261. Holmes, C. & Stanford, W.L. Concise review: stem cell antigen-1: expression, function, and enigma. *Stem Cells* 25, 1339-1347 (2007).
262. Yoshimoto, M.*, et al.* Two different roles of purified CD45+c-Kit+Sca-1+Lin- cells after transplantation in muscles. *Stem Cells* 23, 610-618 (2005).
263. McKinney-Freeman, S.L.*, et al.* Muscle-derived hematopoietic stem cells are hematopoietic in origin. *Proc Natl Acad Sci U S A* 99, 1341-1346 (2002).
264. Salvucci, O., de la Luz Sierra, M., Martina, J.A., McCormick, P.J. & Tosato, G. EphB2 and EphB4 receptors forward signaling promotes SDF-1-induced endothelial cell chemotaxis and branching remodeling. *Blood* 108, 2914-2922 (2006).
265. Schiraldi, M.*, et al.* HMGB1 promotes recruitment of inflammatory cells to damaged tissues by forming a complex with CXCL12 and signaling via CXCR4. *J Exp Med* (2012).
266. Segret, A.*, et al.* Structural localization and expression of CXCL12 and CXCR4 in rat heart and isolated cardiac myocytes. *J Histochem Cytochem* 55, 141-150 (2007).
267. Bleul, C.C., Fuhlbrigge, R.C., Casasnovas, J.M., Aiuti, A. & Springer, T.A. A highly efficacious lymphocyte chemoattractant, stromal cell-derived factor 1 (SDF-1). *J Exp Med* 184, 1101-1109 (1996).
268. Suratt, B.T.*, et al.* Role of the CXCR4/SDF-1 chemokine axis in circulating neutrophil homeostasis. *Blood* 104, 565-571 (2004).
269. Link, D.C. Neutrophil homeostasis: a new role for stromal cell-derived factor-1. *Immunol Res* 32, 169-178 (2005).
270. Tano, N., Kim, H.W. & Ashraf, M. microRNA-150 regulates mobilization and migration of bone marrow-derived mononuclear cells by targeting Cxcr4. *PLoS One* 6, e23114 (2011).
271. Clark, W.M., Lauten, J.D., Lessov, N., Woodward, W. & Coull, B.M. Time course of ICAM-1 expression and leukocyte subset infiltration in rat forebrain ischemia. *Mol Chem Neuropathol* 26, 213-230 (1995).
272. Rhodes, N.P., Hunt, J.A. & Williams, D.F. Macrophage subpopulation differentiation by stimulation with biomaterials. *J Biomed Mater Res* 37, 481-488 (1997).
273. Moriwaki, H., Stempien-Otero, A., Kremen, M., Cozen, A.E. & Dichek, D.A. Overexpression of urokinase by macrophages or deficiency of plasminogen activator inhibitor type 1 causes cardiac fibrosis in mice. *Circ Res* 95, 637-644 (2004).
274. Wells, C.M., Walmsley, M., Ooi, S., Tybulewicz, V. & Ridley, A.J. Rac1-deficient macrophages exhibit defects in cell spreading and membrane ruffling but not migration. *J Cell Sci* 117, 1259-1268 (2004).
275. Yang, L.*, et al.* Cdc42 critically regulates the balance between myelopoiesis and erythropoiesis. *Blood* 110, 3853-3861 (2007).
276. Torchia, E.C., Boyd, K., Rehg, J.E., Qu, C. & Baker, S.J. EWS/FLI-1 induces rapid onset of myeloid/erythroid leukemia in mice. *Mol Cell Biol* 27, 7918-7934 (2007).
277. Wang, J.F., Liu, Z.Y. & Groopman, J.E. The alpha-chemokine receptor CXCR4 is expressed on the megakaryocytic lineage from progenitor to platelets and modulates migration and adhesion. *Blood* 92, 756-764 (1998).
278. Hamada, T.*, et al.* Transendothelial migration of megakaryocytes in response to stromal cell-derived factor 1 (SDF-1) enhances platelet formation. *J Exp Med* 188, 539-548 (1998).
279. Hodohara, K., Fujii, N., Yamamoto, N. & Kaushansky, K. Stromal cell-derived factor-1 (SDF-1) acts together with thrombopoietin to enhance the development of megakaryocytic progenitor cells (CFU-MK). *Blood* 95, 769-775 (2000).
280. Lane, W.J.*, et al.* Stromal-derived factor 1-induced megakaryocyte migration and platelet production is dependent on matrix metalloproteinases. *Blood* 96, 4152-4159 (2000).
281. Avecilla, S.T.*, et al.* Chemokine-mediated interaction of hematopoietic progenitors with the bone marrow vascular niche is required for thrombopoiesis. *Nat Med* 10, 64-71 (2004).
282. Dominici, M.*, et al.* Restoration and reversible expansion of the osteoblastic hematopoietic stem cell niche after marrow radioablation. *Blood* 114, 2333-2343 (2009).
283. Singh, M.*, et al.* Functional roles of osteoactivin in normal and disease processes. *Crit Rev Eukaryot Gene Expr* 20, 341-357 (2010).
284. Friddle, C.J., Koga, T., Rubin, E.M. & Bristow, J. Expression profiling reveals distinct sets of genes altered during induction and regression of cardiac hypertrophy. *Proc Natl Acad Sci U S A* 97, 6745-6750 (2000).
285. Ceriani, L. & Giovanella, L. Cardiac natriuretic peptides after myocardial infarction: relationship with infarct size, left ventricular function and remodelling assessed by 99mTc-sestamibi gated-single photon emission tomography. *Clin Chem Lab Med* 45, 226-231 (2007).
286. Cameron, V.A.*, et al.* Atrial (ANP) and brain natriuretic peptide (BNP) expression after myocardial infarction in sheep: ANP is synthesized by fibroblasts infiltrating the infarct. *Endocrinology* 141, 4690-4697 (2000).
287. Magga, J.*, et al.* Atrial natriuretic peptide, B-type natriuretic peptide, and serum collagen markers after acute myocardial infarction. *J Appl Physiol* 96, 1306-1311 (2004).
288. Calderone, A.*, et al.* Scar myofibroblasts of the infarcted rat heart express natriuretic peptides. *J Cell Physiol* 207, 165-173 (2006).
289. Levy, P.S.*, et al.* Limit to cardiac compensation during acute isovolemic hemodilution: influence of coronary stenosis. *Am J Physiol* 265, H340-349 (1993).
290. Wahr, J.A. Myocardial ischaemia in anaemic patients. *Br J Anaesth* 81 Suppl 1, 10-15 (1998).
291. Nikolsky, E.*, et al.* Impact of anemia in patients with acute myocardial infarction undergoing primary percutaneous coronary intervention: analysis from the Controlled Abciximab and Device Investigation to Lower Late Angioplasty Complications (CADILLAC) Trial. *J Am Coll Cardiol* 44, 547-553 (2004).
292. Lee, P.C., Kini, A.S., Ahsan, C., Fisher, E. & Sharma, S.K. Anemia is an independent predictor of mortality after percutaneous coronary intervention. *J Am Coll Cardiol* 44, 541-546 (2004).
293. Sabatine, M.S.*, et al.* Association of hemoglobin levels with clinical outcomes in acute coronary syndromes. *Circulation* 111, 2042-2049 (2005).
294. Cho, K.H.*, et al.* Value of early risk stratification using hemoglobin level and neutrophil-to-lymphocyte ratio in patients with ST-elevation myocardial infarction undergoing primary percutaneous coronary intervention. *Am J Cardiol* 107, 849-856 (2011).
295. Gagnon, D.R., Zhang, T.J., Brand, F.N. & Kannel, W.B. Hematocrit and the risk of cardiovascular disease--the Framingham study: a 34-year follow-up. *Am Heart J* 127, 674-682 (1994).
296. Mann, J.F. What are the short-term and long-term consequences of anaemia in CRF patients? *Nephrol Dial Transplant* 14 Suppl 2, 29-36 (1999).
297. Etzerodt, A.*, et al.* Plasma clearance of hemoglobin and haptoglobin in mice and effect of CD163 gene targeting disruption. *Antioxid Redox Signal* (2012).

298. Miller, J.S., McCullar, V., Punzel, M., Lemischka, I.R. & Moore, K.A. Single adult human CD34(+)/Lin-/CD38(-) progenitors give rise to natural killer cells, B-lineage cells, dendritic cells, and myeloid cells. *Blood* 93, 96-106 (1999).
299. Zhao, Y.*, et al.* Murine hematopoietic stem cell characterization and its regulation in BM transplantation. *Blood* 96, 3016-3022 (2000).
300. Bandari, P.S.*, et al.* Hematopoietic growth factor inducible neurokinin-1 type: a transmembrane protein that is similar to neurokinin 1 interacts with substance P. *Regul Pept* 111, 169-178 (2003).
301. Shantsila, E. & Lip, G.Y. Monocyte diversity in myocardial infarction. *J Am Coll Cardiol* 54, 139-142 (2009).
302. Dresske, B.*, et al.* Multipotent cells of monocytic origin improve damaged heart function. *Am J Transplant* 6, 947-958 (2006).
303. Bruno, S.*, et al.* Combined administration of G-CSF and GM-CSF stimulates monocyte-derived pro-angiogenic cells in patients with acute myocardial infarction. *Cytokine* 34, 56-65 (2006).
304. Mühlstedt, S., Özcelik, C., Bader, M. Gpnmb/Osteoactivin as a drug target and biomarker in cardiac diseases; EP2460890. (2010).

7 Appendix

7.1 Abbreviations and Letter Symbols

7.1.1 Abbreviations

Abbreviation	
ACE	Angiotensin converting enzyme
ACS	Acute coronary syndrome
AMI	Acute myocardial infarction
Ang	Angiotensin
ANP	Atrial natriuretic peptide
APC	Allophycocyanin
BCA	Bicinchoninic acid
BLAST	Basic local alignment search tool
BM	Bone marrow
BNP	Brain natriuretic peptide
BSA	Bovine serum albumin
CABG	Coronary artery bypass graft
CK	Creatine kinase (muscle-brain)
CM	Cardiomyocyte(s)
CRP	C-reactive protein
DAPI	4’,6-Diamidino-2-pheyindole
DMEM	Dulbecco’s modified eagle medium
DNA	Deoxyribonucleic acid
Echo	Echocardiography
ECM	Extra-cellular matrix
EDTA	Ethylenediaminetetraacetic acid
EF	Ejection fraction
ELISA	Enzyme-linked immunosorbent assay
EPC	Endothelial progenitor cell
FBS	Fetal bovine serum
F	filial
FC	Flow cytometry
Fig.	Figure
FITC	Fluorescein isothyiocyanate
FS	Fractional shortening
GAPDH	Glyceraldehyde-3-phosphate dehydrogenase
GPNMB	Glycoprotein (transmembrane) nmb
Gra	Granulocytes
G-CSF	Granulocyte colony-stimulating factor
Hbegf	Heparin-binding EGF-like growth factor
HCT	Hematocrit
HGB	Hemoglobin
HPRT	Hypoxanthin-phosphoribosyl-transferase
HSC	Hematopoietic stem cell
IFN	Interferon
IL	Interleukin

Int	Intermediate
i.p.	Intraperitoneal
Iso	Isoprenaline
IVSD(/S)	Interventricular septum in diastole(/systole)
LAD	Left anterior descending (artery)
LV	Left ventricle
LVED(/S)D	Left ventricular end-diastolic(/-systolic) diameter
LVED(/S)V	Left ventricular end-diastolic(/-systolic) volume
Lym	Lymphocytes
M-CSF	Macrophage colony stimulating factor
MHC	Myosin heavy chain
MI	Myocardial infarction
MMP	Matrix metalloproteinase
Mo	Monocytes
MRI	Magnetic resonance imaging
MSC	Mesenchymal stem cell
NK-κB	Nuclear factor-kappa B
PAGE	Polyacrylamid gel electrophoresis
PB®	Pacific blue
PBS	Phosphate buffered saline
PCI	Percutaneous coronary intervention
PCR	Polymerase chain reaction
PE	Phycoerythrin
Pf4	Platelet factor 4
PLT	Platelet(s)
PI	Peri-infarct
PWTD(/S)	Posterior wall thickness in diastole(/systole)
qRT-PCR	Quantitative real time PCR
RAAS	Renin-angiotensin-aldosterone system
RBC	Red blood cell(s)
ROS	Reactive oxygen species
RT	Room temperature
SD	Sprague Dawley
SDF-1	Stromal cell-derived factor 1
Sk. muscle	Skeletal muscle
Tab.	Table
TAE	Tris-acetate-EDTA
Tg	Transgenic
Tgfb2	Transforming growth factor beta 2
TLR	Toll-like receptor
Tn	Troponin
VEGF	Vascular endothelial growth factor
Vs	Versus
WB	Western blot
WBC	White blood cell(s)
WKY	Wistar Kyoto
WT	Wild type

7.1.2 Letter Symbols

Letter symbol	
bp	Base pair(s)
c	Concentration
d	Day(s)
g	Relative centrifugal force
h	Hour(s)
kb	Kilobase
kDa	Kilodalton
µl	Microliter
µm	Micrometer
µM	Micromolar
M	Molar
min	Minute(s)
ml	Milliliter
ng	Nanogramm
nm	Nanometer
pmol	Picomole
rpm	Rotations per minute
sec	Second(s)
U	Unit(s)
w	Week(s)

7.2 Danksagung

Ich möchte mich ganz herzlich bei Prof. Dr. Michael Bader für die Möglichkeit bedanken, die Dissertation in seiner Arbeitsgruppe als Teil eines spannenden Projektes zu erarbeiten. Im Besonderen bin ich für die ausgezeichnete Betreuung meiner Arbeit und die erstklassigen Arbeitsbedingungen in seinem Labor dankbar.

Des Weiteren gilt mein besonderer Dank Prof. Dr. Harald Saumweber von der Humboldt Universität zu Berlin für die Betreuung meiner Arbeit.

Prof. Dr. Andreas Lendlein und Dr. Cemil Özcelik danke ich für Ihre Anregungen und konstruktive Kritik.

Ein großes Dankeschön gilt meinen Arbeitskollegen der Arbeitsgruppen Bader und Özcelik. Namentlich erwähnen möchte ich Santhosh Ghadge, Anna Panek und Johan Duchene, die mir stets mit Rat und Tat in allen praktischen und theoretischen Fragen zur Seite standen. Zudem bedanke ich mich bei Maik Grohmann, Susann Matthes, Stefanie Hügel und Daniel Beis für die gute Stimmung und die vielen lustigen Stunden im und außerhalb des Labors. Fatimunnisa (Sayeeda) Qadri danke ich für die unermüdliche Unterstützung bei allen histologischen Fragestellungen. Zudem bedanke ich mich bei Elena Popova für die Hilfe bei der Generierung der transgenen Rattenlinie.

Für die exzellente technische Assistenz bedanke ich mich ganz herzlich bei Tanja Schalow, Astrid Schiche, Jeannette Motthes, Andrea Müller, Thorsten Riepenhausen und Lisa Mallis. Weiterhin gilt mein Dank Sabine Grüger, Manfred Ströhmann, Sina Wohlfahrt, Annegret Dahlke, Monique Bergemann und Franziska Kratz für die ausgezeichnete Betreuung der Versuchstiere.

Für die Möglichkeit, mein Methodenspektrum zu erweitern und etablierte Versuchsanordnungen nutzen zu können bedanke ich mich bei Dr. Arnd Heuser, Martin Taube und Stefanie Schelenz (Echokardiographie), Dr. Andreas Pohlmann und Babette Dieringer (Magnetresonanztomographie), Dr. Herbert Schulz und Gabriele Born (Microarray) sowie Petra Domaing (Kardiomyozytenisolierung).

Für die Finanzierung dieser Arbeit bedanke ich mich bei der *Berlin-Brandenburg School for Regenerative Medicine* (BSRT).

Zuletzt gilt mein ganz besonderer Dank meiner Familie und meinen Freunden. Ich danke euch für die liebevolle Unterstützung und Motivation.

7.3 Selbstständigkeitserklärung

Ich erkläre hiermit, dass ich die vorliegende Arbeit selbstständig und nur unter Verwendung der angegebenen Hilfen und Hilfsmittel angefertigt habe. Alle Stellen, die wörtlich oder sinngemäß aus Quellen entnommen wurden, sind als solche gekennzeichnet. Abbildungen, die anderen Quellen unverändert entnommen oder diesen entlehnt wurden, sind mit der Quellenangabe versehen.

Ich versichere, dass ich mich nicht anderweitig um einen Doktorgrad beworben habe oder einen entsprechenden Doktortitel besitze. Die Promotionsordnung der Mathematisch-Naturwissenschaftlichen Fakultät I der Humboldt-Universität zu Berlin habe ich gelesen und akzeptiert.

Berlin, September 2012 Silke Mühlstedt